Neuroinformatics Group, Bielefeld University

Towards observable haptics

Novel sensors for capturing tactile interaction patterns

Risto Kõiva

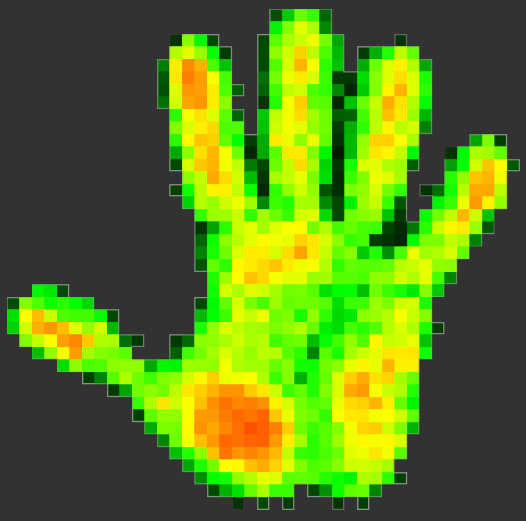

PhD Thesis

Neuroinformatics Group, Bielefeld University

Towards observable haptics

Novel sensors for capturing tactile interaction patterns

Der Technischen Fakultät der Universität Bielefeld
vorgelegt von

Risto Kõiva

zur Erlangung des akademischen Grades

Doktor der Ingenieurwissenschaften.

Gutachter:

Prof. Dr. Helge J. Ritter (Universität Bielefeld)
Prof. Dr. Marc O. Ernst (Universität Bielefeld)
Prof. Dr. Jianwei Zhang (Universität Hamburg)

Prüfungsausschuss:

Prof. Dr. Ulrich Rückert (Universität Bielefeld)
Prof. Dr. Helge J. Ritter (Universität Bielefeld)
Prof. Dr. Marc O. Ernst (Universität Bielefeld)
Prof. Dr. Jianwei Zhang (Universität Hamburg)
Dr. Thies Pfeiffer (Universität Bielefeld)

Vorgelegt am 05. Dezember 2013,
verteidigt am 06. Oktober 2014.

Gedruckt auf alterungsbeständigem Papier nach ISO 9706.

Acknowledgments

The work presented in this thesis was carried out in the Neuroinformatics Group, headed by Prof. Dr. Helge J. Ritter, at the Faculty of Technology, Bielefeld University. It was partially supported by the German Service Robotics Initiative (DESIRE), by the German Cluster of Excellence 277 "Cognitive Interaction Technology (CITEC)", by the EU FP7/2007-2013 project no. 601165 WEARHAP and by the Swiss National Science Foundation project nr. 132700, NINAPRO, (Non-Invasive Adaptive Hand Prosthetics).

During my PhD and write-up, I received helpful comments, remarks, criticism and encouragement from numerous helpful people. The result of this support has made outcome all the more awesome, and therefore in the following I would like to thank each and everyone of them for their valuable input.

Above all, I would like to thank Helge, my principal mentor and the first reviewer of my work, for giving me the opportunity to be a part of his group. His always supporting and enthusiastic attitude have made working with him and his team very enjoyable. Helge's limitless creativity and global perspective on the world of research can really turn a rainy day into a sunny one.

I would like to thank Prof. Dr. Jochen J. Steil for introducing me to Neuroinformatics Group, for his belief in me and for giving me the best possible start into advanced robotics, despite me probably being his most annoying student of all time.

I would like to thank Dr. Thomas Hermann for thinking out of the box, for many creative times together, and for teaching me about the magic of scientific publication. His input on writing tricks has been very valuable to me and has resulted in me getting many accepted publications.

It was my pleasure to share an office with two great colleagues during my PhD, Dr. Till Bovermann and Carsten Schürmann. Thank you both for all the elaborate productive discussions and friendly support. I had such fun working on projects with you guys.

My thanks also goes to Dr. Robert Haschke for his input and down-to-earth realistic ideas, his honest and direct criticism and for his friendly support.

I would also like to thank Dr. Claudio Castellini from the German Aerospace Center (DLR) in Oberpfaffenhofen for lively discussions, superb collaboration and for the great times we had in southern Bavaria.

My big gratitude goes to Dr. Jonathan Maycock for not only proof-reading big parts of this thesis, but also numerous scientific submissions of mine and for his valuable input during the thesis write-up. He is a great friend and his positive attitude of always being outstandingly supportive was of great help to me.

For their invaluable assistance, I wish to thank Matthias Zenker, Sebastian Zehe, Gereon Büscher, Barbara Hilsenbeck, Vitali Pojurov and Simon Schulz. Numerous projects I was involved in would have taken magnitudes of time longer without their assistance/support.

I am much obliged to Petra Udelhoven, Susanne Strunk and Andrea Caio for their assistance in handling the sometimes unavoidable bureaucracy.

I would also like to thank all the members of the Neuroinformatics Group, the Ambient Intelligence Group and the team of the Biology-CITEC joint workshop for ensuring a pleas-

ant workplace and a friendly atmosphere. I would especially like to thank Horst-J. Nosseler from the workshop for taking over a huge amount of my daily workshop tasks during this thesis write-up period.

Additionally, I would also like to thank the members of the disputation committee, Prof. Dr. Ulrich Rückert, Prof. Dr. Jianwei Zhang, Prof. Dr. Marc O. Ernst, Prof. Dr. Helge J. Ritter and Dr. Thies Pfeiffer, for taking the time to review this work.

Deep gratitude goes to my parents, for not only being courageous enough to have me in the first place, but, in addition, for their continuous love and encouragement and for the superb start to life they gave me (tänan, kallid vanemad, Karin & Peeter).

And finally, I want to thank my wife Xuemei, for her love and support - she is my inspiration and motivation.

Abstract

Touch is one of the primary senses humans use when performing coordinated interaction, but the lack of a sense of touch in the majority of contemporary interactive technical systems, such as robots, which operate in non-deterministic environments, results in interactions that can at best be described as clumsy.

Observing human haptics and extracting the salient information from the gathered data is not only relevant if we are to try to understand the involved underlying cognitive processes, but should also provide us with significant clues to design future intelligent interactive systems. Such systems could one day help to take the burden of tedious tasks off our hands in a similar fashion to how industrial robots revolutionized manufacturing. The aim of the work in this thesis was to provide significant advancements in tactile sensing technology, and thus move us a step closer to realizing this goal.

The contributions contained herein can be broken into two major parts. The first part investigates capturing interaction patterns in humans with the goals of better understanding manual intelligence and improving the lives of hand amputees, while the second part is focused on augmenting technical systems with a sense of touch.

tacTiles, a wireless tactile sensitive surface element attached to a deformable textile, was developed to capture human full-body interactions with large surfaces we come into contact with in our daily lives, such as floors, chairs, sofas or other furniture. The *Tactile Dataglove*, *iObject* and the *Tactile Pen* were developed especially to observe human manual intelligence. Whereas *iObject* allows motion sensing and a higher definition tactile signal to be captured than the *Tactile Dataglove* (220 tactile cells in the first *iObject* prototype versus 54 cells in the glove), the wearable glove makes haptic interactions with arbitrary objects observable. The *Tactile Pen* was designed to measure grip force during handwriting in order to better facilitate therapeutic treatment assessments. These sensors have already been extensively used by various research groups, including our own, to gain a better understanding of human manual intelligence.

The *Finger-Force-Linear-Sensor* and the *Tactile Bracelet* are two novel sensors that were developed to facilitate more natural control of dexterous multi Degree-of-Freedom (DOF) hand prostheses. The *Finger-Force-Linear-Sensor* is a very accurate bidirectional single finger force ground-truth measurement device that was designed to enable testing and development of single finger forces and muscle activations mapping algorithms. The *Tactile Bracelet* was designed with the goal to provide a more robust and intuitive means of control for multi-DOF hand prostheses by measuring the muscle bulgings of the remnant muscles of lower arm amputees. It is currently in development and will eventually cover the complete forearm circumference with high spatial resolution tactile sensitive surfaces. An experiment involving a large number of lower arm amputees has already been planned.

The *Modular flat tactile sensor system*, the *Fabric-based touch sensitive artificial skin* and the *3D shaped tactile sensor* were developed to cover and to add touch sensing capabilities to the surfaces of technical systems. The rapid augmentation of systems with a sense of touch was the main goal of the modular flat tactile sensor system. The developed sensor modules can be used alone or in an array to form larger tactile sensitive surfaces such as

tactile sensitive tabletops. As many robots have curved surfaces, using flat rigid modules severely limits the areas that can be covered with tactile sensors. The *Fabric-based tactile sensor*, originally developed to form a tactile dataglove for human hands, can with minor modifications also function as an artificial skin for technical systems. Finally, the *3D shaped tactile sensor based on Laser-Direct-Structuring technology* is a novel tactile sensor that has a true 3D shape and provides high sensitivity and a high spatial resolution. These sensors take us further along the path towards creating general purpose technical systems that in time can be of great help to us in our daily lives.

The desired tactile sensor characteristics differ significantly according to which haptic interaction patterns we wish to measure. Large tactile sensor arrays that are used to capture full body haptic interactions with floors and upholstered furniture, or that are designed to cover large areas of technical system surfaces, need to be scalable, have low power consumption and should ideally have a low material cost. Two examples of such sensors are *tacTiles* and the *Fabric-based sensor for curved surfaces*. At the other end of the tactile sensor development spectrum, if we want to observe manual interactions, high spatial and temporal resolution are crucial to enable the measurement of fine grasping and manipulation actions. Our fingertips contain the highest density area of mechanoreceptors, the organs that sense mechanical pressure and distortions. Thus, to construct biologically inspired anthropomorphic robotic hands, the artificial tactile sensors for the fingertips require similar high-fidelity sensors with surfaces that are curved under small bending radii in 2 dimensions, have high spatial densities, while simultaneously providing high sensitivity. With the fingertip tactile sensor, designed to fit the Shadow Robot Hands' fingers, I show that such sensors can indeed be constructed in the *3D-shaped high spatial resolution tactile sensor* section of my thesis.

With my work I have made a significant contribution towards making haptics more observable. I achieved this by developing a high number of novel tactile sensors that are usable, give a deeper insight into human haptic interactions, have great potential to help amputees and that make technical systems, such as robots, more capable.

Abbreviations and Acronyms

ABS	Acrylonitrile butadiene styrene (a thermoplastic)
ACL	Asynchronous-Connectionless-Link
ADC	Analog-Digital-Converter
AIM	Int. Conf. on Advanced Intelligent Mechatronics
ALS	Amyotrophic lateral sclerosis
ANSI	American National Standards Institute
ASCII	American Standard Code for Information Interchange
ATR	Advanced Telecommunications Research Institute International
BID	Bus Identifier
BioRob	Int. Conf. on Biomedical Robotics and Biomechatronics
BMBF	German Federal Ministry of Education and Research
BT-SPP	Bluetooth Serial Port Profile
CAD	Computer-Aided Design
CAM	Computer-Aided Manufacturing
CITEC	German Cluster of Excellence 277 *Cognitive Interaction Technology*
CLK	Clock signal
CNC	Computer Numerical Control
CR	Carriage Return
$\overline{\textbf{CS}}$	Chip Select (low active)
CTS	Clear-to-Send
DAQ	Data-acquisition
DC	Direct current
DESIRE	BMBF funded project *German Service Robotics Initiative*
DFG	German Research Foundation (Deutsche Forschungsgemeinschaft)
DIY	Do-It-Yourself
DLC	Data-Link-Control
DLR	German Aerospace Center
DOF	Degree-of-Freedom
EEG	Electroencephalography
EMBC	Int. Conf. of the IEEE Engineering in Medicine and Biology Society
EU	European Union
EUSART	Enhanced-Universal-Synchronous-Receiver-Transmitter
FDM	Fused Deposition Modeling
FET	Field-Effect Transistor
FFLS	Finger Force Linear Sensor
FFT	Fast-Fourier-Transform
FMG	Force Myography
fMRI	functional MRI
FSR	Force-Sensing-Resistors
GND	Ground potential

GUI	Graphical User Interface
HAID	Int. Conf. on Haptic and Audio Interaction Design
HMI	Human-Machine-Interface
HRI	Int. Conf. on Human-Robot-Interaction
I^2C	Inter-Integrated Circuit
ICD	In-Circuit Debugger
ICORR	Int. Conf. on Rehabilitation Robotics
ICAR	Int. Conf. on Advanced Robotics
ICRA	Int. Conf. on Robotics and Automation
ICSP	In-Circuit-Serial-Programming
IEEE	Institute of Electrical and Electronics Engineers
IMU	Inertial Measurement Unit
Int. Conf.	International Conference
ISR	Interrupt Service Routine
iObject	Instrumented/Intelligent Object
IROS	Int. Conf. on Intelligent Robots and Systems
I/O	Input/Output
KISS	Keep-It-Simple&Stupid
L2CAP	Logical Link Control and Adaptation Protocol
LBR4	Lightweight Robot 4
LCD	Liquid Crystal Display
LDS	Laser-Direct-Structuring
LED	Light-Emitting Diode
LF	Line Feed
LiPo	Lithium-Polymer
LSB	Least-Significant-Bit
MCU	Microcontroller unit
MEMS	Microelectromechanical systems
MId	Message Identifier
MID	Molded-Interconnect-Devices
MILAB	Manual Interaction Laboratory
MIPS	Million instructions per second
MISO	Master-In-Slave-Out
MMG	Mechanomyography
MOSI	Master-Out-Slave-In
MPASM	Microchip assembly language
MRI	Magnetic Resonance Imaging
MSB	Most-Significant-Bit
NINAPRO	SNSF project Non-Invasive Adaptive Hand Prosthetics
NRMSE	Normalized Root-Mean-Square Error
PC	Personal Computer
PCB	Printed Circuit Board
POM	Polyoxymethylene
PST	Pressure-Sensor-Tactile
QTC	Quantum-Tunneling-Composite
RAM	Random-Access-Memory
RBF	Radial-Basis-Function
RKI	Residual Kinetic Imaging

RTS	Request-to-Send
RX	Receiver
sEMG	Surface Electromyography
SDK	Software Development Kit
SID	Sonic Interaction Design
SMD	Surface-Mount-Devices
SMP	Surface Muscle Pressure
SNSF	Swiss National Science Foundation
SPI	Serial Peripheral Interface
SPP	see *BT-SPP*
SVM	Support Vector Machine
taxel	Tactile pixel
TX	Transmitter
USB	Universal Serial Bus
WEARHAP	EU funded project *WEARable HAPtics*
WHC	World Haptics Conference

Publications

Parts of this thesis have been published or submitted for publications in the following (corresponding author noted with an asterisk):

- *Flexible and stretchable fabric-based tactile sensor*,
  Gereon Büscher, **Risto Kõiva***, Carsten Schürmann, Robert Haschke and Helge J. Ritter. Journal of Robotics and Autonomous Systems, Special Issue on Advances in Tactile Sensing and Touch-based Human-Robot Interaction, Sept. 2014.

- *A highly sensitive 3D-shaped tactile sensor*,
  Risto Kõiva*, Matthias Zenker, Carsten Schürmann, Robert Haschke and Helge J. Ritter. In proceedings of the International Conference on Advanced Intelligent Mechatronics (AIM), Wollongong, Australia, July 2013. Best Student Paper Award candidate nomination.

- *Evaluating subsampling strategies for sEMG-based prediction of voluntary muscle contractions*,
  Risto Kõiva*, Barbara Hilsenbeck and Claudio Castellini. In proceedings of the International Conference on Rehabilitation Robotics (ICORR), Seattle, Washington, USA, June 2013.

- *Using a high spatial resolution tactile sensor for intention detection*,
  Claudio Castellini* and **Risto Kõiva**. In proceedings of the International Conference on Rehabilitation Robotics (ICORR), Seattle, Washington, USA, June 2013.

- *Schreibgeräthülle mit taktil-sensitivem Schaft*,
  Gereon Büscher*, Gerhard Mahlich, **Risto Kõiva**, Carsten Schürmann, Robert Haschke and Helge J. Ritter. Presented at the annual DVE Ergotherapy-Congress, Bielefeld, Germany, May 2013.

- *Tactile dataglove with fabric-based sensors*,
  Gereon Büscher, **Risto Kõiva***, Carsten Schürmann, Robert Haschke and Helge J. Ritter. In proceedings of the International Conference on Humanoid Robots (HUMANOIDS), Osaka, Japan, November 2012. Best Paper Award candidate nomination.

- *Analysis of human grasping under task anticipation using a multi sensory tactile book*,
  Carsten Schürmann*, **Risto Kõiva**, Robert Haschke and Helge J. Ritter. In proceedings of the International Conference on Humanoid Robots (HUMANOIDS), Osaka, Japan, November 2012.

- *Intention Gathering from Muscle Residual Activity for the Severely Disabled*,
  Claudio Castellini* and **Risto Kõiva**. In proceedings of the workshop on Progress, Challenges and Future Perspectives in Navigation and Manipulation Assistance for

Robotic Wheelchairs, held in conjunction with the International Conference on Intelligent Robots and Systems (IROS), Vilamoura, Portugal, October 2012.

- *Flexible and stretchable fabric-based tactile sensor*,
  Gereon Büscher, **Risto Kõiva***, Carsten Schürmann, Robert Haschke and Helge J. Ritter. In proceedings of the workshop on Advances in tactile sensing and touch-based human-robot interaction, held in conjunction with the International Conference on Intelligent Robots and Systems (IROS), Vilamoura, Portugal, October 2012.

- *FFLS: An accurate linear device for measuring synergistic finger contractions*,
  Risto Kõiva*, Barbara Hilsenbeck and Claudio Castellini. In proceedings of the International Conference of the IEEE Engineering in Medicine & Biology Society (EMBC), San Diego, California, USA, August 2012.

- *Experimental Evaluation of Human Grasps Using a Sensorized Object*,
  Maximo A. Roa*, **Risto Kõiva** and Claudio Castellini. In proceedings of the International Conference on Biomedical Robotics and Biomechatronics (BioRob), Rome, Italy, June 2012.

- *Using surface electromyography to predict single finger forces*,
  Claudio Castellini* and **Risto Kõiva**. In proceedings of the International Conference on Biomedical Robotics and Biomechatronics (BioRob), Rome, Italy, June 2012.

- *Sensors for capturing tactile interaction patterns*,
  Risto Kõiva* and Carsten Schürmann. In proceedings of workshop on Advances in tactile sensing and touch based human-robot interaction, held in conjunction with the International Conference on Human-Robot Interaction (HRI), Boston, Massachusetts, USA, March 2012.

- *SonicChair*,
  Thomas Hermann* and **Risto Kõiva**. Sonic Interaction Design - Exhibition Catalogue, Editors Frauke Behrendt and Trond Lossius. Bergen/Oslo, Norway, May 2011.

- *Development of an intelligent object for grasp and manipulation research*,
  Risto Kõiva*, Robert Haschke and Helge J. Ritter. Proceedings of the International Conference on Advanced Robotics (ICAR), Tallinn, Estonia, June 2011.

- *A Modular High-Speed Tactile Sensor for Human Manipulation Research*,
  Carsten Schürmann*, **Risto Kõiva**, Robert Haschke and Helge J. Ritter. Proceedings of World Haptics Conference (WHC), Istanbul, Turkey, June 2011.

- *tacTiles for Ambient Intelligence and Interactive Sonification*,
  Thomas Hermann* and **Risto Kõiva**. Proceedings of Haptic and Audio Interaction Design, Third International Workshop (HAID), Jyväskylä, Finland, September 2008.

Contents

1 Introduction

1.1 Motivation

The term *haptic* was first introduced in the late 19^{th} century and comes from the Greek words *haptikos* and *haptein* meaning to be able to touch, grasp or fasten [Oxf09]. Today we understand haptics to be the study of touch and the study of human interaction with the external environment using touch.

Touch, also known as tactioception, is one of the main senses that humans use for coordinated interaction with the world. The four other most common senses are sight (ophthalmoception), hearing (audioception), taste (gustaoception) and smell (olfacception). The question of how important each sense is to our everyday lives can be answered by temporarily suppressing the sense in question and observing the results. Closing the eyes or wearing noise cancelling earphones are simple examples used to suppress sight and hearing. Table 1.1 gives some examples in which the sense of touch has been suppressed in selected parts of the body.

The non-existence or permanent loss of a sense of touch is fortunately very uncommon in humans, but if it occurs, it can have a significantly stronger negative impact on quality of life than a loss of any of the other main senses. A colorful example of this is given by Cole [Col95], when he described the life of a man who, at the young age of 19, was struck down at work by a rare neurological illness that deprived him of all sensation below the neck. With no chance of neurological recovery, he relearnt over time how to move his limbs using sight as a feedback modality. Using powerful concentration in a tight visual control loop, he was even able to achieve slow independent walking. However, at times when there was a sudden interruption of his visual information, such as during a power outage when everything went dark, he would fall to the ground due to the inability to supervise his body. To avoid slippage, he was forced to use excessive force during grasping and manipulation of objects, thus making interactions with deformable objects almost impossible.

The sensory homunculus in Figure 1.1 shows a representation of how much of the somatosensory cortex is typically dedicated to processing sensory information from different

Area of loss of touch	**Equivalent**	**Consequences**
Hand/arm	Sleeping on an arm	Difficulty controlling/moving the hand/arm and manipulating objects. Numbness.
Leg	A leg that falls asleep	Difficulty walking and maintaining a stable posture. Tendency to fall.
Mouth/tongue	Local dental anesthesia	Difficulty speaking and chewing. Involuntary drooling. Numbness or “fat lip” sensation.

Table 1.1: Understanding the loss of touch through common, everyday situations [RDLT06]. Note: an “asleep” arm or leg might involve disruption of sensory and also motor nerve information due to applied pressure.

Figure 1.1: The sensory homunculus. The body part sizes are drawn in proportion to their corresponding sensory organ areas in the cortex. Note the large hands, denoting sizable cortex areas devoted to the processing of haptic information. (Image from flowering-brain.wordpress.com)

body parts. The distorted appearance of the homunculus results from the fact that the appropriate somatosensory cortex area is not proportional to the size of the actual body part. The resulting sensory homunculus has large hands, bold lips and a big face, as disproportionally large somatosensory cortex areas are used for processing sensory information from these areas.

Although tactile receptors cover almost all of our bodies, the hands are especially interesting for haptics studies due to their dense haptic sensory distribution and amazing ability to perform motor skills. Using our hands, we are able to carry out a wide variety of tasks, such as high precision tasks (example: surgery), accurate timing and force tasks (example: playing piano), high sensitivity tasks (example: braille reading), heavy-duty lifting and carrying tasks. Investigating how humans perform manual interactions may help us to not only produce better robotic systems, but also may give us new insights into the human brain and its processes.

An early experiment demonstrated the importance of tactile feedback for manual interactions. Westling and Johannson [WJ84] anesthetized the skin of the hands of volunteers and thus deactivated their tactile receptors, which resulted in them having great difficulties while they tried to maintain stable object grasps. Similarly, the lack of tactile feedback in today's industrial robots restricts their use to highly structured environments, eliminating the possibility for contact with any uncertainties, including humans. If robots are to operate in unconstrained, general environments, they will need to be endowed with much greater awareness than they currently possess, and thus we can reasonably argue that such technical systems will strongly benefit from force sensing capabilities. An immediate benefit of having force sensing capabilities is the increased safety brought about by having contact detection. Looking towards skillful task execution, having tactile feedback endowed robots will result in an improved capability to manipulate objects under non-deterministic conditions. Some recent work has already been carried out in this area [RHN+11, DWA11, EFS11].

Ritter *et al.* [RHS07] suggested that the study of manual intelligence and its replication in technical systems could lead to the *Rosetta Stone*[1] of grasping and that this is a good step towards having cognitive robots. Therefore, in our journey towards cognitive robots the ability to analyze human hands performing tasks involving touch is a necessary prerequisite endowing artificial hands with humanlike capabilities.

1.2 Contributions and structure of the thesis

The aim of this thesis was to develop and provide numerous research fields (such as robotics, psychology, kinetics, rehabilitation, ubiquitous computing, ambient intelligence) with novel sensors to allow deeper insights into haptic interactions that heretofore have not been possible. The contributions of this thesis can be broken into two major parts. Part A (Chapter 3) concentrates on capturing the interaction patterns of humans, while the focus of Part B (Chapter 4) is on augmenting technical systems with a sense of touch.

Before the main contributions of this thesis are presented, a literature review is given in **Chapter 2**. I first investigate biological tactile sensing by looking into the haptic sensitive organs of humans and their performance in **Section 2.1**. Observing biological systems and trying to mimic them, or taking clues from and applying the design paradigms of biology to technical systems, has not only previously led to new innovative products (e.g., hook-and-loop fastener, lotus-effect paints and coatings, cat's eye road reflectors), but has also led to devices that outperform classical designs (e.g., less drag using shark-skin swimsuits, bionic aircraft and ship hull designs, better cooling of houses modeled after termite mounds, sportswear based on pinecones for improved respiration). A survey of related work on capturing interaction patterns of humans (for the sensors introduced in Part A), and related work on augmenting technical systems with the sense of touch (for the sensors introduced in Part B) is given in **Section 2.2** and in **Section 2.3**, respectively.

In Part A of this thesis I present the developed sensors for capturing haptic interaction data from humans [**Chapter 3**]. Although a variety of possibilities exist to capture human body posture (e.g., marker based optical systems such as Vicon [Vic], LUKOtronic [LUK]; markerless systems such as sensors based on PrimeSense technology [Pri], e.g., Microsoft Kinect [Kin], and computer vision algorithms working on plain RGB-streams; inertial motion based systems such as Xsens Moven/MVN suits [Xse]; magnetic systems such as Ascension Flock-of-Birds [ATC]), there are currently very few options available for observing haptic interaction patterns. As tiny postural changes can cause large force or pressure changes, reliable haptic data cannot be captured by relying solely on postural sensors. In **Section 3.1**, I will introduce a novel wireless modular tactile sensitive surface element that is attached to a deformable textile. It was designed as a cover for surfaces we come into contact with, such as floors, chairs, sofas or other furniture. The sensor is characterized by a robust build, affordable components, and a capacity to cover large areas and curved surfaces. In addition to explaining the developmental details of the sensor, application ideas are sketched in the field of ambient intelligence, gaming and physiotherapy.

[1] The Rosetta Stone is an ancient Egyptian stone containing a ruling that appears in three scripts - ancient Egyptian hieroglyphs, Demotic and ancient Greek. As the texts were almost identical in all three scripts, the discovery of the stone rendered it possible to decipher ancient Egyptian hieroglyphs and as such, the term *Rosetta Stone* has been used idiomatically to represent the crucial key to the process of decryption of encoded information, especially when a small but representative sample is recognized as the clue to understanding a larger whole [Oxf09].

As most of our haptic interaction is performed with our hands, observing the haptics of the fingers and the palm are especially interesting for grasping and manipulation research. A significant part of work on capturing manual intelligence has been performed using postural datagloves (such as the CyberGlove [Cyb]). Only limited research has involved tactile sensing, and most with considerable drawbacks, such as not being practically usable as the devices suffered from unsatisfactory performance (typically not sensitive enough, limited measurement range etc.), or were too fragile and thus not robust enough to survive the forces occurring during normal grasping and manipulation. In Section 3.2 and Section 3.3 I present two robust novel sensors explicitly designed for practical usability in grasping and manipulation research.

Section 3.2 discusses a wearable tactile dataglove that has 54 tactile cells and embedded data acquisition electronics. Sensing is achieved using a fabric-based, flexible, and stretchable tactile sensor introduced by Büscher [Bü11] and capable of seamlessly covering natural shapes. As human skin is mostly a smooth curved surface that is capable of significantly stretching under movement, the practical use of traditional rigid tactile sensor arrays to cover our skin is limited. The data acquisition electronics and the sensor performance evaluation results are presented. The measurements revealed the sensor's ability to measure pressure from a subtle <1kPa up to high pressures of >500kPa, which easily covers the common range for everyday human manual interactions. Countermeasures introduced to tackle the experienced sensitivity degradation due to sweat of the first prototype are also presented. The section concludes by sketching ideas for future dataglove versions that include the addition of goniometer based postural finger joint sensors and IMU-based hand motion sensors.

Section 3.3 presents a novel instrumented object, called iObject, which is equipped with tactile and motion tracking sensors that allow for the evaluation of grasping and manipulation actions. Contact location and contact force, object acceleration in space (6D) and orientation relative to the earth (3D magnetometer) are measured and transmitted in real-time via a cable or optionally a wireless configuration can be used for free movement experiments. By allowing human-human, human-robot and robot-robot comparisons to be made, iObject is a versatile tool that can be used to study manual interaction. In addition to presenting the development details, the section reports on initial applications using iObject. A physiological experiment that evaluated the main parameters of a dual-handed manipulation task was performed. In another experiment, selected grasp quality measures (used typically in robotics to numerically grade the quality of the grasp) were compared with participants' subjective statements of grasp quality goodness.

Losing a hand, regardless of whether it is due to an accident or an illness, can be a very traumatic experience that can have a significant impact on the quality of one's life. The use of prostheses allow many amputees to regain their lost limb not only optically, but with a considerable degree of functionality. Indeed prosthetic devices can also have a positive effect on a patient's psychological state. Current mainstream hand prostheses are typically equipped with only a single active degree-of-freedom (DOF) joint, which facilitates only clamping. The most basic version of such a gripper is actuated purely mechanically, typically via cables that transfer shoulder movement into an opening and closing movement of the hand. More sophisticated versions try to extract patients' intention of closing and opening from muscle remnants using surface electromyography (sEMG). Although popular in numerous active prosthesis research projects, sEMG has significant drawbacks, such as a low signal-to-noise ratio that does not allow very fine-grained and robust control. I argue that controlling advanced multi-DOF hand prostheses over a continuous force manifold

allows for a more robust and natural way of actuation than the current state-of-the-art hand posture classification methods. In **Section 3.4** I present two projects and their results using force/tactile sensing towards the development of more robust and advanced multi-DOF hand prostheses. First, a reference sensor rig that can measure single finger forces from able-bodied participants with unrivaled accuracy was developed to evaluate the effectiveness of intention detection methods, techniques and algorithms. The device, called the *Finger-Force Linear Sensor*, measures the forces applied by the fingertips in both directions (flexion and extension of index, middle, ring and little finger plus thumb rotation and abduction/adduction) and is presented in **Subsection 3.4.1**. It is suitable for several different hand sizes, achieves high measurement accuracy and its signal is guaranteed to be linear for a high range of forces (covering a wider range than a typical person can generate). The output of six analog voltages ($\pm$10V) is suitable for direct processing with a typical data acquisition (DAQ) card. Second, a novel tactile bracelet allowing more robust intention detection from residual muscles will be presented in **Subsection 3.4.2**. Traditionally, intention detection towards controlling prosthetic devices is done using gaze tracking, surface electromyography or electroencephalography, all of which are prone to having noisy signals. In this work a novel way of deducing intention is presented using a high spatial resolution, high dynamic range tactile sensor. Given its similarities to surface electromyography, we have named the technology *tactilemyography*. The developed sensor captures tactile images of muscle bulgings in the forearm during manipulation and grasping tasks and makes the muscle activity clearly visible in the output data. Initial experiments suggest its usability to reliably control future dexterous multi-DOF hand prostheses. And the usage of the sensor is not limited to prosthesis control, as it can also be used to intuitively control exoskeletons and as an input device in gaming and virtual reality scenarios.

Observing the grip force during handwriting could provide an important measure of handwriting effectiveness or skill for the general population in remedial education or during therapy sessions for people with congenital disorders, musculoskeletal disorders or those who have suffered traumatic injury. **Section 3.5** introduces a tactile sensor sheath for a ballpoint pen or a digitizer pen to allow such finger force measurements.

Moving on to Part B of the thesis [**Chapter 4**], I turn my attention to augmenting technical systems with the sense of touch. Unlike industrial robots that perform known repetitive tasks with job-specific grippers, I argue that mastering touch is a prerequisite for having advanced robots that can interact safely with humans and objects in unconstrained situations. Over the last few years, touch sensing has seen immense growth in consumer electronic devices, with the market fully embracing gadgets that have touchscreens, such as smartphones, tablets and recently, somewhat surprisingly, large desktop computer monitors. Such touchscreens are typically implemented as resistive or capacitive sensor arrays, integrated into the rigid liquid crystal displays (LCDs). Similar to touchpads, they are mostly used for registering the positions of fingertips relative to the surface for cursor positioning, navigation or action triggering with predefined gestures. As their main goal is to sense the presence of fingers, these sensors are not capable of providing detailed force or pressure pattern information. In comparison, **Section 4.1** presents the development details of a modular flat tactile sensor that detects the location of an unlimited number of fingers and objects by capturing the true pressure profile. Larger sensor areas can be composed from identical sensor modules, each measuring 80×80mm and consisting of 16×16 tactile pixels. This sensor provides the functionality of a haptic camera, providing technical systems with information about applied pressure profiles on the sensor's 2D surface. The forces applied over the tactile cells are converted to monochrome intensities at corre-

sponding pixel locations. The developed sensor achieves very high sampling speeds of up to 500,000 tactile cells/sec., which equates to sampling rates of up to 1.9kHz when using just one sensor module. Significantly exceeding the highest frequency mechanoreceptors in the human skin, this high sampling rate can be used to detect vibrations created by a slipping object. Using the developed modules, we have assembled touch sensitive tabletops and high spatial resolution robotic end effectors.

Numerous anthropomorphic robots make extensive use of complex three dimensional body parts in mimicry of their biological counterparts, and thus the practical usage of traditional rigid flat tactile sensor arrays is limited. What is needed is a tactile skin that is flexible or has a 3D-shape. The flexible fabric-based tactile sensor, used initially for constructing the tactile dataglove discussed in Section 3.2 to capture interaction patterns of humans, can also be effortlessly used to cover the arbitrary surfaces of robots. Especially its manufacturing technology and choice of materials allow the cost-effective augmentation of larger surfaces with the sense of touch. **Section 4.2** presents the design of sensor system to cover the middle (2 tactile sensor regions) and proximal (3 tactile sensor regions) phalanges of the Shadow Robot Hand and a sensor that covers the palmar area with 12 sensor regions.

Section 4.3 presents a ground-breaking new way of producing high spatial resolution and highly sensitive 3D-shaped tactile sensors. A laser structuring technology is used to augment freeform surfaces with conductive tracks, paving the way for the manufacturing of tactile sensors of almost arbitrary shape. The signal acquisition electronics can be effortlessly embedded on the backside of an artificial layer of skin, eliminating the necessity of additional printed-circuit-boards and thus making the tactile sensor highly compact. Fine laser-printing technology and modern surface-mount electronic components allow this sensor to be built in very high, sub 5mm tactile spatial resolutions. The developed sensor performance was evaluated and results are presented. As an exciting application, we produced tactile sensors for the fingertips of the Shadow Robot Hand, each incorporating 12 tactile sensor regions and embedded signal acquisition electronics. The integrated microcontroller is able to capture force patterns with a frame-rate of up to 1kHz, allowing object slippage to be detected.

The thesis closes with a summary of this work and a discussion, before outlining possible future work in **Chapter 5**.

2 Background and related work

The human sense of touch is remarkably robust and performs astonishingly well. It is as yet unsurpassed by current artificial sensory systems. Our senses are often taken for granted until they start performing poorly at which point a person might require glasses or a hearing aid. However, we do not typically notice any degradation of the sense of touch and thus are much less actively aware of this marvel of nature. As the development of technical systems can benefit from observing and taking clues from nature, and a performance comparison with biological systems is informative, the next section gives an introduction into the human sense of touch, the sensing organs and their performance.

Before the main of the thesis, namely the developed novel sensors for observing haptics in humans and augmenting technical systems with the sense of touch are presented in the following chapters, related work in these two fields is given in Sections 2.2 and 2.3, respectively.

2.1 Human sense of touch

When developing technical systems it can be very inspiring to take a look at what evolution has produced. Human skin with its sensory receptors, found in high concentrations in the hand and especially in the fingertips, is of special interest to this thesis.

The sense of touch in human hands augments our capabilities by not only providing feedback for effortless grasping and manipulation, but also allows us to perceive and recognize objects. This becomes especially interesting when our more dominant object recognition sense, vision, becomes impaired, for example due to occlusions or unfavorable lighting conditions. By grasping and probing objects, we are able to extract 3D information about shape and size in addition to other details such as surface texture, compliance, elasticity, thermal conductivity and weight.

For humans and many animals, touch or tactioception perception, results from the activation of neural receptors. They are mainly located in the skin, but can also be found in a number of internal organs, such as the tongue and throat. The skin is our largest organ, accounting for about 12 to 15% of total body weight and covers about a 1.5 to 2m^2 surface area [MN08]. The skin is part of our integumentary system, an organ system with multiple layers that covers and protects our muscles, bones, ligaments and internal organs and plays an important role in regulating body temperature. The protection given by the integumentary system is threefold, providing as it does, chemical, physical/mechanical and biological barriers. It is composed of 3 main tissue layers: the epidermis, dermis and hypodermis [Figure 2.1].

With a thickness of between 0.03 to 4mm, the epidermis forms the outermost and initial protection layer of our body. It consists of four cell types, keratinocytes (which produce keratin to waterproof the body), melanocytes (which produce pigment and protect us from ultraviolet light), Merkel cells (sensory nerve endings that detect slight pressure) and Langerhan's cells (macrophages that function as a defense by digesting cellular debris and

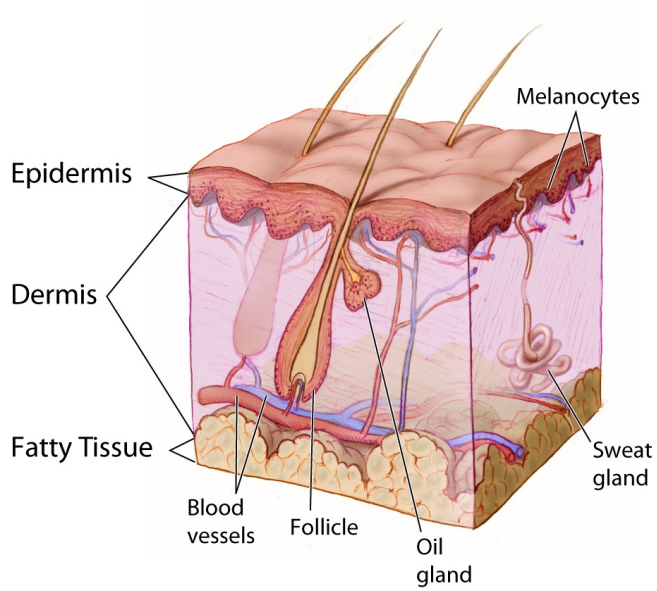

Figure 2.1: Human integumentary system with epidermis, dermis and hypodermis (*fatty tissue*) layers. (Image from Wikimedia Commons, License: Public Domain)

pathogens). The fingernail is a special form of epidermis, in which the protein keratin has hardened the tissue.

Below the epidermis lies the dermis, a strong and flexible tissue layer containing the endings of blood vessels, nerves, hair follicles and sweat glands. The receptors for temperature, touch, pressure, vibration and pain are also located in the dermis.

The deepest and final layer of the integumentary system, the hypodermis, stores fat and functions as a connector to internal tissues that lie beneath it. The hypodermis contains larger blood vessels and nerves than are found in the dermis, and it also functions to cushion the body and helps with temperature regulation in the body.

2.1.1 Mechanoreceptors of the skin

The skin contains a number of different mechanoreceptors, the sensory receptors that respond to mechanical pressure or distortion by firing action potentials into the nervous system [Figure 2.2]. Vallbo and Johansson investigated the mechanoreceptors in the human hand with regards to the sense of touch [VJ84]. In hairless skin, there are five mechanoreceptors: Meissner's corpuscles, Pacinian corpuscles, Ruffini's corpuscle end-organs, Merkel's disks and free nerve endings. Additionally, hair follicle receptors are located at the base of hair strands and sense changes in the position of hairs.

In its simplest form, we can divide the mechanoreceptors into two groups by evaluating their rate of adaptation. The "output" of the mechanoreceptor, the firing frequency or action potential, depends on the amplitude of the stimulus. Some receptors, however, will adapt to a constant stimulus faster than others, thus a categorization into slowly adapting (Ruffini corpuscle end-organs and Merkel's disks) and rapidly adapting (Meissner's corpuscles and Pacinian corpuscles) is possible. The rapidly adapting mechanoreceptors have evolved to detect flutter-vibration [TDSM68] and slip on the skin [WJ87, JW87]. Table 2.1 displays the main mechanoreceptors found in the human hand and their characteristic properties [JF09, SLPD09, KSJ10, Hal11].

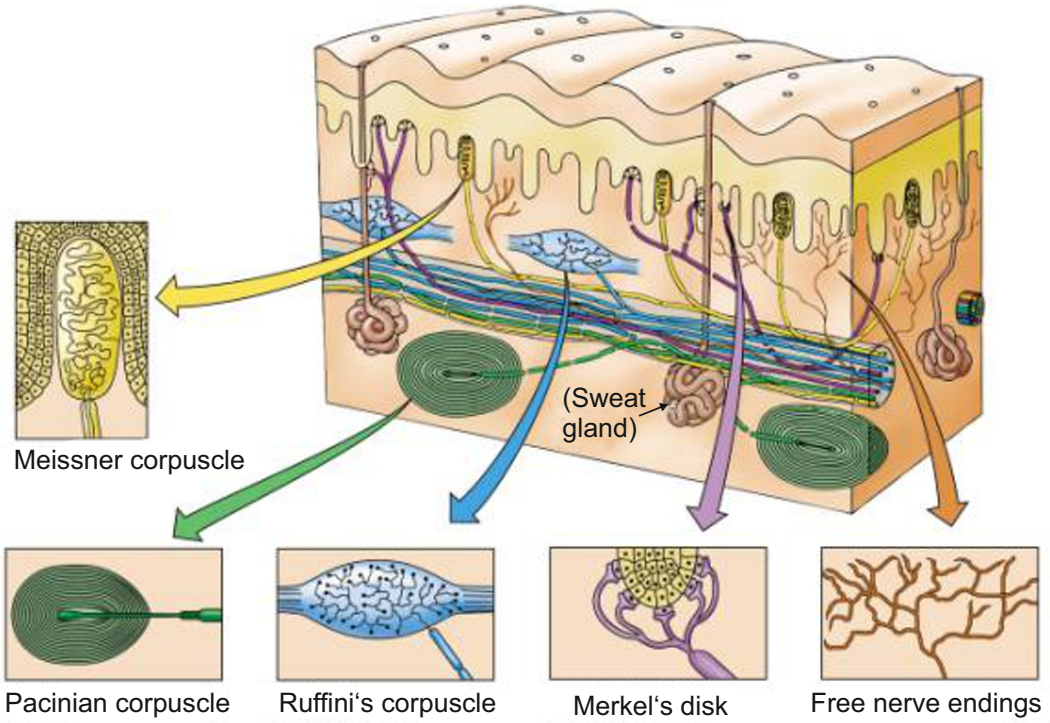

Figure 2.2: Mechanoreceptors in the hairless human skin.
(Adapted from an original image by Dr. Anthony Uzwiak, Rutgers University found here: http://www.rci.rutgers.edu/~uzwiak/AnatPhys/ChemicalSomaticSenses.htm)

Meissner's corpuscles are located just beneath the epidermis and are responsible for sensing light touch. They are very small, measuring approximately 30 to 140μm in length and approximately 50μm in diameter. They have the lowest sensitivity threshold and can sense dynamic skin deformations (vibrations) in the range 5 to 50Hz [JF09]. They are insensitive to static force, do not detect pain, and their concentration is highest in the fingertips (up to 140 cells per cm^2). Furthermore, they are the most common receptor in glabrous (hairless) skin. It is interesting to note that the number of Meissner's corpuscles in the fingertips drops to a quarter of their initial number between the ages of 12 and 50 [TM81].

Mechanoreceptor	**Afferent type**	**Frequency range**	**Density [1/cm^2]**	**Main detection of**
Meissner's corpuscles	rapidly adapting	5 to 50Hz	up to 140	changes in texture
Pacinian corpuscles	rapidly adapting	40 to 400Hz	up to 20	high-frequency vibrations
Merkel's disks	slowly adapting	up to 5Hz	up to 70	sustained force and pressure
Ruffini's corpuscles	slowly adapting	up to 5Hz	up to 50	stretch and heat

Table 2.1: Summary of main mechanoreceptors in the human hand and their main parameters [JF09, SLPD09, KSJ10, Hal11].

Pacinian corpuscles are extremely sensitive to mechanical transients and high frequency vibrations propagating through tissues. They are sensitive from 40 to 400Hz, with optimal sensitivity centered around 250Hz, which is the frequency generated by the fingerprint structure of the fingertips when rubbed against surfaces with fine textures under 200μm [SLPD09]. Thus they are used to detect the roughness of a surface. Pacinian corpuscles are located deep in the dermis and are physically oval in shape, approximately 1mm in length and already due to their large size considerably fewer in number than Meissner's corpuscles (up to 20 cells per cm^2). Similar to Meissner's corpuscles, they are in the rapidly adapting group and are insensitive to static force.

Merkel's disks on the other hand are especially sensitive to static force and low-frequency dynamic skin deformations ($<\approx$5Hz), and therefore detect sustained touch and pressure. They are extremely sensitive to tissue displacement (displacement detection of as little as 10μm has been shown in [JV79]). Merkel's disks are located in the same region as Meissner's corpuscles, in the upper section of the dermis close to the border of the epidermis [Figure 2.2]. In the hand, their density is highest in the fingertips (with 50 cells per cm^2 beneath the ridges of the fingertips). Merkel's disks belong to the slowly adapting group, which can be further split into two types of which they belong to the first type that is characterized by irregular inter-spike intervals when a static stimulus is present. These cells fire fastest when the skin is probed by objects with small surface areas and have a slow output activity when larger objects with flat surfaces or shallow curvatures are contacted [KSJ10].

Ruffini's corpuscles, also called Ruffini's end organs, are spindle-shaped receptors that are sensitive to sustained pressure and tension. They have a low dynamic sensitivity and are very slow to adapt [Hal11]. Due to being sensitive to tension changes, Ruffini's corpuscles register the angle changes of the joints. Interestingly they are also sensitive to heat, but not cold (cold temperatures below the ambient surrounding body temperature are detected in the skin by the *Kraus end bulbs*, which are not classified as mechanoreceptors). The concentration of Ruffini corpuscles is almost uniform over the whole surface of the hand with roughly 50 cells per cm^2. Within the slowly adapting group, they belong to the second type characterized by having a highly regular pattern of inter-spike intervals.

Free nerve endings are unencapsulated afferent nerve endings that have no complex sensory structure, unlike the mechanoreceptors listed above. Free nerve endings are mainly used to detect pain. In addition they can detect temperature and mechanical stimuli, such as touch, pressure or stretching. The free nerve endings, along with the Meissner's corpuscles and Merkel's disks, originate in the dermis close to the border of the epidermis. They infiltrate the middle layers of the epidermis and also surround hair follicles. Free nerve endings exist as both slowly and rapidly adapting afferent types.

Hair follicle receptors are located at the base of hair strands and sense the position changes of hairs. They are rapidly adapting mechanoreceptors, and therefore do not detect static forces. The most sensitive mechanoreceptors in humans are hair follicles found in the cochlea in inner ear, which transduce air pressure waves into nerve signals. It is also here where the highest frequency agitations of up to 20kHz can be detected.

2.1.2 Performance of the mechanoreceptors in the hand

The human hand, especially in the fingertip area, is remarkably sensitive being able as it is to detect high spatial resolutions and a wide range of temporal signals [LP93]. In an early experiment, Weinstein investigated skin pressure sensitivity and measured the detection threshold of the hand to be at best approximately 0.16mN [Wei68]. In a similar

experiment, Johannson and Vallbo determined the minimal absolute static displacement threshold of the finger touch sensors to be about 10μm (for a hemispherically tipped probe of 0.45mm diameter) [JV79].

The spatial resolution at the fingertips was experimentally found to be in the range of 0.9 to 1.7mm according to a number of studies [JP81, VJ84, SZ96, VHK$^+$00, TMD$^+$05]. Spatial resolution, here, is defined as the minimal discriminable distance possible between two objects while still being individually detected. Peters *et al.* [PHG09] showed that fingertip spatial resolution increases as a function of decreasing fingertip size, and therefore as women on average have smaller fingers than men, they have on average a higher tactile resolution.

Another property of skin, especially interesting for detecting slip, is the temporal resolution describing performance in time. Gescheider and Verrillo found that participants could detect two separate stimuli with 1ms duration if the pulses were at least 5.5ms apart [GV79]. In another experiment, Bolanowski *et al.* did a series of vibratory stimulations and detected responses from different mechanoreceptors in a range of 0.4 to 500Hz [BJGVC88].

When developing artificial tactile sensors, it could be beneficial to take the properties and performance of biological mechanoreceptors into account. For example, prototyping the distribution of humanoid robot skin tactile sensors according to biological pattern gives at the very least a good starting point for further investigations. When evaluating the developed tactile sensors that are presented in the next chapters, a comparison with the performance of human mechanoreceptors allows for an estimation of their usability. Although, current state-of-the art tactile sensors are still far away from exceeding or even matching the full potential of the human sense of touch, first significant achievements have already been made when single disciplines are considered in isolation (e.g., detecting structures, maximum force measurement, spatial resolution).

2.2 Sensors for observing human tactile interactions

In this section I will first look into sensors that capture tactile interaction patterns from the whole body, before turning my attention to sensors that have been developed for the hands.

2.2.1 Full-body tactile sensors

Many commercial solutions are available to capture human body posture, such as marker-based Vicon Motion Capture systems [Vic] and wearable Xsens Moven/MVN inertial measurement suits [Xse]. Widely used by the motion picture industry and research institutes, these systems output robust measurements, but are very expensive. With less robustness, human posture can be also tracked using 3D-depth cameras, paired with body posture mapping or skeleton fitting algorithms. Initially developed as an intuitive gaming input device, the Microsoft Kinect [Kin] provides affordable body tracking capabilities. The sensor is based on PrimeSense [Pri] hardware and software development. Similar depth-sensing technology was recently made available in other sensor variations, such as SoftKinetic DS325 [Sof], explicitly designed for tracking hands. The Leap Motion Controller [Lea] allows finger movements in mid-air to be optically tracked using stereo-vision. Another more common way to perform hand tracking is to use postural datagloves, such as the very popular CyberGlove [Cyb] which has been used extensively in our institute's research labs [Ste10] (see also a survey of datagloves by Dipietro *et al.* [DSD08]). A further solution

Figure 2.3: TapTap by Bonanni *et al.* [BVLZ06], a haptic wearable scarf for recording and playing back haptic sensations. (Images included with permission from Dr. Leonardo Bonanni)

for human hand and body posture tracking is to use wearable ultrasound beacons made by soft2tec GmbH in their Nexonar product family [Nex].

When the human body is in contact with objects, tiny changes in body posture can evaluate to significant changes in force and pressure. Using posture capture sensors alone can therefore not reveal detailed information about the involved haptics. Numerous attempts have been made to capture the haptics of the human body, typically concentrating on specific body areas only. Chi *et al.* presented wireless force sensing protectors that measured impacts during martial arts sports [CSC04]. The piezoresistive sensor inside the protector is simple in design, but at the same time robust enough to withstand the enormous forces and impacts created in such sports. Takahashi *et al.* presented an intriguing, but arguably controversial, project called *Sense-Roid* [TOO+11] – a wearable jacket that allowed self-caressing to be experienced using tactile sensing and haptic sensation generators. Integrated pressure sensors and micro switches capture the generated hugs and caresses, and McKibben pneumatic actuators are used to replay the sensations. Similarly, an air-inflatable jacket, although targeted for remote hugging, was presented by Mueller *et al.* [MVG+05]. Their system was output-only and thus not equipped with tactile sensing at all. Gemperle *et al.*, presented *The Hug* [GDFY03], a haptic telecommunication pillow with simple switches as input and vibration motors and heat generators as output. A clever, but unusual usage for force-sensitive-resistors was presented by Samani *et al.* with the *Kissenger* (Kiss Messanger) [SPR+12] robot system. Two wirelessly paired orb shaped bots with force-sensitive and motion controlled lips were designed to facilitate remote kissing. Bonanni *et al.*, presented *TapTap* [BVLZ06], a haptic input/output scarf for haptic telecommunication or emotional therapy [Figure 2.3]. The shape and the form of the scarf allows the haptic input/output device to be worn in numerous ways and thus around

a wider selection of body parts. The work was strongly biased towards haptic sensation generation rather than haptic sensing. As also described by the authors in their paper, the weakest point and the one requiring most attention in future versions was the touch sensing, which was available only as binary touch signal. As one can easily notice, the common criteria for many devices is the low fidelity of the tactile sensing, often available only as contact/no contact binary input channel. Unsurpassed sensitivity of less than 5Pa (not kPa!) was recently achieved by groundbreaking strain-gauge based tactile sensor using interlocking platinum-coated nanofibers [PLK+12]. Positioned over the wrist, the sensor performance has impressively been shown to be able to measure the heartbeat. Practical applications using a high number of tactile cells are difficult due to the required complex data acquisition electronics needed for each tactile cell.

Fujimori *et al.* presented an interesting solution to capture haptic data from the full body by developing a wearable motion capture suit that combines optical tactile sensing and inertial motion sensing [FOHK09]. Unfortunately the authors do not reveal their tactile sensor performance characteristics, which casts a shadow over the practical usability of the work. In a recent article Donati *et al.* [DVDR+13] presented a similar opto-electronic pressure sensor technology that is designed to capture upper- and lower-limb tactile interactions. The sensing principle is to use silicone to close the gap between an LED and a photodiode according to the applied load, effectively converting force to a light intensity received by the photodiode. The authors demonstrated sensor arrays of up to 8×4 elements and a spatial resolution down to 6mm. Although sensors with an 8.3kPa measurement range have been presented, information regarding the crucial starting sensitivity values of otherwise very interesting sensor design are unfortunately not provided.

Human presence detection and limited tactile information from floor mats was explored before in [RLFP04,SBQK05,AGH10]. Rigid construction or limited flexibility of the sensors restricted the usage of these systems to hard surfaces only. Interactive console games have also experimented with capturing haptic information from feet, with examples from Nintendo with *Wii Fit* [Nin] and Konami with the binary only tactile output *DanceDanceRevolution* [Kon] mats. Another approach towards capturing foot haptics was achieved with the *Smart Sock* by Alpha-Fit [Sma], a wearable sock with embedded tactile sensors that was designed with orthopedic applications in mind [Figure 2.4].

Tekscan's Body-Pressure-Measurement-System (BPMS) [Teka] is a commercially available sensor designed for capturing full-body haptics, such as the pressure distribution over seats, mattresses, cushions, and backrests. For a large area tactile sensor, it provides a very high spatial resolution of just 10mm and connects to the data processing system via a USB-cable. *Alphamat* [Alp] from Alpha-Fit GmbH is another commercial sensor with the same goal. In comparison to these commercial solutions, the tactile sensor for observing full-body haptic interactions presented in Section 3.1 provides an affordable and wireless large area tactile sensing solution.

The following two creative research projects benefited from out of the box thinking on the topic of augmenting arbitrary surfaces with the sense of touch. First, Wimmer and Baudisch [WB11] demonstrated how with conductive tape almost any surface can be made (single-) touch sensitive using time domain reflectometry. Second, Sato *et al.* [SPH12] presented *Swept Frequency Capacitive Sensing* that can augment arbitrary objects with the sense of touch, such as tables or door knobs. Although no force or pressure information can be measured with the proposed system, limited classification of persons or postures is possible due to the sensors ability to detect different capacitance at different probed frequencies throughout the spectrum.

Figure 2.4: Pressure sensitive sock *Smart Sock* [Sma] by Alpha-Fit GmbH. (Photograph taken with the permission of booth personnel during a visit to the Medica Fair 2013)

2.2.2 Hand tactile sensors

Most of our daily active haptic exploration is done using our hands and therefore being able to observe the haptics of the hands should go a long way to revealing the secrets of grasping and manipulation. In an early experiment, Westling and Johansson [WJ84] demonstrated the importance of tactile feedback for manual interactions: without the sense of touch, subjects had severe difficulties to maintain a stable grasp. Tactile sensors measuring interaction forces at the human skin will allow for studies of human motor-control processes at a new level of detail. Nowadays existing knowledge in this field stems largely from positional information, such as posture datagloves or vision-based tracking systems as used in our Manual Intelligence Lab [MDE+10]. In addition to posture and position tracking studying tactile feedback in human interaction experiments will provide not only a better understanding of human grasping and manipulation processes, but will also give valuable insights into the design of robotic manipulators and manipulation algorithms, which cannot be obtained from existing sensor technologies alone. Thus sensors allowing human haptics to be observed are not only important if we are to gain a picture of the neurological processes behind manual interactions, but can also lead to significantly more robust robots with more universally usable end-effectors and grasping strategies. Optimally, such measurement devices should be wireless, without the presence of intrusive cables in order to minimize possible behavioral errors and disturbances to the natural manipulation action.

As humans have smoothly curved body parts, the practical usage of traditional rigid flat tactile sensor arrays is limited. There exist many attempts to develop flexible tactile sensors. A common technology employs flexible printed circuit boards (PCBs) [KWW03, LKLP04, KLK+09], which can be bent in one dimension at a time. Cutting the flex-PCB film carrier, tactile sensors capable of covering two dimensional curvatures have been demonstrated as well [OKN06, CMMS08, FOHK09]. In our research group, our very first tactile dataglove prototype used commercially available FSRs at fingertips [GBH+11]. Due to thick semi-rigid sensors, the glove did not allow fine haptic sensations to be transferred, had suboptimal wearing comfort and provided sensing only in fingertips. Stretchable ma-

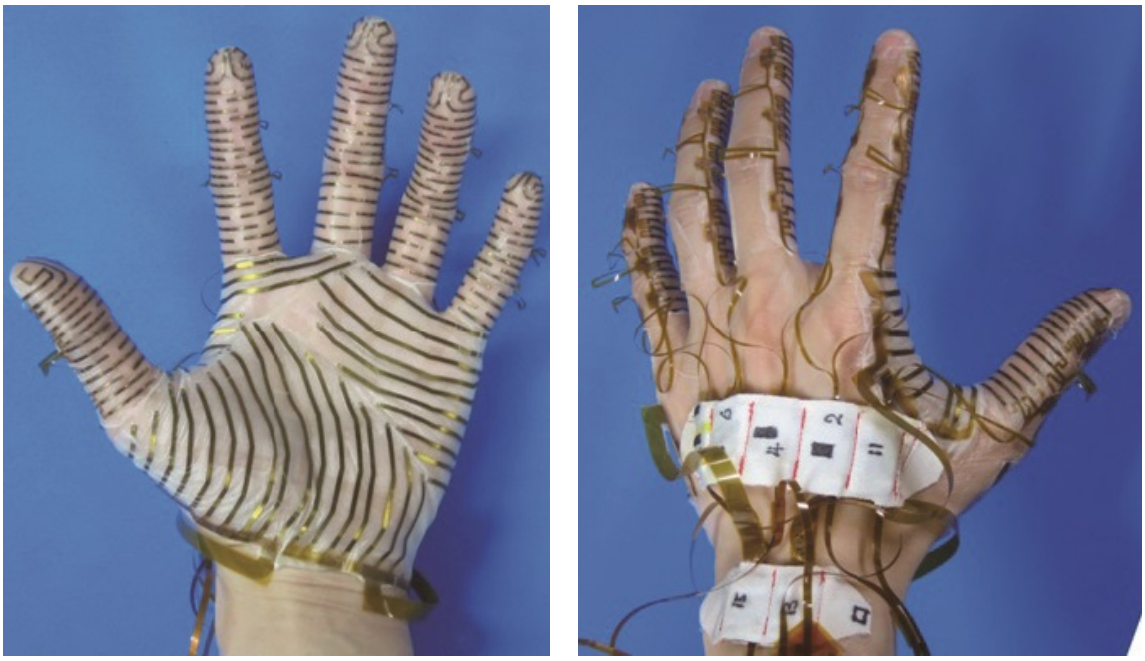

Figure 2.5: High-density conformable tactile glove by Sagisaka *et al.* [SOK+11]. Long preparatory sessions were required to construct the glove around every participant's hand. The sensor foils were robust enough to be removed after an experiment and reused in another glove. (Images included with permission from Dr. Takashi Sagisaka)

terials can much better adapt to arbitrary, even dynamically changing surfaces. A sensor using gold-plated copper wire interwoven into conductive rubber was presented by Shimojo *et al.* [SNI+04]. Although simple in construction, it lacked robustness due to exposed fragile wiring on the outside surface of the sensor. A mechanically simpler sensor based on a sheet of pressure sensitive conductive rubber that was used as the sensor material was introduced by Alirezaei *et al.* [ANK07]. It used a technology called electrical impedance tomography to gather the tactile data from connectors only attached to the boundary of a uniform sheet. Although simple in mechanical design, the electronics required to sample the values was relatively complicated limiting the compactness of the design and the output signal could exhibit negative effects such as ghosting and mirroring. An interesting approach to produce a complete wearable tactile suit employed a conductive fabric, but suffered from almost binary output [IHN+96]. Sato *et al.* presented Sensor Glove MKIII [SSS+96], with pressure sensitive conductive rubber and stitched gold plated copper strings. The dataglove was very advanced for its time. However, the readout was done by multiplexing the tactile cells rows and column wise, which lowered the maximum tactile data acquisition speed. Ying *et al.* presented an interesting approach to measure stress at the body surface using silicon nanomembranes [YBL+12]. Although the presented prototype finger cot shaped device with nanomembrane coating provided only a proof-of-concept, the dual idea of tactile sensing and the possibility of sensation generation with embedded electrotactile stimulators is very intriguing and could result in very capable wearable haptic input/output datagloves. Very high tactile sensor spatial resolution was demonstrated by Sagisaka *et al.* [SOK+11] using a glove made from a sprayed-on silicone elastomer. The glove, with 1052 tactile cells, was assembled around participant's hands and thus required a long preparatory session to attach the numerous delicate sensor foils for each measurement session [Figure 2.5]. According to

correspondence I had with Mr. Sagisaka, a new and at the time of speaking (April 2013) unpublished version was developed that is more robust and is built on an elastomeric mold copied from the wearer's hand, decreasing significantly the effort required by eliminating the tedious preparatory sessions for participants. Micro-machined strain gauges on Kapton film were developed by Engel *et al.* [ECL03] and they allow for a high spatial resolution, but are unfortunately not very robust due to exposed miniature mechanical components. Our fabric-based tactile dataglove design [Section 3.2] overcomes all the aforementioned drawbacks: it is flexible, stretchable and robust, and allows independent sampling of multiple tactile cells in a relatively high spatial resolution. Plusea [PW] and KobaKant [SPW] are two inspiring websites, collecting different Do-It-Yourself (DIY) projects with creative ideas, and some of the recent contributions use similar conductive and piezoresistive fabrics to our design towards capturing tactile information from humans.

There are only a very few commercially available tactile sensing datagloves. The most promising model, the *X-IST Data Glove HR3* from No-DNA [noD] provided 5 pressure sensors at each fingertip and was targeted towards novel music making, but unfortunately has been discontinued. *Pinch Glove* from Virtual Realities [Vir] provided binary digit contact sensing and was designed to be used in virtual reality scenarios for the manipulation of objects. However the production of Pinch Glove has also been discontinued. *The Peregrine Glove* from the company of the same name [Per] was designed towards computer gaming and provides, similar to the Pinch Glove, only binary contact information. The Peregrine Glove is equipped with a considerably higher count of active contact points (18 touch points and 3 activator pads that allow for over 30 user-programmable actions to be triggered). *Grip* from Tekscan [Tekb] is a force-sensitive-resistor foil matrix with 349 tactile cells and a high sample rate of up to 850Hz and was developed for grip force and pressure measurement [Figure 2.6]. The sensor foils are not stretchable and thus do not confirm optimally around the curvatures of human hand, and because of this its rigidness can be disturbing when capturing natural manual interactions. Wang *et al.* discussed these problems and provided some solutions when using this system [WHB07].

Capturing human hand haptics can also be achieved using instrumented objects. Krause [Kra02] presented a haptic ball with force-sensitive-resistors designed to allow interactive music creation. Kondo *et al.* [KUMO04,KUO08] presented a cylinder with a tactile sensitive surface and magnetic field motion tracking designed for hand haptics research. However, the device was connected to the data acquisition system with a disturbingly thick cable that must affect human behavior. Two tactile pens, made to measure finger grip forces, were developed by Kutz *et al.* [KWM+09] and by Matsuo *et al.* [MMH+09]. Both use force-sensitive-resistors as sensing elements, connected with inflexible cables to the external data processing system, which limits the quality of natural interaction capturing. The developmental details of an instrumented object that not only provides cable-free tactile image capture of a human hand, but can also measure the orientation and movements generated is presented in Section 3.3. Initial experiments and their results validating the usability of the device are also presented.

2.2.3 Natural intention detection sensors

Intention detection is the interpretation of biological signals in Human-Machine-Interface (HMI) with the aim of automatically, reliably and naturally understanding what a human subject intends to do. It is particularly interesting for people who can no longer use standard

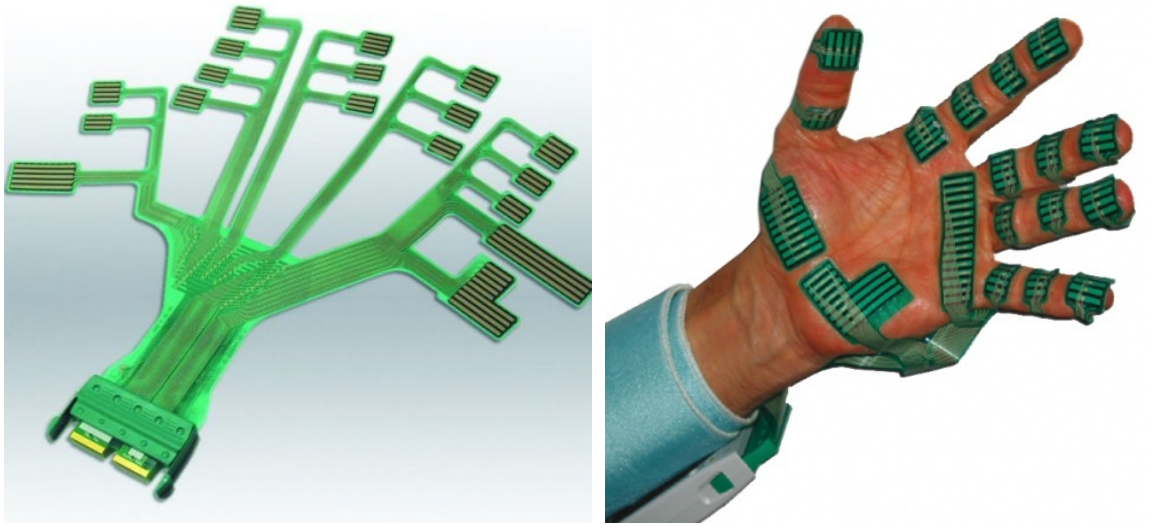

Figure 2.6: *Grip*, commercially available force and pressure measurement system from Tekscan [Tekb]. (Images included with permission from Stephen Weber of Tekscan, Inc.)

control devices such as a joystick, mouse, keyboard, voice control, etc. In these cases, more subtle messages coming from the person's body must be interpreted. Although intention detection is not restricted to disabled people, such methods can be crucial in improving a patient's life, e.g., aiding control of a prosthesis or a robotic device, e.g., an arm or wheelchair.

Traditionally, intention detection has been achieved using either gaze tracking, surface electromyography (sEMG) or electroencephalography (EEG). sEMG in particular is a non-invasive technique that measures muscle activation potentials and has been actively researched since the 1960s [Bot65] in the rehabilitation robotics and machine learning communities, as it can be used to predict the hand posture and overall grip force. The main advantages of this technique are that it requires no surgical intervention and is relatively cheap, although interpreting the signal is difficult [De 97, ZMCD02].

The standard application involves, after an amputation has been performed and the wounds have healed, designing and building a custom socket and placing it at the location of the amputee's high-activity forearm muscle remnants, where a limited number (typically just two) sEMG electrodes are placed over the signal sources. The patient is then trained to separately contract two or more muscles in order to open and close a prosthesis that can mimic robotic gripper functionality (such as shown in Figure 2.7). A detailed survey of sEMG and its applications can be found in [MAB$^+$10b, MAB$^+$10a].

Over the past 20 years however, dexterous mechanical hands have appeared which could enable an amputee to control the movement of single fingers, if only a sensible control system were available. To this end the scientific community has augmented the number of electrodes (up to 32 [TRF$^+$09]) and adopted sophisticated statistical and machine-learning methods to decode the signal and associate it to a desired hand posture. These methods range from Linear Discriminant Analysis [LGLM11] and Neural Networks [BvdS06] to Support Vector Machines [CvdS09]. The approach has also been successfully applied to amputees [SRL05, TRF$^+$09, CGDS09, CAC$^+$11].

So far, however, only a few attempts have been made to predict the intended force by a

Figure 2.7: Single degree-of-freedom hand prosthesis. (Photograph taken with permission of booth personnel during a visit to the Hannover Fair 2006.)

subject using voluntary muscle contractions. In contrast to the traditional approach, mainly based upon static hand posture classification, the force control schema can considerably widen the usable actions of an artificial limb, as classification restricts the user's control of a prosthesis to a finite (usually small) number of predefined grip patterns. The prediction of finger force from voluntary muscle contractions on the other hand would allow hand control over an infinite manifold of force configurations. Predicting forces has at least the following two benefits over predicting postures:

1. Position control is effective only in the absence of obstacles, which is seldom the case when a hand is engaged in grasping and/or manipulation

2. sEMG is known to be related to *force* rather than to position, so regression on positions from sEMG really is regression on isotonic muscular configurations (theory supported by recent results on sEMG-based direct position control of robotic arms [AK10, VCvdS11])

Moreover, a control that targets grip force is more natural and would be driven by the patient's will, which would greatly improve the usability and acceptance of prostheses [CAC+11, PBW+11].

In a recent work, Nielsen *et al.* [NHJ+11] tried to estimate the force of a single voluntary muscle contraction. The authors implemented artificial neural network to predict the proportional force in the wrist joint. One force-torque sensor, strapped around forearm, was used to measure the wrist forces during the experiments. Concentrating on the wrist alone though, will not produce very general hand prosthesis, and thus controlling finger

forces should also be considered. Towards this end, a reference sensor that can capture the finger forces of able-bodied participants would help to create appropriate mappings between muscle activations and exerted finger forces. Measuring finger forces has been tried before, using wearable fingertip sensors [JRW91, MA01], gloves [SSS+96] or instrumented graspable objects such as [KKYS10], but most of these devices are unidirectional and thus usable only to measure finger flexion forces, omitting the forces that occur during finger extensions. Subsection 3.4.1 presents the developmental details of a novel bidirectional reference finger force sensor with unrivaled accuracy.

A radically different idea to infer intention for hand prosthesis actuation was presented in an early paper by Lucaccini *et al.* in 1966 [LKL66]. The authors proposed observing the pressures exerted by muscle bulges in the stump. Their simple, but at the time groundbreaking system, used pneumatic switches to control the opening and closing of the *French Electric Hand*. More recently, but in the same vain, Craelius *et al.* have explored the use of a hard socket fitted with 8 to 32 myo-pneumatic sensors [CFC01] and 14 force-sensing resistors (FSRs) [WKC08]. In both experiments, single-finger motion discrimination was demonstrated. The same research group has recently applied the FSR-based approach (with 8 sensors) to gait control [YWB+11] and brain injury rehabilitation [YC12]. Gait control was also realized in this way in an earlier paper by Lukowicz *et al.* [LHSS06].

The idea of detecting muscular activity via the changes induced by the activity itself on the body surface has been called in turn SMP (surface muscle pressure), FMG (force myography) and RKI (residual kinetic imaging). Of great relevance to the work presented in Subsection 3.4.2 is the comparison between SMP and the mainstream approach to non-invasive prosthesis control, namely, surface electromyography (sEMG), carried out in [YWB+11]. They show that, at least for the experiment considered, SMP yields a more stable and repeatable signal than sEMG with less variance and more robustness over the medium-term and across participants.

However, all these approaches lack the high spatial resolution needed to obtain a faithful representation of the activity of different muscles, which the work presented in Subsection 3.4.2 shows to be important to gain a much richer and more robust insight into subjects' intended actions. As a tactile sensor plays a central role in the presented method, *tactilemyography* seems to be an appropriate name for the novel technology.

A slightly different approach, called mechanomyography (MMG) relies on the vibrations induced by muscle activation in the muscles themselves. Research in this direction (e.g., [Ori05, Nd04, YKA09, Bec10, DBS12]) seems also very promising, and indeed it should be possible to use the sensors presented in Subsection 3.4.2 to perform this technique (this will be verified in future work).

2.3 Sensors that augment technical systems with the sense of touch

Touch is one of the main senses that humans use to perform coordinated interactions. The lack of tactile feedback in today's industrial robots constrains their use to highly structured environments, eliminates the possibility of having contact with any uncertainties, including humans. It is not hard to see that technical systems could benefit from an artificial sense of touch. Not only will it be possible to drastically improve the safety of such systems by endowing them with contact detection abilities, object manipulation capabilities could also significantly be advanced. This idea is backed up by the experiment discussed in Section 1.1

by Westling and Johannson [WJ84] that looked at the human sense of touch. When the subject's tactile receptors were suppressed, they showed immense difficulties in being able to perform grasps. This leads to the obvious conclusion that a robot without tactile sensors should also have great difficulty in performing grasps, especially considering the added disadvantage that a robot lacks real world experience by humans.

In this section I will first look at tactile sensors that are designed to gather haptic information from large surfaces of technical systems, e.g., from the body of a robot. Next, I will look into sensors designed especially for robotic hands, where features such as high spatial resolution and miniaturization play a crucial role.

2.3.1 Tactile sensors to cover large areas of technical systems

Artificial tactile sensitive skin development is an active research field, with numerous previous interesting designs. One of the most widely used sensors in the (humanoid) robotics community to cover large areas of robots was presented by Cannata *et al.* [CMMS08]. By cleverly cutting large flex-print-PCBs into separated triangle shaped units, each equipped with 12 capacitive tactile cells, surfaces with moderate curvatures can be covered. The authors demonstrated this by skinning large parts of the child-sized humanoid robot iCub [SMM+11]. The same technology, although in a slightly miniaturized form was used by the authors to equip the iCub robot fingertips with a sense of touch. Their sensor can accomplish up to 5kPa sensitivity, but compared to resistive tactile sensor technologies it is more sensitive to noise and further miniaturization is strongly limited due to crosstalk between the tactile cells.

Mittendorfer & Cheng presented hexagonal sensor modules [MC11] that could also cover large robot surfaces. Instead of direct force or pressure measurement sensing, they used optical proximity sensors to detect close-by surfaces. The disadvantage of this technology is that it cannot directly sense force or pressure. As one of the very few artificial skin proposals for technical systems, their hexagonal modules are also equipped with temperature sensing, allowing easier differentiation of human contact from non-human contact.

Technical systems with considerable mass and power, which are typically the features required to be able to perform tasks such as everyday object lifting and manipulation, might pose a health risk if they unintentionally come into contact with other objects or humans. If such systems are to operate in unstructured environments with unpredictable humans, unwanted contacts are unavoidable. Therefore such mobile technical systems must be able to sense collisions and be equipped with logic for taking countermeasures to avoid harm or damage. As a moving mass cannot be instantly stopped, it is important that the outer layer of technical systems is soft and compliant. Elkmann, Fritzsche and Schulenburg *et al.* [FE09, EFS11] presented such a soft tactile sensor for safe human-robot interaction. The authors developed a clever sleeve for the Kuka LBR robot arm using flexible sensor mats. Unfortunately their design suffered from significant false positives when flexed and stretched around a cylindrical robotic arm [Figure 2.8].

In a recent work, Strohmayr [Str12] presented a flexible tactile sensor skin with an admirable 1.25mm spatial resolution. A grid of intersecting triangle shaped extruded miniature conductive polymer wires formed the sensing element. By applying a load to an intersecting location of two triangle shaped wires, the sharp edges of these wires are pushed into each other, effectively lowering the electrical resistance between the wires. The sensor is compliant and can achieve up to 8kPa sensitivity. Long time performance has not yet been demonstrated, which is especially important as natural abrasion can have a strong

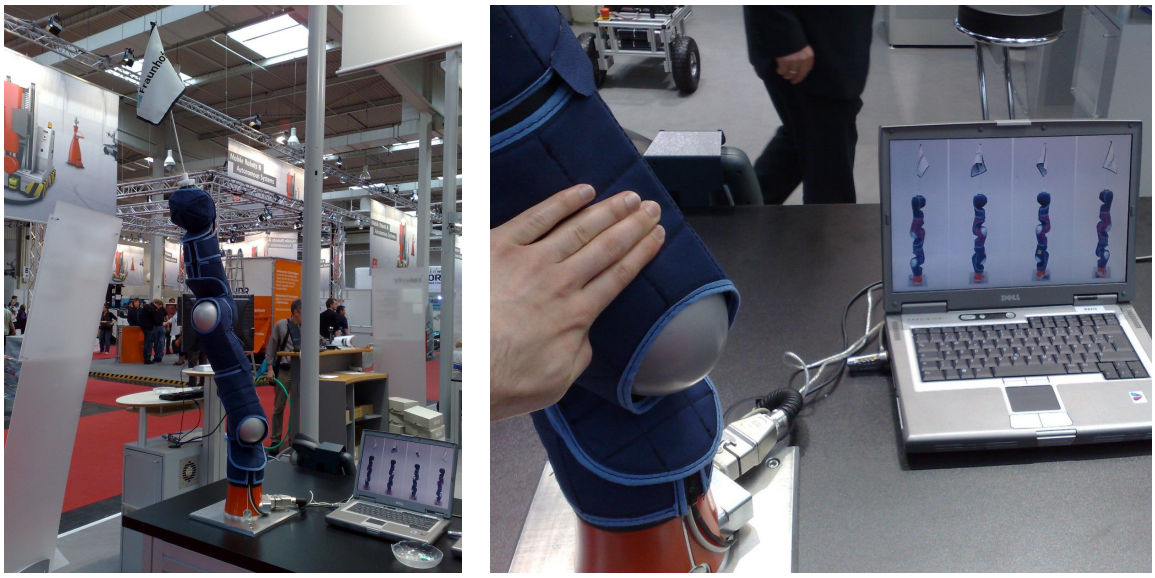

(a) Kuka LBR robot arm sleeve with flexible sensor mats.

(b) Sensor shown to be unfortunately exhibiting false positives on areas with no contact.

Figure 2.8: Live demonstration of tactile sensors [FE09, EFS11] at Fraunhofer Institutes booth in Hannover Fair 2009. (Photographs taken during experiment with permission of booth personnel.)

negative effect on the performance of this sensor design, which depends on the sharp edges of the triangle shaped wires.

Fritzsche *et al.* [FSE12] recently demonstrated a 3D shaped tactile sensor using thermoforming. A flat piezoresistive sensor foil was heated and formed into the desired shape by pressing it into a mold. The technical specifications were optimized towards collision detection (10N detection threshold and large tactile cell areas) and as such, the sensor is not usable for fine force or pressure measurements.

Sato *et al.* [SPH12] presented Touché, a clever sensor design that uses swept frequency capacitive sensing to augment arbitrary conductive objects with sensing capabilities to distinguish between different touches. Although not directly usable for force or pressure measurement, the sensor enables classification of persons and grasp types. The sensor's working principle is based on the fact that the measured capacitance of the object being touched changes at different sampling frequencies depending on the person touching the object and also on the used grasp type. A frequency sweep over the whole spectrum of the sensor reveals patterns unique to the specific contact situations, allowing recognition of previously learned contact situations.

Large area touch mats have received broad acceptance in a variety of consumer electronic devices. Sensor grid arrays are used to capture the control signals from users using custom digitizer pens or fingers alone. Current state-of-the-art trackpads and touchscreens that use this technology can detect multiple contact points simultaneously [VIR+09, App]. Figure 2.9 displays the capacitive sensor array of the Apple Inc. Magic Mouse that can detect finger gestures. For capacitive sensors to detect a change, the dielectric near the electrode has to change from the ambient electric field. Thus, such sensors are not able to detect arbitrary materials (for example wearing a glove typically renders fingers undetectable). The capacitive sensor grids, mostly used in such products, are used as presence detectors,

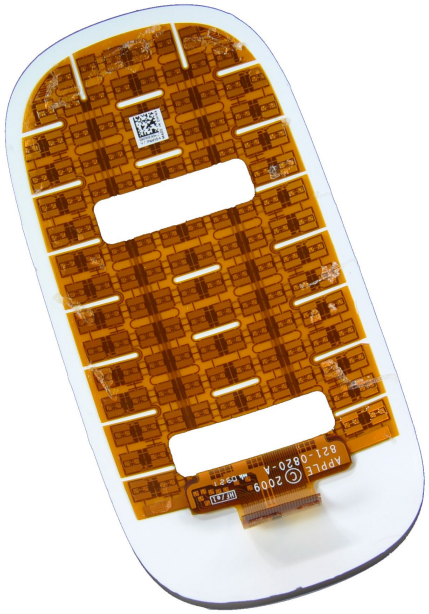

Figure 2.9: The foil based electrode sheet of capacitive touch sensors of the gesture recognition capable Magic Mouse by Apple Inc. Notice the cutouts necessary to fold the flex-print PCB foil with electrodes into the concave 3D-surface. (Image included with permission from iFixit, source: http://d3nevzfk7ii3be.cloudfront.net/igi/UyyKmUFBEB5WBCOW)

but they cannot directly measure the interaction forces or pressures.

2.3.2 Tactile sensors for robotic hands

The dexterity of the human hand is especially fascinating for the robotics community and as yet is still not close to being replicated in current robotic hands that are clumsy when operating in natural environments with objects originally developed for humans. Even if a robot is able to move in its workplace, with the help of wheels or legs, and the objects to be handled can be localized and recognized using computer vision, the daunting task of grasping and manipulating them is still mostly unsolved for arbitrary objects by current state of the art robot hands, which is also due to missing or inadequate tactile feedback.

One can argue that the current infant state of industrial and research robots performing generic grasping and manipulation tasks is due to the lack of, or extremely inferior, haptic sensing capabilities when compared to biological systems. Active ongoing research on artificial skin and on hand and fingertip tactile sensors has yet to match the high spatial resolution and sensitivity of human fingertips. The limited amount of available space in anthropomorphic robot joints, especially for the case of human-sized hands, is one of the greatest limitations.

Augmenting robotic hands with a sense of touch is also a very active research field. In an early paper, Butterfaß *et al.* [BGLH01] introduced the four-fingered DLR Hand II, which is approximately twice the size of an adult human hand, and has single 6D force/torque sensors located in each fingertip [Figure 2.10]. A single sensor has the drawback that all of the forces in its area of coverage are summed leading to the loss of potentially important

Figure 2.10: DLR-Hand II with integrated 6D force/torque sensors located in each fingertip [BGLH01]. (Photograph taken with permission from booth personnel during visit of Hannover Fair 2004.)

spatial information. Robotic hands that use tactile sensor matrices are able to capture finer grained contact location and force amplitude data. Oddo *et al.* [OBMC09] demonstrated a 2×2 MEMS-based strain-gauge sensor that was human fingertip sized. Due to the required relatively complicated signal conditioning electronics and the limited available space inside the finger joints, the addition of further tactile pixels (taxels) into the fingertip was not achievable. An interesting approach that succeeded in attaining a high sensor density by using inductive coils embedded in the finger flesh was recently demonstrated by Wattanasarn *et al.* [WNMS12]. However, their approach also suffers from the necessity to have complicated electronics for each single taxel. In a different approach, Ohka *et al.* [OTK$^+$09] demonstrated an optical tactile fingertip sensor that was more than twice the size of a human fingertip. Using a high-definition camera, this allowed very high spatial resolutions to be achieved, although due to sensor design, the sensor spatial resolution decreases with increasing applied force. Computer vision algorithms were applied to the images captured by a fiberscope in order to convert the visually detected shape changes into force vectors. The lack of a compact embedded design and the need to sacrifice the majority of the available space in the fingertips in order to capture an unobstructed field-of-view are two major drawbacks of their design.

Resistive and capacitive tactile sensors typically require much simpler signal conditioning and can thus be produced with relative ease in higher taxel counts. Often in these sensors, printed circuit boards (PCBs) are used as sensor electrodes [KWW03, GGW09]. Section 4.1 highlights a flat modular sensor based on PCBs that we developed. It can cover large surface areas with high spatial resolution tactile sensitivity. The highlight of

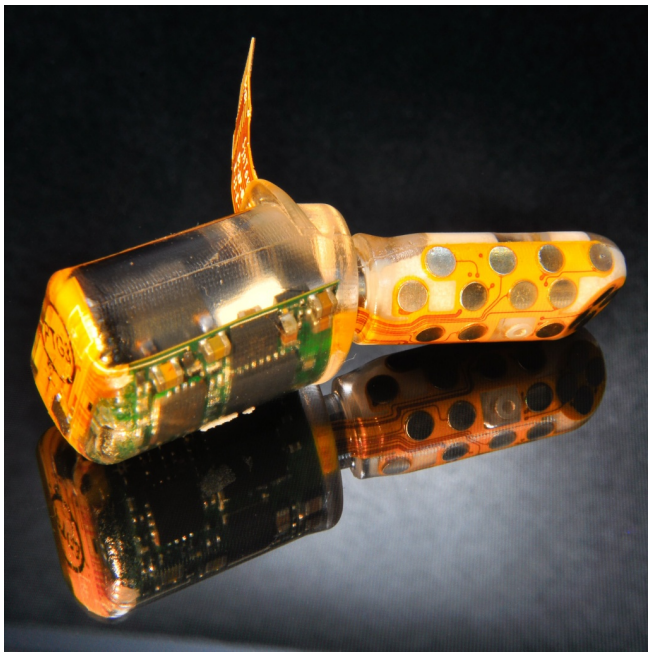

(a) Sensor without its outer rubber shell.

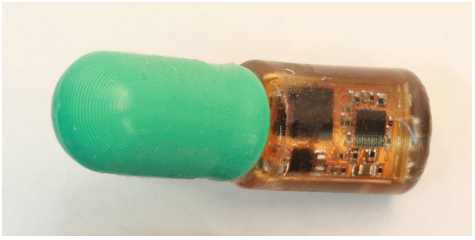

(b) Sensor with shell containing the conductive fluid (pictured in green).

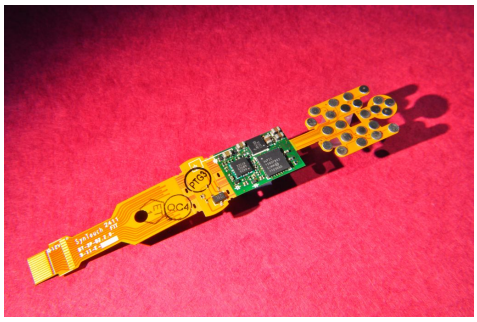

(c) Sensor electrodes and electronics.

Figure 2.11: SynTouch BioTac fingertip tactile sensor [Syn] by Wettels and Loeb [WL11]. The outer rubber shell keeps the conductive fluid, used to measure the applied pressure, inside the sensing chamber. The sensors and data acquisition electronics are molded in resin. It can measure temperature (1 sensor), has 19 taxels and one separate fluid pressure sensor to measure pressure transients over the whole fingertip surface. (Images included with permission from Matt Borzage of SynTouch, LLC)

our design is a very high sampling speed, allowing slippage be detected by capturing the vibrations occurring during such events. Using flexible substrates, such as Kapton instead of fiberglass, which is commonly used in rigid PCBs, tactile sensors having flexibility in a single dimension can be built [WW04, NKK+06]. With a clever design that cuts the flex print PCB, tactile sensors capable of covering two-dimensional surfaces with limited radii have also been demonstrated [OKN06, SMM+11].

The Shadow Robot Company [Sha] tried Quantum-Tunneling-Composite (QTC) sensors to augment finger phalanges with tactile sensing capabilities. We performed usability experiments in our lab with this technology and unfortunately experienced a significant sensitivity drop in a timeframe of a maximum of 2 weeks from sometimes very high initial sensitivity of 0.1N/taxel to no output at all. This unfortunately strongly undermined the usability of this technology.

Another option to augment curved surfaces with tactile sensing is to directly use flexible and stretchable materials capable of taking near arbitrary shapes. Section 4.2 presents just such a sensor design, based on solely layers of conductive and non-conductive fabrics covered with silicone for increased human flesh mimicry.

In a recent paper, Wettels and Loeb demonstrated a multimodal fingertip sensor capable of sensing thermal flux, micro-vibration and force [WL11] [Figure 2.11]. The performance of the sensor is impressive, but due to the electronic circuitry extending (in a rigid manner) deep into the middle phalange of the fingers, joint movement between distal and middle phalanges is eliminated.

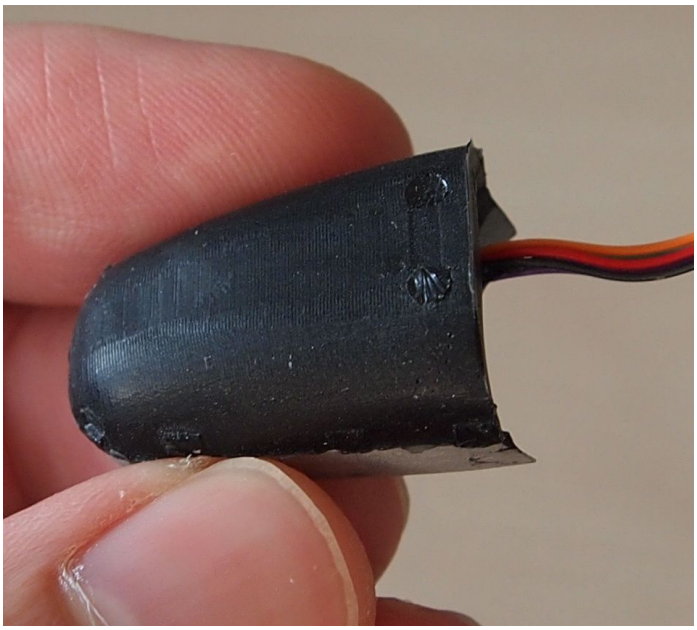

Figure 2.12: Fingertip tactile sensor for robotic hands from Shadow Robot Company [Sha] based on pressure sensing inside a single airtight chamber.

Pressure-Sensor-Tactile (PST) is another interesting fingertip tactile sensing development from the Shadow Robot Company [Sha] [Figure 2.12]. The simplistic design is based on a hollow fingertip with an embedded miniature barometric pressure sensor and is covered in an airtight rubber casket. Applying force on the sensor increases directly the air pressure inside the casket, which is then measured. The PST-sensor is very sensitive, with a detection threshold of just 1kPa, but due to only a single chamber and sensing element for the whole fingertip, it is unable to provide detailed contact pattern information.

To overcome all these drawbacks, Section 4.3 introduces our developed compact tactile sensor with embedded electronics using a laser structuring process. This process can be applied to almost arbitrarily shaped surfaces, allowing tactile sensing to be added to object surfaces previously not possible.

3 Making human tactile interactions observable

Observing human haptic interactions allows not only the statistical gathering of contact and pressure information, but can provide deeper insights into the cognitive processes behind such actions, and indeed can facilitate the development of improved technical interactive systems[1]. This chapter introduces a number of novel sensing systems that enable natural haptic information gathering.

Section 3.1 introduces a sensor with a simple, but clever design, that can capture full-body haptic interactions. The main design criteria of the sensor was that it should be a robust, flexible and low-cost big area sensor. It achieves a spatial resolution exceeding 20 tactile pixels (taxels) per m^2.

As a significant part of our daily interactions are performed using our hands, capturing haptic data from the fingers and palm requires higher spatial resolutions with more fine grained sensors. The next two sections present tactile sensors that facilitate this criterion. In Section 3.2, a wearable tactile dataglove with 54 taxels and embedded data acquisition hardware allows the observation of haptic data from hands while they manipulate arbitrary objects. Section 3.3 approaches the question of capturing haptic manual interaction from an orthogonal direction and presents an instrumented object that not only captures high-resolution tactile patterns, but also the relative linear and rotational motion parameters, rendering novel experiments possible for a wide spectrum of research.

Section 3.4 presents two sensors that are designed to aid in the development of intuitively usable hand prosthesis for amputees. The first sensor provides an unrivaled quality in finger force reference sensing that could be useful for prosthesis control algorithm development. The second sensor, in the form of a tactile bracelet, detects intended finger forces over an infinite manifold from muscle bulgings of the forearm. Although initially targeted towards hand prosthesis control and capturing intentions of upper-limb amputees, the sensor can be used by able-bodied people in different scenarios as well, such as in virtual reality or in interactive gaming.

Section 3.5 introduces Tactile Pen, a sheath for a ball point pen or a digitizer pen, to measure the grip force during handwriting. Whether in remedial education or during therapy for congenital disorders, musculoskeletal disorders or traumatic injury, such a tactile sensitive pen can in combination with handwriting analysis tools give feedback about the effectiveness of the performed therapy.

3.1 Capturing full-body haptic interactions with tacTiles

This section introduces *tacTiles*[2], a novel flexible tactile sensor mat that can equip surfaces with tactile sensitivity. It allows spatially resolved pressure profiles caused by contact with

[1] In this thesis the terms *haptic* and *tactile* are both used and unless otherwise stated mean the same thing.
[2] The name *tacTiles* comes from mixing the words *tactile* and *tiles*.

Figure 3.1: A version of *tacTiles* touch sensitive mat to cover an office chair.

a human user to be observed. It is built using commercially available and reasonably priced force-sensitive-resistors (FSRs) that are attached to a deformable textile and designed as a cover for surfaces we touch with our body, such as floors, chairs, sofas or other furniture.

This project was done in co-operation with Dr. Thomas Hermann and was published and presented at the Third International Workshop on Haptic and Audio Interaction Design (HAID 2008) [HK08]. A specially contoured version of tacTiles, called *SonicChair* which was used to cover office chairs and was paired with an audio synthesis program, has received considerable media attention after a Reuters newscast. During the summer months of 2011, SonicChair was one of eleven showcase pieces displayed at a special exhibition on Sonic Interaction Design (SID) in Oslo's Technical Museum in Norway, where visitors had a hands-on possibility to experience the developed sensor designed to observe full-body haptics [HK11].

My contribution to the project was the design, development and construction of the prototypes, including the design of the data acquisition electronics circuitry and the development of the embedded microcontroller firmware. The graphical user interface and the sonification[3] of the SonicChair were developed by Dr. Thomas Hermann and are therefore not discussed in detail in this thesis.

An initial prototype of tacTiles in the form of a cover for office chairs is presented in Figure 3.1. Versions for other everyday-objects such as sofas, mattresses, doormats, yoga mats, backpacks etc., were also considered.

Tactile sensor-equipped chairs had previously been presented, such as the *sensingChair* [TSP01] and the *SenseChair* [FDZ+05], and references can also be found to tactile input mats [see Section 2.2]. In comparison, tacTiles is not limited to chairs or floor mats; it can also be combined to form larger patches, e.g., to cover larger sofas, floors or walls. Furthermore, our solution is wireless and the software and hardware designs are freely available as open source.

[3]Sonification is the auditory display of information [Kra94].

tacTiles enables the capturing of rich haptic data from full-body interactions. Apart from just gathering the haptic interaction data from users, numerous clever applications using the technology can be considered. In its simplest form tacTiles can be used to detect the presence and location of people. Due to its proportional force output, tacTiles is well suited to monitor the ergonomics of users, e.g., the ergonomics of sitting, when produced in the shape of a chair cover. Users can be identified using total pressure measurements (corresponding to their weight) and novel security checks can be imagined (e.g., password entrance using a motion shift sequence). As a floor mat in front of a standard computer workplace, it allows feet to be used as an input device for the computer - think for instance of a painting program where you can interactively modify the brush size by foot pressure. As a door mat, it allows registration of people entering or leaving a room, e.g., as an alarm system or as a general floor mat used as a support system for room intelligence to shut off the lights and to control the temperature in unused rooms. In connection with interactive sonification, eyes-free audiomotoric games, similar to AcouMotion by Hermann *et al.* [HHR06], can be considered. Furthermore, tacTiles can be used to couple several users by registering their interactions with the mat and reflecting, for example, differential information so that a synchronous performance can be practiced. Such applications could even be interesting for training programs in dance or performance. The design and applications presented in this section therefore represent only a proof-of-principle into the field of full-body tactile mediated interactions.

The construction of tacTiles cover mat for office chairs is presented in Subsection 3.1.1 and then some example applications are given in Subsection 3.1.2.

3.1.1 Construction of tacTiles

This subsection describes the mechatronical construction of tacTiles, including the design ideas for the sensor mat and the electronic circuits needed to acquire and process measurements into a live Bluetooth-broadcasted sensor data stream. Although, the presented hardware details concentrate on tacTiles for office chairs, they apply without significant changes for other shapes and designs as well.

Sensor mat design

The tacTiles sensor cover designed for office chairs incorporates 8 FSRs from Interlink Electronics [Int] of type FSR-406, each comprising of a 40×40mm active sensing area, with a saturation point of 100N/cm^2 [Figure 3.2a].

To make the most use out of as few sensors as possible, the FSR's were not positioned in a grid or in a fixed pattern, rather the positioning was especially optimized towards usage in office chairs. The positions of the sensors were derived from tests done with numerous people of different heights and sizes to optimize the area of greatest contact with the seat and back area. From these experiments, 4 sensors were placed on the horizontal seating area in an X pattern, and 4 sensors were placed on the back of the chair with T pattern to measure how much a person leaned [Figure 3.2b].

The FSR-406 sensors were glued [Figure 3.2c] to a 5mm thick foam (the same material is also used in many camping mats), which forms a sturdy base and protects the sensors from over-elongation. The foam was cut into a form that fits a typical office chair's seating and back areas. Two flexible wires emanating from each FSR-sensor were glued with Pattex Express into the carved grooves on the backside of the mat and connected to the signal

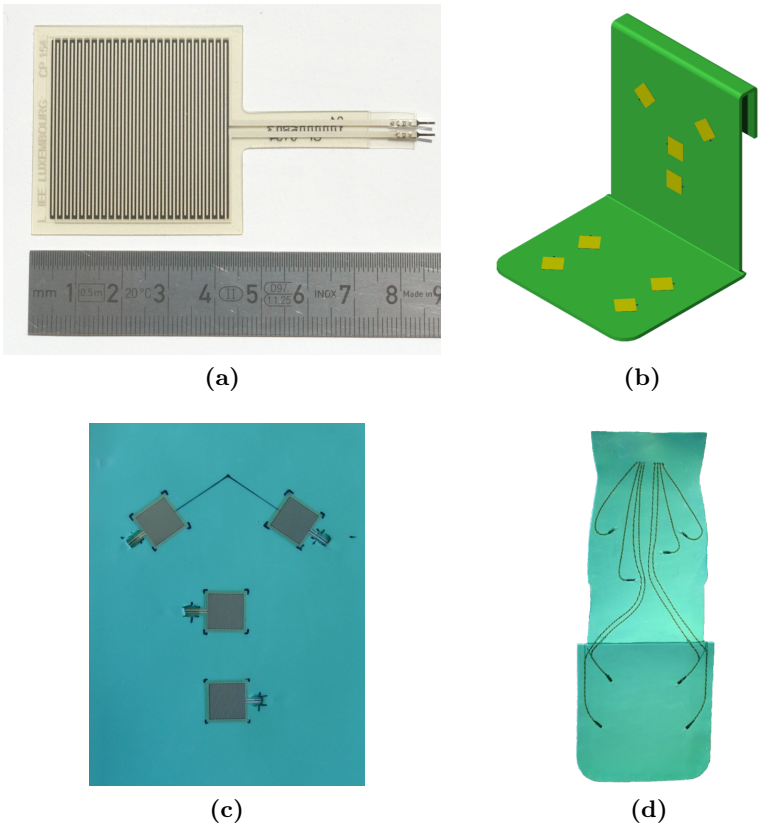

(a) **(b)** **(c)** **(d)**

Figure 3.2: Illustration of tacTiles sensors and chair cover mat assembly. **(a)** Interlink Electronics FSR-406 Force Sensitive Resistor used in tacTiles, **(b)** CAD model of the chair cover mat showing the sensor placements, **(c)** Close-up of 4 glued sensors on the back area, **(d)** Photo of the foam mat showing the routing of cables between the sensors and the electronics on the backside of the mat.

processing electronics, which are located on the backside of the seat cover [Figure 3.2d]. The grooves in the foam protect the cabling and at the same time ensure the user does not feel them. The sensors are located in the top layer of the mat and an additional thin layer of silk was glued with numerous glue spots around the sensors to avoid shearing and tearing the sensors from their positions. A rubber coated textile, sewn in the form of a bag, with a side zipper for easy access to its inside was used to wrap the foam with glued sensors and silk protection.

Data acquisition and wireless transmission electronics

The electronics unit, located in a protective box behind the backrest of the chair [Figure 3.3], consists of a Microchip PIC18F4580 microcontroller with an integrated 10-bit analog-digital-converter. The 8 FSR values are read with the help of a constant pull-up resistor-network to produce a voltage output from the sensors. The converted values are sent as an ASCII stream to a Free2Move [Fre] F2M01 Bluetooth Serial-Adapter, which is connected to the Enhanced-Universal-Synchronous-Receiver-Transmitter (EUSART) output pin (TX) of the microcontroller. Thanks to the F2M01 module, the tacTiles sensor mat has a wireless coverage of more than 10m indoors, even through non-metallic walls. Easy interfacing is guaranteed thanks to a Bluetooth Serial Port Profile (BT-SPP) that is

(a) Initial electronics unit with push-button ON/OFF switches.

(b) Extended electronics unit version targeted especially for public exhibition with hidden reed (magnetic) ON/OFF switches.

Figure 3.3: Electronics unit located on the backrest of SonicChair.

supported out-of-the-box by numerous desktop and mobile operating systems. Optionally the module allows encrypted communications, which are important for authentication applications and will be discussed in the next subsection. The user interface of the electronics is derived from the KISS (Keep-It-Simple&Stupid) ideology, and employs just ON/OFF buttons, status LEDs and a charging jack. The tacTiles sensor chair cover mat was paired with sonification abilities to become SonicChair and in time for an exhibition on Sonic Interaction Design (SID) in Oslo, Norway, the ON/OFF buttons were replaced by reed-switches [Figure 3.3b]. This allowed the system to be switched on before opening and switched off after closing on a daily basis by exhibition personnel using a small but strong neodymium magnet. This ensured that visitors could enjoy the SonicChair experience in full without having to worry that the previous user might have inadvertently powered down the system.

tacTiles mat is powered by 2-Cell Lithium-Polymer (LiPo) battery. An early prototype used a model with 700mAh capacity that could provide power for up to 8h of continuous operation. To achieve an uninterrupted extended working day operation with reserve power, the original battery was replaced with 1500mAh model, thus more than doubling the operating duration of the original battery. The microcontroller monitors closely the battery voltage, warns the user of low battery status and shuts the unit off if the voltage drops to less than 3.4V/cell, an important feature to prolong the lifespan of the LiPo-chemistry based battery.

The schematic of the tacTiles/SonicChair electronics unit is displayed in Figure 3.4 and the component listing can be found in Appendix 6.2. An educated eye will immediately notice, by glancing at the parts listing [Appendix 6.2], the simplicity and the very low total price achieved, which is due to a low parts count and the use of common components and was a criteria that was especially aimed for during development.

As can be seen in the schematic [Figure 3.4], at the heart of the electronics unit is an 8-bit flash-based reprogrammable PIC18F4580 microcontroller (IC2) from Microchip. It incorporates 11 analog-digital-converter (ADC) inputs, 9 of which are used in the circuit to sample the 8 FSRs and the battery voltage. The integrated ADCs have a 10-bit resolution, thus allowing 1024 different voltage levels to be sampled. The FSR resistance change is converted to a voltage change that is sampled by the ADCs with the help of 10kΩ resistors

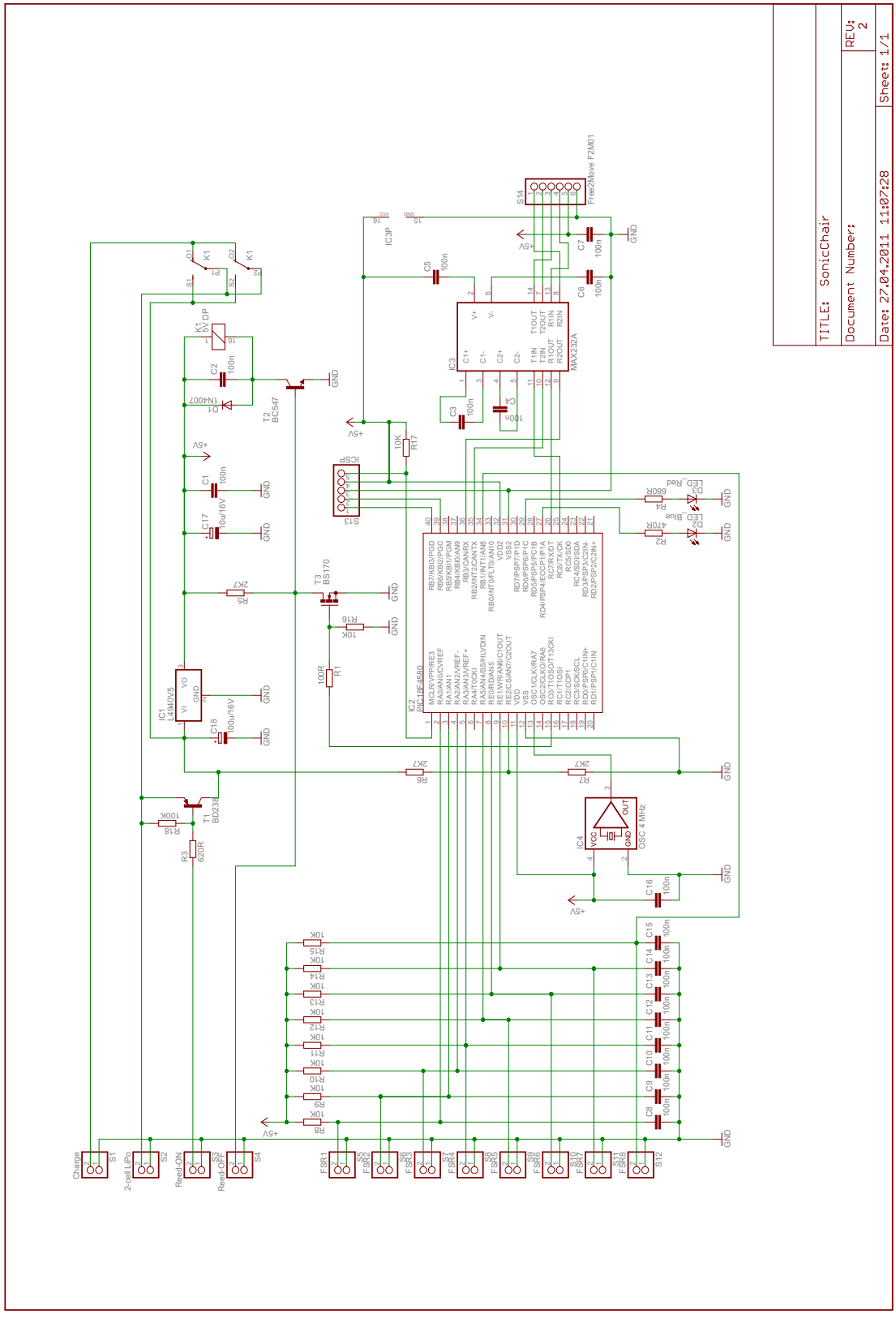

Figure 3.4: The schematic of tacTiles electronic unit. Eight force-sensitive-resistors (FSRs) are sampled using a PIC18 internal analog-converter module and the gathered digitized data is made available over RS-232C serial connection. Connected to a serial-to-Bluetooth module, such as the Free2Move F2M01, tacTiles can wirelessly transmit the tactile data.

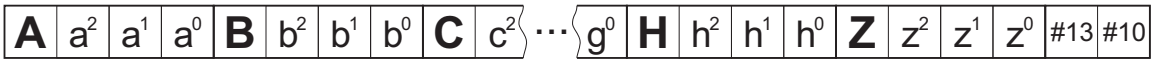

Figure 3.5: Human-readable simplistic communications protocol of tacTiles office chair cover in ASCII. A-H are tactile sensor identifiers, Z designates battery voltage. Packet is terminated with carriage return and line feed bytes.

(R8-R15). To smoothen possible ripple, 100nF ceramic capacitors are used (C8-C15). The battery voltage is measured through a voltage divider (R6-R7) with 1:2 division to match the battery voltage (with a typical range 6.0 to 8.5V) to the input range of the ADC (up to 5.0V). An external oscillator is used to drive the microcontroller and it emits a 4MHz square-wave signal. A microcontroller-integrated EUSART is used, driven over a MAX232A RS-232 line driver/receiver, to communicate with a Free2Move F2M01 Bluetooth module. The PIC18F4580 provides in circuit programming and debugging thanks to the integrated in-circuit-serial-programming (ICSP) port.

To avoid deep discharging of the Lithium-Polymer battery and thus considerably shortening its life span, power control circuitry was implemented. At its core, a double throw (xPDT) relay (K1) was used, which switches the battery positive pole between the charging jack and the tacTiles circuitry. To turn on the system, the ON pin header (S3) is shorted, which activates the BD238 PNP-transistor (T1) that then powers the low-drop positive 5V regulator L4940V5 (IC1). The output of IC1 flows through R5 to BC547 NPN-transistor (T2) activating relay K1 and bridging BD238 (T1), thus the ON pin header (S3) can be released and the system remains powered. The PIC-microcontroller (IC2) is programmed to periodically measure the battery voltage through the voltage divider (R6-R7) on its AN7 analog-input mode configured pin. In the event the sensed voltage drops below a preprogrammed threshold of 3.4V/cell, the microcontroller activates the BS170 N-channel field-effect-transistor (FET) T3, which cuts the power flow to BC547 (T2), thus deactivating the relay K1 and resulting in the powering off of tacTiles.

Communication protocol

The readout values of the 8 FSR sensors plus the battery voltage are sent using a simplistic human-readable ASCII protocol shown in Figure 3.5. ASCII characters A to H are used to identify the tactile sensors (A-D for seat, E-H for back), and the battery voltage is identified in the data stream with a leading Z. The designators are followed by 3 ASCII numbers, ranging from 000 to 999, where higher values correspond to higher force applied on the sensors. The battery voltage value is provided in the data stream without an explicit decimal symbol after the first digit (thus an example value of 673 relates to a battery voltage of 6.73V). The data packet is terminated with carriage return (CR) and line feed (LF) characters (hexadecimal byte values 0x13 and 0x10 respectively), allowing for the possibility to easily look at the values using arbitrary terminal programs. At a combined sampling rate of 10Hz for all inputs, the electronics utilizes very low data rate (3800 baud/sec.) and at the same time still achieves a crisp performance with no noticeable lag in reaction. A theoretical maximum sampling rate with the used electronic components and 8 sensors is 300Hz. However for practical purposes a frame rate of 10Hz is completely sufficient to observe real-time changes in the pressure profile of individuals sitting on the chair.

Microcontroller firmware

The embedded PIC18F4580 microcontroller in the tacTiles electronics unit includes 32 Kbyte of internal flash program memory and starts the program execution as soon as power is applied and an oscillating clock is present. The firmware of the PIC18F4580 was written to be compiled with Microchip MPLAB C compiler for PIC18 microcontrollers (an ANSI'89 compliant C compiler especially for the PIC18 family of 8-bit microcontrollers).

After executing the code for initialization, the microcontroller firmware remains in an endless execution loop handling hardware input/output. During the initialization, the directions of input/output port pins and their functionality (digital or analog), if appropriate, are configured as required by the hardware design, and the initial state of the output pin values are set. Time is given for the Bluetooth module to initialize, thereafter further modules such as EUSART for communication and Timer0 for generating internal 100ms time base are initialized. As only a single interrupt (Timer0) was implemented, no special prioritization is necessary and thus all interrupts are vectored to a fixed program memory location 0x8. In the interrupt service routine the global trigger variable is incremented and Timer0 hardware reconfigured to notify the end of next 100ms period.

The main program loop continues executing only if semaphored by the Timer0 trigger variable, thus effectively limiting the main loop runs to 10Hz. When triggered, the microcontroller reads all the enabled analog inputs (FSRs and battery voltage), sends out the measured values according to the communication protocol and checks if the battery is depleted.

3.1.2 Applications for tacTiles

A brief introduction to realized practical examples using tacTiles in different context scenarios, published initially in [HK08], is now provided. The prototype tacTiles office chair cover with 8 sensors, physically split in two functional groups for back and bottom, allows intuitive deduction of pressure patterns and related posture from the sensor output. The tendency of the presented applications to use auditive channels for feedback is due to this project's co-author, Dr. Thomas Hermann, whose primary interest is in the field of sonification.

Figure 3.6 depicts the graphical user interface for a basic controller application that shows the sensor data as pressure profile and histogram plot (left/middle) together with computed dipole vectors for back and seat area (right). All the example applications presented below run in real-time and allow recorded data vectors to be stored for later processing. In the video examples presented on the project website[4], it can be seen that the latency is low enough to ensure real-time operation.

I will now present four applications that were built using tacTiles technology.

Real-time monitoring of human haptic interactions

In the first application, tacTiles was used as a cover for an office chair to demonstrate real-time monitoring of working style. The processed signal from tacTiles was presented to the user using audio feedback. Only the dynamic output of tacTiles was considered for this application and thus the output is silent when the pressure profile on tacTiles is constant. The pressure values were mapped to the generated pulse rate of the audio, so that

[4] tacTiles project website: `http://www.sonification.de/publications/HermannKoiva2008-TFA/`

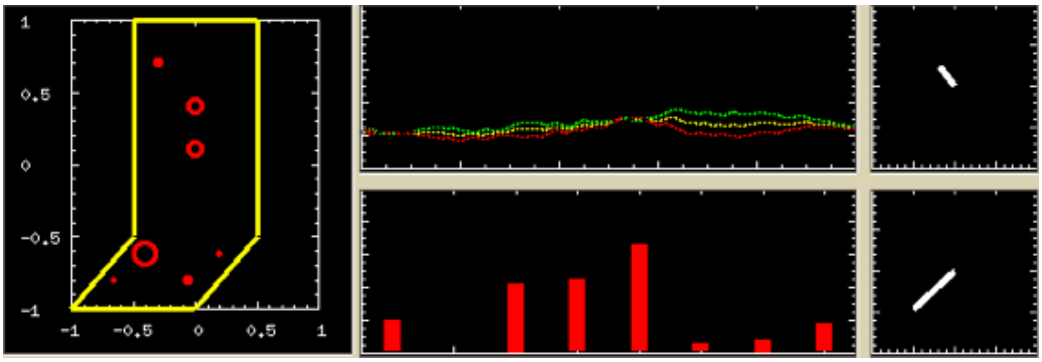

Figure 3.6: Screenshot of the real-time tacTiles Controller application showing real-time pressure profiles (left and middle bottom plots), sensor sums for the back, seat, and the total (red, yellow, green respectively) as a time series in the middle upper plot, and back and seat dipole vectors on the right side. (Application programmed in Neo/NST[5]and screenshot taken by Thomas Hermann.)

sensors that experience a higher pressure were heard as pulsing at a higher rate, similar to a Geiger counter that ticks more frequently with a higher radioactivity level. There is little immediate benefit from receiving such a direct auditory feedback on the sitting style, however, the controls are useful to check proper operation of the chair, and perhaps such sonifications might be interesting for visually impaired users who wish to gain a sense of activity in crowded offices.

Rapid scanning of long-lasting haptic interactions

The second application collapses the recorded data from long-lasting haptic interactions, such as a whole working day on an office chair equipped with tacTiles, into a short time of a few seconds. This allows the interaction, in this case the work pattern, to be reviewed and summarized very quickly. As an example, we compressed one hour of recorded tacTiles data into just 10 seconds, allowing the overall interaction pattern the subject showed to be perceived. A natural extension of this work would be to monitor the sleep of patients using tacTiles as a sensor mattress. This could greatly enhance the monitoring capabilities present in hospitals.

Activity feedback

A third application was based on activity feedback. Here extended periods of unchanging pressure profiles was interpreted as being unhealthy and was portrayed by an ambient information display involving sound and visuals in form of a facial feedback for the estimated degree of inflexibility. Every physical activity on the chair was used to recharge the sensors activity accumulator. If the activity fell under a threshold, increasingly motivating sound events began and the facial expression turns into a sad emotion. Becoming more active on the chair rapidly recharged the underlying accumulator and the happiness level of the system. This could be used as a reminder to people who sit for long periods at work and it has the potential to reduce back problems.

[5]The Graphical Simulation Toolkit Neo/NST. `http://ni.www.techfak.uni-bielefeld.de/neo/` Links last checked on November 18^{th}, 2013.

Figure 3.7: An example of a tacTiles mat audio-induced balance-game application.

tacTiles-based cooperative balancing

Another application of tacTiles was a cooperative balancing game. The idea was to have two players stand on the tacTiles sensor mat, facing in opposite directions as shown in Figure 3.7. The goal of the game was to keep a simulated canoe in balance on rough water. In the created application, the canoe angle was displayed auditorily using sonification. Both players needed to cooperatively balance their body weight in order to compensate for the external disturbance to keep the canoe level. Games such as this one can help to train or develop body balance.

3.2 Wearable dataglove for observing hand haptics

A significant part of our everyday tactile exploration is done with our hands, thus being able to observe the manual haptic interactions is important if we are to understand the involved processes. This section discusses a tactile dataglove with integrated data acquisition hardware, which facilitates the capture of pressure patterns during grasping and manipulation of arbitrary objects.

The curved shape of human hands restricts the practical usage of rigid tactile sensors. A sensor capable of capturing tactile information from human hands during common daily activities should be flexible, sensitive and robust enough to discriminate and withstand the forces occurring in everyday grasping and manipulation tasks. Furthermore it should provide a sufficient number of taxels to acquire distinguishable spatiotemporal tactile patterns. After an exhaustive search for such a device [see Section 2.2], no single, flexible, tactile sensor design was found that fits all these specifications.

In 2011, Gereon Büscher, in his diploma thesis [Bü11] carried out in Bielefeld University of Applied Sciences in cooperation with our institute, started developing fabric-based flexible

and stretchable tactile sensors. His design used 4 layers of conductive and non-conductive fabrics layered together to form a resistive tactile cell with a thickness of approximately 1.5mm. Due to purely fabric based components, the sensor could be cut and sewn in the same way as a common fabric, which allows a wide variety of shapes to be produced.

As an important milestone, Büscher discovered that the selected conductive coating material was etchable with a ferric chloride ($FeCl_3$) solution, a common etchant used in printed-circuit-board development to remove the copper between tracks. By etching the areas between desired tactile pixels (taxels) on one electrode sheet, it was effectively possible to isolate taxels from each other within a single fabric patch, which allowed the building of multi-taxel flexible fabric sensors. A first tactile dataglove prototype with 54 taxels was started and the mechanical construction finished by Büscher during his diploma.

After Gereon Büschers graduation, he continued working on the project solely in our institute together with Carsten Schürmann under my guidance and officially supervised by Dr. Robert Haschke and Prof. Dr. Helge J. Ritter. We performed exhaustive sensor performance evaluation, added embedded data acquisition electronics to the glove and created graphical user interface software. In addition to being involved in the data acquisition electronics schematic development, my main contribution to this project was that I was the main writing lead of the two successful publications eminating from the project, I coordinated sensor performance measurements and performed the programming of the host data acquisition software. The developmental details of the first dataglove prototype with integrated data acquisition electronics were published and presented at the International Conference on Humanoid Robots (Humanoids 2012) [BKS+12] and this work was one of the finalists for the best paper award. Further testing of the dataglove in our laboratory revealed significant sensor performance degradation of the original design due to sweat. The findings and exhaustive performance evaluation results have been accepted in a revised form for publication in the Journal of Robotics and Autonomous Systems, Special Issue on Advances in Tactile Sensing and Touch-based Human-Robot Interaction [BKS+14].

In order to understand the functionality of the tactile dataglove, construction details of the underlying fabric-based tactile sensor by Büscher [Bü11] are now briefly given. The sensor performance evaluation results are displayed in Subsection 3.2.2. Subsection 3.2.3 recaps briefly Büschers original tactile dataglove construction, introduces the added data acquisition electronics, presents solutions to protect the sensor from performance degrading moisture and introduces the developed data acquisition software. This section concludes by providing a discussion about future work in Subsection 3.2.4.

3.2.1 Underlying sensor construction

The sensor itself is based on the piezoresistive effect, in which the electrical resistance of a material changes under mechanical pressure. The main component is the piezoelectric, stretchable knitted fabric (72% nylon, 28% spandex), manufactured by Eeonyx [Eeo], whose individual fibers within the fabric are coated on a nano-scale with inherently-conductive polymers. By placing the piezoresistive fabric between two highly conductive materials, a change in the resistance is measured at the two outer layers when pressure is applied to the compound. These outer layers constitute the low impedance electrodes for transporting current into and out of the sensor with minimal losses. The low impedance of less than 2Ω/sq.[6] is achieved by plating nylon knitted fabric (78% polyamide, 22% elastomer) with

[6]Unit Ω per square as used by the manufacturer. The meaning is that the given resistance applies to arbitrary size square specimen.

pure silver particles. Signal repeatability was increased, especially in the subtle pressure range of 0 to 50kPa, when an additional non-conductive meshed layer was added between the middle piezoresistive and one of the electrode layers. Sensor sensitivity was found to depend on the thickness of the meshed layer and on the size of the mesh openings, with larger openings and thinner layers producing better sensitivity to first touch (determined by the smallest detectable force). Büscher evaluated meshes with openings in the range of 0.2 to 5mm and chose in the final design a 0.23mm thick meshed fabric with a honeycomb structure and mesh openings accounting for ≈70% of the surface with an opening size of ≈2mm.

With this additional mesh layer, the sensor has a very high resistivity (in the range of GΩ for a 50x50mm sample) when not acted upon, which is achieved by the introduced gap between the electrode and the piezoresistive layer. Due to the minimal force required to close this gap, the sensor still remains sensitive to subtle forces. In later tests, performed in our lab, 0.1N was experimentally found to be a reliable threshold using a $3mm^2$ probe tip. Above this threshold, the sensor operates as a parallel circuit of force sensitive resistors. The high resistance in its idle state has the additional benefit of minimizing the current flow through the sensor and thus minimizing the energy loss. This ensures a longer runtime of battery powered portable systems and simultaneously has the positive side-effect of significantly reducing the heat produced by the sensor. Especially in large-scale applications, such as covering the floor of a room, this becomes an important feature.

3.2.2 Sensor performance evaluation

To evaluate the performance of the fabric-based tactile sensors, we used our custom built measurement bench discussed in Appendix 6.1. In tests we used circular plastic (POM) probe tips with 1, 3 and $5cm^2$ tip areas. The fabric sensor sample was connected via a constant 1.0KΩ resistor to a regulated 5V voltage source. The voltage drop over the sensor, the supply voltage and the strain gauge reference sensor were sampled with a National Instruments PCIe-6259 DAQ-card with 16-bit analog input resolution. We limited our measurements to an upper value of 35N, as in a recent experiment we found the typical maximum finger force produced by humans to be no higher than 30N (see Section 3.4.1 for further details).

First we measured the tactile sensor hysteresis by exerting force using a $1cm^2$ probe tip. We loaded the sensor from idle to 35N and retracted the probe tip back to idle again. For this, we loaded the unstretched fabric tactile sensor and iteratively moved the probe tip downwards in steps of 0.1mm. At each step we waited for 0.3 seconds for the mechanics to stabilize and performed simultaneous measurements of the test sensor and the reference strain gauge sensor. We continued until a force of 35N was produced, after which we retracted the probe tip in the same fashion to produce measurements in both directions. Approximately 320 data points were gathered in a single trial, lasting approximately 3.5 minutes. Figure 3.8 depicts the sensor output over 10 consecutive trials. As can be observed from the graph, the sensor repeatability is high. We found that with increasing iteration count, the load curve converges to the unload curve. This can be explained by an increasingly better intertwinement of the fibers in the sensor fabric with an increased number of trials.

Second we evaluated the response of the sensor using in addition to the $1cm^2$ POM circular flat probe tip, 3 and $5cm^2$ tips [Figure 3.9]. As can be observed, the smaller the area of contact, the more hyperbolic the output resistance curve becomes. This can be

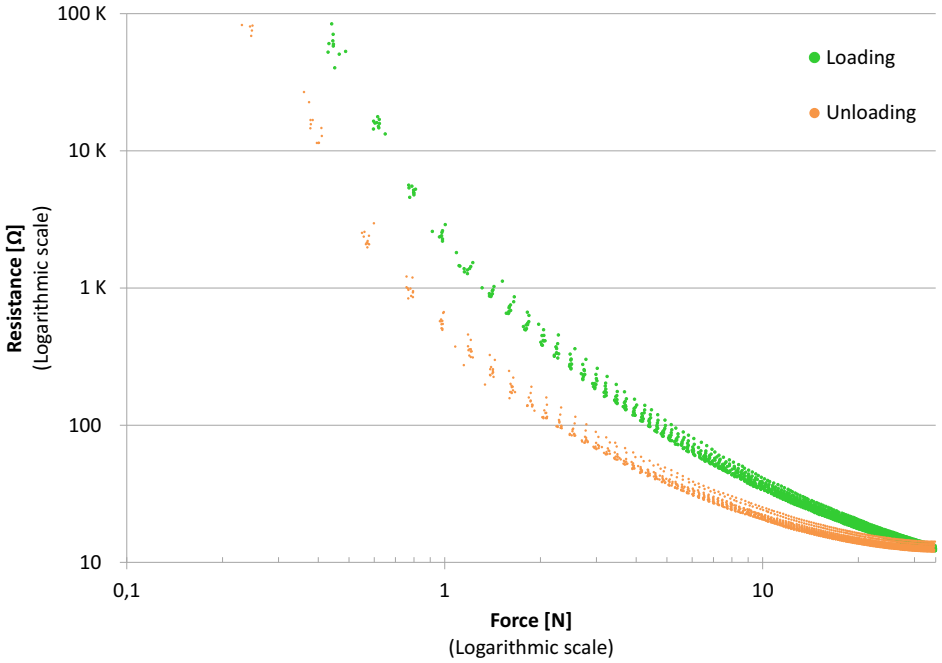

Figure 3.8: Fabric-based tactile sensor performance as measured using the 1cm^2 POM circular flat probe tip over 10 trials. Green points depict the loading phase from idle to 35N and the orange curve shows the measured points captured during the unloading phase. A single trial from idle to 35N and back to idle lasted approximately 3.5 minutes.

explained by a faster saturation of the piezoresistive material produced by a smaller tip.

In Büschers fabric based tactile sensor there are two effects of changing resistance working in parallel: the piezoresistive change of the material and the parallel arrangement of resistances, according to the surface area of contact. Both these effects are themselves nonlinear and their sum can be observed in the resulting output curves.

Figure 3.10 demonstrates the sensor resistance against pressure, by exerting up to 120kPa using the same probes. As can be observed, the curves overlap more strongly when the applied force is normalized to pressure, especially when considering only the bigger probe tips (3 and 5cm^2). This lets us conclude that the sensor is more suitable for pressure measurements than for direct force measurements, especially when the contact surface is considerably larger than the spacer layer mesh opening.

The composite 4-layer sensor remains stretchable up to 25%, limited by the mesh layer (the electrodes and the piezoresistive material alone remain stretchable up to 100%). We verified the sensor operation while stretched by bulging it over a convex POM surface with an 80mm radius using numerous stretch ratios and a 3cm^2 concave probe tip [Figure 3.11]. The sensor output in its stretched state is shown in Figure 3.12. Starting from an ≈10% stretch ratio, the idle resistivity decreases as the usually required force threshold has already been overcome. Apart from the first touch behavior, the sensor exhibits only marginal output differences between unstretched, 5% and 15% stretched states.

To evaluate how the sensor behaves in time, we measured the sensor output over 10 minutes by constantly loading it with 1N using a 1cm^2 plastic cylindrical probe tip. Figure 3.13 displays the relative change of resistance compared to the initially recorded value. The resistance decreases in the first minute strongly and then slowly stabilizes at values

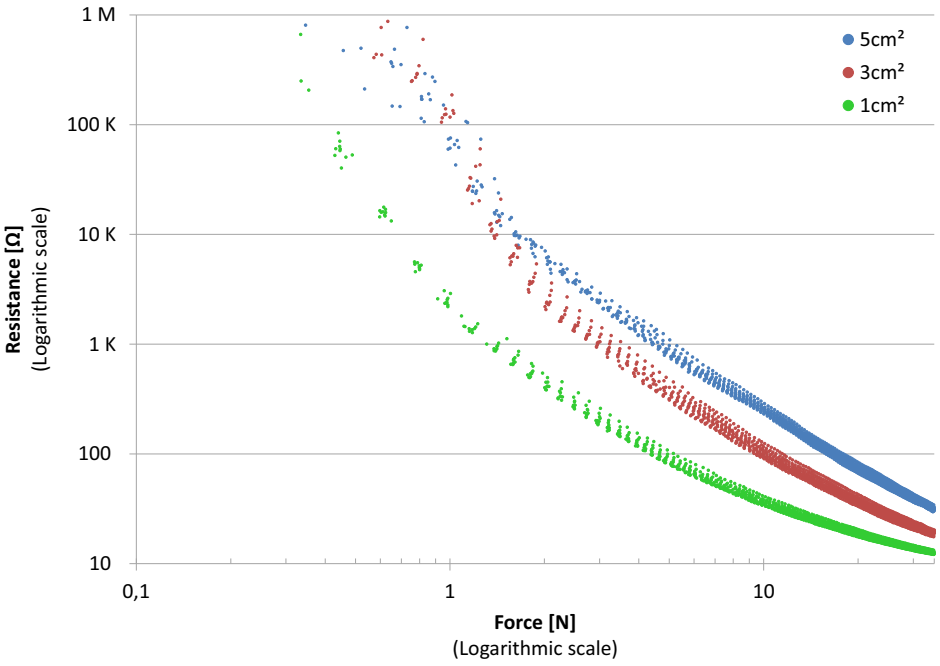

Figure 3.9: The resistance of the tactile sensor while applying forces in the range of 0 to 35N using 1, 3 and 5cm^2 POM circular flat probe tips (green, red and blue data points accordingly). Each trial was repeated 10 times.

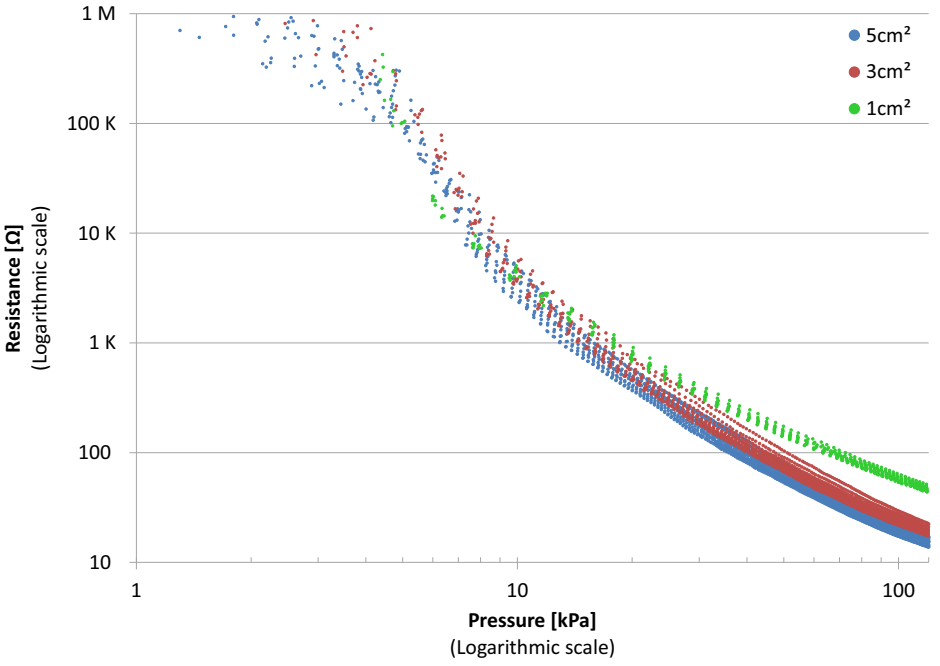

Figure 3.10: The sensor resistivity, normalized to pressure. 1, 3 and 5cm^2 flat circular probe tips were used and forces up to 12, 36 and 60N were exerted, resulting in all cases to pressure in the range of 0 to 120kPa. The graph shows every measurement curve repeated 10 times.

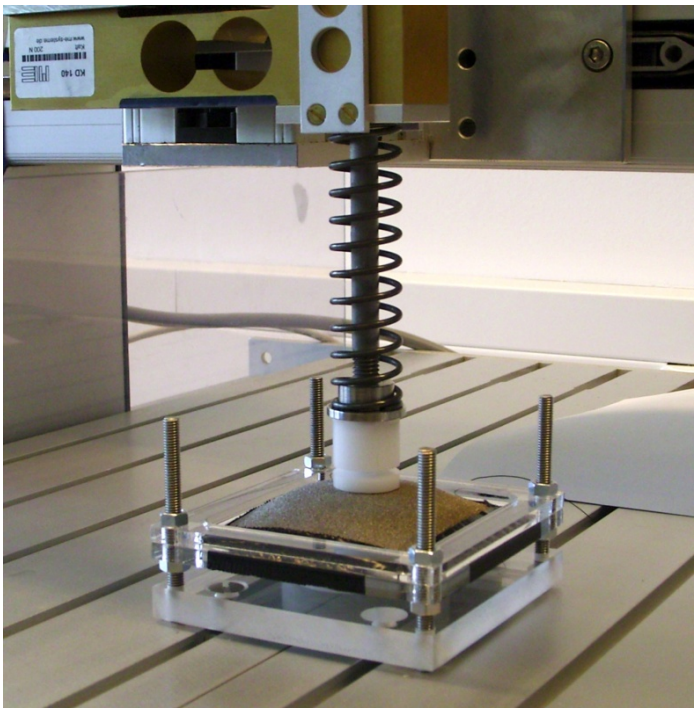

Figure 3.11: The sensor performance was evaluated with our custom built measurement rig (for further info about the rig, see Appendix 6.1). Exchangeable circular plastic probe tips with various surface areas were used during testing. The picture shows a fabric-based tactile sensor patch being tested, the probe and the strain-gauge reference sensor. This close-up shows a measurement of the sensor in a stretched state, in which the fabric tactile sensor is stretched over a convex surface with a radius of 80mm (the probe tip fits this surface). (Image source: [BKS+14])

3–4% smaller than the initial value. This effect can be explained due to material creep in the fabric as explained in [HMS07].

The quantitative results underline the developed fabric-based sensors usability for pressure measurements typically found in human manual interaction. The repeatability of the sensor is high and the hysteresis of the sensor remains in a similar range to that of other flexible tactile sensors [SNI+04, OKN06, ANK07, CMMS08, SOK+11]. Flexibility, stretchability and simple construction result in a robust and universal tactile sensor that can capture pressure information from free-form surfaces.

3.2.3 Completion of the Tactile Dataglove

In his diploma defense talk, Büscher [Bü11] presented a finished mechanical construction of the first Tactile Dataglove prototype with 54 taxels. To separate the taxels inside a single fabric area, Büscher used a heated (≈60°C) solution of 30 mol/m^3 of ferric chloride dissolved in water. A cleverly designed custom etching rig was built to achieve uniform etch result without etchant creeping into material areas not destined to be removed from conductivity.

To form a glove shaped device, he added an additional layer in the form of a fine mesh with approximately 0.2mm openings to the 4-layer tactile sensor design in order to mount the tactile sensor fabric patches. All the layers were sewn together and thin Teflon coated

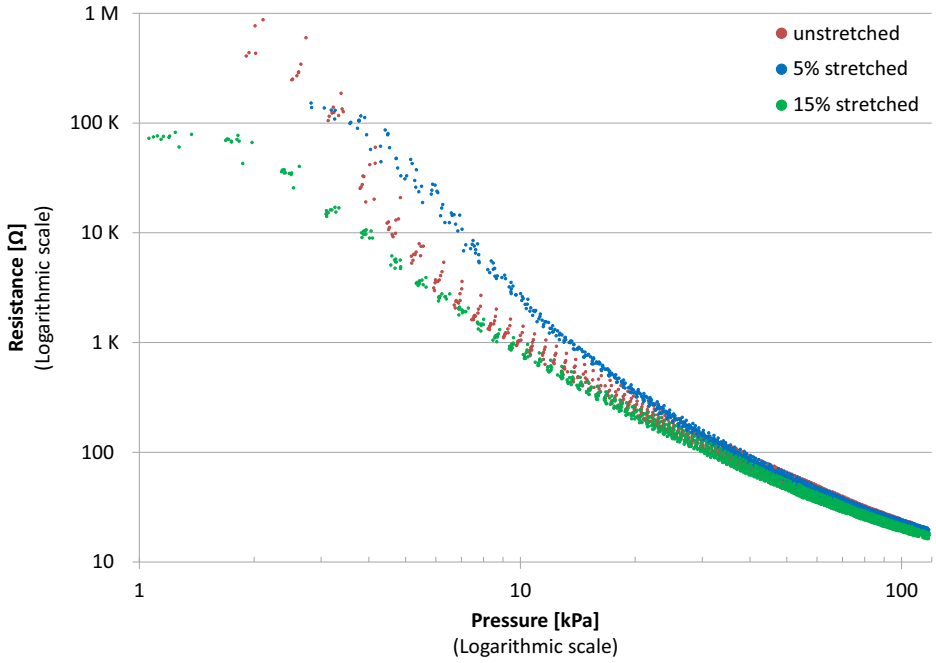

Figure 3.12: Stretched sensor output as measured on top of an 80mm radius convex surface using a 3cm^2 matching concave probe with 3 stretch levels: 15% (green), 5% (blue) and unstretched sensor (red data points). All measurements were repeated 10 times.

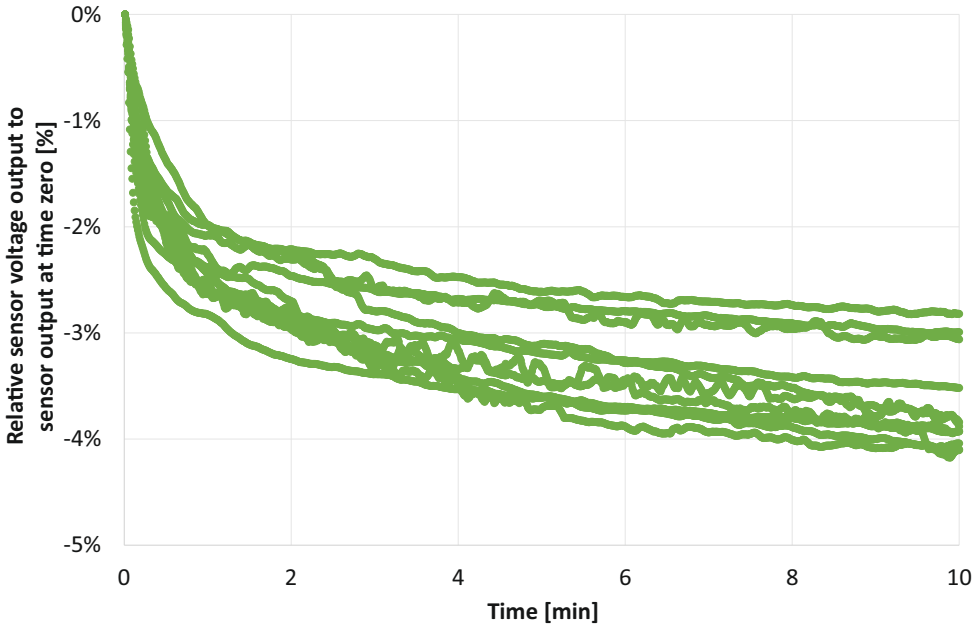

Figure 3.13: The relative resistance change of the sensor as gathered over the course of 10 minutes while exerting a constant force of 1N with a 1cm^2 probe tip (10 repetitions). The irregular fine oscillations can be explained by small vibrations in the building, conveyed through the floor onto the measurement rig.

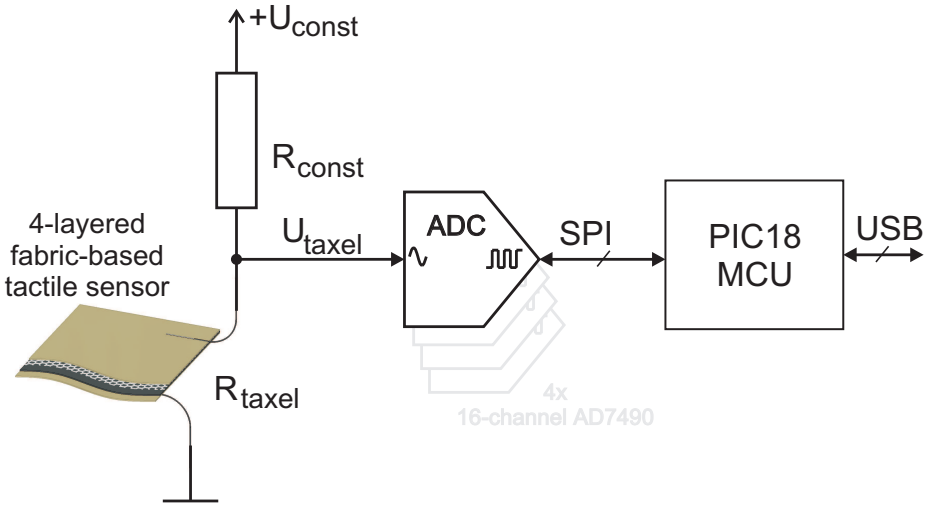

Figure 3.14: Tactile sensor signal acquisition schematic. A voltage divider circuitry, consisting of a constant pull-up resistor with 1KΩ resistance and the tactile sensor cell, converts the sensor resistance change into a voltage change. An ADC provides the sampled value in digitalized form over the internal SPI-bus to the microcontroller (MCU). The microcontroller is used to gather data from all taxels and to perform the communication over a USB connection with an external system, such as a PC.

wires (⌀0.3mm) were connected to the sensor patches by removing the insulation from the tip of the wire and interweaving them into the electrode layers.

Tactile data acquisition

As the tactile sensor is based on the piezoresistive effect, an applied load results in a change of output resistance. Using a voltage divider circuitry [Figure 3.14], we convert the resistance change into a voltage change. By implementing a fixed pull-up resistor setup, the output voltage U_{taxel} only depends on the resistance of the taxel:

$$U_{taxel} = \frac{U_{const} \cdot R_{taxel}}{R_{pull-up} + R_{taxel}}. \tag{3.1}$$

The output of the voltage divider is sampled using an ADC and converted into a numeric value. Each individual taxel is sampled by a dedicated ADC input channel. A total of four 16-channel input ADC chips are used to sample all 54 taxels of the glove. The ADC chips are connected via an SPI bus to a microcontroller that relays the data to a connected host system via USB. Employing dedicated ADC channels for all taxels avoids crosstalk and ghosting and allows high sampling rates to be achieved. As a consequence, for each taxel a fixed resistor and an ADC input channel is needed, along with the components to generate the supply voltage and the electronics needed to transmit the acquired data to the USB host. To sample the ADCs and relay the gathered information to a host system, a PIC18F24J50 microcontroller was employed, running at 48MHz. On the USB bus, the microcontroller registers as a CDC device, such that the tactile data can be received by the host via a virtual serial port. The power for the Tactile Dataglove is also taken over the same USB connection.

The data acquisition board layout was created, its components soldered and the microcontroller programmed by Carsten Schürmann.

Figure 3.15: Second prototype of a wearable right hand dataglove with 54 taxels and embedded data acquisition electronics.

Protection against sweat

During the evaluation of the initial Tactile Dataglove prototype, we noticed a significant non-recoverable drop in sensor sensitivity after prolonged use. We found this to be due to moisture, such as the natural sweat produced by the hands, reacting with the silver-coated electrode layers, which resulted in a reduction of the conductivity and thus elevated the electrode layer's resistivity.

To avoid the performance decrease of the sensor due to moisture, a second prototype was built with an additional layer that is impervious barrier to moisture, and is placed between the glove base-material and the sensor-patches. The barrier consists of a ductile polyethylene-foil with a thickness of just 0.01mm. Figure 3.15 depicts the finished second prototype of the tactile glove including the embedded data acquisition electronics located in a housing mounted around the dorsal side of the arm.

To completely seal the sensor patches, a rubber coating to the outer surfaces of the sensors was investigated. However, due to the added layer, the haptic feel when wearing the glove worsened.

Figure 3.16 displays the proposal to swap the sensor layer order in a future prototype. Having the ground electrode layer as the most outer layer, will eliminate the false contacts observed in previous designs when different taxels came into contact with each other, which is easily possible e.g., by adducting the fingers or making a fist.

Data acquisition application

An application to visually observe the haptics of the hand and to save the captured data was developed. Figure 3.17 demonstrates the Tactile Dataglove and the corresponding .NET data acquisition and visualization application during operation while grasping an apple. On the right image the resulting output of the sensors is displayed. In the *Humanoids 2012* conference in Osaka, Japan, this combination was successfully presented in a live demonstration. For an interested reader we prepared an online video, available through our institute's YouTube channel [BKS+].

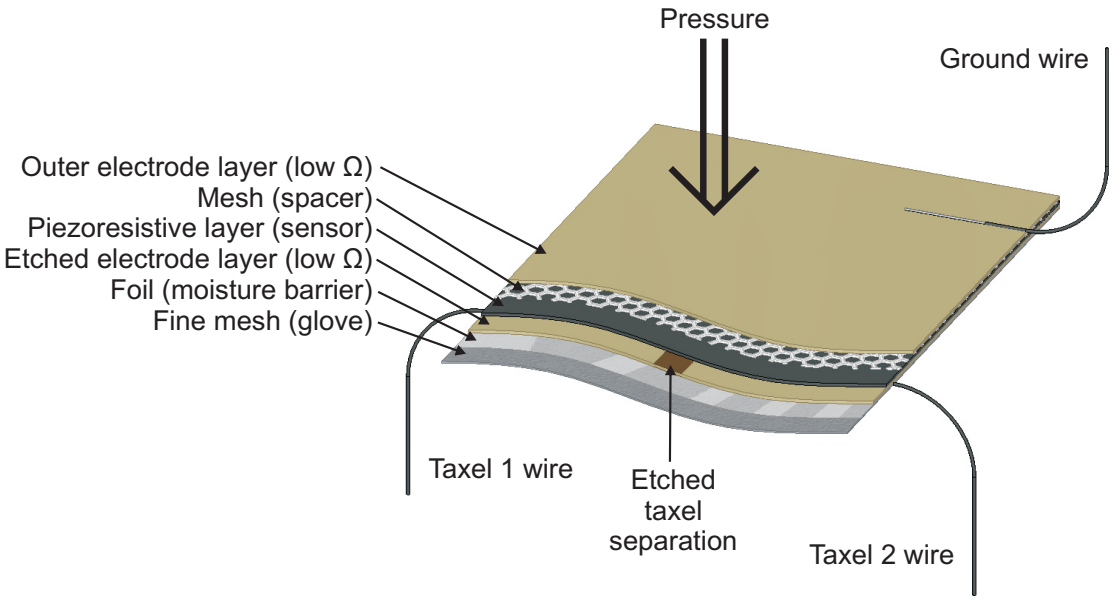

Figure 3.16: The proposed layer order for the next Tactile Dataglove prototype, shown as an example two taxel sensor patch. Swapping the ground electrode to the outer side will eliminate the false positives observed in previous designs when taxels came into contact with each other.

(a) The grasp. **(b)** Graphical sensor output.

Figure 3.17: Grasping an apple using the right hand Tactile Dataglove. On the right image, the output of the sensors is depicted graphically. The color coded pressure scale goes from dark green for no contact, through light green and yellow to red for high pressure (in the displayed configuration 100kPa).

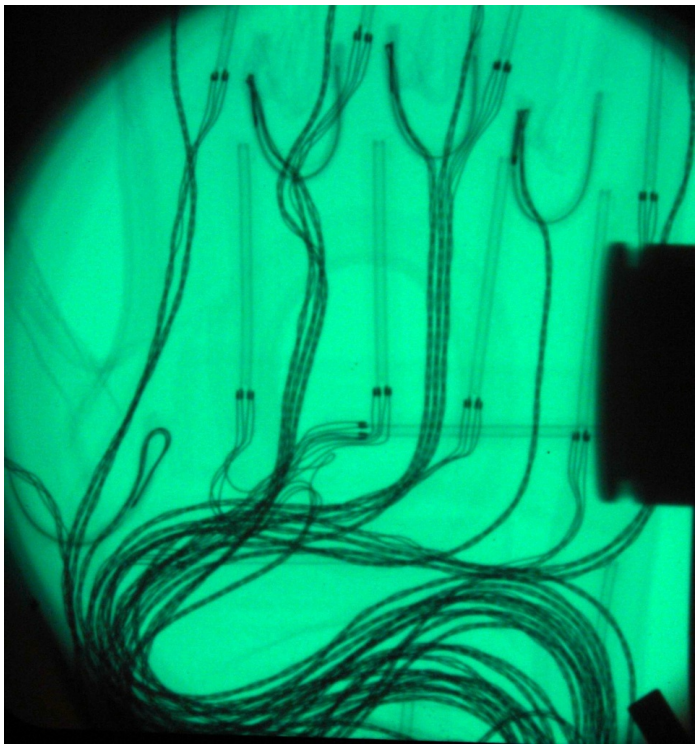

Figure 3.18: Combining tactile sensing with postural sensing is an immediate next step in our future dataglove development. This X-ray image shows the popular CyberGlove II postural dataglove [Cyb], as an example of such flex sensors with cabling. (My gratitude goes to Mr. Hans Bartels from the Faculty of Physics for helping with the X-ray machine.)

3.2.4 Future improvements

As the fabric tactile sensor design allows for its integration into almost arbitrary garments, numerous other applications for capturing tactile patterns can be explored, for example in research, entertainment, health-care and ambient intelligence. Section 4.2 discusses a tactile sensitive artificial skin for robots implementing the same sensor technology.

Plans are afoot to develop improved data acquisition electronics that incorporate a wireless real-time data transmission module in addition to an on-board micro-SD card slot to allow later offline data analysis similar to work presented in [SKHR12]. We would also like to integrate additional sensors into the glove to capture the posture of the hand, as this has been shown to be important in [SEHR10, SMR11]. Some practical options for sensors measuring finger joint angles and integrated in wearable portable datagloves are force sensitive bend sensors, for example the *Flex Sensor* from Spectra Symbol [Spe], used also in the famous gaming input device *PowerGlove* by Mattel [Mat], and magnetic goniometric sensors, such as those presented by Portillo-Rodriguez *et al.* [PRAS$^+$07]. Figure 3.18 displays the joint posture sensors and cabling of the popular CyberGlove II dataglove [Cyb]. Kramer *et al.* [KMSW11] present an interesting stretchable curvature sensors based on specially treated thin elastomer film development that possibly would suit best for integration in the dataglove.

The developed Tactile Datagloves will be used to investigate human manual intelligence in our group's Manual Intelligence Lab [MEH$^+$11] together with numerous other sensor

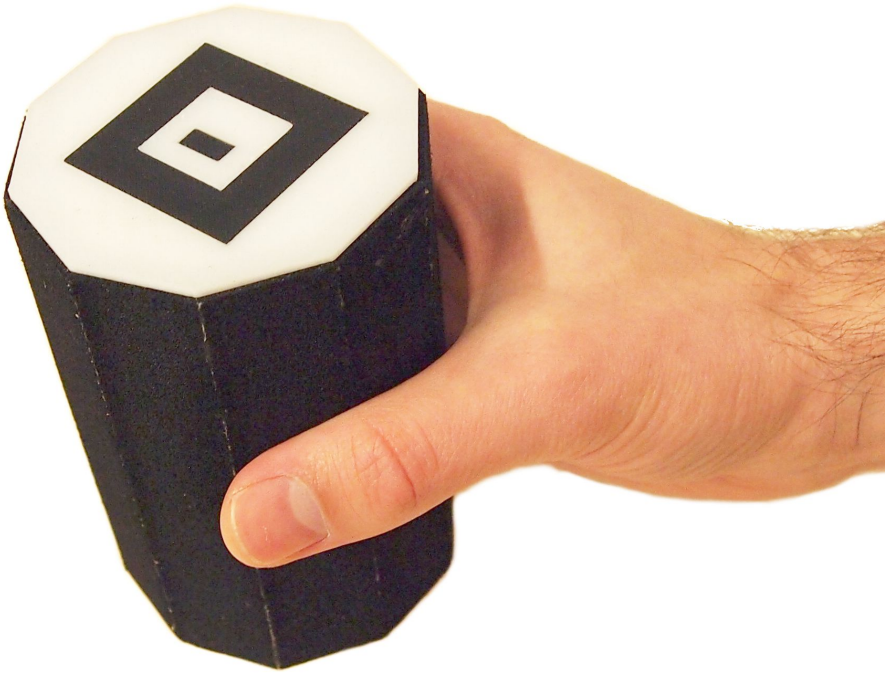

Figure 3.19: Beverage can shaped iObject grasped by a human hand.

modalities, such as *Vicon* [Vic] and eye tracking, to better understand how humans perform grasping and manipulation. A right-left pair of Tactile Datagloves is also a deliverable in an ongoing EU-funded FP7/2007-2013 project no. 601165 WEARHAP (WEARable HAPtics) [WEA].

3.3 Instrumented object for observing manual intelligence

This section introduces *iObject* (abbreviation for Instrumented/Intelligent Object) - a versatile multi-modal sensory tool designed to study manual intelligence [Figure 3.19]. Embedded tactile and motion tracking sensors allow the actions of a human or an anthropomorphic robotic hand (roughly the size of an adult hand) to be evaluated. Finger and hand contact location and force, object acceleration (linear 3D + rotational 3D) and orientation relative to the earth (3D magnetometer) are measured and transmitted wirelessly in real-time over a Bluetooth connection. If the user additionally wears a postural data glove (such as the popular CyberGlove [Cyb]), hand posture, contact location, contact intensity and motion data (linear and rotational) can be simultaneously captured.

This project was carried out by me and was supervised by Dr. Robert Haschke and Prof. Dr. Helge Ritter. The development of iObject was published and presented at the 15^{th} International Conference on Advanced Robotics (ICAR 2011) [KHR11].

The construction details of iObject are given in Subsection 3.3.1. There, the details of the sensing principle of the implemented tactile cells, iObject's mechanical construction, power management, wireless connectivity and elementary on-board data preprocessing are

explained. Subsection 3.3.2 introduces iObject's flexible mounting interface facilitating its use in various research disciplines by allowing a wide variety of active and passive add-on modules to be attached. A brief introduction to operating the iObject is given in Subsection 3.3.3. Subsection 3.3.4 discusses the communication and data protocol. iObject's tactile sensor characteristic and the signal propagation latency are then presented in Subsection 3.3.5. Some preliminary applications are presented in Subsection 3.3.6. Finally, Subsection 3.3.7 discusses future work and presents the improvements of a second generation model currently under construction.

iObject provides a good basis for a broad range of possible future research in numerous fields, including, but not limited to, robotics, psychology, sport, art and medical sciences. Human, as well as robotic, grasping and manipulation parameters such as contact position, contact magnitude and motion are measured. Furthermore, a distinguishing feature of iObject is that it is cable free, which facilitates more natural interactions.

Imitation learning [Sch99] has seen an explosion of research activity in recent times. iObject can be used in the first stage of imitation learning, the observation stage, to learn the relevant features of human grasps. I expect that this will contribute to endowing robot hands with more dexterous capabilities. Another interesting direction for iObject is as a control device in a virtual reality setting. For example, a sculpting application could be developed in which iObject is used as a virtual carving chisel with tactile control for the applied chisel type and magnitude, and the position and orientation of the tool are given by the motion tracking sensor.

3.3.1 iObject construction details

iObject was designed to measure contact and motion data, to be cable-free to maintain maximum comfort, and to measure data in a robust way while being used. For the initial prototype, a standard 330ml beverage can, an object that allows both a firm grasp, as well as numerous single or dual handed manipulations to be carried out, was chosen as the shape and size for the model. Thus the dimensions of iObject are approximately 80mm (diameter) $\times$ 120mm (height), which provides ample interior space for the numerous required electronic components. Next, the components and working principle of iObject are introduced. Figure 3.20 gives an overview of the internal component blocks and their connections.

Tactile sensors

To measure the contact pressure location and amplitude of a human or robotic hand, a custom built tactile sensor array was implemented throughout the whole cylindrical surface of iObject with a spatial sensor cell separation of 10mm [Figure 3.21]. The tactile sensors are based on a resistive working principle, where the interface resistivity between two surfaces changes according to the applied load. The invention dates back to late 19^{th} century, when a French electrical engineer, Theodore du Moncel, discovered alternation in the current flowing between a sooted metal plate and a nail when acoustic waves were present. This paved the way for the invention of the carbon microphone, which revolutionized telephony [dM78]. iObject is equipped with a more modern version of the resistive tactile sensor and instead of sooted plates and nails, uses a chemically golded Printed-Circuit-Board (PCB) surface as electrodes and a conductive elastomer foam as the sensor material, a technique first introduced by Weiß and Wörn [WW05]. The tactile sensor cell resistance, R_t, is the sum of

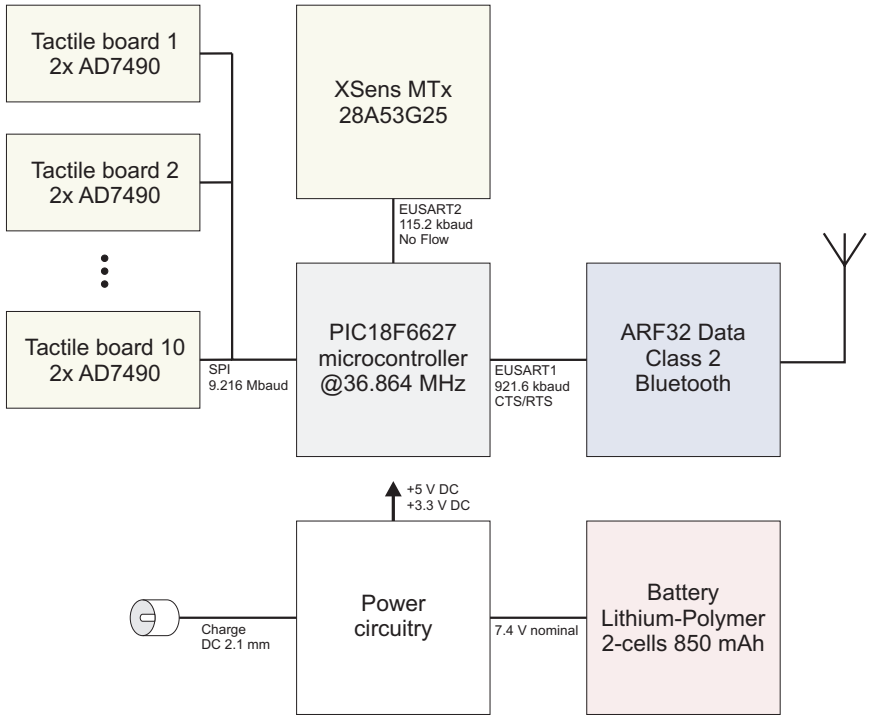

Figure 3.20: iObject's internal components and their connection.

Figure 3.21: iObject's tactile sensors as seen through rendered translucent sensor material.

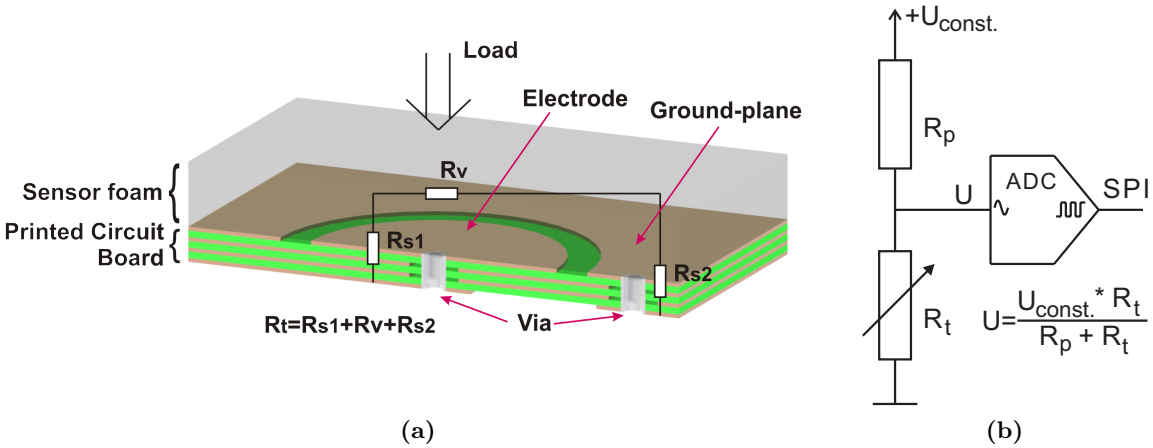

Figure 3.22: Single resistive tactile sensor cell of iObject. (a) The cell resistance R_t is a sum of sensor foam volume resistance R_v and surface resistances at the sensor foam contact points with electrode R_{s1} and ground plane R_{s2}. (b) Sensor cell resistance R_t digitalization with a constant pull-up R_p and analogue-to-digital-converter (ADC) with serial-peripheral-interface (SPI) bus output.

three parts – the variable surface interface resistance, made up of $R_{s1} + R_{s2}$, and a constant sensor material volume resistance R_v [Figure 3.22].

The resistive sensor approach was chosen as in comparison to capacitive sensors it is robust to electromagnetic interference, and in comparison to load cells it is relatively easy to implement. Resistive sensors also have a very desirable hyperbolic style characteristic between the applied load and the resistance. This is especially interesting for tactile sensors, as it allows detection of first contact and a wide measurement range, although resolution is sacrificed at higher loads. Due to the simple construction of resistive tactile sensors, they are also very insensitive to abuse, such as vibration and overload.

Ten identical sensor array boards, measuring 20 × 115mm and each containing 2 × 11 tactile sensitive elements, form the decagon surface of the iObject [Figure 3.23]. The schematic of the sensor array board is shown in Appendix 6.3.3 and the utilized electronic components are listed in Appendix 6.3.4. The tactile sensor electrode layer of the 4-layered PCB includes 22 taxels surrounded by a common ground-plane. Signal conditioning circuitry on the backside of the PCB forms the basis of the tactile sensor. Numerous candidates for the needed conductive sensor material were evaluated, and a high viscosity elastomer foam from Weiss-Robotics [Wei] was selected. It features a favorable low creep and strength to cope with shear forces without easily rupturing. 5mm thick sheets of the foam were processed with a CNC milling machine into a trapezoid form and glued with flexible glue (Pattex Express [Pat]) to form an exact fit over the electrode decagon ring of sensors.

The resistance measured between the electrode and a common ground-plane, electrically connected with the conductive elastomer foam, is converted to voltage with a constant pull-up resistor attached to a constant power supply [Figure 3.22b]. The voltage of 22 taxels in one sensor board is measured with two 16-channel 12-Bit successive-approximation analog-to-digital converters (ADCs), model AD7490, which provide the internal Serial Peripheral Interface (SPI) bus with data that can be further processed. Altering the value of a pull-up resistor allows us to shift the measurement range. Higher resistance allows lower pressures to be measured, at the cost of inducing a higher signal noise and narrowing the sensor bandwidth. The typical contact forces required for normal handling of iObject were

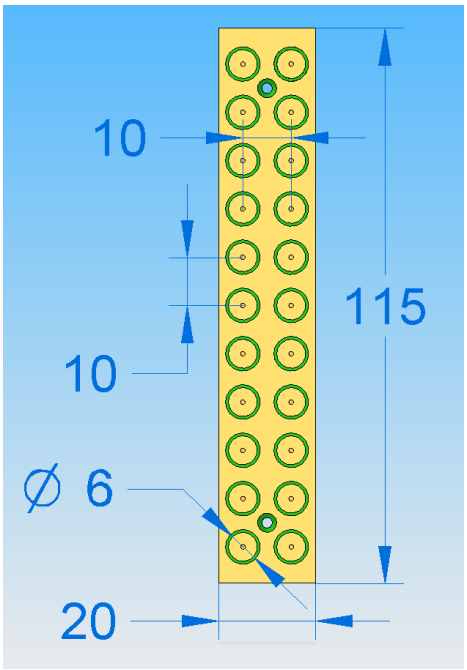

Figure 3.23: Single tactile sensor array board of iObject with dimensions of 20×115mm. The electrodes of the tactile cells, with a diameter of 6mm, are arranged in a 10mm grid.

measured to be in the range of 5 to 15kPa, resulting in an optimal pull-up resistor value of 100kΩ. The tactile sensor sensitivity evaluation can be found in Subsection 3.3.5.

If we were to unroll the 10 × 2 × 11 tactile sensors of the decagon surface, it can be imagined to be a 20 × 11 pixel tactile monochrome camera with 220 tactile pixels (taxels), thus offering the possibility of processing the contact pressure data with numerous existing algorithms from the computer vision domain.

Motion and orientation sensor

To measure the motion and orientation of iObject, commercially available MTx-28A53G25 motion tracker internals from Xsens [Xse] were embedded [Figure 3.24]. The MTx incorporates and provides measurement for:

- 3D linear acceleration sensors (full scale 50m/s^2 ≈ 5G, bandwidth 30Hz)
- 3D rotational acceleration (rate-of-turn) sensors (full scale 1200deg/s, ≈ 3.3 full rotations/s, bandwidth 40Hz)
- 3D magnetometer sensors (± 750mGauss, bandwidth 10Hz)
- Ambient temperature sensor

The MTx outputs the measured and digitalized data on a standard serial RS-232 interface at 115.2kbaud with a maximum update rate of 120 frames per second using onboard processing. Appendix 6.3.7 describes the internal details, such as the low level protocol, internal states, wakeup procedure, and lists the packet formats for some of the in iObject used communication packet types of the Xsens MTx motion tracker. iObject does not reply

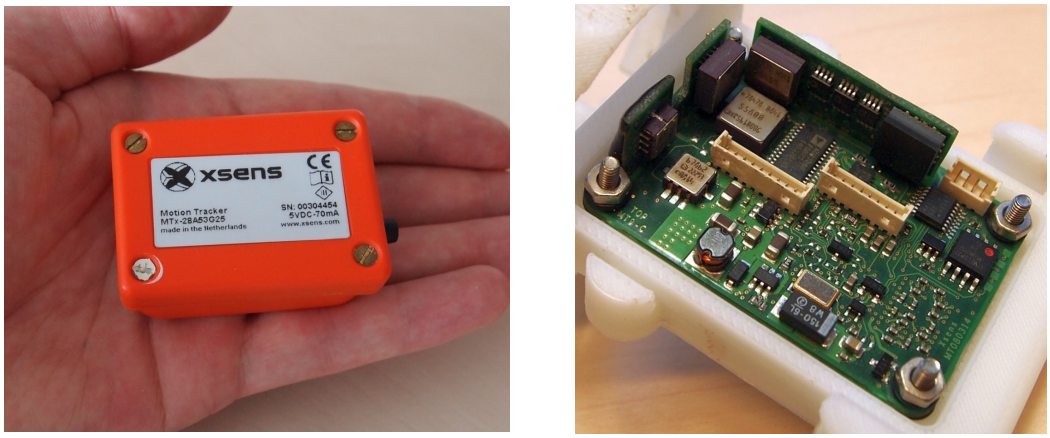

Figure 3.24: Xsens MTx motion tracker sensor (left - in original casing, right - the bare electronics, shown assembled in iObject's frame).

to the WakeUp message sent by Xsens during power-up, forcing Xsens MTx automatically into *Measurement mode* (see Appendix 6.3.7 for further details).

As the Xsens MTx in iObject is deliberately configured not to send acceleration and orientation data out automatically (for this, internally in MTx the SkipFactor configuration value is set to *0xFFFF*), the data has to be polled by iObject with a *ReqData* message (see Appendix 6.3.7 for more information). The polling rate is constantly adjusted according to the available wireless connection bandwidth. The acceleration, orientation and ambient temperature sensor information of Xsens MTx is sent out in an MTData message (for further information, also see Appendix 6.3.7).

The format the *MTData* message uses is configurable by the user. The user can decide between raw or calibrated data to be outputted by MTx (both cannot be outputted simultaneously). If calibrated data is chosen, many different calculated value types may be selected or deselected to be included in the message. The required data mode and/or data fields must be configured in *Config state*, the selection is saved in Xsens MTx internal EEPROM and thus is not cleared by power cycling the iObject.

The easiest way to perform the selection of outputted *MTData* message format is to use Xsens MT Manager Software, which is part of MT Software Development Kit (SDK). The Xsens SDK provides tools and wizards for the configuration, making the configuration easy. Nevertheless, the settings can also be made with a standard terminal program capable of sending out arbitrary characters (a terminal program not limited to 7-bit ASCII and capable of outputting full value range from *0x00* to *0xFF* must be used).

The *MTData* message itself does not include information about which sensor data is included nor its coding, thus one should note the configuration of Xsens either by saving the configuration packet sent after power-up, requesting the configuration explicitly with an *ReqConfig* message or explicitly setting the *MTData* format.

If the raw (uncalibrated) data output mode is selected, the *MTData* message contains the raw data output of the accelerations, rate of turn and magnetic field sensors in all X, Y and Z axes. The 16-bit unsigned integer values are directly forwarded from the analog-digital-converters of MTx. Including the temperature value, the raw values of the sensors are contained in 20 bytes.

In calibrated data output mode the *MTData* message can be more granularly configured by choosing the format for the data (such as quaternion, Euler angles or 3×3 rotational

matrix for orientation), the precision of float values sent in 3 steps, plus single sensor modalities that are to be included in the packet can be individually selected. Thus, in calibrated data output mode, the length of the *MTData* message is variable. The order of information in a *MTData* message is however fixed and as follows:

1. Ambient temperature
2. Calibrated data
3. Orientation data
4. Status
5. Sample counter

A standard value field in the *MTData* packet is 4 bytes long and describes a single precision 8.24 floating point value (as defined in the IEEE 754 standard [IEE08]). Optional fixed point signed 12.20 (also 4 bytes long, but with different distribution between significant and exponent) and 16.32 (6 bytes long, for higher precision) formats are also configurable.

Power supply

iObject's internal components are powered by a 2-cell Lithium-Polymer (LiPo) 850mAh battery providing nominally 7.4V. LiPo chemistry was used due to its outstanding power to weight ratio and good availability in numerous sizes and forms. With an average power consumption of ≈120mA, the selected battery can provide around 7h of continuous usage on a single charge. Extra care is taken to avoid deep discharge of the battery in iObject, which is done by powering down the complete device if the voltage drops below 3.0V/cell.

An external directly accessible charging socket is provided with a standard cylindrical 2.5mm DC-plug and with a negative terminal on the shield. Finally, Lithium-polymer capable chargers with up to 1A charging current can be used.

Wireless connectivity

To extract realistic grasping and manipulation data, a wireless design without disturbing cabling was decided upon. An *Adeunis ARF32 Data* Class 2 Bluetooth Module [Figure 3.25] was chosen due to its relatively high 723kbps theoretical maximum data rate. Using wireless communication has the added benefit of actively being able to control key data sampling parameters in an online fashion from the control system. A class 2 Bluetooth module was chosen over the considerably higher range Class 1 module due to power consumption concerns (see Table 3.1 for further information about Bluetooth classes). Nevertheless, the best wireless range is achieved with a Class 1 communication partner, as these modules

Class [Blua]	**Maximum Transmission Power** [Blua]	**≈Operating Range** [Blub]
Class 1	100mW (20dBm)	100 meters
Class 2	2.5mW (4dBm)	10 meters
Class 3	1mW (0dBm)	1 meter

Table 3.1: Bluetooth Power Classes.

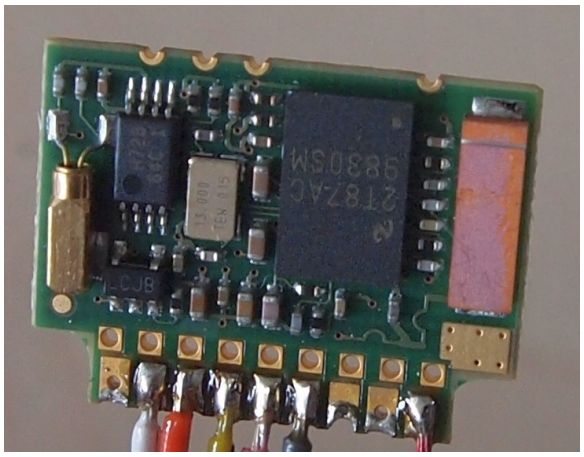

Figure 3.25: *Adeunis ARF32 Data* Bluetooth Class 2 module with an integrated antenna.

usually embed higher grade components and thus have in addition to considerably higher transmitting rates also more sensitive receivers.

The actual over-the-air data rate is very dependent on the environment, thus hardware flow control with Clear-to-Send/Request-to-Send (CTS/RTS) is actively used to avoid overflowing the buffers and invalidating data packets. The sensors (tactile and motion) are polled at the maximum rate possible for transmission.

In iObject the ARF32/LMX9830 wireless module is configured to use transparent mode after link establishment, which means that all data from both sides are transferred one-to-one without any parsing or processing by the wireless module. One speaks of this as cable-replacement or transparent mode. The opposite is command mode, in which each packet has to be capsuled in defined transmission packets. Command mode must be used for multipoint communications, which is not required with iObject. If the link is dropped by the communication partner or due to bad radio quality, the ARF32/LMX9830 falls back to command mode.

Appendix 6.3.8 discusses the relevant low level communication details of the ARF32 wireless module.

Data processing

The sensor data from all sensors is internally collected, encoded and sent to the Bluetooth module for transmission by a custom built main processing unit PCB (electronic schematic shown in Appendix 6.3.1, component listing in Appendix 6.3.2). At the heart of the main processing unit is the Microchip PIC18F6627, an 8-Bit FLASH-based reprogrammable microcontroller unit (MCU) which runs at 36.864MHz and provides computational capabilities up to a theoretical limit of 9.216 million instructions per second (MIPS). The microcontroller collects the data from the pressure sensor boards over a SPI Bus; the data from accelerometer and orientation sensor over an enhanced-universal-synchronous-receiver-transmitter (EUSART) and communicates with the client via a Bluetooth module that is connected to the second EUSART port of the microcontroller.

To optimize the usage of its limited wireless bandwidth, the microcontroller transmits only the taxel values that are above the set threshold. In a typical grasping situation only a low percentage of cells are contacted [Figure 3.26], thus the selective transmission

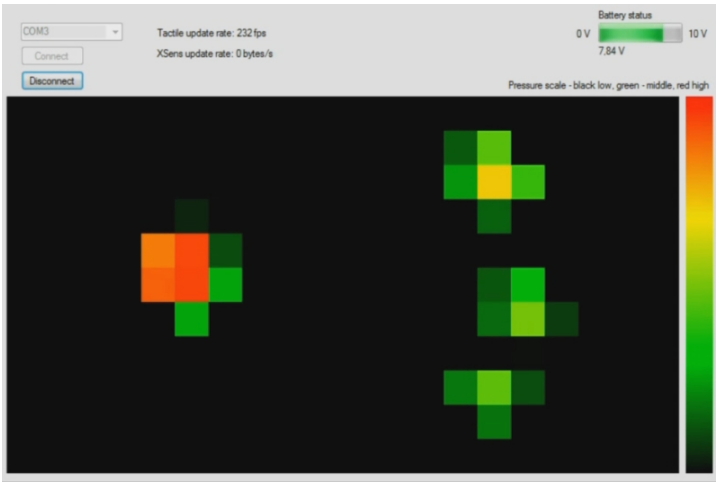

(a) Graphical User Interface (GUI) displaying the tactile data of the cylinder surface, rolled out flat (cell pressure is colored from black for no contact to red for maximum pressure).

(b) Matching grasp for **(a)** with 4 contact points (thumb plus 3 fingers are in contact with iObject).

Figure 3.26: Typical grasp scenario, where only a small number of taxels have contact. Transmitting only the values of non-zero taxels allows because of this in most grasping situations a significant reduction in the amount of data, resulting in computationally very cheap, but effective, data compression.

compression algorithm allows considerably higher frame rates to be achieved.

The iObject PIC18 microcontroller code is completely written in Microchip assembly language (MPASM). The main reason for choosing assembly language over higher generation languages, such as C, was to have more precise timing control and maximum processing efficiency. The MPASM assembler and linker required to build the firmware for the MCU are included in the freely available Microchip MPLAB IDE development environment [Mic].

The main entry points for the start of the program and Interrupt Service Routines (ISRs) are defined in absolute code blocks (as required by the PIC18 hardware), while the rest of the iObject MCU code is written as relocatable code. With relocatable code, the addresses of the variables and procedure entry points are first defined by the linker and not by the coder, which makes code more readable and facilitates less error-prone programming in assembly language.

A big drawback of using assembly language to program PIC18 microcontrollers is that the programmer has to consider data memory banking. With the used PIC18F6627, the available data memory, including the control registers, are divided into 16 256-byte sized blocks (of which a total of 3936 bytes of RAM are available for user variables). Most instructions in the instruction set (a 16-bit wide program memory with a typical 16-bit wide instruction length) are however only able to address 8-bits, and thus only variables inside a single data memory bank. To address more than a single bank, bank select bits need to be set by the programmer with an extra instruction(s) before accessing a variable on a different bank, regardless if one is reading or writing information. When using relocatable code (as is the case with the iObject), the exact bank is mostly not known during programming and thus the bank switching (the required bank selection value) is left for the linker process to decide. Nevertheless the linker directive *banksel <variable>* for selecting the bank needs to be implemented in source code before each access to a variable on a different bank.

The simplified operation of MCU code in iObject is displayed in Figure 3.27. After

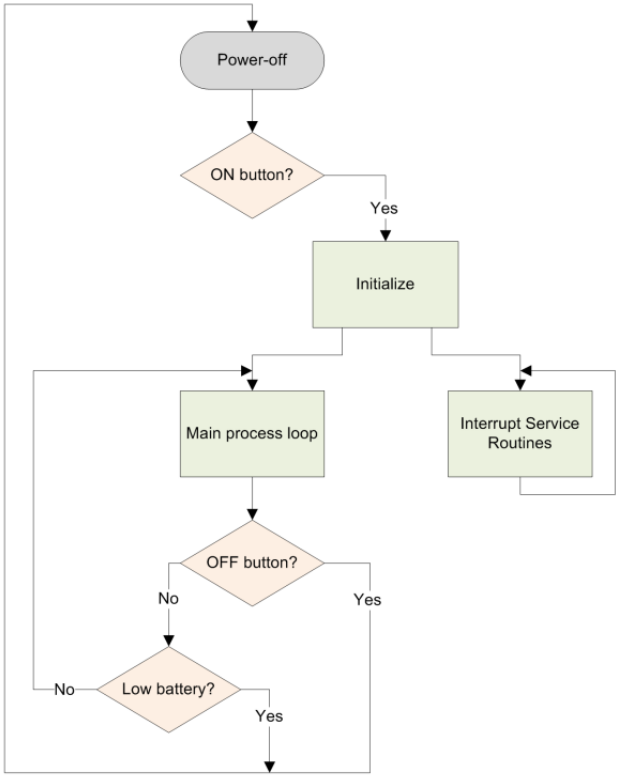

Figure 3.27: Operation diagram of the PIC18F6627 microcontroller in iObject MPU (flowchart with considerable simplification).

iObject is powered up, the Input-/Output (I/O) pins, internal state, global variables and PIC18F6627 modules used (such as EUSART, SPI etc.) are initialized and interrupts from the modules are enabled. The main process enters a loop. After each iteration the iObject's power-off button state and battery voltage state are checked. If the power-off button is not pressed and the battery voltage is above a fixed threshold, the loop is continued from the start, otherwise the microcontroller is powered down and power flow from battery is cut, effectively powering iObject down. Parallel to the main process, the peripheral modules of the PIC18F6627 can cause asynchronous interrupts, which are handled with higher priority than the main loop (as PIC18F6627 MCU only has a single processing core, the main loop processing is paused for the time that code from Interrupt-Service-Routines (ISRs) are processed).

The main loop does the following:

- Triggers the polling of the *Xsens MTx* motion sensor if the user has enabled iObject to receive motion data from *MTx*
- Parses and processes the incoming data of the two EUSART modules (one module is attached to Xsens *MTx*, the other to the *ARF32 Data* Bluetooth module)
- Generates the data packets to be transmitted from iObject over the Bluetooth link and manages their transmission priority

The ISRs handle the asynchronous events due to external input (e.g., physical pin level change, incoming data) or internal events (e.g., timer overflow, internal module ready with processing). The following ISR handles were implemented in the source code:

- Bluetooth module receive event
- Bluetooth module transmit finished event (triggers the transmission of the next byte, if one is available in the transmit buffer)
- Bluetooth module Clear-To-Send (CTS) flow control pin change
- Motion and orientation sensor module receive event
- Motion and orientation sensor module transmit finished event (triggers the transmission of next byte, if one is available in the transmit buffer)
- PIC-internal ADC conversion finished event
- Timer overflow events (multiple hardware timers are used, e.g., for an internal fixed time base and for asynchronous event timing)

Mechanical construction

The body of iObject was constructed to serve the dual duty of having good integral strength especially important to allow for firm grasps, and at the same time being an optimal mount for all the internal components. The mechanical parts were all designed in Computer Aided Design (CAD) software. The plastic parts were manufactured from Acrylonitrile Butadiene Styrene (ABS) thermoplastic using a Fused Deposition Modeling (FDM) [Str] rapid prototyping 3D-Printer and the metal parts were milled using a Computerized Numerical Control (CNC) machine from a very strong aluminum alloy (type 7075). An explosion view of iObject's internal construction is shown in Figure 3.28.

The bottom surface incorporates a power on/off switch, a charging jack, status LEDs and a debugging/programming port for the microcontroller. On top there is a custom mount for exchangeable modules [Figure 3.29] that provides instant mounting with Neodymium (Nd) magnets for light modules with limited mechanical loading and threaded M4 (x3) and M36×1 mounts for modules that need firm attachment. The base of the mount provides a 4-pole jack for power and digital I/O to be used by active modules.

3.3.2 Exchangeable modules

To adhere to the fundamental idea of a generic grasp and manipulation measurement tool, iObject allows for the mounting of numerous exchangeable modules. Some examples are shown in Figure 3.30. An ARToolKit [Kat] marker module can be used for absolute position localization, for pointing purposes a module can be fitted with a laser diode, and even specific tools can be mounted (table tennis bat mount, arbitrary tools, or objects with passive grippers). In the event none of the existing modules suit the particular task, an appropriate module can be constructed and built swiftly without the need for modifications to iObject. Technical drawings of the mounting so that custom modules can be developed can be found in Appendix 6.3.5 and Appendix 6.3.6.

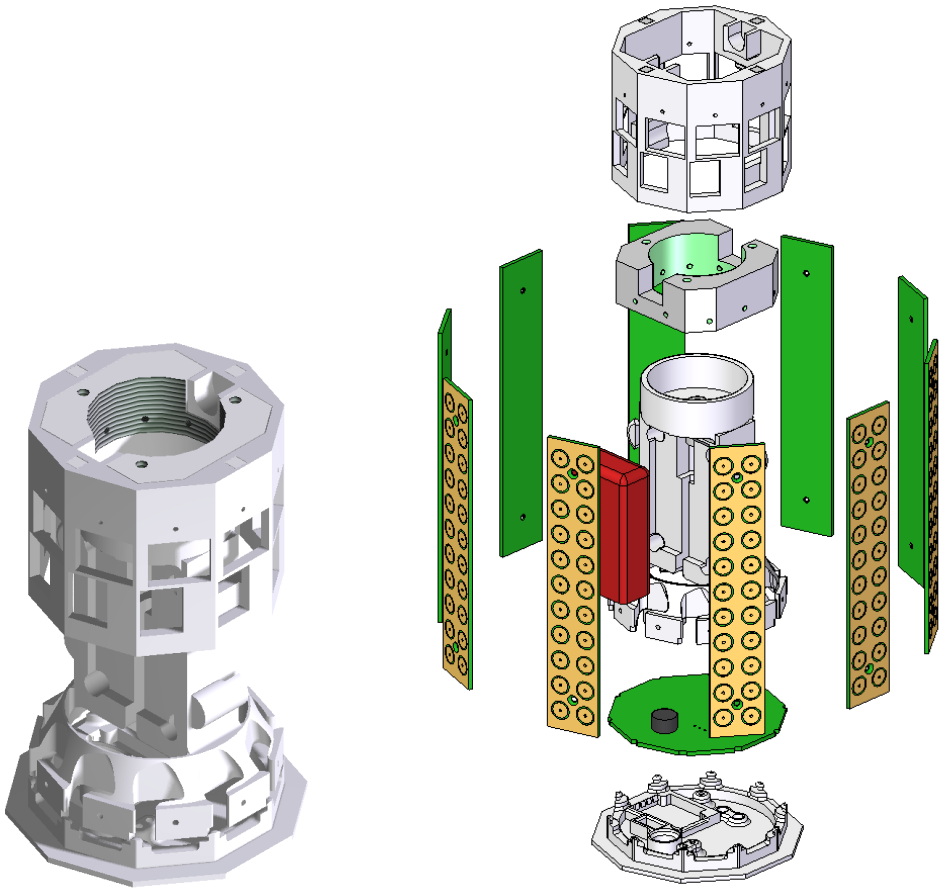

(a) Internal frame of iObject. **(b)** Explosion view of iObject's internals.

Figure 3.28: Mechanical construction of iObject.

3.3.3 Operating the iObject

The user interface of iObject can be found on the bottom plate [Figure 3.31]. To turn iObject on, a short press of the red button marked *ON* is required. To power iObject down, the black button marked *OFF* needs to be kept pressed for a minimum of 1 second. To protect the internal Lithium-Polymer battery from deeply discharging and thus resulting in damage to the battery, iObject shuts itself off if the battery voltage drops below 6.0V (whereas a normal battery voltage of 7.4V can be expected for the two Lithium-Polymer cells). According to the original datasheet of the used Lithium Polymer battery, it should not drop below a voltage of 2.6V per cell (5.2V for 2-cell battery), and therefore a 6.0V threshold provides an adequate level of protection for the battery.

To allow easy charging of the internal battery, iObject provides an externally accessible common 2.5mm DC-jack on the bottom plate. Only chargers, especially developed for charging Lithium-Polymer cells and capable of charging 2 cells in series, should be used. The middle pin of the 2.5mm DC-jack is connected to the positive terminal of the battery, the shield with the negative terminal. The battery used in iObject has a recommended charge rate of 1C, which results in an optimal charging current of 850mA. A maximum allowed charge rate is 2C (1.7A).

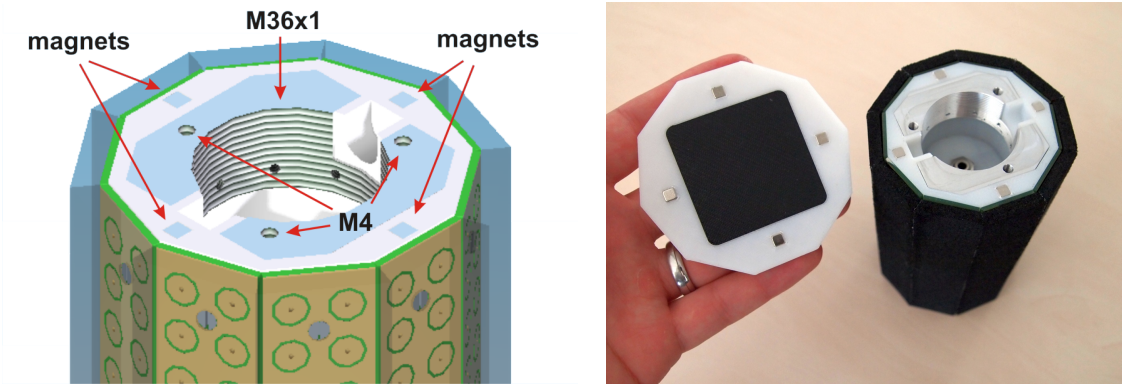

(a) Multiple mounting options for exchangeable modules.

(b) An example module with magnetic mounting.

Figure 3.29: Versatile mount for exchangeable modules.

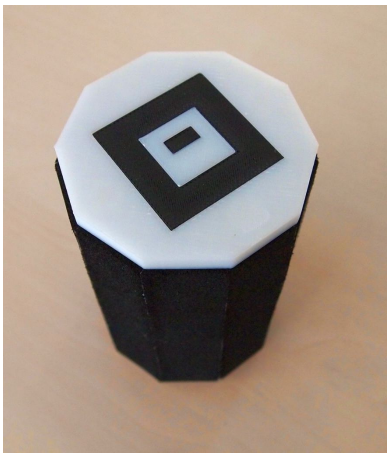

(a) ARToolKit marker

(b) Laserpointer

(c) Table tennis bat

(d) Small passive gripper

(e) Big passive gripper

Figure 3.30: Some examples of add-on tool modules.

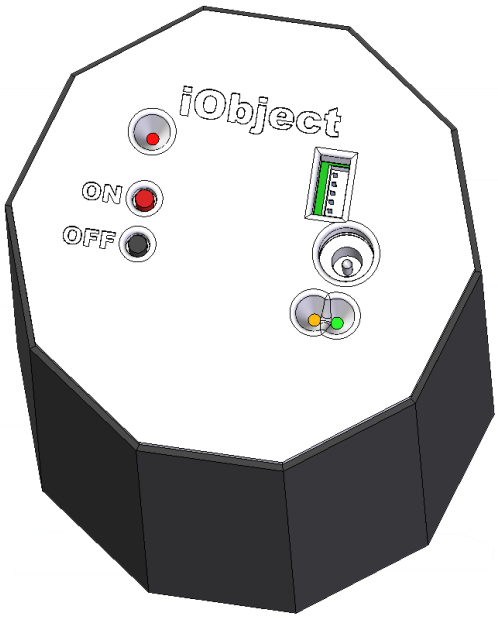

Figure 3.31: The main control user interface of iObject can be found on its bottom plate.

Although the electronics of iObject are also capable of operating during the charging process, nevertheless this is not recommended as the concurrent current draw to the battery and iObject simultaneously can possibly disturb the charging program of the charger and this might result in a false detection of an end of charge or indeed cause overcharging and damage the battery.

The bottom plate of iObject contains in addition to ON-OFF power switches:

- Red power LED that lights up if the iObject is powered
- Green status LED that lights if the iObject MPU has not encountered any errors
- Orange transmission flow LED is turned on for 1 second if the input buffers of the Bluetooth module are full and it cannot receive new data for further transmission (for example due to a sub-optimal radio signal quality the transmission speed needs to be throttled by the MCU)
- Microchip in-circuit-debugger (ICD) port for debugging and re-programming the PIC18F6627 microcontroller found on the MPU

After turning on, iObject waits for a connection from Bluetooth host. After the wireless link with the host is established, by default iObject starts streaming:

- Tactile data packets (with the maximum frame rate possible, limited by the Bluetooth wireless link signal quality)
- Battery status packets (at 1Hz)
- Internal status packets (at 1Hz)

As iObject powers-up and the link to communication partners over Bluetooth is established, iObject listens to numerous commands over the Bluetooth link [Table 3.2]. The

Activate	Deactivate	Action controlled
A	a	Global Bluetooth packet transmission
B	b	Battery status transmission
T	t	Tactile sensor data transmission
X	x	Acceleration and orientation data transmission
<none>	p	Command parsing

Table 3.2: ASCII-commands supported by iObject (default state after power-up is displayed in red).

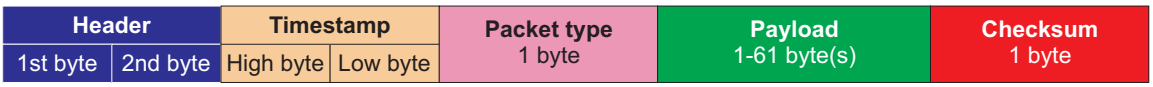

Figure 3.32: Data protocol used by iObject.

transmission of the motion tracker data is not enabled by default on power-up and needs to be enabled explicitly by user by sending the appropriate activation command.

After disabling Bluetooth link parsing by sending the ASCII character *p*, iObject enters direct communication mode with the Xsens MTx motion and orientation sensor, meaning all data sent over the Bluetooth link is relayed 1-to-1 to the motion tracker. This mode is required to re-configure Xsens MTx or to use proprietary software like Xsens original SDK/MT Manager to communicate with MTx. To re-enable command parsing, a power-cycle (OFF− >ON) is required.

3.3.4 Communication and data protocol

The Bluetooth communication module provides communication over a Bluetooth Serial-Port-Profile (SPP) that is easiest to interact with using a virtual serial port at host. The data transmitted from the main processing unit uses a custom data protocol shown in Figure 3.32.

iObject implements 4 packet types for outgoing messages:

- Tactile data packet
- Acceleration and orientation data packet
- Battery status packet
- Internal status packet

A custom packet format was developed [Figure 3.32]. A two byte header packet (constant bytes *0xF0*, *0xC4*) is used to allow easy synchronization by the receive parser. A timestamp value (16-bit counter) describes the internal time the packet is constructed in MPU and is incremented internally each millisecond and thus overflows approximately once every minute.

The packet type identifier flag is coded as:

- *0x0?* - tactile data packet, where ? is a placeholder for an allowed range of between 1 and A, informing the originating tactile board with an ID from 1 to 10 (A being 10)

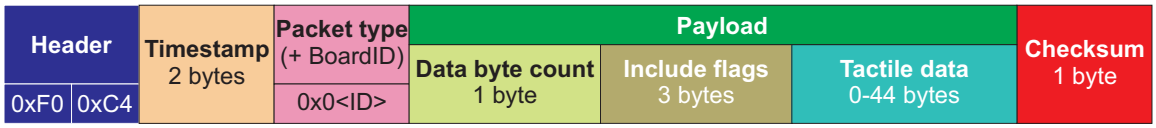

Figure 3.33: Tactile data packet used by iObject.

- *0x80* - battery status packet
- *0x90* - acceleration and orientation data packet
- *0xA0* - internal status packet

All type values not explicitly listed above are illegal and should lead the communicating host software to discard the packet and signal that there is a communication error. The payload and its length are packet type dependent and will therefore be explained in more detail in specific packet type sections below.

The checksum field is used to validate the packet and is calculated by a simple addition over all bytes (including header bytes). As the checksum field is only 1 byte long, only the last 8 bits of the sum are used (modulo *0xFF*). The simple additive method for the checksum calculation is not the most error-tolerant possible (for example it is not immune to a byte order switch, nor if one byte has the same amount subtracted as another one has added), but it is the fastest to calculate on a low-power microcontroller which does not provide a checksum calculation instruction as a hardware function.

A single packet is always considered atomic and thus cannot be interrupted with another packet.

Tactile data packet

iObject uses 10 identical pressure sensor boards, each equipped with 22 pressure sensitive cells. The main-processing unit (MPU) of iObject embeds pressure sensor data from each pressure sensor board into its own tactile data packet. Therefore 10 tactile data packets, one from each pressure sensor board, are required to transmit the complete iObject pressure sensor pattern. The MPU sends data from the pressure sensor boards in a cyclical manner starting with the first through to the tenth and then looping back to the first.

In the transmission stream, the MPU can decide to transmit other packet types (such as acceleration and orientation data packets, an internal status packet or a battery status packet).

The tactile data packet schema is illustrated in Figure 3.33. The high nibble of the packet type field for the tactile data packet is 0. Tactile boards are numbered from 1 to 10, thus the allowed range for the packet type field is *0x01* to *0x0A*. As this information requires only half of a byte, the data is crammed into the packet type lower nibble field, which would have been unused otherwise.

To save the limited wireless bandwidth, a data compression scheme was implemented, in which only taxel data with a higher than predefined threshold value is included in the payload. Through experimentation, I observed that in most grasp scenarios only a small number of the pressure sensors have contact, as could also be seen in Figure 3.26. Each taxel with a higher than threshold pressure uses 16-bits (2 bytes) in the tactile data field. The higher 4 bits of the 16 represent the internal A/D channel number, and the remaining

12-bits represent the digitalized value (with 4096 different levels). 3 flag bytes are used to indicate which pressure sensor data is included in the tactile data packet.

The digitalized value range of a single cell is from *0x000* to *0xFFF*, where *0xFFF* represents no contact and *0x000* represents maximum pressure (maximum measurable pressure, where higher pressure applied would saturate the output). The threshold for inclusion in iObject is programmed to be *0xFFE*, therefore the taxels with higher pressure values (as measured by the ADC to be in the range from *0x000* to *0xFFD*) are included in the tactile packet and will be transmitted. Depending on the included taxel count, a tactile packet from one sensor board can have from 0 to 44 payload bytes [Figure 3.34]. If the pressure value is above the threshold, the data value is included in the tactile data field and the corresponding bit in flag bytes is set (to 1), otherwise the flag bit is cleared (to 0).

Figure 3.35 displays an example of a tactile packet including the detailed flag bytes. In this tactile data packet the pressure for 8 taxels on board number 6 was above the threshold - cells 1,2,5,6,9,10,16 and 19. The data contained in this packet is extracted and displayed in Table 3.3.

Battery status packet

If sending the battery status is enabled (which by default is the case), iObject emits a battery status packet once every second. The MPU may choose automatically to omit sending the periodical battery status packet in cases where the radio wave conditions are very difficult in order to save bandwidth for the more important sensor value packets (e.g., tactile, acceleration and orientation data).

The payload length of the battery status packet is just 1 byte and it indicates the battery value on a linear scale. A value of *0x00* represents 0.0V and the maximum value of *0xFF* represents 10.0V. Note that due to the automatic low-power-shutdown feature, iObject is shut-down if the battery drops below 6.0V for more than 1 second, which means that iObject will not send a value smaller than *0x99* (that corresponds to 6.0V).

The battery status packet is displayed in Figure 3.36a. In the example [Figure 3.36b] a nominal battery value of 7.4V (*0xBC*) is transmitted. The checksum is calculated as (*0xF0 + 0xC4 + 0xF5 + 0x38 + 0x80 + 0xBC*) & *0xFF*, that results to *0x1D*.

Acceleration and orientation data packet

The factory configuration of the embedded Xsens MTx motion and orientation tracker is set to send the collected data at a predefined frequency of 100Hz. For iObject this property was not suitable, as the wireless data throughput depends heavily on the wireless Bluetooth link quality, and means that it is possible for high rate of the motion tracker data to oversaturate the link. Thus, the embedded MTx motion tracker in iObject is configured to work in a polled mode, where the MPU controls the polling frequency based on the wireless link quality.

Acceleration and orientation data is polled from MTx only if following conditions are met:

- Xsens transmission is enabled (this is not the default case when power-up is initiated, see Subsection 3.3.3 for the power-up procedure of iObject)
- The previous Xsens packet is completely transmitted over the Bluetooth link

Flag byte 1								Flag byte 2								Flag byte 3							
-	-	21	20	19	18	17	16	15	14	13	12	11	10	9	8	7	6	5	4	3	2	1	0
-	-	AD2-Ch10	AD2-Ch9	AD2-Ch8	AD2-Ch6	AD2-Ch5	AD2-Ch4	AD2-Ch3	AD2-Ch2	AD2-Ch1	AD2-Ch0	AD1-Ch11	AD1-Ch10	AD1-Ch9	AD1-Ch8	AD1-Ch7	AD1-Ch6	AD1-Ch5	AD1-Ch4	AD1-Ch3	AD1-Ch2	AD1-Ch1	AD1-Ch0

Figure 3.34: Taxel numbering and mapping of ADC channels to flag bytes in the tactile data packet.

Header		Timestamp		Packet type (+ Board ID)	Payload												Checksum
					Data byte count	Include flags			Tactile data, 16 bytes (0x10 bytes)								
F0	C4	04	F8	06	10	09	06	66	1E,B0	2E,4D	5F,F6	6C,97	9F,BF	AF,0B	4F,E0	8E,49	FA

(a) Tactile data packet from BoardID 6 with 8 active taxels.

Flag byte 1, 0x09								Flag byte 2, 0x06								Flag byte 3, 0x66							
-	-	21	20	19	18	17	16	15	14	13	12	11	10	9	8	7	6	5	4	3	2	1	0
-	-	0	0	1	0	0	1	0	0	0	0	0	1	1	0	0	1	1	0	0	1	1	0

(b) Include flag bytes *0x09*, *0x06* and *0x66* of an example tactile data packet of **(a)** expanded.

Figure 3.35: Example tactile data packet.

Cell number	AD+channel	Data Word	Channel	Pressure value
1	AD1-Ch1	0x1E 0xB0	0x1	0xEB0
2	AD1-Ch2	0x2E 0x4F	0x2	0xE4F
5	AD1-Ch5	0x5F 0xF6	0x5	0xFF6
6	AD1-Ch6	0x6C 0x97	0x6	0xC97
9	AD1-Ch9	0x9F 0xBF	0x9	0xFBF
10	AD1-Ch10	0xAF 0x0B	0xA	0xF0B
16	AD2-Ch4	0x4F 0xE0	0x4	0xFE0
19	AD2-Ch8	0x8E 0x49	0x8	0xE49

Table 3.3: Extracted tactile data for the example packet shown in Figure 3.35.

Header		Timestamp 2 bytes		Packet type	Payload	Checksum 1 byte
0xF0	0xC4			0x80	Battery value 1 byte	

(a) Battery status packet format.

Header		Timestamp		Packet type	Payload	Checksum
0xF0	0xC4	0xF5	0x38	0x80	0xBC	0x1D

(b) An example of battery status packet indicating 7.4V.

Figure 3.36: Battery status packet with an example.

- The last packet was not polled less than 20ms ago (limits the effective transmission to maximum of 50Hz)

The polling is achieved by the MPU transmitting the *ReqData* message to the MTx. For further information on the Xsens protocol, please see Appendix 6.3.7. The data from the Xsens MTx motion sensor are transported 1-to-1 into an iObject acceleration and orientation data packet shown in Figure 3.37, except when:

- the incoming message from MTx to the MPU exceeds 60 bytes, in which case the originating packet will be split at each 60 bytes into multiple acceleration and orientation data packets
- The incoming message from MTx to the MPU takes longer than 6.0ms to arrive, in which case the packet will also be split at the 6.0ms mark into separate packets

An example of complete Xsens MTx *MTData* message embedded into an iObject acceleration and orientation data message payload can be seen in Figure 3.38. For further information on the Xsens internal message format, please see Appendix 6.3.7. Figure 3.39 demonstrates an example of a possible split of the same MTx *MTData* packet data displayed in Figure 3.38.

Internal status packet

If sending the internal status is enabled (which by default is the case), iObject emits an internal status packet once every second. The payload length of the internal status packet is 9 bytes and contains the following data in the order listed:

- State flags, 1 byte [Table 3.4]
- Error flags, 1 byte [Table 3.5]
- Bluetooth connection $\overline{RTS}$ signal count, 1 byte (limited to upper value of 255)[7]
- MPU Bluetooth port status flag, 1 byte [Table 3.6]
- MPU receiver buffer peak value for ARF32 (Bluetooth), 1 byte
- MPU transmit buffer peak value for ARF32 (Bluetooth), 1 byte
- MPU MTx port status flags, 1 byte [Table 3.6]
- MPU receiver buffer peak value for MTx, 1 byte
- MPU transmit buffer for peak value for MTx, 1 byte

The internal status packet format is displayed in Figure 3.40. The internal Bluetooth and MTx receive and transmit buffers are 250 bytes in size, thus the value of the appropriate flag bytes can be in between *0x00* and *0xFA*. An example of the internal status packet for normal error-free operation is displayed in Figure 3.41.

[7] This counter is incremented each time a hardware flow control (Request-To-Send) signal is cleared by the *ARF32 Data* Bluetooth module to notify the MPU that it's input buffers cannot handle new data at the present time.

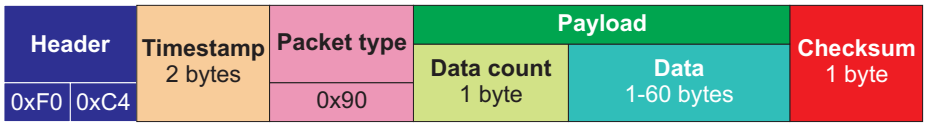

Figure 3.37: Acceleration and orientation data packet format.

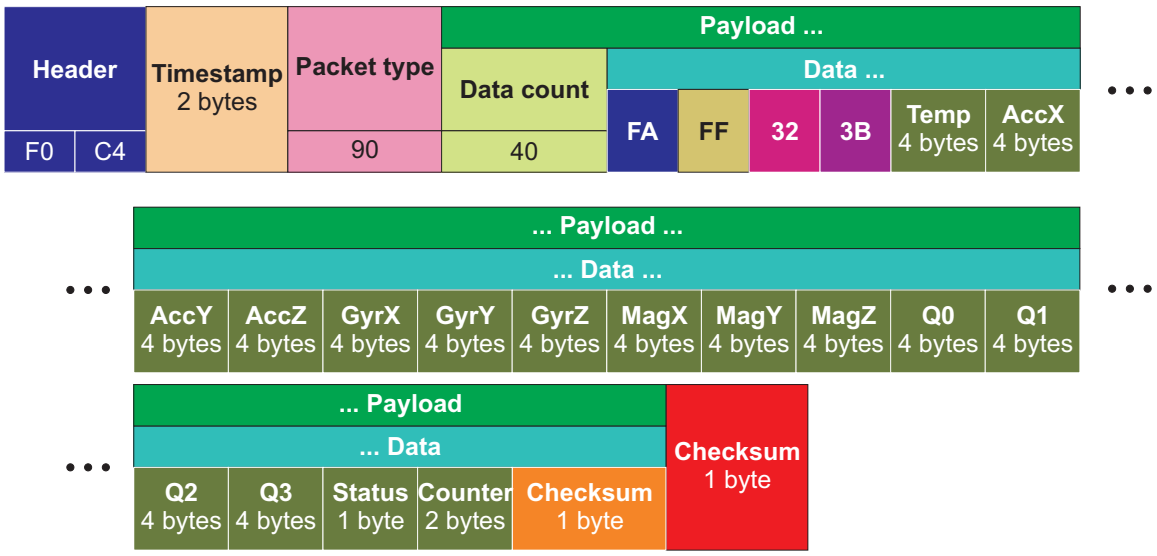

Figure 3.38: An example of an acceleration and orientation data packet with Xsens MTx *MTData* packet and with a calibrated data payload (orientation in quaternion mode). For further information see Appendix 6.3.7.

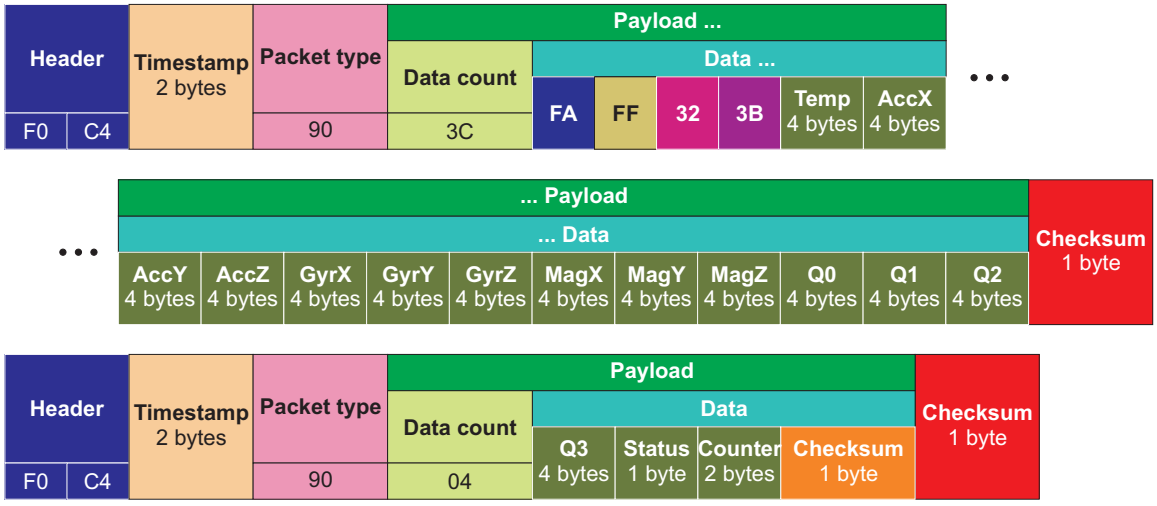

Figure 3.39: The same Xsens MTx *MTData* packet content as in Figure 3.38, but split into two iObject's acceleration and orientation packets.

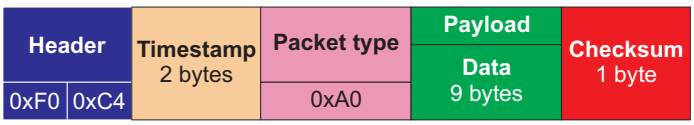

Figure 3.40: Internal status packet format.

Bit	Description
0	(internal timing flag, gets set every second)
1	if set (=1), Bluetooth port input parsing on MPU is enabled
2	if set, transmitting the internal status packet is enabled
3	if set, transmitting the pressure sensor packet is enabled
4	if set, transmitting the acceleration and orientation packet is enabled
5	if set, transmitting the battery status packet is enabled
6	if set, global Bluetooth communication is enabled
7	if set, the internal battery voltage is higher than low-battery threshold

Table 3.4: State flag bit mapping of iObject's internal status packet (Most-Significant-Bit (MSB) is bit 7, Least-Significant-Bit (LSB) is bit 0).

Bit	Description
0	Battery value packet transmission was skipped at least once (for example due to a heavy load on Bluetooth link)
1	MTx port input buffer has overflown and thus become invalid
2	Bluetooth port input buffer has overflown and thus become invalid
3	MTx port transmit buffer has overflown and thus become invalid
4	Bluetooth port transmit buffer has overflown and thus become invalid
5	MPU internal pressure sensor buffer has overflown
6	MPU internal ADC was triggered before last conversion was ready
7	Pressure board ADC replied with an other than requested channel data

Table 3.5: Error flag bit mapping of iObject's internal status packet (MSB is bit 7, LSB is bit 0).

Header		Timestamp	Packet type	Payload								Checksum
F0	C4	2 bytes	0xA0	FE	00	00	04	00	A4	04	3C	01	22

Figure 3.41: Internal status packet example.

Bit	Description
0	Transmit buffer full (no error, just information)
1	Receive buffer full (no error, just information)
2	Receive buffer empty (no error, just information)
3	Receive UART module error
4	Receive buffer overflow
5-7	unused

Table 3.6: Status flags of MPU Bluetooth and MTx ports (MSB is bit 7, LSB is bit 0).

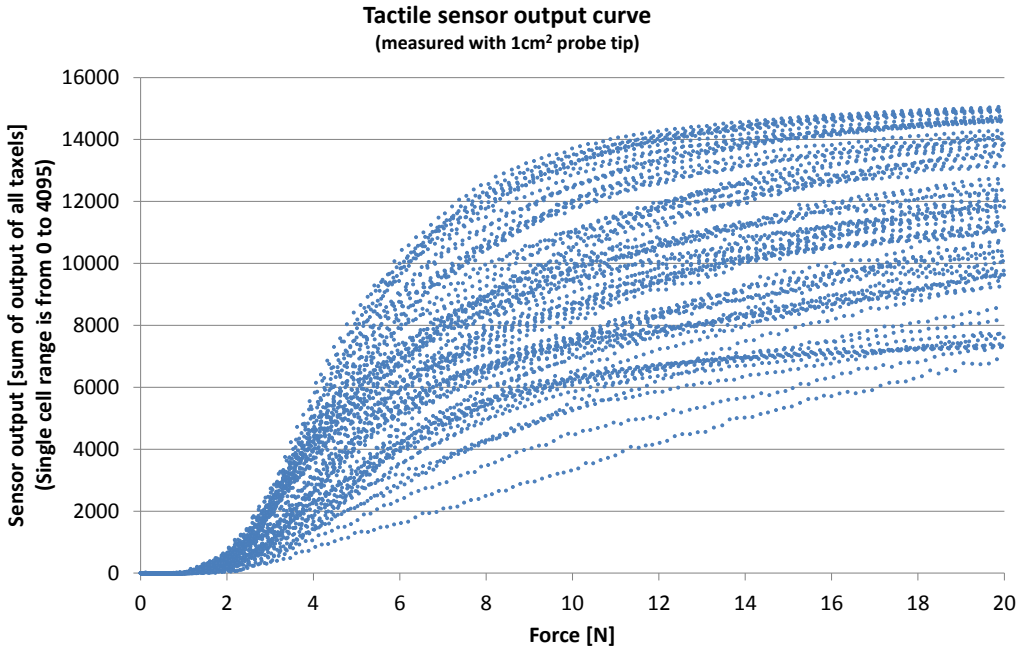

Figure 3.42: Characteristic hyperbolic output of resistive tactile sensor cell in iObject.

3.3.5 Performance evaluation

With favorable wireless link conditions, up to 250 tactile data frames per second can be achieved for a typical grasp scenario while simultaneously transmitting motion tracking data at up to 50 frames per second.

Data capture and live visualization software for Linux and Windows hosts were implemented (the initial Linux port from my original .NET host program was done by Tobias Röhlig).

The sensitivity of the tactile sensors, their signal curve and the latency of the system, which is an important parameter for time critical tasks such as the real-time control of robots, were evaluated and are now reported upon.

Tactile sensitivity

The tactile sensor signal curve was verified using the custom measurement rig presented in Appendix 6.1 by ramping up the force on different tactile cells using a push-style scale with a 1.0cm^2 circular flat probe tip and simultaneously reading out the ADC output of all cells. The resulting characteristic curve over 50 trials is shown in Figure 3.42. The usable tactile sensor pressure is in the range of 4 to 200kPa.

As can be observed, the variance of the output is unfortunately large and results from the simple circular taxel shape, implemented in the first iObject, that is very dependent on the position of contact relative to electrodes and the ground-plane border. Subsection 3.3.7 discusses a considerably improved version that is currently under construction.

Latency measurement

To evaluate the suitability of iObject for controlling devices in real-time (e.g., robotic body parts such as arms, hands, head), the latency of iObject was measured. The effect on latency was examined for factors such as the wireless range, applied pressure magnitude, concurrent transmission of motion data and concurrent transmission of tactile data with different amounts of taxels active (to evaluate the impact of the implemented tactile data compression scheme). To take high accuracy temporal measurements, a custom built measurement device based on a PIC18 microcontroller and a probe clamp was constructed that can achieve 250ns timing accuracy. One taxel in iObject was designated for the latency measurement and connected to the test device electrically with spring probes [Figure 3.43]. Each measurement run started with a field-effect-transistor in series with a resistor closing and thus imitating an instantaneous pressure exertion. 5 different resistor values were used (short-circuit, 1K, 47K, 470K, 4.7M) simulating pressure values from approximately 3 to 100kPa. To simulate a typical grasp scenario with approximately 20% of iObject taxels in contact, a rubber-ring was wrapped around the sensor surface exerting pressure an arbitrary 20% set of iObject taxels [Figure 3.44]. To test the worst case scenario of maximal tactile sensor transmission, numerous rubber rings were evenly distributed along the cylindrical surface to generate non-zero sensor readings on taxels [Figure 3.45]. For each test case a minimum of 100 measurements were performed in the presence of other active wireless equipment on the used 2.4GHz band (e.g., wireless LAN, other Bluetooth devices).

As expected, concurrent transmission of other sensor values has a strong impact on latency as is illustrated in Figure 3.46. In contrast, the applied pressure (or resistance value) has no statistically significant effect on latency (with statistical significance considerably greater than 0.05). The distance of the wireless connection increases the latency by approximately 2ms per meter (if a linear regression model is assumed). In looking at Figure 3.46 we notice that for the case of the large area contact, which is not very likely to happen in a real world scenario, the average latency was doubled to 82ms compared to the 38ms latency observed for a single activated taxel. The transmission of motion data adds a insignificant 2ms to the average tactile sensor latency. As can be seen from the graph, although the standard deviation is relatively narrow, minimum and especially maximum raw values (displayed by the whiskers) vary more heavily, which can be explained by the nature of wireless link which has fixed transmission timeslots and data re-transmission in case of packet loss.

The average latency of iObject has a similar range to that of typical vision sensors used for robotic control (e.g., cameras outputting 25/30 fps). This allows iObject to be even used as a real-time input controller for robotic devices, provided that the rare situations of higher peak latency, induced by wireless disturbances, are intelligently handled.

3.3.6 iObject Applications

In this section two initial iObject studies are discussed. In the first, iObject was used in a psychology and sport sciences study to investigate the difference between bimanual rotation when performed alone and then afterwards with a partner. In the second application, iObject was used to evaluate different grasp quality metrics that are commonly used to grade the quality of grasps in robotics. Done with real people, the participants subjective grasp quality perception was compared to a mathematically calculated grasp quality from the data captured using the tactile sensors around the iObject hull.

Very recently, Twardon *et al.* [TFR13] presented a novel way of controlling robotic ma-

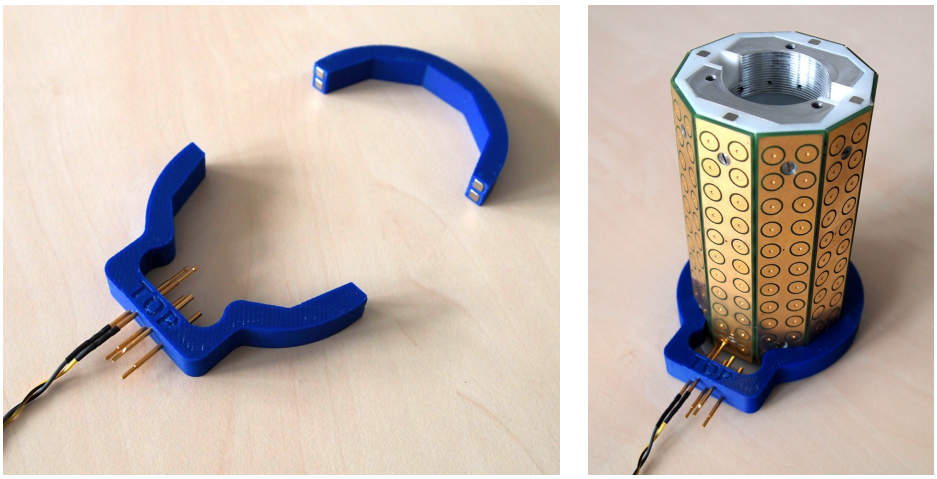

(a) Spring probe clamp.

(b) Attached measurement clamp.

Figure 3.43: Spring probes clamp for latency measurement.

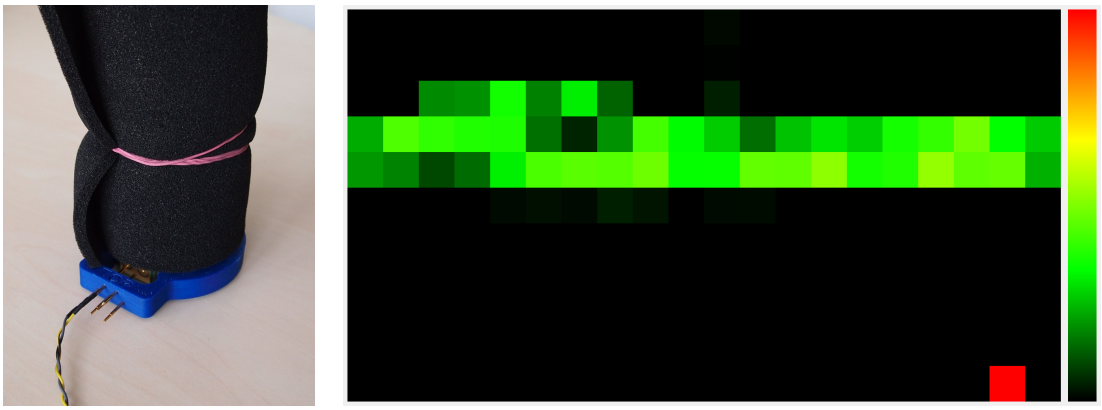

(a) Rubber ring simulating a typical grasp scenario.

(b) Matching GUI output displaying tactile data. (The red taxel in bottom right is the probe taxel)

Figure 3.44: Simulating a typical pressure pattern of approximately 20% of taxels in contact.

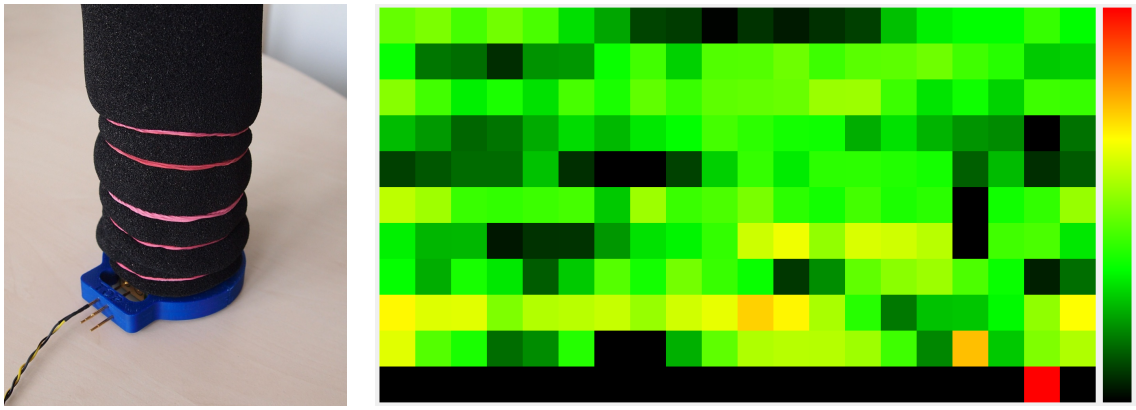

(a) Multiple rubber rings simulating full contact.

(b) Matching GUI output displaying tactile data.

Figure 3.45: Simulating the worst case scenario for tactile data compression algorithm with most taxels having non-zero values.

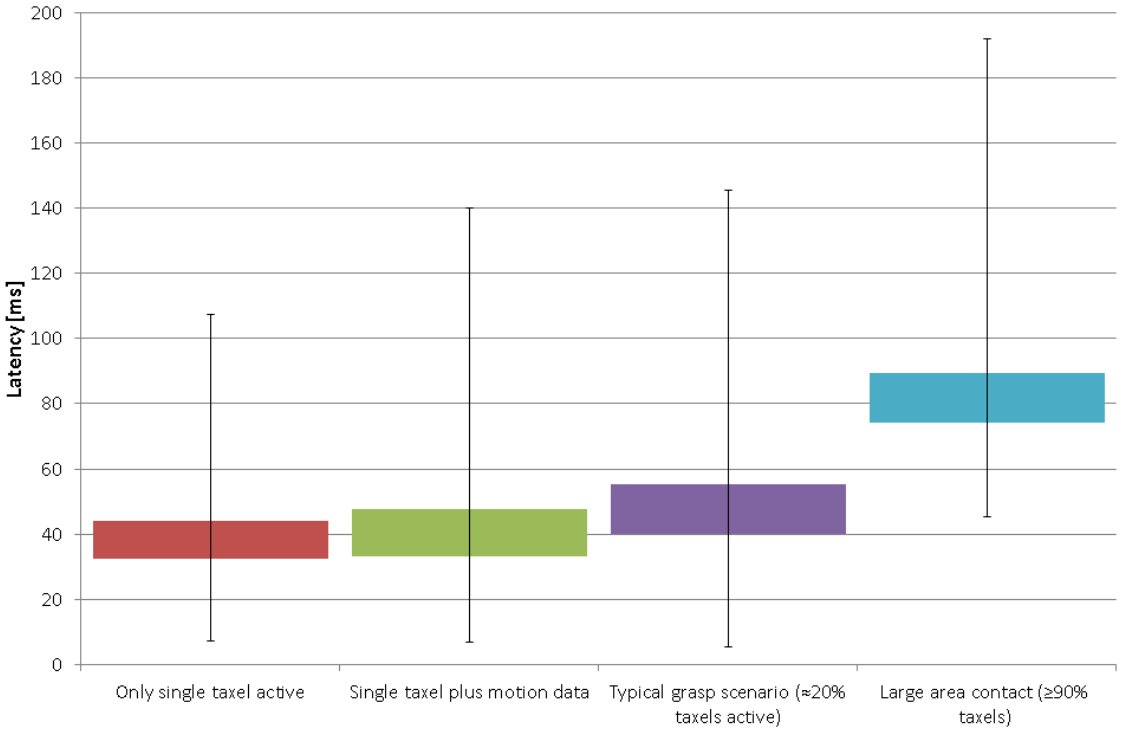

Figure 3.46: Latency of iObject as measured over the Bluetooth link under different conditions. The color blocks display the standard deviations, while the whiskers show the minimum and maximum values measured.

nipulators using iObject and eye-tracking equipment. The joint or end-effector to be manipulated was selected using gaze, and the control was activated by squeezing the iObject. The subsequent movement of the selected joint or tool center point was then controlled by intuitively rotating or shifting iObject to desired positions.

Evaluating cognitive load through hand motion - study 1

The goal of this preliminary experiment was to compare the main motion parameters when bimanually rotating iObject around its major axis at maximum comfortable speed, a task similar to the turning motion needed to screw/unscrew caps. The first part involved one participant performing the rotation alone. To successfully rotate iObject, all subjects used a strategy by which one hand rotated the object while the other hand had no contact, then a switch took place and the opposite occurred. This was repeated for the duration of the trial. In the second part, a dyadic situation was setup in which two participants were evaluated as they cooperatively turned the object with one hand each. The direction of rotation and the hand chosen for rotation in the second part of the experiment were not dictated to the participants.

8 participants took part in the experiment, each one performing a bimanual iObject rotation by themselves once and then performing a cooperative rotation with a partner once (the measurement set therefore consists of 8 solo and 7 twin runs).

The duration of contact for each hand (from contact of the first finger to contact loss of the last finger) was evaluated separately, as well as the accumulated pressure applied to iObject (sum of all taxels during contact) divided by the duration of contact.

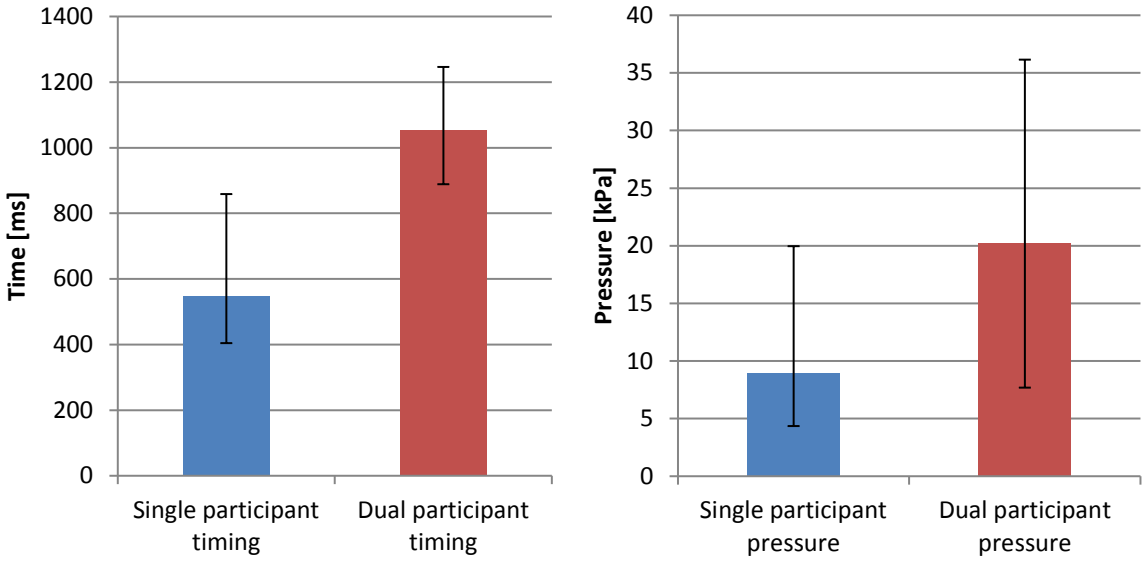

Figure 3.47: Bimanual rotation timing and pressure differences between the single participant case and the dyadic case. The whiskers show the minimum and maximum values measured.

The experiment revealed the following (also see Figure 3.47):

- Participants performing the rotation alone had an average left/right hand switching time of 0.55 seconds (with standard deviation of 0.15) while exerting an average pressure of 8.97kPa per hand (with a high standard deviation of 4.65).
- When doing the experiment with a partner, the inter-subject hand switching time increased by 93% to 1.05 seconds. The applied average pressure also increased by 116% to 20.24kPa.

The experiment highlights the higher cognitive load required (slower turnaround time) and higher importance of tactile feedback due to uncertainty (higher pressure exerted) when the manipulation was performed cooperatively. In future work, the captured raw data could be analyzed in more detail, including information such as the contact order of the fingers, overlapping finger time durations, rotation speed or angle per hand, and rotational symmetry. This information has the potential to provide new insights into human grasping and could extend and improve our current robotic setup, which is already capable of opening a jar in an unconstrained setting [SEHR10].

Evaluation of grasp quality metrics - study 2

Grasp quality metrics have been long studied, due to their importance to evaluate the quality of a grasp made with a robotic hand. However, the application of these quality metrics to grasps made by humans has only recently begun to receive some attention [BXB+10]. In this experiment we evaluated and compared different grasp quality metrics using data obtained from iObject's tactile sensors and subjective grasp quality data gathered orally from participants. The experiment includes power grasps and precision grasps with differing number of contact fingers. The results give hints towards how realistic or usable such grasp quality metrics are, e.g., in the field of robotic grasping.

Figure 3.48: Experimental setup for grasp quality metrics evaluation. iObject was picked up and placed down by participants between two predefined positions on the table using a grasp type and pace according to presented visual and audio stimuli.

This experiment was done in cooperation with Dr. Maximo A. Roa and Dr. Claudio Castellini from the German Aerospace Center (DLR), Institute of Robotics and Mechatronics and the results were published in 4th IEEE RAS & EMBS International Conference on Biomedical Robotics and Biomechatronics (BioRob 2012) [RKC12].

For this experiment two modifications were made to the iObject design. First, the original sensor material, the Weiss-Robotics conductive foam, was replaced with a softer version with higher electrical conductivity, shifting effectively the measurement range of the tactile sensor from the original 4 to 200kPa range into a 1 to 30kPa range and thus providing better insights into subtle grasps. Second, as only very short and simple object movements were targeted in this experiment, the wireless Bluetooth connection was replaced by a more reliable cable based USB 2.0 connection, which allowed iObject to be powered from the PC and remedying the necessity to have to care for the charging of the internal battery.

The task presented to the participants, who were seated comfortably in front of a table, was to grasp iObject using 9 different grasp types and to move iObject between two predefined marked positions on the table [Figure 3.48]. The 9 grasps consisted of a single power grasp to the side of the iObject and 8 precision grasps with 2,3,4 and 5 fingertips to both the side and top of iObject [Figure 3.49]. The specific grasp types and timing were presented on a laptop using visual and audio stimuli. After each movement was completed, participants retracted their hands to a rest position. Each grasp type was repeated 6 times in total, resulting in a total of 54 recordings for every subject. Tactile sensor data from iObject was collected at 300 frames per second, and was saved to a laptop. The data collected was analyzed using six separate well established grasp quality metrics, commonly used in robotic grasp planning:

M1 *Largest minimum resisted wrench.* This is the most common quality measure used in grasp planning and is the largest perturbation wrench that the grasp can resist independently of the perturbation direction [FC92]

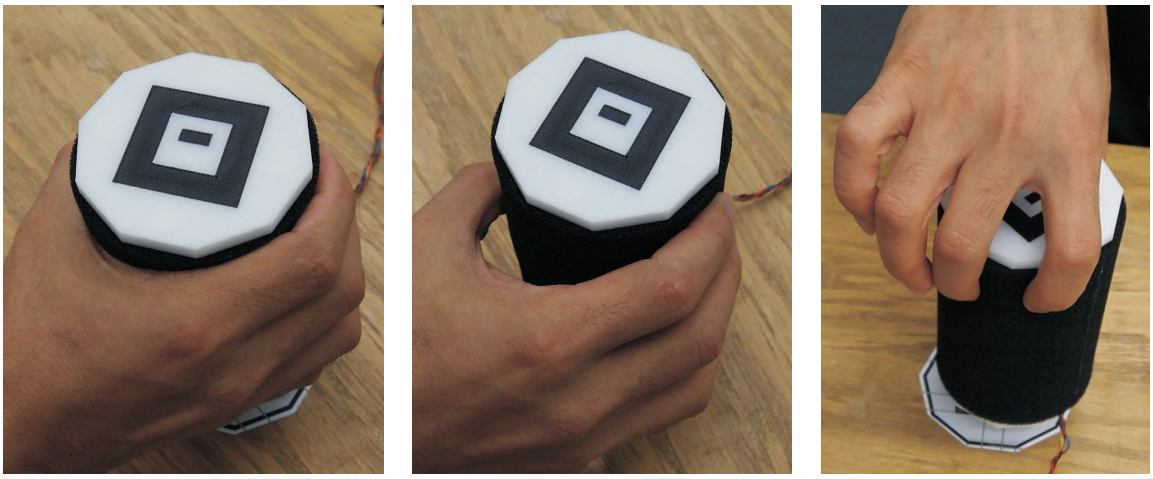

(a) **(b)** **(c)**

Figure 3.49: Some examples of the used grasp types: **(a)** Side power grasp. **(b)** Side precision grasp with 5 fingers. **(c)** Top precision grasp with 3 fingers.

M2 *Volume of the convex hull* is a measure independent of the reference system used in torque computation [MA99]. The maximization of the criterion leads to more robust grasps in general, although with the same volume a grasp could stand much less force than another one in a certain direction

M3 *Distance between the centroid of the contact polygon/polyhedron and the center of mass of the object.* Minimizing this distance minimizes the effect of the inertial and gravitational forces on the grasp [PSS+97]

M4 *Volume of the grasp polyhedron.* This metric is based on the volume of the convex hull of the contact points and is a generalization of the idea of maximizing the area of a triangle for a tripod grasp [CFMdP03]

M5 *Minimum singular value of the grasp matrix.* Larger values of this metric indicate that the grasp is farther from a singular grasp configuration (i.e. that the grasp loses the ability to withstand external wrenches in one or several directions) [Shi96]

M6 *Grasp isotropy index of grasp matrix.* This metric looks for a uniform contribution of the contact forces to the total wrench applied on the object, i.e., it tries to balance the internal forces of the grasp [Shi96]

For more information on the grasp quality metrics evaluated and for greater detail on the experiment itself, please refer to the original publication from this experiment [RKC12].

The large amount of data generated during the experiment allows different types of comparisons to be evaluated. First, metrics *M1* and *M2* were used to compare the estimation of grasp quality, for the case of region contact. Second, we evaluated the quality of different grasp types and the influence of the number of fingers involved in the grasping action with all considered quality metrics (*M1* to *M6*), this time when the region is approximated by a single point of contact (which is a common assumption in grasp planning).

The subjective impression of grasp robustness that the users reported in the oral survey that was performed in parallel with the experiment is summarized in Table 3.7.

Grasp type	Average ± Std.Dev.
Side, 5 fingers	6.00 ± 1.16
Side, 4 fingers	5.29 ± 1.38
Side, 3 fingers	4.43 ± 2.07
Side, 2 fingers	2.71 ± 1.70
Side, power grasp	7.00 ± 0.00
Top, 5 fingers	5.29 ± 1.11
Top, 4 fingers	4.71 ± 1.60
Top, 3 fingers	3.57 ± 1.27
Top, 2 fingers	2.00 ± 0.81

Table 3.7: Subjective impression of grasp robustness using a 7-point Likert scale[8](the higher the value, the better the grasp robustness). (Table source [RKC12])

M1		M2		M3	M4	M5	M6
region	point	region	point				
0.94	0.93	0.82	0.75	0.49	0.92	0.93	0.92

Table 3.8: Correlation index between the analytical metrics and the subjective perception of grasp robustness for the 6 grasp quality metrics considered. (Table source [RKC12])

To provide an assessment on the relation between the subjective perception of the participants and the analytical results, Table 3.8 indicates the Pearson product-moment correlation coefficient between the quality metrics and the results of the perception survey. The coefficient was computed taking into account only the grasps where each quality measure was valid (for instance, the case of 2 finger grasps is not considered for *M5* and *M6*). Our experiment revealed that the best correlation is obtained for *M1 region*. Despite the underestimation of grasp quality that the punctual approximation to the contact region creates, the correlation index was also very high for the case of *M1 point*. Other quality metrics with high correlation coefficients were *M4*, *M5*, and *M6*, although in the case of *M4* the measure was only valid for 4 and 5 finger grasps.

For an improved grasp quality assessment, a combined index that mixes the results of several quality metrics could be worth exploring. Such a combined index could also include quality metrics that take into account the posture of the grasping hand, which was not considered in this experiment.

3.3.7 Future work

As one of the biggest observed drawbacks of iObject that was noticed in some of the experiments conducted was its relatively low tactile sensor spatial resolution of 10mm. Increasing the spatial tactile sensor resolution and the sampling rate using the current sensor technology is possible, as will be demonstrated in a later project (Section 4.1) in which the high sampling rate was used for slip detection [SSPR10].

The next generation iObject, called *iObjectPlus*, is currently under development. It

[8] *Likert scale* is a metric used to represent people's attitudes to a topic and was named after its developer Rensis Likert [Oxf09].

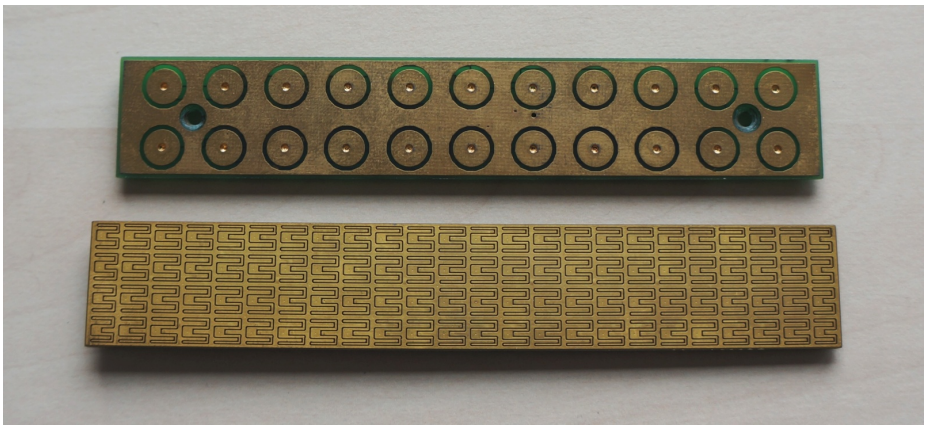

(a) iObject (top) and iObjectPlus (bottom) sensor board comparison. Notice the new electrode shape and increased taxel count from 22 to 96.

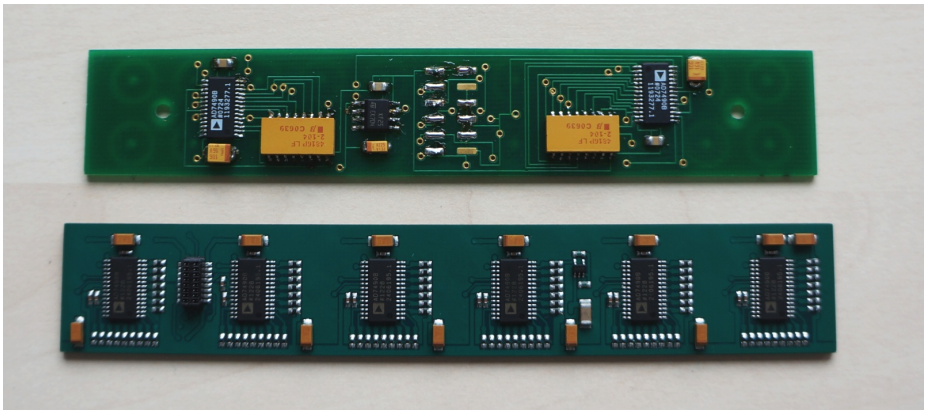

(b) The component sides of iObject's (top) and iObjectPlus' (bottom) sensor boards. iObjectPlus' sensor board incorporates six AD7490 ADCs instead of only two on the original version.

Figure 3.50: Sensor board comparison of the original iObject and the improved iObjectPlus.

introduces a newer, more sensitive, electrode shape (see Section 4.1 for details) and will have double the spatial resolution resulting in a more than quadrupled taxel count. The original iObject sensor boards were hard-wired with flexible cables to the mainboard, whereas in iObjectPlus a connector based attachment will allow considerably less tedious maintenance tasks to be carried out. Figure 3.50 displays the prototype of the iObjectPlus sensor board next to the original iObject sensor board. Appendix 6.3.9 presents the schematic of the new iObjectPlus sensorboard.

The benefit of increased spatial resolution can be visually observed in Figure 3.51, in which a high resolution tactile image of two fingers touching the new sensor are depicted. Compared to the original iObject, the tactile image of the two fingers in contact has significantly higher detail (see Figure 3.26 which shows a much reduced spatial resolution reading at the fingertips).

However the increased tactile sensor spatial resolution necessitates increasing considerably the wireless bandwidth of iObjectPlus. Instead of 220 taxels, data from 960 taxels in the new iObjectPlus need to be transported. Wireless LAN (IEEE standard 802.11) will

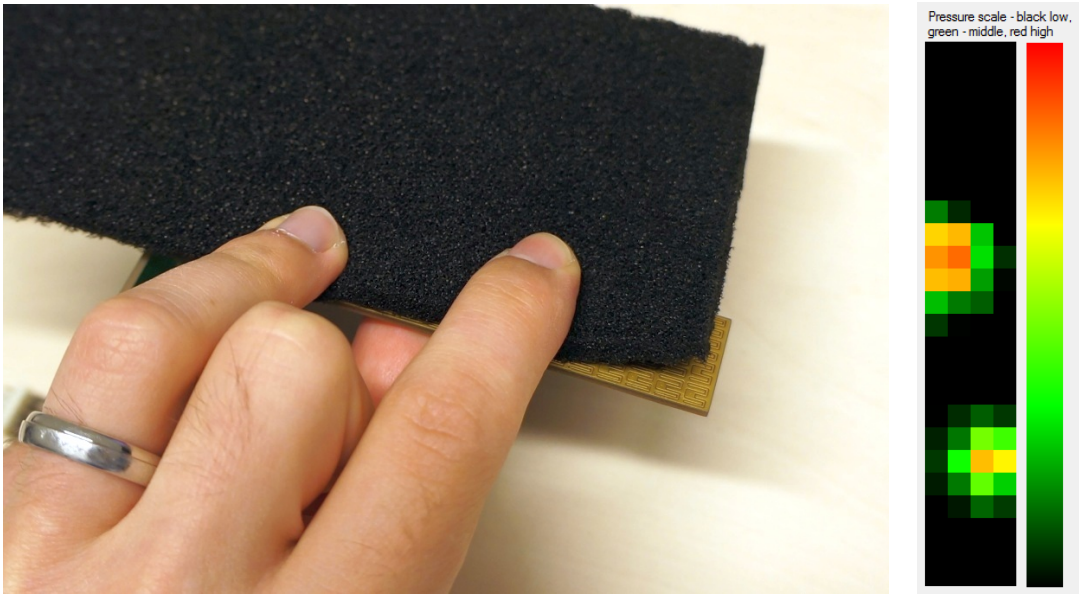

(a) Touching the iObjectPlus sensor sheet with 2 fingers.

(b) Sensor output.

Figure 3.51: Example output of iObjectPlus sensor sheet with 96 taxels while touching the sensor with 2 fingers. Notice the informative rich sensor output due to four times higher taxel density than original iObject.

allow for a magnitude improvement in data throughput, with only a slightly higher space allocation needed for the components and a slightly increased current draw. The latter can be circumvented as the development of batteries based on Lithium-Polymer chemistry has advanced since the initial iObject was developed and will ensure full-day operation can be maintained using the same physical sized battery as in the original model. A new prototype utilizing Texas Instruments CC3000 wireless LAN module is at the time of writing under development. iObjectPlus will support, as an alternative to wireless communication, USB cable based data transmission for studies in which high mobility is not required.

Motion sensing in iObjectPlus will be performed with an InvenSense MPU-9250 [Inv] nine axis microelectromechanical systems (MEMS) device instead of Xsens MTx motion tracker. This decision was influenced by significantly reduced sensor cost and considerably smaller space requirements, while at the same time achieving similar sensor performance.

A number of further improvement ideas for future iObject versions are also being discussed. Instead of streaming real-time sensory data over radio waves, an interesting option would be to use modulated light as a signal carrier instead. IEEE has devised a standard 802.15.7 for visible light data communication [RRL12] and research in this direction has already been presented [LVX, Fra]. For psychological or sport science experiments it would be beneficial to integrate humidity and surface temperature sensors to sense further modalities of human participants. Finally combining tactile sensors with haptic feedback devices on the surface of iObject would allow active feedback to be given to the user. In its simplest form it could take the form of a simple global vibration or indeed more fine grained localized vibrations could be produced. This could open up opportunities for many interesting new research directions.

3.4 Towards natural control of dexterous hand prosthesis

In case a hand is lost, for example either due to illness or injury, a hand prosthesis can often regain some of the lost functionality. Common more affordable hand prostheses, although visually mostly undistinguishable from the normal human hand, have significant capability drawbacks, providing mostly just simple single degree-of-freedom (DOF) gripper functionality. Although, lately a small number of multi-DOF mechanical hands have emerged, the problem of naturally and reliably controlling such complex devices has until today been yet unsolved. Rehabilitation community has experimented for decades using surface electromyography (sEMG) as means of input. By placing the sEMG electrodes around the lower arm on top of the muscles driving the fingers, a non-invasive way to gather (also remnant) muscle activity is possible. However, as the lower arm contains a high number of finger driving muscles, and the muscles are closely packed side-by-side and sometimes also intertwined, the signal captured by sEMG electrodes from the surface of the arm is a noisy mixture of single muscle activity. Machine learning algorithms have been demonstrated that allow posture classification by extracting relevant data from such noisy sEMG signals [BvdS06, CGDS09, CAC+11]. However, such current state of the art hand prosthesis control, relying on surface electromyography (sEMG) and hand posture classifications has at least 3 disadvantages:

- it forces the user to select from a limited set of predefined grip types
- the stability of the prosthesis depends heavily on the accuracy and decision making speed of the classifier
- it enforces no control over the force the prosthesis applies

The projects explained in this section try to fight these problems by concentrating on prediction of finger forces over the continuous manifold. Towards this end, two sensor systems were developed. First, a finger force measurement reference system is introduced in Subsection 3.4.1. Second, a bracelet with tactile sensing for capturing the intended finger forces from the muscle bulgings in the forearm is presented in Subsection 3.4.2.

3.4.1 Apparatus for precisely measuring single finger forces

In the first step towards development of control algorithms towards multi-DOF force driven hand prosthesis, we propose to investigate the correlation between muscle activations and single finger forces on able bodied participants. This would then, in a later step, provide us a basis for controlling the finger forces in the hand prosthesis using the muscle activations alone, as would be the case in real prosthesis used by amputees.

To be able to perform such studies for creating the mapping, in addition to capturing muscle activations, a reference finger force measurement is necessary. Our initial experiment, conducted together with Dr. Claudio Castellini from German Aerospace Center (DLR), implemented a modular tactile sensor array (see Section 4.1 for further technical details of the sensor used) for capturing the exerted finger flexion forces. Figure 3.52 displays the experimental setup. The participants wore sEMG electrodes around the forearm, laid the hand on the 48×48 tactile sensor array and instructions how to flex the fingers were presented on the computer screen in front of the participant. The large tactile sensor array detected the force applied orthogonally to its surface, and was therefore used for capturing

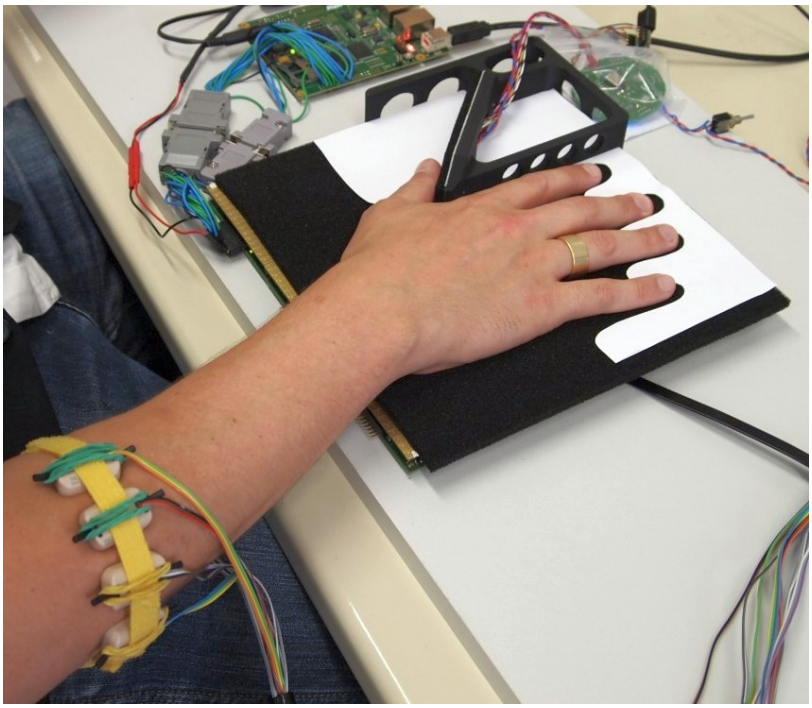

Figure 3.52: An experimental setup to capture the mapping of single finger forces to muscle activations using sEMG electrodes around the forearm and tactile sensor array below palm and fingers for force measurements.

the finger flexions (including thumb rotation). An additional tactile sensor was mounted orthogonally onto the large tactile sensor array surface to detect the thumb adduction. The experiment and the results were published in [CK12b].

We found several drawbacks of the used setup, the biggest being not able to measure forces in both finger directions (flexion AND extension). In addition, the used tactile sensor array was developed towards high initial sensitivity and high-speed sampling and not optimized to perform precise and accurate measurements.

Here, I present a novel finger force measurement device focusing on exactly these drawbacks. The developed finger force linear sensor (FFLS) can accurately and simultaneously measure the force applied by the human fingertips in both directions. It captures flexion and extension of index, middle, ring and little finger plus thumb rotation and abduction/adduction. The sensor can be easily adapted to several different hand sizes, enforces high measurement accuracy (reaching an overall accuracy of $\pm 0.35\%$ over the nominal measurement range) and is guaranteed to be linear in a high range of forces (100N in both directions for each finger). It outputs six analog voltages in the range of ± 10V, suited for processing with a data-acquisition (DAQ) card. To the best of my knowledge, no comparable device measuring simultaneously the finger forces of all fingers was available on the market or was previously presented in the scientific community.

The FFLS was developed mostly by me, I received help from Dr. Claudio Castellini from German Aerospace Institute (DLR) by providing input on the best possible hand positioning and targeted measurement range. An initial experiment to measure the maximum single finger forces was performed together with Ms. Barbara Hilsenbeck (DLR) and the results presented including the hardware development details in the 34^{th} International Conference

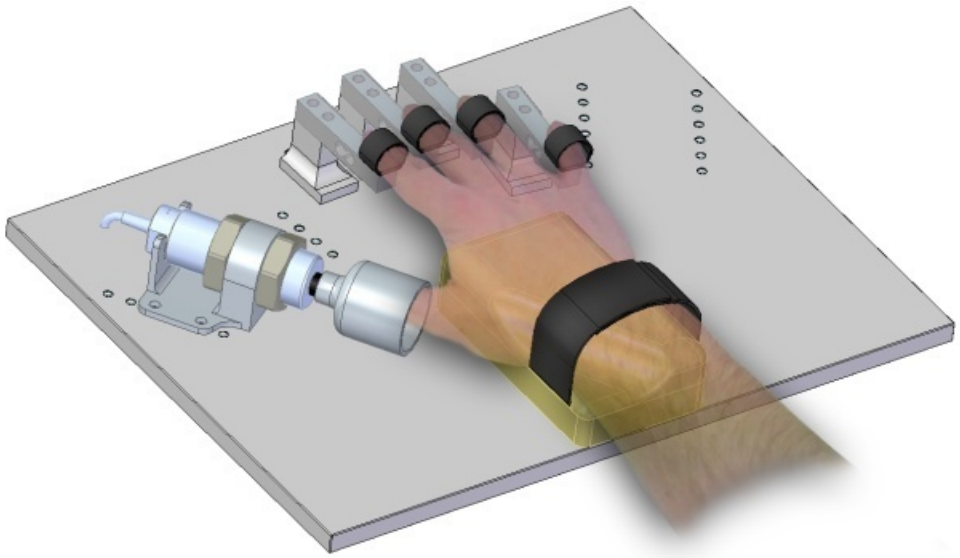

Figure 3.53: CAD-rendering of the FFLS, configured for right-hand finger force capturing.

of the IEEE Engineering in Medicine & Biology Society [KHC12]. This work was partially supported by the Swiss National Science Foundation project nr. 132700, NINAPRO (Non-Invasive Adaptive Hand Prosthetics).

The goal of the sensor in this project was to simultaneously and accurately measure the flexion AND extension forces of the fingers. Strain gauge-based sensors were chosen, commonly used in laboratory and industrial environments, where high accuracy, robustness, repeatability, bipolarity and low hysteresis are important. Unsurpassed linearity is an additional plus of this force measurement sensor type.

The requirement to accurately capture single finger forces of most adult hands with respect to various hand sizes and the hand used (left or right) necessitated a highly configurable platform for the sensors.

Figure 3.53 shows a CAD-rendering of FFLS using four single-axis strain gauge sensors for measuring the finger forces and a single two-axis force sensor for measuring the forces of the thumb. All force sensors are mounted on a sturdy aluminum plate providing a high number of adjustable positions for the sensors. Palm is supported on a CNC-milled wooden plate and direct hand contact to metal (rig and sensors) is avoided to minimize unpleasant thermal conductivity that could possibly alter the finger forces exerted by participants.

Finger force capture

The index, middle, ring and little finger flexion and extension forces are captured using an ME-Meßsysteme GmbH KD60-100N [ME-c] industrial strain gauge sensor for each finger, which is capable of measuring up to ±100N (push/pull). The sensor is very precise and has a linearity error of less than 0.1%, a hysteresis error of less than 0.1% and a drift of less than 0.1% over 30 minutes. The strain gauge bridge output is rated at 0.5mV/V. The KD60 sensors are connected to ME-Meßsysteme GmbH GSV-1L 010/250/2 signal amplifiers [ME-a] with 2mV/V input bridge sensitivity, resulting in ±2.5V output for KD60 ±100N loading. The integrated low–pass filter cutoff (-3dB) frequency of the GSV-1L amplifier is set at 250Hz.

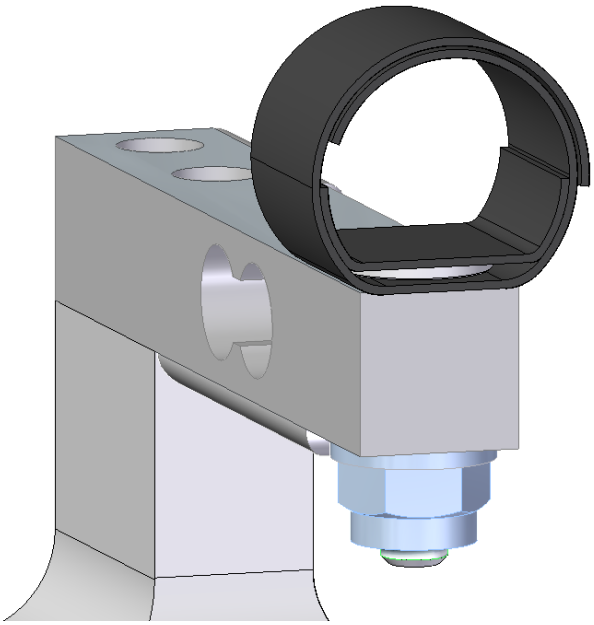

Figure 3.54: A close-up showing the adjustable hook-and-loop finger attachment mounted to the industrial strain gauge force sensor. The top of the custom metal M5 bolt is covered with another piece of hook-and-loop band to avoid direct finger on metal contact which ensures greater comfort.

The fingers are attached to the sensors using adjustable hook-and-loop bands, which are connected to the strain gauge sensors with a custom bolt [Figure 3.54]. This allows a robust connection of fingers of different sizes and shapes to sensors with minimal slack.

Thumb force capture

Thumb forces are measured across two axes, thumb flexion/extension and thumb adduction/abduction. An RFS-150XY-100-8-3 radial dual–axis strain gauge sensor [Hona] from Honigmann Industrielle Elektronik GmbH with ±100N range is used for this purpose. It has an accuracy class of 0.25 with a rated output tolerance of less than 0.2%. Each axis of the RFS-150XY is connected to a Tensiotron TS503 strain gauge amplifier [Honb] from the same manufacturer, with an accuracy class of 0.1. Nominally, a ±100N loading on the RFS-150XY produces an output of ±10V on the TS503s. The TS503's integrated low-pass filter cutoff (-3dB) frequency is set at 55Hz.

In tests it proved difficult to strap the thumb to the sensor with the hook-and-loop bands and simultaneously avoid slack in both movement axes. Therefore, instead of a hook-and-loop solution, the thumb is attached to the sensor using an exact gypsum cast that is custom made for each participant and that allows a perfect fit between the thumb and the sensor.

Data acquisition and sensor calibration

The output of each force sensor axis is connected to a dedicated signal amplifier, which converts the applied force loading into voltage [Newtons→Voltage]. The analog voltage outputs of the converted force signals are provided on a 68-pin male SCSI connection, which exactly matches the standard for the popular National Instruments DAQ-cards.

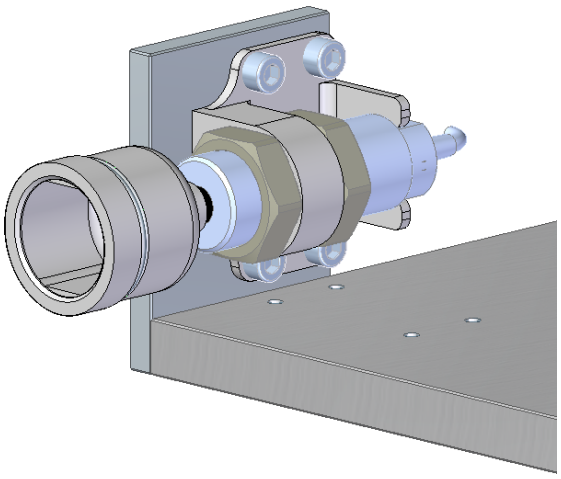

Figure 3.55: 2-axis thumb sensor in a 90° rotated position for calibrating the thumb adduction/abduction axis with a calibration mass.

Sensor calibration is essential if high quality measurements are to be attained. As the strain gauge based-sensors are highly linear, a two point calibration is sufficient. First, the zero-point is calibrated (with no external forces applied). GSV-1L strain gauge amplifiers support a digital taring function, triggered with the help of a push-button. The 2-axis thumb sensor, connected to dual TS503 amplifiers, must be manually tared using multi-turn trimmers in the TS503s, for each axis separately.

The second calibration point is optimally chosen near the end of the measurement range. We used an exact mass of 8kg (in an exemplary gravitational field of $9.81 m/s^2$, a mass of 8kg evaluates to 78.48N). Special positions are available on the baseplate to calibrate the KD60 and RFS-150XY sensors (also in 90° rotation to calibrate the second axis with a mass [Figure 3.55]).

Experiment: maximum comfortable finger forces

As an initial test of the FFLS, we measured the maximum comfortable single finger forces for each finger in both directions, exerted by seven healthy human participants (all right-handed; 5 male, 2 female; age 27.9 ± 5.3yrs, min. 23, max. 39). The participants sat on an office chair, adjusted for each subject for maximum comfort, with the armrest kept at the same level of the FFLS palmrest. Their right hand fingers were then comfortably tightened to the sensors.

A large monitor displayed a visual stimulus to the subjects, which consisted of a set of bars indicating which finger should be actuated and in which direction [Figure 3.56]. The participants were instructed to flex, extend, rotate, adduct or abduct the indicated finger with the *maximum comfortable force*, which was the highest force that participants felt comfortable executing over prolonged durations. Each contraction was stimulated once for 5 seconds, and five times for a duration of 2 seconds. Three seconds of rest were allowed between every contraction in the stimuli in order to avoid muscle fatigue. Thus, each subject generated 72 contractions, lasting approximately 7 minutes. Data from the FFLS was sampled with a 12-bit National Instruments PCMCIA DAQCard-6024E at 250Hz.

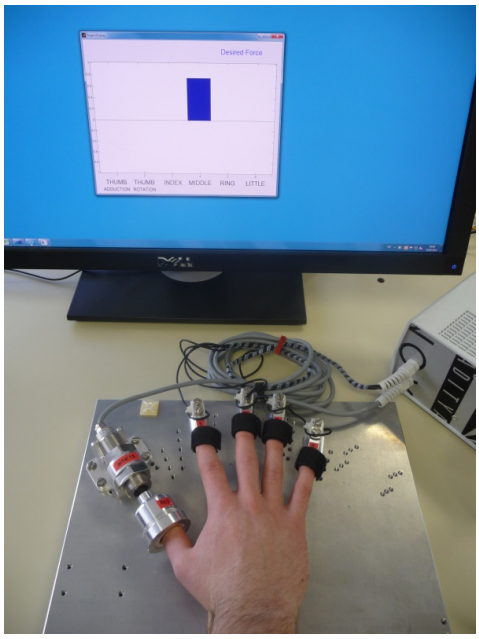

Figure 3.56: Experimental setup capturing maximum comfortable forces. Monitor displays visual stimulus, fingers and thumb are attached to FFLS. (Image source: [KHC12])

Figure 3.57 shows an example of the gathered data. Positive values denote extensions while negative values denote flexions. The graph reveals that participants were able to generate more force while flexing their fingers than when they extended them. During the experiment, all participants reported that it was easier to perform flexions than extensions.

In order to evaluate the average exerted force for each participant over both finger contraction directions, the raw data was split according to the stimuli; the delay between the stimuli and the force was accounted for, by selecting those samples for which 75% of the force maximum absolute value during the stimulus was reached. The average force over this interval was then evaluated, generating 72 values for each subject.

Table 3.9 shows the results for the five repetitions of the 2 second sequences (the results obtained for the 5 second sequences were found to be not significantly different from these and therefore for the sake of brevity are omitted). As the results show, the middle finger and the thumb produce similar forces during flexion; during extension, the thumb reaches higher values than the other fingers. Significantly smaller forces can only be generated by the ring and the little fingers, especially during extension. All subjects could produce the highest force while adducting the thumb. All this is in agreement with everyday experience, and no sensor limit of the FFLS was ever reached. Finally, no subject reported fatigue or discomfort during the experiment.

Improved version of FFLS

From the maximum comfortable forces measurements (Table 3.9), we concluded that the range of ±100N is in fact far too generous. A follow-up experiment [Figure 3.58] which evaluated different subsampling strategies towards online mapping learning [KHC13] and the experiments by Gijsberts *et al.* [GAC+] in the context of the NINAPRO-project (Non-Invasive Adaptive Hand Prosthetics) gave us inspiration for further modifications and led to the design of a revised version of FFLS.

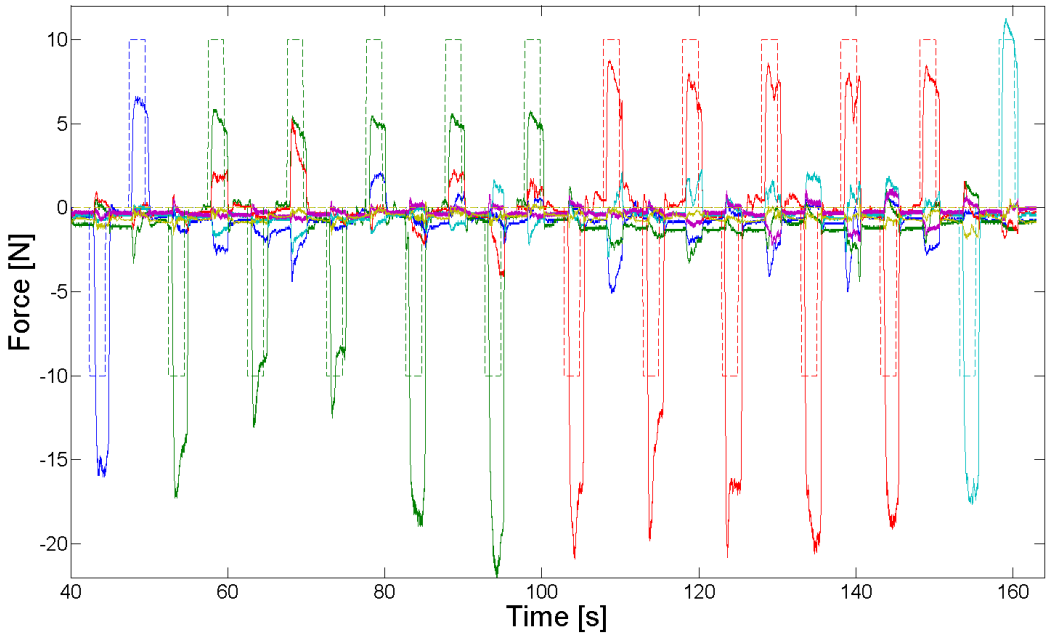

Figure 3.57: An example of acquired trial data (2 minute excerpt from 7 minute trial): stimulus (dashed line) and force values (continuous lines) of the little (blue), ring (green), middle (red) and index (cyan) fingers. (Graph source: [KHC12])

As ±100N was experimentally found to be too large range, the improved version of the FFLS, called FFLSv2 [Figure 3.59], was designed for to only have ±40N measurements. The decrease in the range was achieved by replacing the dual-axis thumb sensor RFS-150XY-100-8-3 (±100N) with a lower range RFS-150XY-40-8-3 [Hona] (±40N) sensor and the finger force sensors KD60-100N (±100N) with KD60-10N (±10N) sensors. An alert reader will have noticed an inconsistency with the finger force sensors only being ±10N instead of ±40N - this is not an error. As the KD60 series is designed for four-fold overloading, the KD60-10N sensor will output in combination with the same GSV-1L signal amplifiers used in the original FFLS at ±40N correctly ±10V and still remain inside the allowed specifications. Decreasing the measurement range resulted in a 2.5 fold signal-to-noise improvement in the thumb sensor and a very significant one magnitude improvement in the finger sensors [Figure 3.60].

	Flexion [N]	**Extension [N]**
Index	15.15 ± 4.48	5.67 ± 1.42
Middle	14.99 ± 2.29	5.63 ± 1.76
Ring	13.02 ± 1.66	3.83 ± 1.33
Little	13.20 ± 2.99	3.50 ± 1.31
Thumb	16.12 ± 5.18	8.96 ± 1.27
	Adduction [N]	**Abduction [N]**
Thumb	20.03 ± 6.73	8.25 ± 3.26

Table 3.9: Maximum finger forces. Mean values in Newtons over all subjects, plus/minus one standard deviation. (Table source: [KHC12])

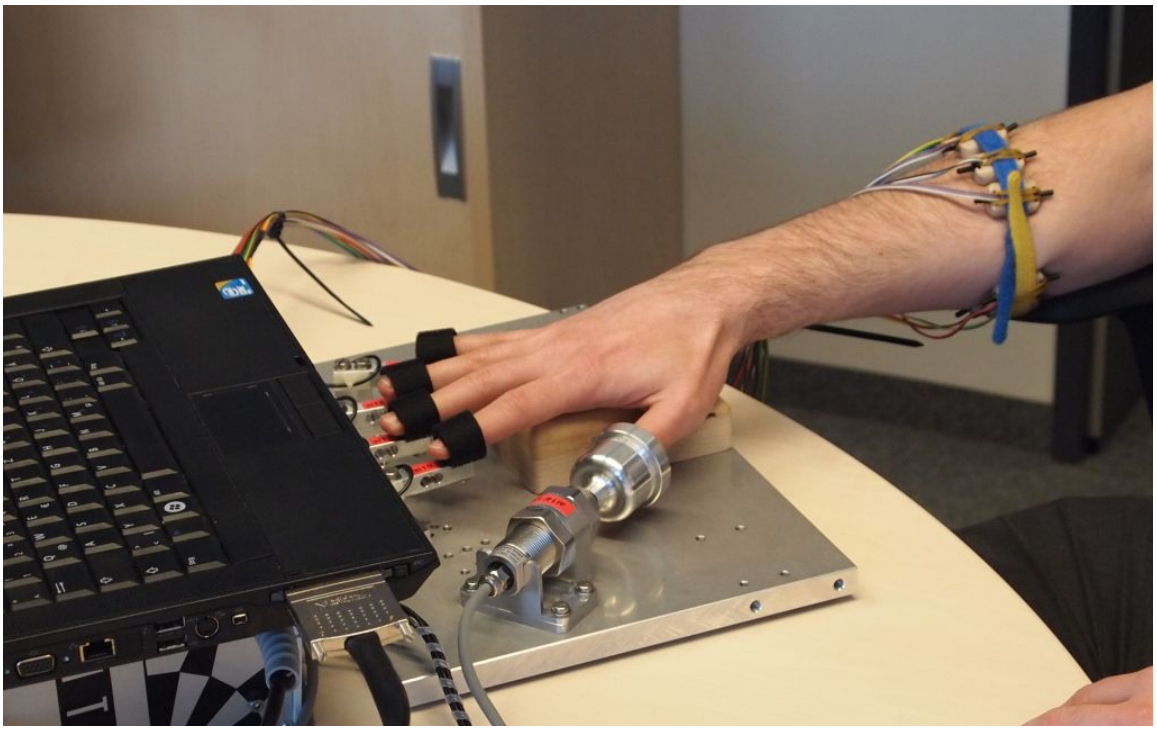

Figure 3.58: An experiment employing the FFLS to gather synergistic muscle activations [KHC13].

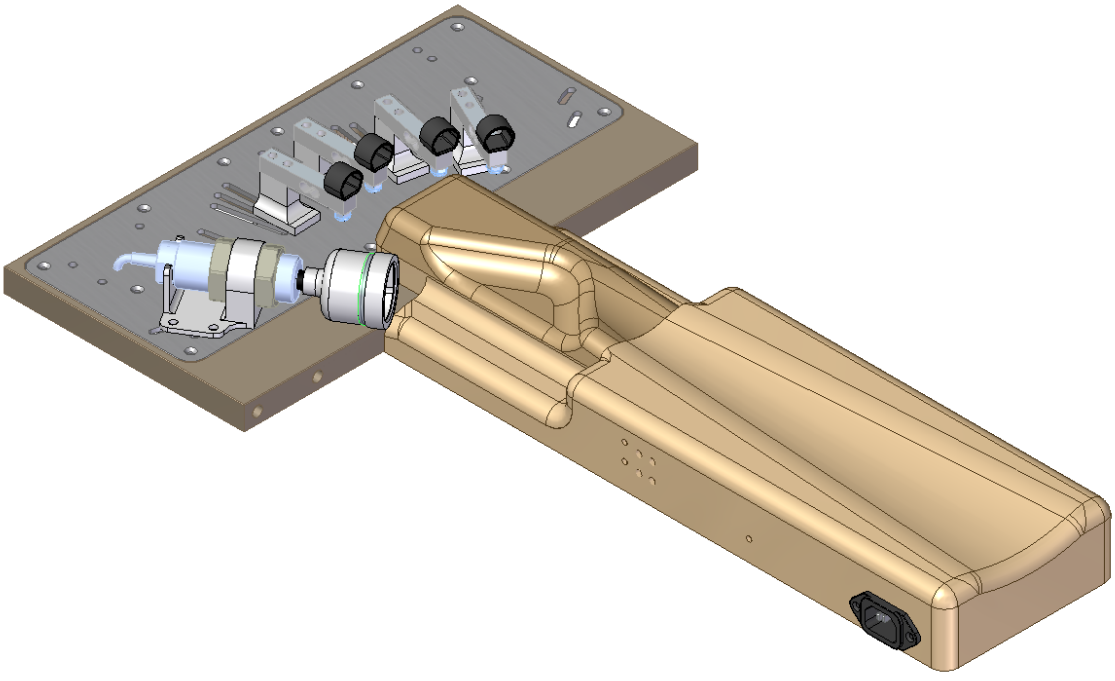

Figure 3.59: CAD-design of the FFLSv2, an improved version of the original FFLS with increased signal-to-noise ratio, easier transportability due to a lower weight, increased comfort due to continuous force sensor positioning and the availability of a full armrest, and less cluttered experiments thanks to integrated power distribution and signal conditioning components inside the armrest.

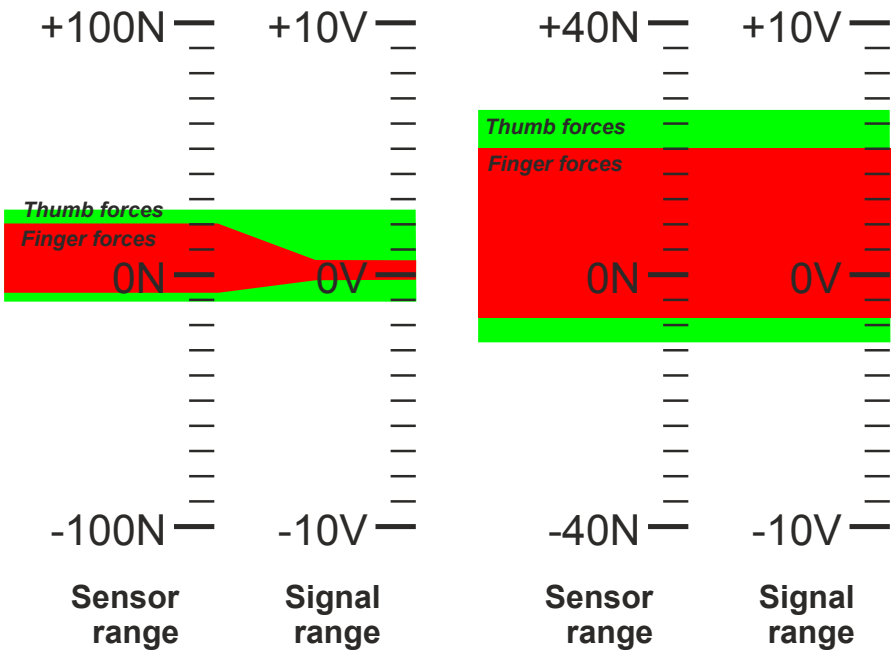

(a) FFLS (original). **(b)** FFLSv2.

Figure 3.60: A decreased measurement range in the improved version of the FFLS, the FFLSv2, significantly improves the signal-to-noise ratio. The green area shows the typical range for thumb forces, while the red area depicts the typical range of finger forces (according to measurement results from Table 3.9).

The original FFLS allowed each of the force sensors four positional adjustments in 11mm increments in order to match the appropriate finger lengths of participants. Although all of our participant's hand sizes were covered within this range, the worst case positional adjustment error was still 5.5mm resulting in sub-optimal finger or thumb mounting and less than maximum possible comfort during experiments. The FFLSv2 solves this problem by introducing continuous attachments slots over the full range. This was achieved without compromising measurement results by ensuring flexing or bending of the system does not occur using a modified force sensor attachment employing a wider surface, which distributes the force across a greater surface area on the baseplate.

During prolonged experiments, participants requested a means of resting their arm instead of having to support it in midair. FFLSv2 incorporates in addition to palmrest, an integrated wooden armrest for increased comfort as well.

Numerous experiments using the original FFLS at institutions distributed around Europe, called for simpler transportability of the sensory equipment. The FFLSv2 was designed with this in mind - it is lighter and more compact than the original and the whole sensory system including necessary accessories fit neatly into a sturdy carrying case, small enough to be taken as cabin luggage during air transportation [Figure 3.61]. A weight reduction was achieved by a considerable increase of parts produced from wood and plastics instead of metal in the original FFLS.

Numerous experiments with FFLSv2 are planned in the near future, hopefully leading to further insights into muscle activation and finger force couplings.

(a) Force sensor plate.

(b) Armrest with embedded signal conditioning and power distribution electronics.

Figure 3.61: FFLSv2 was designed specifically to fit inside a sturdy transportation case, small enough to be carried as cabin luggage during air travel. The FFLSv2 is stowed in two parts for transportation: the force sensor plate and the armrest with embedded electronics. Accessories, e.g., required tools and calibration jigs also have their designated luggage compartments.

3.4.2 Detecting manual interaction intentions from the forearm using tactile sensors

For almost half a century in the rehabilitation community, surface electromyography (sEMG) has been pursued as a means of detecting intentions, and is especially interesting in terms of gathering control signals from residual limbs [Bot65]. The main advantages of sEMG are that it requires no surgical intervention and the sEMG sensors can be manufactured at no significant cost. Nevertheless, clinical acceptance has been low due to signal instability [De 97, PBW+11]. Proposals to control multi-DOF hand prostheses have implemented machine learning algorithms to classify a finite (typically low) number of hand postures from the gathered sEMG signals [BvdS06, CGDS09, CAC+11]. The practical use of sEMG is still not clear, especially as far as the reliability of such classification algorithms is concerned, and the fact that the signal can be expected to significantly change over time due to sweating, muscle fatigue and position shifting of the electrodes.

The original idea of capturing muscle bulgings of residual limbs using force sensors was published as early as 1966 by Lucaccini *et al.* [LKL66], but has since found very little resonance (see also Subsection 2.2.3 for further related work). In the original experiments, high density tactile sensor technology was not yet available and the authors used simple bulky pressure sensitive binary switches to detect actions.

The project introduced in this subsection, and performed in cooperation with Dr. Claudio Castellini from the German Aerospace Institute (DLR), comes at the problem using modern tactile sensors.

Figure 3.62: The experimental setup to verify the usability of a sensitive tactile sensor array towards manual intention detection. Flexion/extension and ab-/adduction forces of the index finger were measured using a two-axis strain gauge sensor (in the photo the participant has his right index finger in the hollow of the sensor). The changes in the ventral side of the forearm were measured using a tactile sensor array (black rectangle under the forearm) with 48×48=2304 taxels. The stimulus, the force vector captured from the index finger by the strain gauge sensor, and the pressure pattern of the forearm are displayed on the screen.

Background of intention detection using a tactile sensor

Our main idea was to use a tactile sensor with a high spatial resolution to detect changes in the force distribution at the body surface induced by a person's attempt to express their intention. This is especially interesting for amputees or persons who can still produce a stable, albeit possibly minimal, muscular activity, such as for example the case of degenerative muscular disorders (Gehring, ALS, etc.) or various types of spinal injuries. For example, trying to flex a finger results in the thickening of the corresponding flexor muscle; this in turn produces increased pressure on the surface of the skin, above the location of the muscle. Small as these bulges sometimes are, as the preliminary experiment described in the next subsection shows, they can be detected well using a sensitive tactile sensor array, which paves the way for a novel non-invasive human-machine interface.

Our initial idea of using a high spatial resolution tactile sensor towards intention gathering was presented at the International Conference on Intelligent Robots and Systems (IROS2012) Workshop on Progress, Challenges and Future Perspectives in Navigation and Manipulation Assistance for Robotic Wheelchairs [CK12a].

Preliminary experiment using a tactile table

To validate our idea of reliably detecting participants manual interaction intentions from muscle bulgings using a state-of-the-art tactile sensor, we conducted a preliminary experiment, consisting of a two-axis force sensor, a tactile sensor table (see Section 4.1), and control software with stimulus visualization and data gathering processes [Figure 3.62].

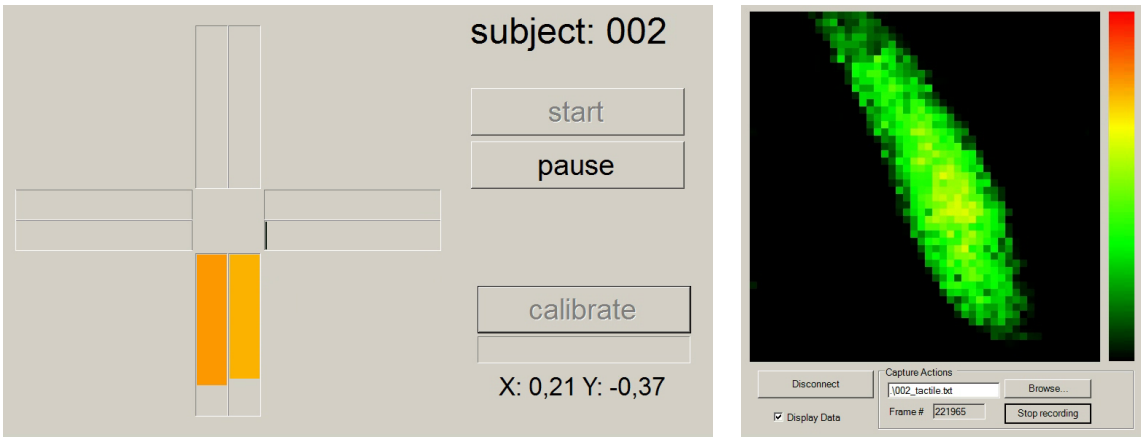

Figure 3.63: (Left) Screenshot of the visual display shown to participants during the trial. The stimulus direction and amplitude were displayed as a cross in the left window. Next to the stimulus bars, the live-captured values of the two-axis strain gauge sensor were shown as a feedback to the user. **(Right)** The visualization of the pressure pattern of the arm, as captured by the tactile sensor system. (Source of images: [CK13])

Along with the stimulus, live visual feedback about the exerted force was provided to aid the participants more easily match the desired force patterns. Participants were instructed to exert small forces with their index finger in two axis (up/down and left/right), while a tactile-sensing board recorded the corresponding muscle bulgings occurring on the ventral side of the forearm. The experiment and the results were published and presented at 13th International Conference on Rehabilitation Robotics (ICORR2013) [CK13].

The index finger flexion/extension and abduction/adduction forces were gathered using the original FFLS (Subsection 3.4.1) radial dual axis strain gauge sensor with a ±100N range. The index finger was attached to the dual-axis sensor using different sized gypsum casts, allowing a slack-free fit between the finger and the sensor.

In order to capture muscle bulges on the ventral side of the arm we used a 3×3 array of modular tactile sensors (explained in detail in Section 4.1). Each of the modules has 16×16 tactile pixels (taxels), resulting in a total of $48 \times 48 = 2304$ taxels covering an area of 240×240mm. The characteristic hyperbolic output of implemented tactile sensor allows a fine-grained insight into subtle hand movements, while still being able to output discriminating values for high muscle bulge forces (with a main measurement range between 1 and 30kPa).

The stimulus was presented to the participants on a large computer monitor as a set of colored bars displaying the requested force pattern of the index finger. Alongside the stimulus bars, feedback bars displaying the measured force magnitudes and directions were shown in real-time, so that the task was reduced to that of matching the stimulus bars [Figure 3.63 shows a screenshot of the stimulus].

Nine able-bodied, healthy subjects (all male, right-handed, aged 29.9 ± 5.1yrs) participated in the experiment, which lasted about 15 minutes. The stimulus consisted of four levels of desired forces, 1 to 4N (in 1N increments), applied either up (index finger extension), right (adduction), down (flexion) or left (abduction). During the experiment, each force magnitude and direction combination was repeated 7 times (in a non-random manner), in order to generate a learning effect.

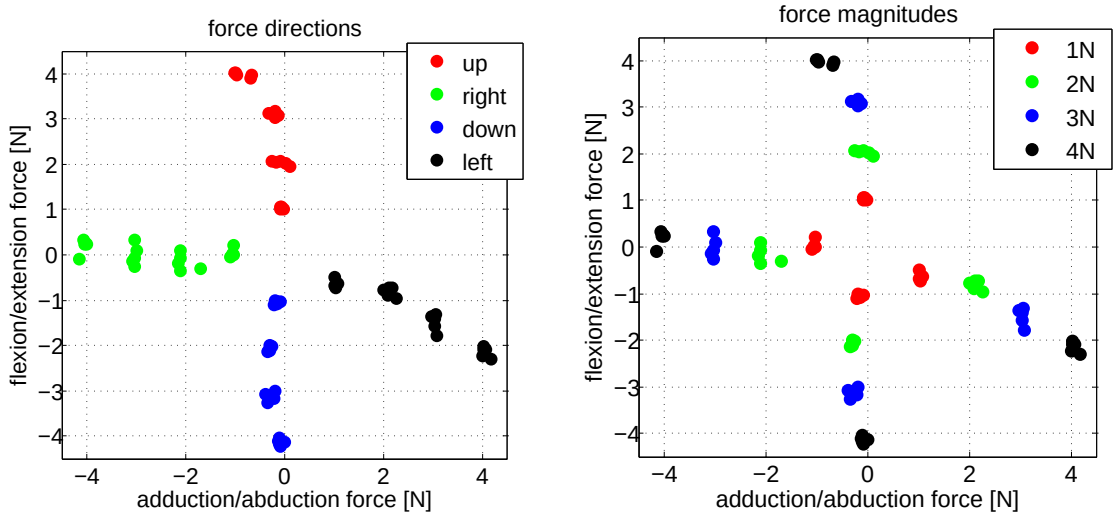

(a) Force Directions.

(b) Force Magnitudes.

Figure 3.64: Typical captured index finger force data for a single participant plotted on a 2D-graph. **(a)** displays the clustering of captured data in force directions, **(b)** displays the data from the same experiment, clustered according to force magnitudes. Notice the skewness of the adduction forces [Figure 3.64a, black samples]. In this case the participant could not avoid flexing the index while adducting. (Source of images: [CK13])

Figure 3.64 displays a typical experiment run. As one can see, the force vectors are perfectly clustered according to either the required force direction or the magnitude. This is true for all participants, notwithstanding slight distortions of the clusters due to each participant's anatomy. In Figure 3.64a, for example, this participant could not avoid flexing the index finger during adduction - this is reflected in the inclination of the black cluster in the graph.

The data analysis was performed by Dr. Claudio Castellini and therefore the main results are only briefly presented here. In order to classify the tactile samples according to force magnitude and direction, a Radial-Basis-Function (RBF) SVM was used [BGV92, CST00]. Leave-One-Out error evaluation was used since the number of samples was relatively small. Table 3.10 shows the results [CK13].

The table clearly shows that classification is in many cases perfect or near perfect, and that the highest classification error observed was 6.25%. Perfect classification in some rows of the table can be explained by the relatively small number of samples used.

Furthermore, the experiment tested the prediction of the exerted forces and their direction depending on the magnitude and direction of the stimulus. Figure 3.65 shows the results for pooled abduction/adduction (X) and pooled flexion/extension (Y) force vector prediction errors, aggregated according to the force direction (Up,Right,Down,Left) prediction errors and force magnitude errors (1N to 4N, in 1N steps). Error bars denote the average plus/minus one standard deviation, evaluated over all participants. The error measure is the normalized root-mean-square error (NRMSE) over the range of measured index finger forces (about 8.5N). The global NRMSEs are $1.09\% \pm 0.35\%$ along the index finger ab-/adduction directions and $1.12\% \pm 0.31\%$ along the flexion/extension directions

Participant#	Direction error	Magnitude error
1	1.25%	0%
2	0%	0%
3	6.25%	2.5%
4	0%	1.25%
5	1.25%	2.5%
6	1.25%	0%
7	0%	0%
8	1.25%	0%
9	0%	0%
mean±std.	$1.25\% \pm 1.98\%$	$0.69\% \pm 1.10\%$

Table 3.10: Classification errors for force magnitudes and directions, and their related statistics. (Table source: [CK13])

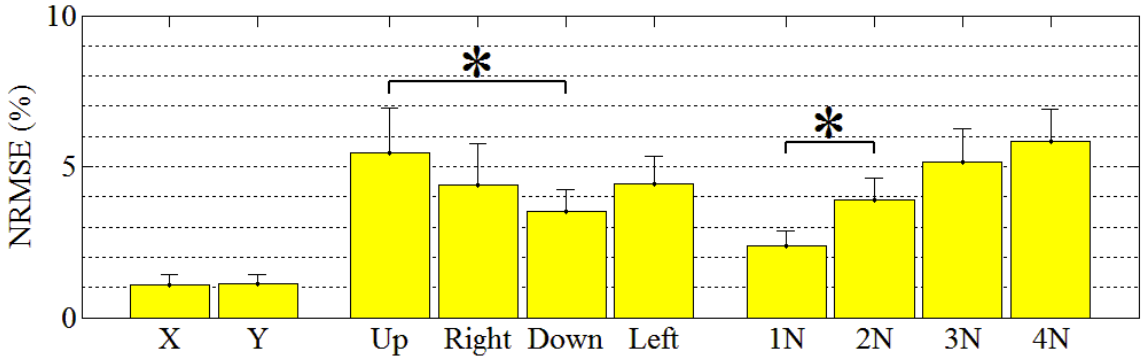

Figure 3.65: The NRMSE obtained while predicting finger forces using the spatial linear approximations of the tactile images. **(left)** Global values for sensor directions X (index ab-/adduction) and Y (flexion/extension); **(middle)** Values aggregated over force directions; **(right)** Values aggregated over force magnitudes. The asterisks denote two pairs of statistically significant (Student's t-test, $p < 0.01$) error rates. (Image source: [CK13])

(these values are particularly low since they include all the resting phases). As far as force direction is concerned, whereas there seems to be no difference between abduction and adduction (*Left* and *Right* columns in the figure), there is a statistically significant difference between extension (column *Up*, NRMSE $5.46\% \pm 1.48\%$) and flexion (column *Down*, NRMSE $3.51\% \pm 0.74\%$). This can be explained by the fact that extending a finger is intrinsically harder to do than flexing it, which leads to a lower signal-to-noise ratio. The graph also clearly shows that the error increases as the forces increase. Taking into account that the range of forces was about 8.5N in both measured index finger movement axes, this evaluates to an absolute error of about 0.2N when the applied forces were 1N, and about 0.5N when the applied forces were 4N. Figure 3.66 shows exemplar true and predicted forces. Such high finger force prediction accuracy will allow fine grained finger force control of future hand prosthesis, and is a significant step towards enabling hand amputees to regain the ability to perform delicate grasps and fine manipulations.

Figure 3.67 shows six exemplary tactile images of a participant engaged in the exertion of 4N forces. The images were obtained during three repetitions of the force-up and force-

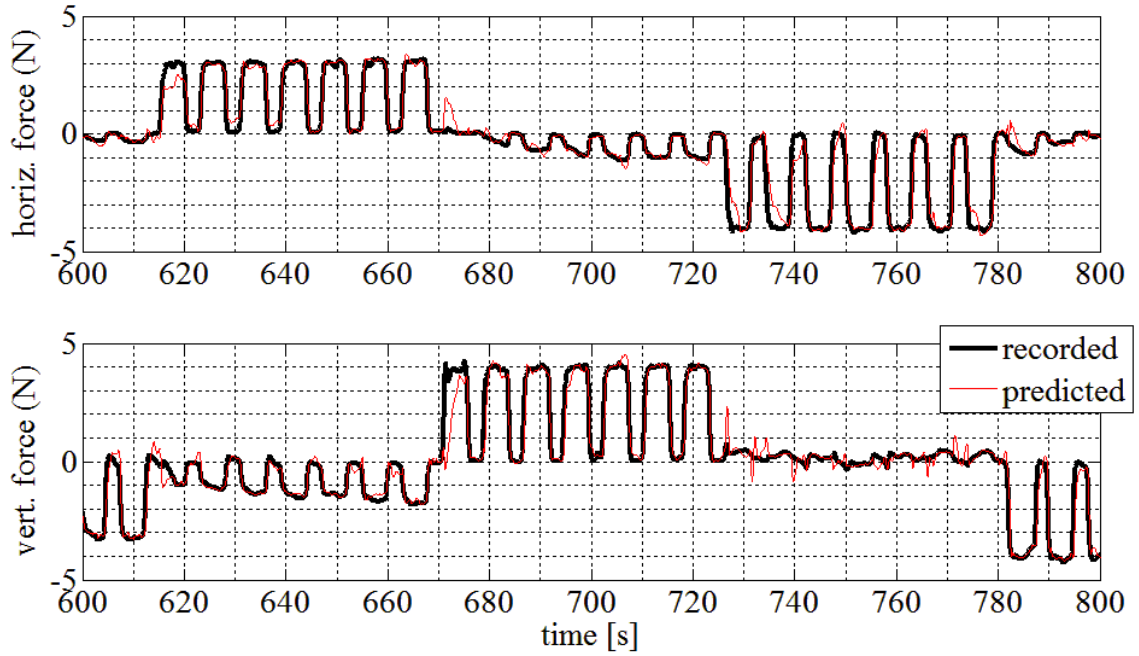

Figure 3.66: Exemplar recorded and predicted forces for one selected participant. **Upper panel:** Along the finger ab-/adduction direction (horizontal force); **Lower panel:** Along the finger flexion/extension direction (vertical force). The resulting ab-/adduction and flexion/extension NRMSE are 1.14% and 1.31%. (Image source: [CK13])

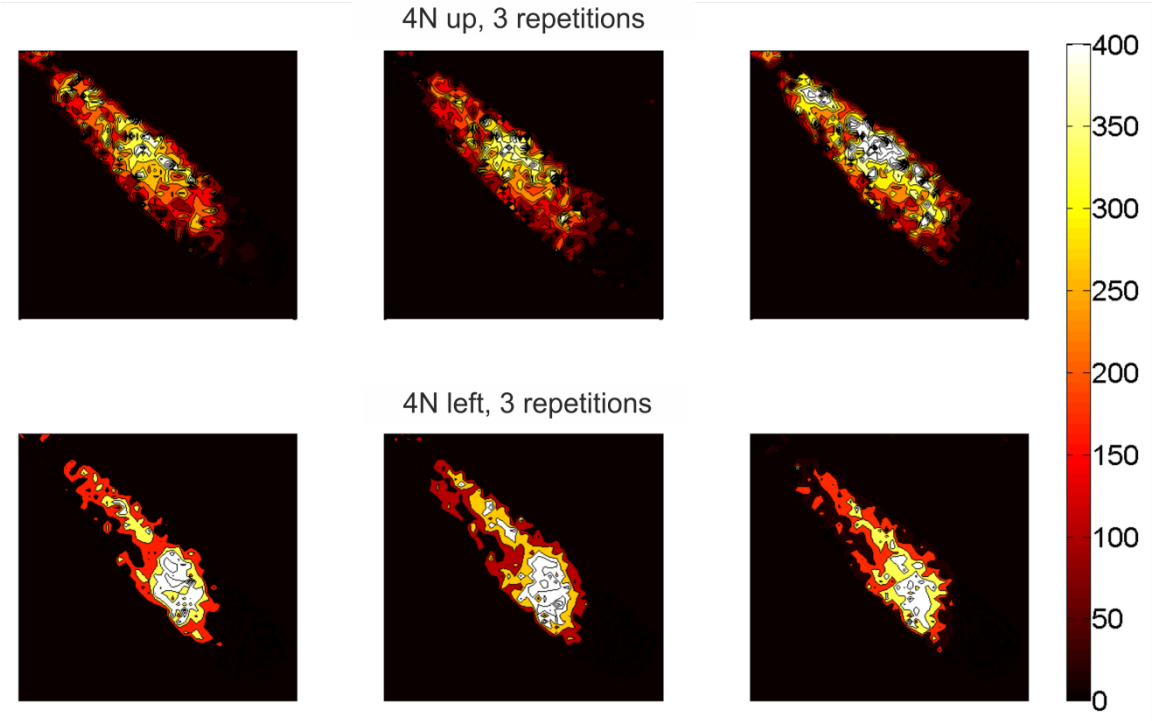

Figure 3.67: Differential tactile images of a typical participant's forearm while exerting a 4N force with the index finger towards up (top row) and towards left (bottom row). Similar muscle activations are clearly visible in the repetitions. (The force scale displayed is a unitless 12-Bit value, provided by the tactile sensor system.) (Image source: [CK13])

left patterns, while the resting state was extracted from the force images. In the top row a high-pressure zone can be clearly seen in the middle region of the forearm, while the elbow (situated in the bottom-right corner of the images) does not produce much of an effect; this is consistent with a strong extension of the index finger, during which a reaction force towards the bottom appears. In contrast to this, in the bottom row two high-pressure regions appear near the elbow and over the distal section of the forearm (upper-right corner of the arm footprint in the images), again consistent with the exertion of a finger force directed to the left. Notice that these activation patterns are visually consistent across the repetitions.

These results validate the usage of a high-resolution tactile sensor as an effective human-machine interface for detecting manual interaction intentions. The results indicate that even small finger forces (one to four Newtons) can be predicted with a high degree of accuracy. A qualitative examination of the flat tactile images shows that the deformation in the arm is clearly and consistently detectable from the captured and processed visual tactile pattern.

Tactile Bracelet

As the results from the preliminary experiment using a flat tactile sensor in contact with one side of the arm were very promising, further development effort was put into an improved system. A tactile bracelet was devised to capture muscle bulgings from around the circumference of the arm. Furthermore, we decided to miniaturize the tactile sensor system and make it portable [Figure 3.68]. The Tactile Bracelet, including the design, mechanics and electronics circuitry, was developed by me.

The bracelet design uses up to 10 tactile sensor boards and a single mainboard which collects the tactile data from the sensorboards and also provides motion tracking capabilities (for schematics, see Appendix 6.4.1 and Appendix 6.4.3, respectively). To enable optimal covering of different arm circumferences, the amount of connected sensorboards is made variable by design.

The tactile sensors are based on the second generation instrumented object, *iObjectPlus*, tactile sensor design (see Subsection 3.3.7). Each sensor board in the Tactile Bracelet incorporates 4×8 taxels that are sampled using two 16-channel ADCs (of type AD7490) in parallel. The specifications and performance of the sensor is thus similar to iObjectPlus sensors. The digitalized data is provided internally on the SPI-bus. With a sensor board width of 20mm, an adult can typically fit all 10 sensorboards around the circumference of the arm, resulting in a very high resolution tactile image of $10 \times 4 \times 8 = 320$ taxels.

The mainboard of the Tactile Bracelet has an embedded PIC32 microcontroller that collects, as the SPI-master, data from up to 20 ADCs over the internal SPI-bus. Motion tracking of the bracelet (and by extension the human arm) is achieved using a 9-axis InvenSense MPU-9150 Inertial-Measurement-Unit chip connected to microcontroller over Inter-Integrated-Circuit (I^2C) bus. The mainboard also includes the power unit, taking the +5V DC provided by USB host, smoothes it using a 5V in/5V out DC/DC converter, and generates the +3.3V required by some components in the circuitry using a linear low-drop voltage regulator. The gathered sensor data is relayed as a serial stream over the USB 2.0 bus. Future versions can also be equipped with wireless connectivity if required by the application. A design implementing a Texas Instruments CC3000 wireless-LAN module has already been sketched for possible future iterations to achieve cable-free operation.

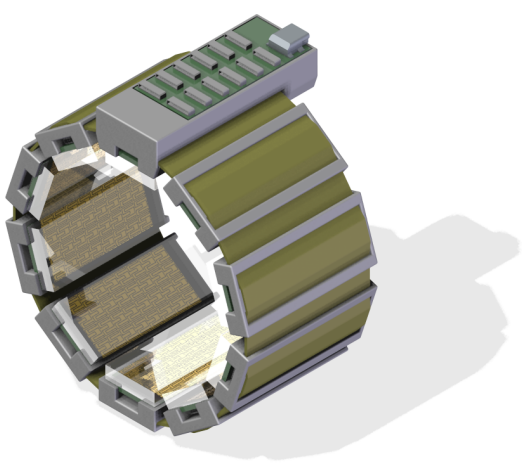

(a) CAD-Rendering.

(b) Photograph of first prototype.

(c) Tactile Bracelet in rolled out state showing the 10 sensor pads. Each sensor pad is equipped with 4×8 taxels.

Figure 3.68: CAD-rendering and photographs of the Tactile Bracelet prototype designed to gather manual interaction intentions by capturing muscle bulgings with high spatial resolution and highly sensitive tactile sensors.

Experimentally we found that a wide double sided hook-and-loop band was the optimal solution for mounting the sensor and data collector boards around a human arm. This allows for quick individual sensor position and overall bracelet circumference adjustment, while providing a sturdy attachment. Appropriate fasteners were designed and 3D-printed for attaching the printed circuit boards to the hook-and-loop band.

At the time of writing, the first prototype of the Tactile Bracelet is almost finished. Preliminary trial runs of the system indicate great potential thanks to the tactile sensors' high spatial resolution and high sensitivity, allowing muscle bulgings to be observed by inspecting the tactile image around the arm. This makes the developed Tactile Bracelet a solid candidate to enable single finger control of future dexterous hand prosthesis. The usability of the Tactile Bracelet is not limited to upper-limb amputees, but extends to for example future virtual reality systems, gaming and manual intelligence research studies.

Figure 3.69: Tactile sensitive pen sheath prototype for measuring grip force during handwriting. A standard ball point pen or a Wacom digitizer pen can be attached into the sheath and used for writing.

3.5 Tactile Pen to monitor grip force during handwriting

Bad handwriting can be caused by simply limited or bad handwriting skill teaching, or can also be an indicator of motor dysfunction, such as e.g., cerebral palsy, or musculoskeletal disorders, such as carpal tunnel syndrome. Observing handwriting skills before and after treatment can allow conclusions about the effectiveness of a treatment to be drawn. Software, such as the *MovAlyzeR* from NeuroScript [Mov] are commercially available to analyze handwriting using digitizer tablets. This can not only reveal subjects' ability to perform movements such as matching a given pattern, ability to perform round or sharp movements, the regularity of the produced patterns, but also gather information about the pressure applied to the writing surface, speed and temporal uniformity of movement data. Nevertheless, a very interesting and clear tension indicator is the force used to grip the pen, and thus far this data has been neglected in such writing experiments due to a lack of appropriate hardware. Mr. Gerhard Mahlich, an ergotherapist whose practice is close to Bielefeld, motivated us to develop a tactile sensitive pen.

This ongoing project is a cooperation with Gerhard Mahlich, Gereon Büscher, Carsten Schürmann and me, and is officially supervised by Dr. Robert Haschke and Prof. Dr. Helge J. Ritter. Our proposal was to create a sheath with attached tactile sensors for digitizer pens and normal ballpoint pens in order to measure the grip force. For tactile sensing we chose the fabric-based tactile sensor, the underlying sensor technology of the tactile dataglove, discussed in Section 3.2.

Figure 3.69 displays our first prototype, assembled by Gereon Büscher, for testing purposes with 3 tactile sensors with differing measurement ranges on the pen sheath. Our initial idea including the prototype tactile pen sheath was published in [BMK+13]. Currently a newer prototype version with embedded data acquisition electronics and designed to be mass produced is under development.

The usage of pen grip force measurement can also be advantageous in general schools during early handwriting education, in which a teacher would receive much clearer information about the quality of grasp and force, and could enable earlier intervention.

4 Augmenting technical systems with a sense of touch

A sense of touch is critical to enable humans to master intricate manual interactions. It follows that technical systems, such as robots, operating in non-deterministic environments, will benefit enormously from artificial haptic sensing systems. This chapter describes work done on three tactile systems that were developed as artificial touch sensors for technical systems. A main design decision taken in the development stage of these sensors was to aim for high sensitivity, even if that meant that measurement accuracy had to be compromised. The benefit of choosing sensitivity over accuracy can best be illustrated with an example. If a rolling ball on a flat surface is to be grasped, failure to detect initial contact could mean that the ball simply continues to roll away. Biological sensors, such as the mechanoreceptors in human hand, follow similar a principle and have a strong bias for sensitivity over accuracy [GK90, JF09].

Section 4.1 discusses a versatile modular tactile sensor system with a very high speed and spatial resolution. The modules can be used to augment different sized flat areas with the sense of touch. A tactile sensitive table or palms of a robotic device are just some examples of where this sensor could be used.

The tactile sensor in Section 4.2 does not reach the high spatial resolution or the speed of the previous sensor, but due to its fabric-based design, it is flexible and stretchable and can thus cover curved surfaces, such as the body of humanoid robots or palms of anthropomorphic artificial hands.

Human fingertips are equipped with the highest number of mechanoreceptors in our skin [JF09]. As we perform most fine-grained manipulation tasks using our fingertips, it seems logical to equip robotic hand fingertips with high grade tactile sensing as well. Section 4.3 introduces a very recent 3D-shaped tactile sensor, with very high sensitivity and spatial resolution, developed in the form of a fingertip with a soft outer surface, but rigid "bone"-like inner structure.

4.1 Modular flat tactile sensor system

Traditional scene analysis and object tracking relies mainly on data from vision cameras. To overcome limitations such as occlusion and a lack of 3D spatial information, numerous cameras, stereo-matching-algorithms and special depth measurement devices, such as the popular Microsoft Kinect [Kin], are commonly used. A tactile sensitive surface on the other hand provides an orthogonal approach to extend such scene analysis setups. A high-resolution tactile surface can supply information about the shape and position of multiple objects and also deliver information about the weight and pressure distribution of objects. To be able to augment different sized surfaces with tactile sensitivity, our main criteria for such a system was that it had to be modular, but at the same time simple to use and to reconfigure. After an exhaustive search for such a system, to the best of our knowledge no such system was available, and therefore we initiated our own development.

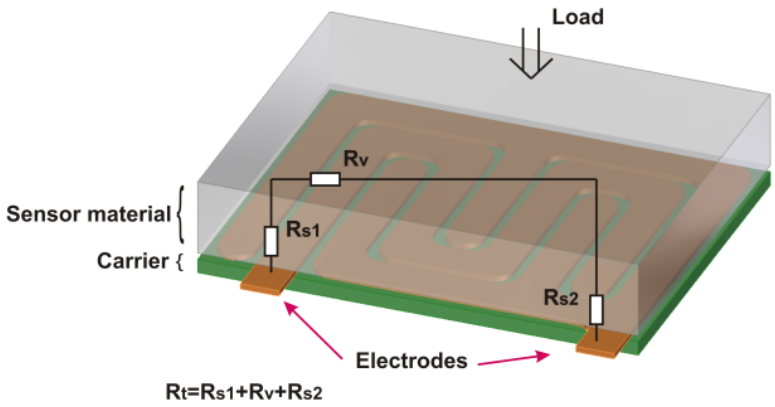

Figure 4.1: The resistance of a single resistive tactile sensor cell, measured between two electrodes, is the sum of sensor material volume resistance and contact resistances between the sensor material and the electrodes. The contact resistance changes according to the applied load on the sensor foam.

This project started out as a diploma project for Carsten Schürmann [Sch08], who was mainly supervised by me. The sensor developmental work was published at the World Haptics Conference in 2011 [SKHR11] and at Human-Robot Interaction conference in 2012, at a special workshop on Advances in Tactile Sensing and Touch [KS12].

4.1.1 Tactile sensing

The modular flat tactile sensor system implements a resistive tactile sensor array with a conductive foam used as the sensor material, similar to instrumented object from Section 3.3. Compared with numerous competing sensor technologies, such as broadly used capacitive or load cell based systems [ECL03, CMMS08, OBMC09], the resistive tactile cells are robust to electromagnetic interference, tolerant to overloading and require very few mechanical and electronic components making them easier to implement, especially for higher taxel counts. The applied pressure to output resistance has a hyperbolic characteristic, which enables high output resolution at low pressures, while simultaneously allowing a wide measurement range. Figure 4.1 depicts the components of the resistive tactile sensor cell's resistance, R_t. R_t is the sum of 3 parts – variable surface interface resistances $R_{s1} + R_{s2}$ and a constant sensor material volume resistance, R_v. Varying the applied load, varies the surface interface resistance (R_{s1} & R_{s2}), thus allowing simple data acquisition with a constant pull up or pull down resistor and an analog-digital-converter. In his diploma thesis, Carsten Schürmann optimized the shape of the tactile cell form (a sample of various shapes tested can be seen in Figure 4.2) and found the M-shaped cell to be most desirable as it was very responsive to input load changes and the output was least dependent on contact location inside one taxel.

A single tactile sensor module sized 80×80mm is composed of 3 layers [Figure 4.3a] - a databus layer (bottom), a sensor electrode layer (middle), and a conductive elastomer foam layer (top). The sensor electrode layer is made out of standard FR4 printed-circuit-board (PCB) material. The top layer consists of 16×16 M-shaped electrodes and on its underside 16 analog-digital-converters (of type AD7490) with 16-channels. The bottom databus layer implements a PIC32 microcontroller to collect the data from the top electrode layer. All

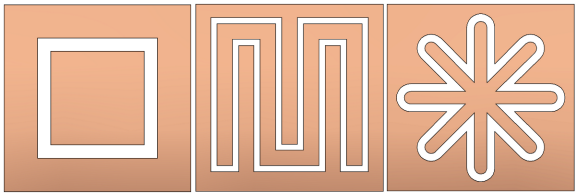

Figure 4.2: A sample of the tested resistive tactile sensor cell shapes. The middle "M" shape was experimentally found to perform best as it hat the most uniform sensitivity across a taxel. (Image source: [SKHR11])

four sides of the databus PCB have connectors that can be used for interconnecting further sensor modules to the system, allowing large 2D areas to be made tactile sensitive. The proprietary parallel bus has a bandwidth capability of 500,000 taxels/second, allowing up to 1.9kHz sampling to be achieved using a single sensor module (if the number of sensor modules on a bus is increased, the frame-rate drops accordingly). As master-controlled bus arbitration is used, there are no packet collisions, allowing all of available bandwidth to be utilized at all times. We have successfully evaluated such active table systems consisting of up to 6×6 sensor modules (480×480mm). Finally, the conductive elastomer foam on the top provides the necessary change in resistance according to applied load.

A single interface board based on an AVR32 microcontroller is connected to one of the corners of the databus modules and converts the data on the proprietary parallel bus to a standardized USB-Video-Class protocol. Typically used by USB-Webcams, this protocol allows tactile data to be delivered to a USB-host (e.g., PC) as a video stream, where each pixel corresponds to a pressure value of a taxel. An example of such a tactile image can be seen in Figure 4.3b, in which a right hand was placed on top of a tactile plate built from 3×3 sensor modules. It is also interesting to note that numerous algorithms from the computer vision domain can be used to process the tactile data. Furthermore, the USB-Webcam connection standard makes the tactile sensor usable with numerous closed source programs in the vision domain in which proprietary systems cannot as easily be connected.

4.1.2 Applications

As an initial sensitivity demonstrator of the system, software was developed to detect the location of the handle of a cup by just observing the tactile image [SKHR11]. The additional weight of the handle allowed immediate directional recognition due to the fact that more weight was distributed towards the handle. For all the cups tested, the directional prediction error remained under 20°.

In [SSS+09], Schöpfer *et al.* used two of the sensor modules to manipulate deformable materials. Each of the modules were attached as a tool on the end of two 7 degrees-of-freedom robotic arms to form two movable tactile sensitive grippers. Using only tactile feedback, a *Play-Doh* compound was explored and successively deformed into a round ball.

In a similar robotic setup, Schöpfer *et al.* [SSPR10] took advantage of the high frame rate of the modular flat sensors and used them to detect object slippage. Slip was detected using a Fast-Fourier-Transform (FFT) on the tactile data followed by a trained artificial neural network to detect specific characteristic slip patterns in the frequency domain, which even allowed a discrimination between different surface textures.

Schürmann *et al.* [SKHR12] analyzed the end state anticipation on grasp control for two pick and place type tasks with similar starting, but different ending conditions. For this

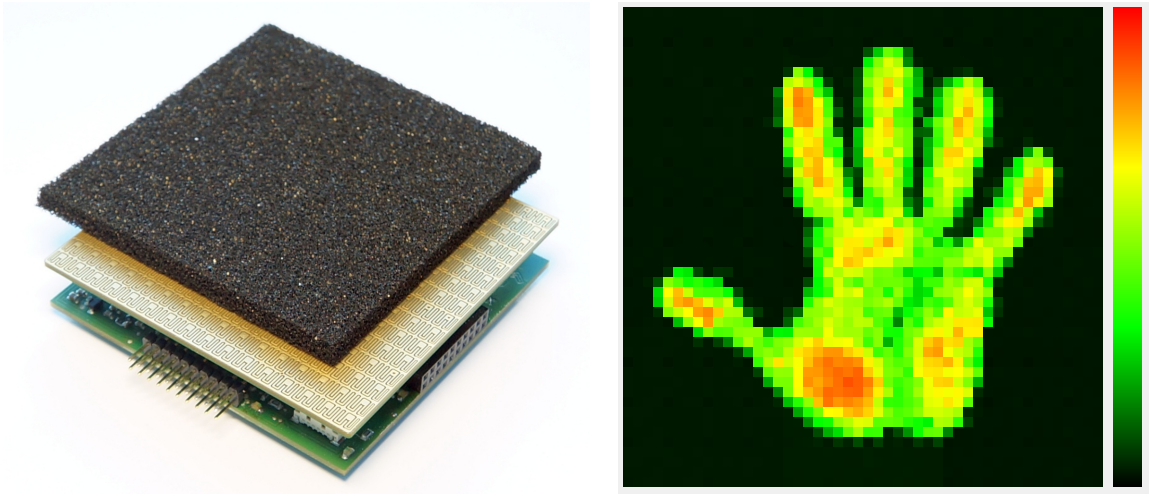

(a) Single tactile sensor module with 16×16 taxels, measuring 80×80mm.

(b) Tactile image of a right hand on a 3×3 tactile module system.

Figure 4.3: Modular tactile sensor system with a high-speed USB-Video-Class interface. The system allows data to be captured at a rate of 500,000 taxels/second. For the case of a single module, this results in a frame rate of approximately 1.9kHz.

experiment, we built a small book sized tactile object using four of the sensor modules - two on each side, and added an additional 6D motion tracking sensor. The results clearly showed the different positioning strategies of the hand on the object in relation to the anticipated task. Depending on the task's desired end state, participant's chose postures from the beginning of the movement right through to the end of the movement that ensured the hand was in a comfortable position at the final goal state of the task (in psychology the term used for this is *end state comfort* [RvHC96]). Regarding the finger forces used by participants during the pick and place tasks, the experiment revealed no surprises - the results were in line with the expected forces required to maintain a steady grasp of the tactile book, showing slightly elevated forces during the acceleration phases.

An experiment by Naceri *et al.* [NME13], used a similar book-type arrangement of the tactile sensor modules, additionally attached on both long sides to two PHANToM [PHA] 6 degree-of-freedom haptic device simulators to investigate the strategy of humans in distributing finger positions and forces under external force perturbations. The experiment revealed a substantial systematic variability of finger placement between participants, however, within participants the placement was rather constant across numerous trials. More importantly the experiment revealed the fast haptic learning curve of the participants - all learned to compensate for the expected external perturbations after only the first trial.

Recently, Maycock, Essig, Schack and Ritter secured funding through CITEC, Bielefeld University, for a project, entitled *Single and Dyadic Visuo-Haptic Task Learning* to investigate human haptics and other characteristics of participants as they solve maze game. The goal of the currently running project is to gain insights into how humans acquire a new manual skill. To achieve this, posture, eye-tracking and haptic data is to be gathered and analyzed. The tactile data is being gathered using four of the tactile sensor modules presented in this section. The modules are attached to the sides of the maze, two on each side measuring the top and bottom interaction forces [Figure 4.4]. The CAD development and construction of the tactile maze mechanics were done by me.

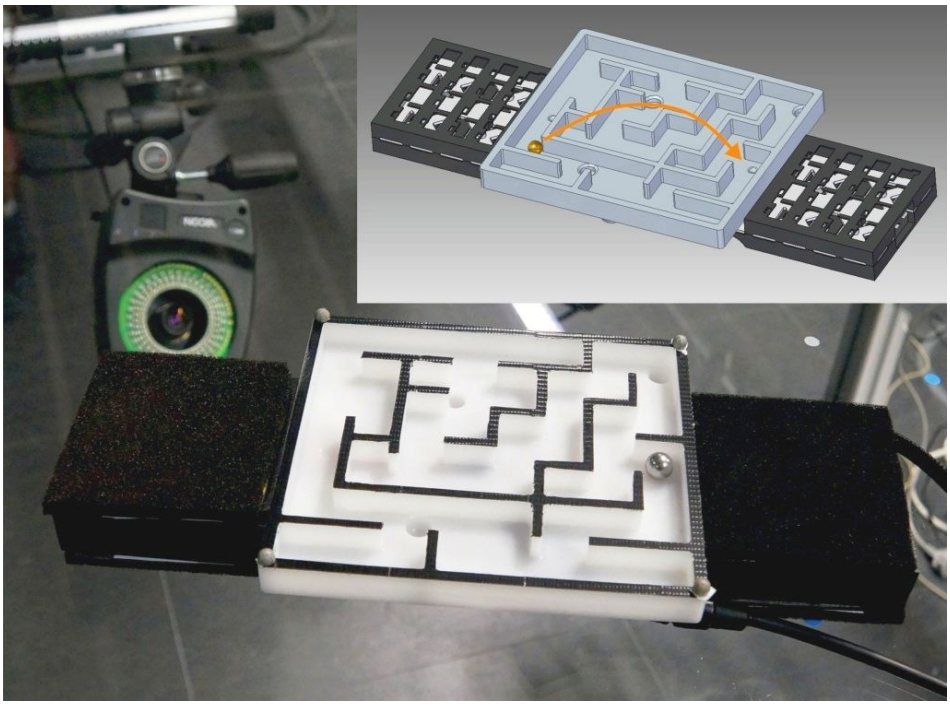

Figure 4.4: Maze with four modular tactile sensors, two on the left and two on the right (top and bottom), to capture the tactile interaction patterns while participants solve the maze. The inset shows the underlying CAD construction.

4.2 Augmenting curved surfaces with a sense of touch

Numerous anthropomorphic robots make extensive use of complex three dimensional body parts in mimicry of their biological counterparts. The use of traditional flat rigid tactile sensors, as discussed in previous section, is therefore limited due to their inability to take on the required smooth curved form. Numerous attempts in this direction have been taken before (see Section 2.3), but only a very limited number of developments have matured to the point that they could be used to cover significant surface areas of real intelligent interactive systems [CMMS08, EFS11, KWW03]. Our proposal is to use the underlying fabric-based tactile sensor of the Tactile Dataglove, discussed in detail in Section 3.2, to cover the curved surfaces of technical systems. The fabric-based tactile sensor has numerous benefits that overcome many of the drawbacks of previous attempts, such as great conformability to curved surfaces, relatively high spatial resolution, great sensitivity and no need to have complex bulky data acquisition electronics.

The next subsection presents the latest results of an ongoing project to augment the palm and fingers of a robotic hand with an artificial sense of touch using the fabric-based tactile sensor technology. Then, subsection 4.2.2 introduces an idea to implement the same sensor technology as a sensitive type of bed linen in order to control the active anti-decubitus beds according to a measured pressure pattern.

In addition to these two projects, the field of Ambient Intelligence can benefit from large scale tactile sensors by allowing the augmentation of rooms and furniture with tactile sensing and thus making them responsive to the presence of people and pets. Furthermore, novel and more intuitive ways of interacting with computers and computer games using touch and the sensors discussed in this section open up new possibilities.

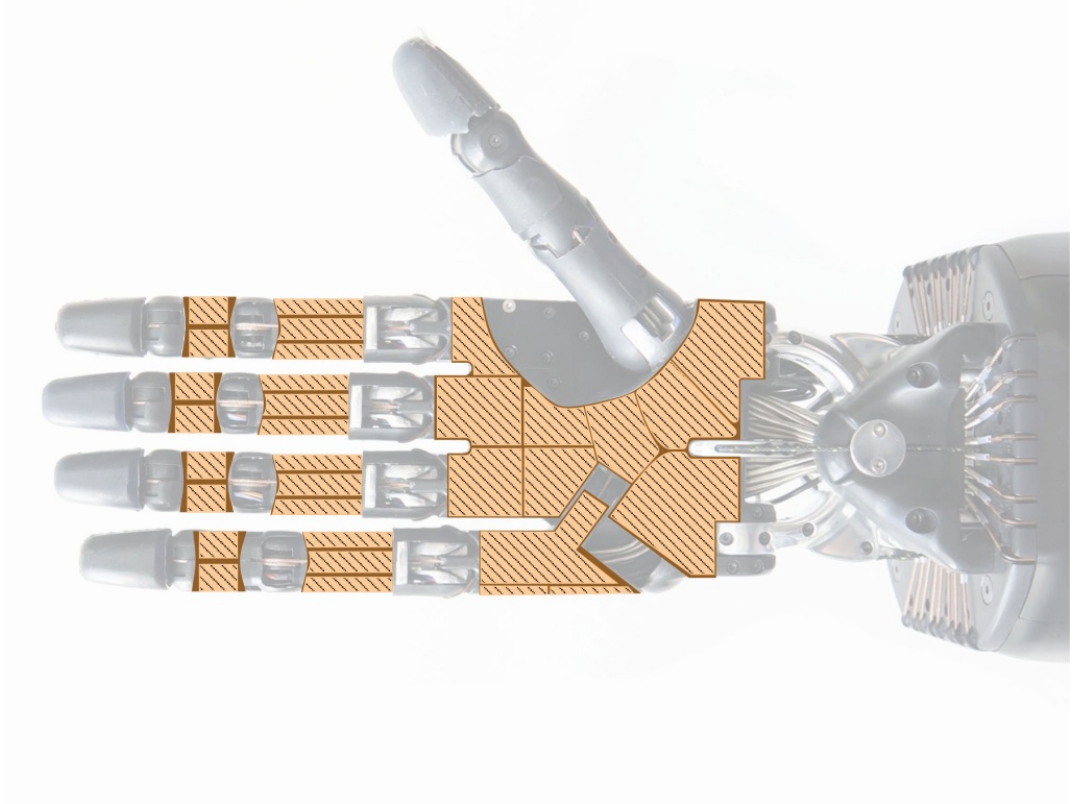

Figure 4.5: Tactile sensing of the palmar side of the Shadow Robot hand in our lab is being developed using fabric-based tactile sensor technology. Striped surfaces depict the taxels and the darker brown area shows the shape of the planned sensor patches. Note that I separately discuss a solution for fingertip tactile sensors in Section 4.3.

4.2.1 Tactile sensor for the palm and fingers of robot hands

In an ongoing project with the Shadow Robot Company [Sha], me and Gereon Büscher, under the supervision of Dr. Robert Haschke and Prof. Dr. Helge J. Ritter, are currently in the process of finishing the prototype fabric-based tactile sensors that will be used to cover the palm and fingers of the Shadow Robot Hands, effectively augmenting large areas of the palmar surfaces of the robot hand with the sense of touch. Although the current development targets the Shadow Robot Hand, it can also, with minor changes, be used with other similarly sized robotic or prosthetic hands.

The data acquisition electronics were developed in cooperation with the Shadow Robot Company and are already integrated into the current version of the motor hand, type E2M3X. For the Shadow Robot Company, it was only possible to add 2 taxel inputs for the middle phalange, 3 for the proximal phalanges and 12 for palmar surface. With this limitation in mind, a taxel distribution layout using all available input channels was devised. Figure 4.5 depicts the proposal by dividing the middle finger phalange sensor into two symmetrical taxels, the proximal phalange into symmetrical right/left taxels and a middle taxel for palm normal direction contacts, and the perimeter and distribution of 12 taxels around palmar surface of the robotic hand, taking into account the movability of the thumb and little finger carpometacarpal joints. The middle and proximal phalange tactile sensors are attached using brackets on the dorsal side of the fingers, whereas the palmar sensor is

Figure 4.6: An initial tactile sensor prototype for the middle phalange of Shadow Robot hand, mounted on the index finger. The two taxel sensor is embedded in a silicone covering and cast in the shape of an original non-sensorized middle phalange skin.

planned to be attached with a hook-and-loop band, allowing easy removal and maintenance of the hand. Figure 4.6 displays the initial prototype of the middle phalange tactile sensor. The connection to the data acquisition electronics, located in the finger phalange, is made using a JST SUR-type connector with a low 0.8mm pitch using ⌀0.38mm wires. Although our initial development concentrates on palmar surface of the robotic hand only, this sensor technology can be used throughout the entire surface of anthropomorphic robot body.

4.2.2 Pressure distribution sensor for intelligent decubitus beds

The usability of this tactile sensor technology is by no means limited to humanoid robots. Numerous other usage scenarios are very likely, for example in the field of medicine. Patients with very limited or no movement (e.g., coma patients), can easily develop pressure ulcers if left sitting or lying in the same position for extended time periods, due to pressure on an area which blocks blood flow. Not only are pressure ulcers very painful, they typically cause tissue and surrounding muscles to die, resulting in extreme cases even in death, if not treated early enough. For long-term patients with little or no movement, active anti-decubitus beds are commonly used in hospitals, with cyclic loading and unloading of different parts of the body. This can be achieved, e.g., by the pumping and releasing of compressed air in a number of chambers forming the bed (an example of such bed is shown in Figure 4.7). The effectiveness of such systems could be enhanced with large area tactile sensor mats, by using the captured pressure information to control the loading and unloading frequency and intensity. Plans are currently afoot to incorporate our fabric-based tactile sensor as a means of gathering such pressure pattern information for more intelligent control of anti-decubitus bedding systems.

Figure 4.7: Anti-decubitus bed with air-chambers for cyclical loading and unloading of body parts. Tactile sensors can make such beds more intelligent by explicitly controlling the applied pressure pattern. Picture showing a commercial product of CareConcept mahnke.

4.3 3D-shaped high spatial resolution tactile sensor

Although the fabric-based tactile sensor, discussed in Section 4.2, has great potential to cover most surfaces of technical systems, it reaches its limitations when it comes to small bending radii and in situations where greater spatial densities than ≈10mm are required. To overcome this limitation, we have developed a groundbreaking new tactile sensor, based on Laser-Direct-Structuring (LDS) technology, to augment freeform surfaces with conductive tracks. It paves the way for the manufacturing of almost arbitrary 3D-shaped tactile sensors. The signal acquisition electronics were embedded on the backside of the sensor layer. To validate our idea, we produced a tactile fingertip sensor for the Shadow Robot Hand, which incorporates 12 tactile sensor regions and embedded signal acquisition electronics.

This project was done in cooperation with Matthias Zenker and Carsten Schürmann, and was supervised by Dr. Robert Haschke and Prof. Dr. Helge J. Ritter. The development and initial measurement results were published and presented at the International Conference on Advanced Intelligent Mechatronics (AIM 2013) [KZS+13] and the work was one of the finalists for the best student paper award. The idea of using LDS to create tactile sensor electrodes came to me during a visit to the Hannover Messe trade fair in which LPKF Laser & Electronics AG and LaserMicronics GmbH presented their LDS machines. My contribution to this project was to coordinate it, to develop the electronic schematic and the data acquisition host software with a graphical user interface for the prototypes, to develop sensor validation measurements, and to write and present the scientific publication [KZS+13]. This project was sponsored by numerous external companies, whom I would like to thank for their help. We received help with injection molding from König Kunststofftechnik GmbH. Ticona GmbH and BASF SE provided us with thermoplastic samples and LPKF Laser & Electronics AG and LaserMicronics GmbH supported us with the LDS-process computer data preparation, laser direct structuring machinery and chemical baths during the production of fingertip tactile sensor prototypes. A significant part of the CAD-works and the mechanical construction, including the design of the injection mold, was performed by Matthias Zenker during his job as a student assistant in our institute.

Figure 4.8: Resistive fingertip tactile sensor with an anthropomorphic 3D shape with 12 tactile cells and embedded signal processing electronics for a human sized dexterous robotic hand. (Note that the cutout in the sensor material covering the electrodes is for illustration purposes only.)

The next subsection introduces our free-form shaped tactile sensor design and describes its construction steps in detail. Subsection 4.3.2 demonstrates an innovative application for the developed sensor in the form of a compact embedded robotic fingertip [Figure 4.8]. In Subsection 4.3.3 the sensor performance is evaluated and measurement results are given. Subsection 4.3.4 discusses future work.

4.3.1 Tactile sensor design

The tactile sensor designed for free-form surfaces is based on the same resistive working principle described in Section 4.1. This project extends the previous design by allowing the sensor to be manufactured in almost arbitrary 3D free-form shapes. To produce 3D-shaped electrodes we use the LDS process, which is described in detail in the next section. To produce curved sensor material (conductive elastomer), we found that high-speed milling in combination with vacuum clamping produced the best results.

Laser Direct Structuring

The LDS process, developed by LPKF Laser & Electronics AG in the late 1990's, allows circuit layouts to be produced on complex three dimensional carriers, also called Molded-Interconnect-Devices (MIDs) [LPK12]. With LDS, the laser beam structures the desired pattern directly onto the (possibly curved) plastic piece. At least two other methods are available for creating MIDs: multi-component injection molding and hot stamping. How-

ever, both have considerably higher manufacturing costs, making them especially unviable in smaller production runs due to additional required specific mold tools needed to create the circuit on the piece. Another considerable benefit of the LDS method is the possibility of creating very fine structures, down to 100μm.

The production of tactile sensor electrodes with LDS technology is a five-step process. The first step is to choose a material for the plastic carrier, which narrows some of the design parameters for the later laser structuring step. A number of laser-activatable thermoplastics are available, differing not only in mechanical properties such as density, tensile modulus or melting temperature, but also in their LDS process parameters, such as the method for creating vias (through-hole connections for creating electrical connection between different sides of the MID). We chose Ticona's Vectra E840i LDS liquid crystal polymer thermoplastic material, due to its dimensional and thermal stability, and its unique property of allowing very tiny vias to be directly punched by laser during the structuring process. As the second step towards producing the LDS-MID, a one component injection mold for the required 3D-shaped form must be constructed and produced. After the tools are ready, the dried and pre-heated plastic granulate is injected under high pressure into the mold, where the MID-blanks can be extracted after the cooling phase. In the third step, the blanks are structured with a laser. The laser-activatable thermoplastic contains a special additive in the form of an organic metal complex, which is activated by a physical-chemical reaction induced by the focused laser beam. This cracks open the complex compounds in the doped plastic, and breaks off the metal atoms from the organic ligands. These act as nuclei for subsequent chemical copper coating. For our tactile sensor electrodes we chose an interwoven M-shaped electrode track that provides the highest sensitivity to first touch as previous experiments have shown (see Section 4.1). In the fourth step, the activated MID's are treated in a number of sequential chemical baths, such as a cleaning bath to remove laser debris, an additive built-up bath to add copper, and a bath to chemically add a thin, final layer of gold to avoid oxidation. In the fifth and final step, the electronic components, such as the data acquisition electronics, are soldered directly to the LDS-MID's, making the final design extremely compact and robust.

Signal digitalization

The resistance measured between two electrodes, or an electrode and a common ground-plane shared by all taxels of a sensor array, is converted to voltage with a simple constant pull-up resistor attached to a constant power supply (voltage divider circuit, as already displayed in Figure 3.22b]. The voltage at the junction of the resistors can be sampled by an ADC, which provides the data in a digital form for transmission or further signal processing. Altering the value of the pull-up resistor allows us to shift the measurement range. Higher resistance allows lower pressures to be measured, at the cost of inducing a higher signal noise and limiting the maximum measurable force.

4.3.2 Fingertip sensor for artificial hand

Our tactile sensor technology is ideal for fingertips, which play a crucial role in human grasping and manipulation and have the highest spatial resolution of the tactile sense in humans [Nap56, JF09]. The tactile sensor is not only usable for dexterous anthropomorphic robotic hands, but could also be implemented in hand prostheses to allow patients regain a sense of touch and thus considerably improve their abilities.

The size of the developed fingertip sensor was chosen to match that of the fingers in the Shadow Robot Hand [Sha], which are approximately the size of adult human fingers. Numerous hand prostheses are also created using similarly sized fingers, such as RSL-Steeper's *BeBionic3* [RSL] or Otto Bock HealthCare GmbH's *Michelangelo* [Ott] hands.

Fingertip sensor construction

The LDS process allows us to embed tactile sensor electrodes and the printed circuit board into a single 3D shaped plastic part. During the shape design process, four basic constraints had to be considered:

- The ability to manufacture the form with an injection mold
- Electrode tracks could not be placed under the mold ejectors
- The maximum material depth was limited to 0.2mm in via locations (to allow the laser to punch a hole through it)
- Access to all desired conductive tracks for the laser beam had to be ensured

The last restriction is less rigorous, as the laser beam is allowed to hit the material with an angle of up to 75° w.r.t. the surface normal. The areas of the parting lines of the injection mold need to have a very high quality to avoid burrs that can cause cracks in the conductive tracks if they cross these areas on the MID. As recommended by Ticona-Celanese, the plastic granulate manufacturer, we used 1.2343 electroslag remelting cavity plates, eroded to a surface roughness of R_a 0.4μm (extremely smooth), to achieve a reliable LDS process [Figure 4.9]. To provide a sturdy mechanical fingertip attachment, our design embeds a mounting dome with a threaded hole directly in the MID carrier, further decreasing the required component count. Figure 4.10 shows the injected plastic fingertip MIDs ready for further processing.

In contrast to common 2D electronic printed circuit boards, the design of the tracks with 3D-shaped MIDs also has to be developed in 3D. Figure 4.11 shows the result of the 3D CAD circuit, with the tracks of the tactile sensor electrodes on the outside and the tracks for the attachment of Surface-Mount-Devices (SMDs) on the inside of the fingertip MID.

Figure 4.12 displays the laser system with a gimbal table used for punching the vias and activating areas to be chemically metallized in a later processing step.

In the next step, the MIDs are processed in numerous chemical baths to apply conductive particles in areas where the laser has activated the material [Figure 4.13]. The final bath before the last washing step applies a thin layer of gold to avoid oxidation.

To produce the required 3D-shaped sensor material that covers the electrodes, we used a conductive elastomer from Weiss Robotics. Thanks to a relatively high ductility, this material can be produced in the desired shape using a high-speed mill. Milling the foam is a two-step process. First, the outer shape is milled on a flat vacuum table, and this is followed by milling the inner cavity in a negative vacuum to form the outer shape. The mill with a custom built vacuum clamping rig is displayed in Figure 4.14a. Our design uses a uniform sensor foam thickness of 2.0mm, which was the minimal thickness we were able to reliably manufacture. The milled sensor foam is glued to a plastic bracket, keeping the foam within the limits of the desired clearance to the electrodes [Figure 4.14b]. The tactile fingertip sensor is mounted onto the robotic hand using a screw, which ensures a firm fit of the bracket and the MID.

(a) A single shot, two-plate custom mold for creating fingertip MIDs in the injection molding machine. A single mold can be selectively used to produce fingertip MIDs or the slightly larger thumb-tip MIDs, by turning the sprue bush in the middle of the mold 180°.

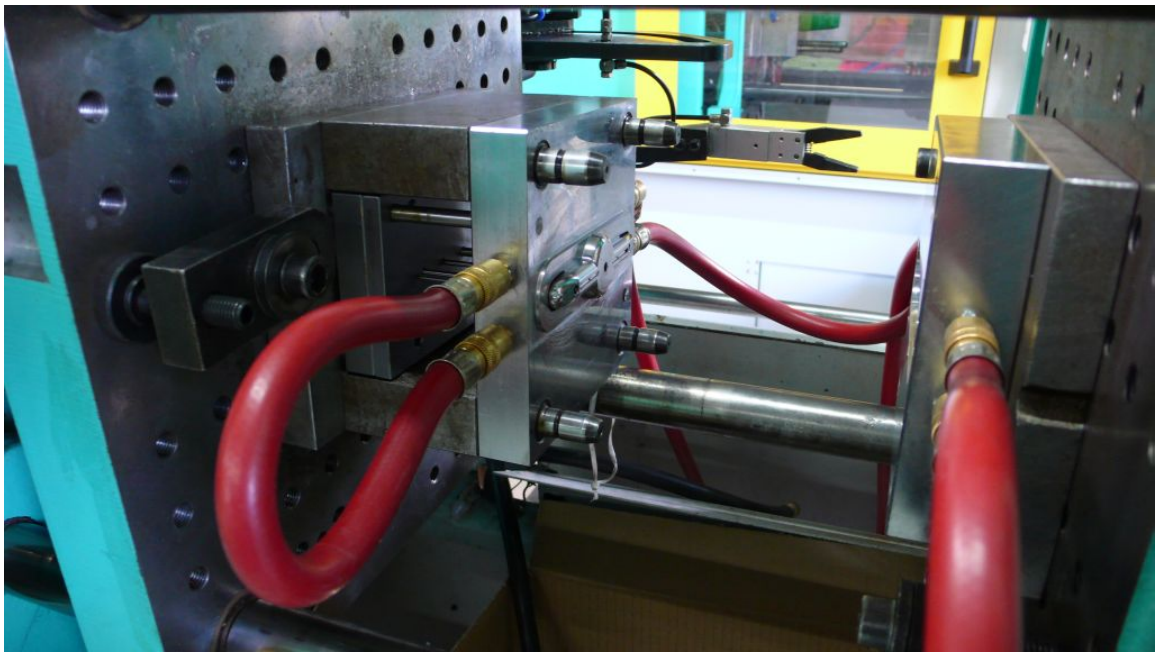

(b) Mold mounted in the injection molding machine with red cooling fluid tubes attached.

Figure 4.9: Injection mold for creating fingertip MIDs. (Both photographs taken by Matthias Zenker at König Kunststofftechnik GmbH during the injection molding process.)

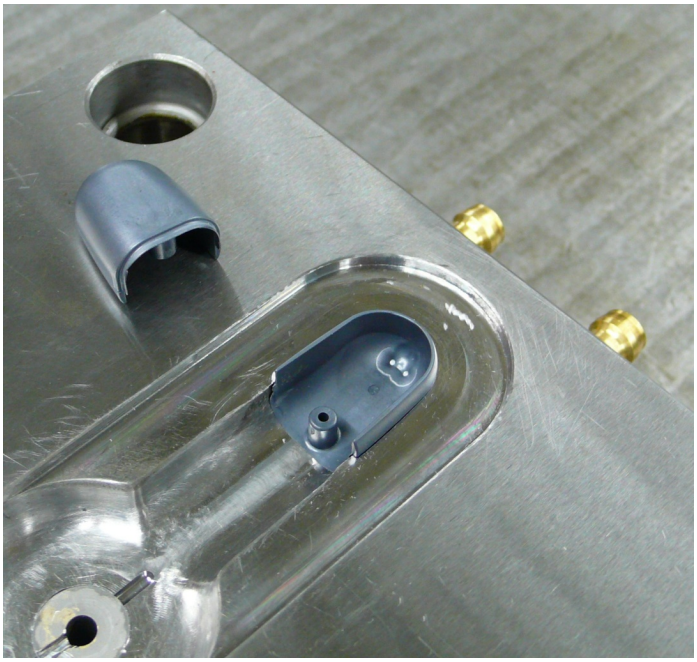

Figure 4.10: Injected fingertip blanks. Notice the embedded mounting dome and cavities near the tip of the MID for laser-punching the vias in a later processing step. (Photo taken by Matthias Zenker at König Kunststofftechnik GmbH.)

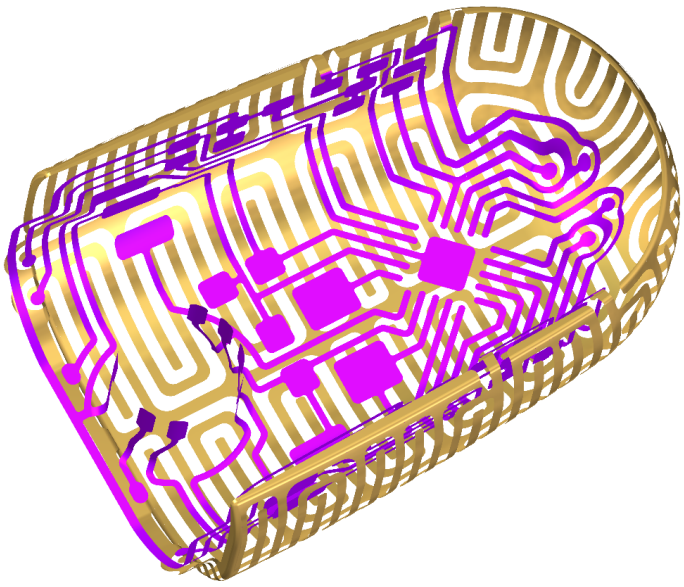

Figure 4.11: CAD screenshot of constructed 3D-shaped tracks. The tactile sensor electrode tracks on the outer surface are displayed in gold, the inner circuitry attaching to data acquisition electronics are displayed in violet.

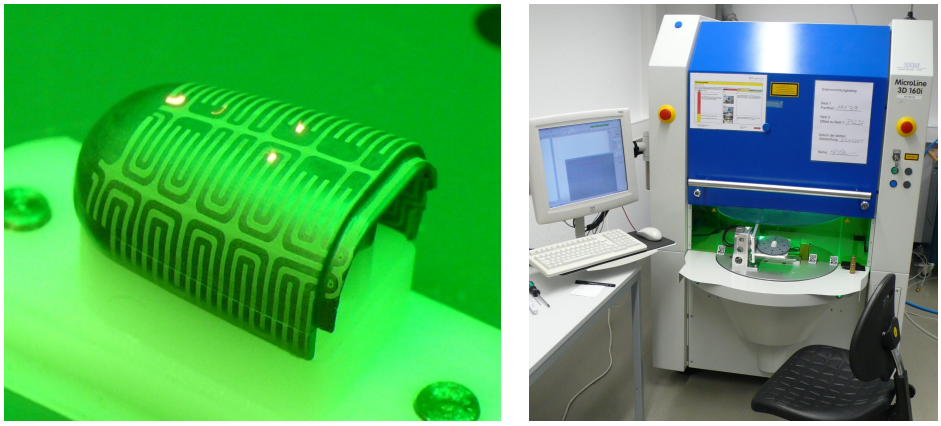

Figure 4.12: **(Left)** A laser beam punches the vias and activates the surface of the MID at areas to be metallized in a later processing step. The picture shows multiple laser points due to the slow shutter speed of the camera. **(Right)** A LPKF MicroLine 3D 160i laser system with gimbal table was used for this processing step. (Both photographs taken by Matthias Zenker at LaserMicronics GmbH)

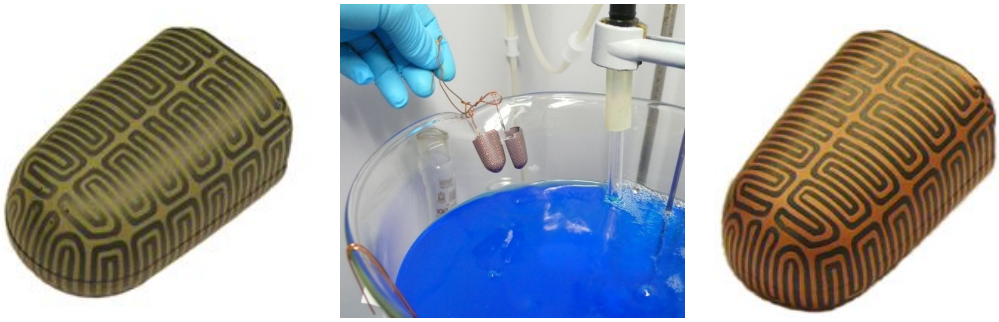

(a) Fingertip MID after 3D lasering.

(b) Chemical baths to apply conductive tracks.

(c) Fingertip MID after chemical baths.

Figure 4.13: After laser activation, the MID undergoes numerous chemical baths and washing sessions. A layer of gold covers the final fingertip MID in **(c)** to protect the tracks from oxidation. (Photographs (a) and (b) taken by Matthias Zenker at LaserMicronics GmbH)

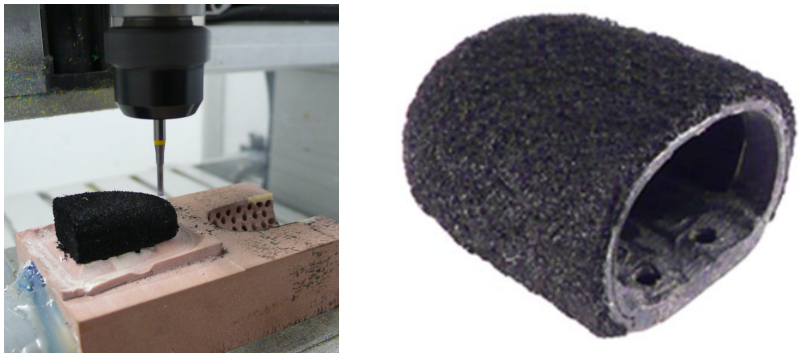

(a) CNC-milling of the elastomer foam.

(b) Finished 3D-shaped sensor material with mounting bracket.

Figure 4.14: The conductive elastomer sensor material must match the 3D surface of the electrodes. For this high-speed CNC-milling with vacuum clamping was utilized. (Both photographs taken by Matthias Zenker)

Data acquisition

Although we explicitly targeted the fingertip of the Shadow Robot Hand [Sha], the manufacturing steps and the developed data acquisition electronics can be used with no or very minimal alterations to build similar tactile fingertip sensors for numerous other robotic or prosthetic hands. In the Shadow Robot Hand, the fingertips are provided with +5V DC and are connected with a 2MHz Serial Peripheral Interface (SPI) bus to the main control board of the hardware. These were the main limiting factors for our data acquisition scheme – in addition to the very confined space that is available. For an improved signal-to-noise ratio and due to the availability of the digital bus, the circuitry for analog voltage measurements and the digital communication was directly integrated into the fingertip. Instead of relying on a stock ADC with an integrated SPI-bus, we decided to use a programmable module in the fingertip for higher protocol configurability and thus better adaptability to different hardware systems.

When grasping and manipulating, humans can detect object slippage using Pacinian corpuscles – mechanoreceptors in the human skin, capable of registering vibrations up to 400Hz (see Subsection 2.1.1). In another tactile sensor project, discussed in detail in Section 4.1, we showed that slip detection is possible with our resistive tactile sensor design employing high sampling rates of up and above 1kHz. Therefore, a major design goal of this project was to maintain or improve on this capability.

From these considerations a single reprogrammable microcontroller chip was chosen to perform both the analog sampling and the digital communication. The microcontroller used is an 8-bit ATtiny40 in a 3×3mm QFN package. Using an internal 8MHz clock, this chip needs only one capacitor and a resistor (as external components) to function. It features 12 ADC inputs with a sampling resolution of 10 bits and a maximum combined sampling frequency of 40kHz. It enables our fingertip sensor to be equipped with 12 taxels, resulting in an average spatial resolution of ≈5.5mm. In terms of digital communication it is employed as a slave device with an SPI clock rate of up to 2MHz.

The LDS process allows data acquisition electronics to be directly embedded on the backside of the sensor [Figure 4.15]. As the electrical components are fitted in the inside of the fingertip, the electrodes on the outside have vias to connect to the ADC channels of the microcontroller. Additionally a dedicated pull-up resistor is connected between each taxel and the supply voltage of +5V.

A reflow-oven was used to solder all the electronic components at one time. To keep the components on their positions on the concave inner surface during the reflow process, they were first glued to their targeted positions using Loctite *Chipbonder* surface mount adhesive. Appendix 6.5.1 shows the schematic of the tactile fingertip sensor and Appendix 6.5.3 gives the corresponding taxel mapping.

4.3.3 Sensor evaluation

The tactile sensor performance was evaluated using the custom built measurement bench presented in Appendix 6.1. To test the tactile sensor discussed in this section, we used a circular plastic probe tip with a $1cm^2$ tip area. Measurements were done using flat probes on a flat tactile sensor specimen [Figure 4.16], considerably simplifying the experimental setup with regards to freeform specimens. As the sensor array output depends only on the applied force and the contact surface area, no error to the measurement results was expected due to this simplification.

Figure 4.15: Finished fingertip electrode prototypes displaying the soldered data acquisition electronics embedded on the inside of the MID.

As a sensor material we used a conductive foam from Weiss Robotics with a milled thickness of 2.0mm, similar to our 3D-fingertip milled elastomer material. Each taxel of the sensor was connected via an exchangeable pull-up resistor to a regulated +5V voltage source. The selection of the pull-up resistor value allows the force region of interest to be shifted as is demonstrated in the results of the measurements. The voltage drop over the sensor, the supply voltage and the strain-gauge reference value were sampled with a 16-bit DAQ-card. We limited our measurements to an upper value of 10N (which equates to 100kPa using a $1cm^2$ probe tip), as the output signal is close to saturation at this force level. An experiment discussed in Subsection 3.4.1 showed that typical human fingertip forces do not exceed this value.

During the measurement trials we loaded the sensor from idle to 10N and retracted the probe tip back to idle again. For this, we positioned the probe above the measured taxel and iteratively moved the probe tip downwards in steps of 0.1mm. At each step we waited for 0.3 seconds for the mechanics to stabilize and performed simultaneous measurements of the test sensor and the reference strain gauge sensor. We continued until a force of 10N was reached, after which we retracted the probe tip in the same fashion to produce measurements in both the positive and negative directions. Over 500 data points were gathered in a single trial, which lasted approximately 6.5 minutes. Figure 4.17 depicts the sensor output over 10 consecutive trials for two pull-up resistor values of 100kΩ and 1MΩ. Noticeable hysteresis in the sensor output can be observed and is indeed found in many tactile sensors [DMVS10]. Using a higher pull-up resistor shifts the measurable force range towards lower forces thus makes the sensor more sensitive, but also limits the maximum discriminable force.

Figure 4.18 displays the calculated sensor resistance. The sensor is highly sensitive to first touch and the signal repeatability is very high. With a 1MΩ pull-up resistor, reliable detection of $0.03N/cm^2$ was demonstrated.

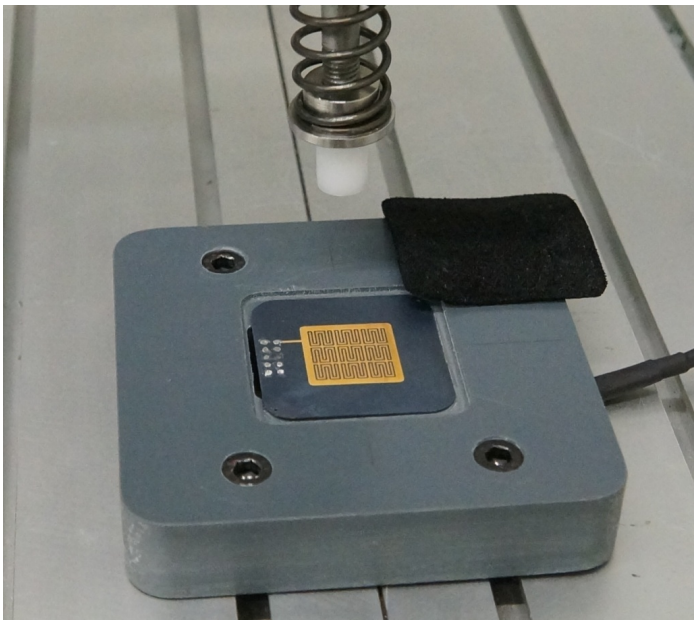

Figure 4.16: Sensor performance measurement using a 3×3 flat tactile sensor produced with LDS-technology explicitly for evaluation purposes. The picture also shows the Weiss-Robotics conductive sensor material milled to 2.0mm thickness (black rectangular part in picture), and the circular 1cm^2 plastic probe (white).

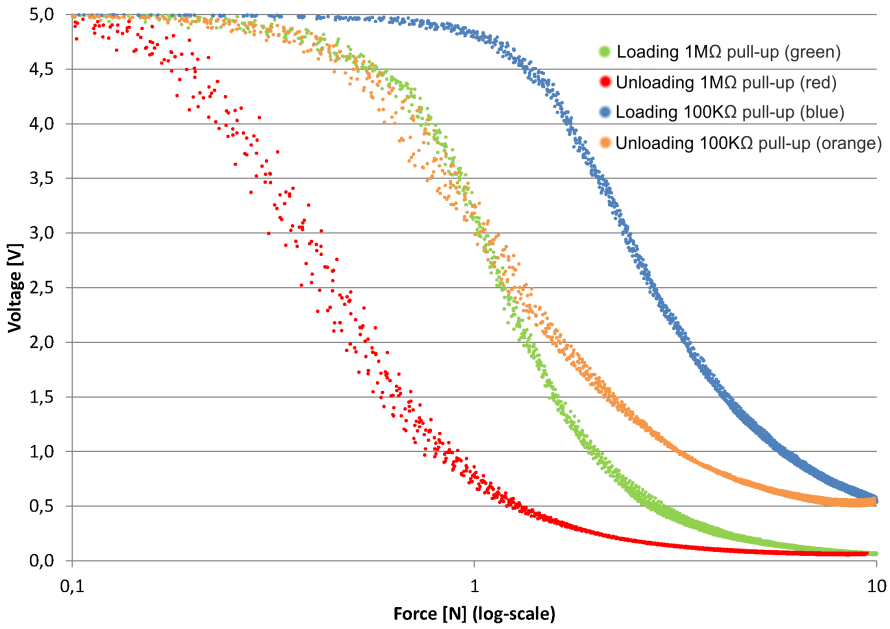

Figure 4.17: The sensor output as measured using a 1cm^2 plastic (POM) flat probe tip using 100KΩ and 1MΩ pull-up resistor values, while the voltage divider circuit supply was a constant +5V. Green and blue points depict the loading phase from idle to 10N, while the red and orange curves show the measured points captured during the unloading phase. Each trial was repeated 10 times.

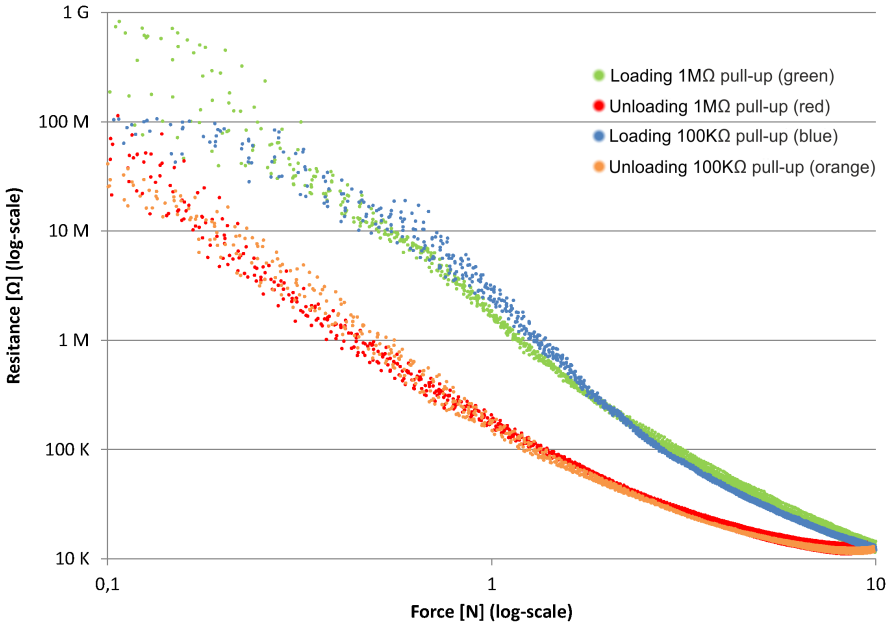

Figure 4.18: The calculated resistance of the tactile sensor from the input data of Figure 4.17. 0.03N was experimentally found to be a reliable detection threshold using a 1cm^2 probe tip and a 1MΩ pull-up resistor.

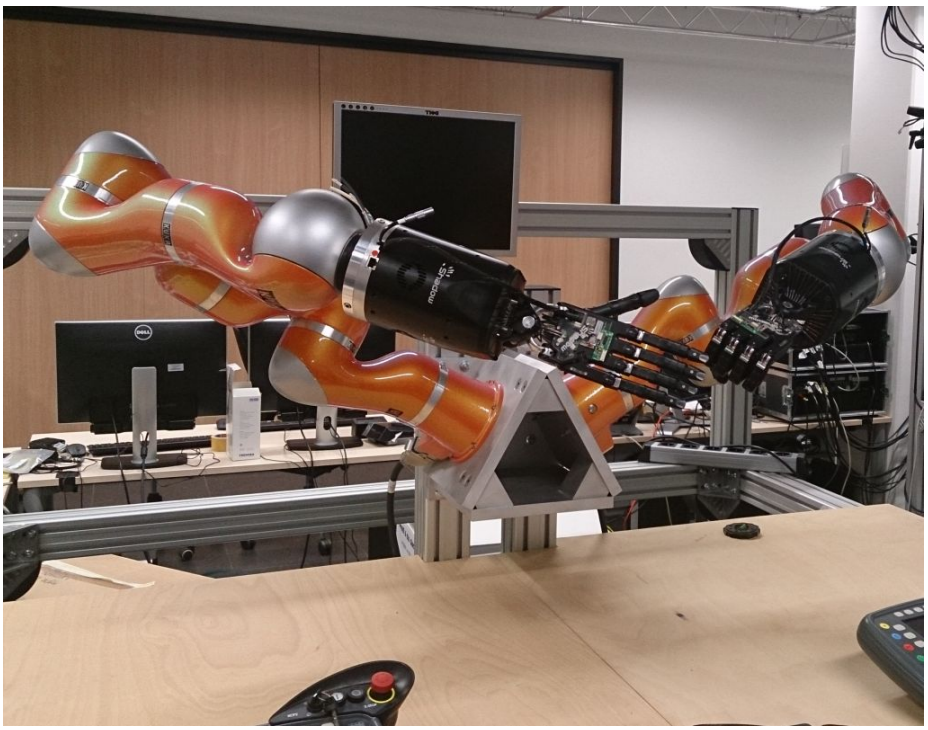

Figure 4.19: Our institute's new bimanual robot laboratory. A right-left pair of E2M3X Shadow Robot Motor hands mounted on two Kuka Roboter GmbH *Lightweight Robot 4* (LBR4) arms will be used for grasping and manipulation research. The novel fingertip tactile sensors will soon be integrated into the robot hands.

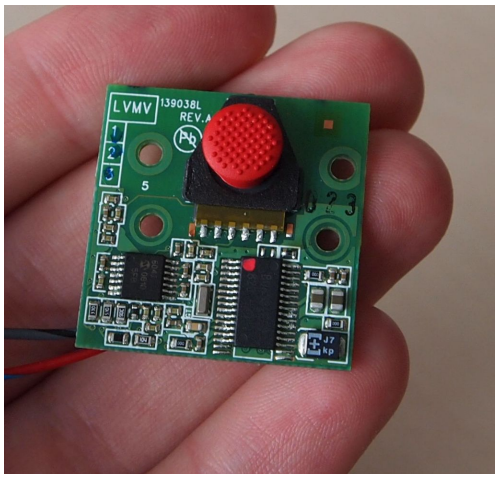

(a) *TrackPoint* mouse input device unit as taken from IBM/Lenovo keyboard.

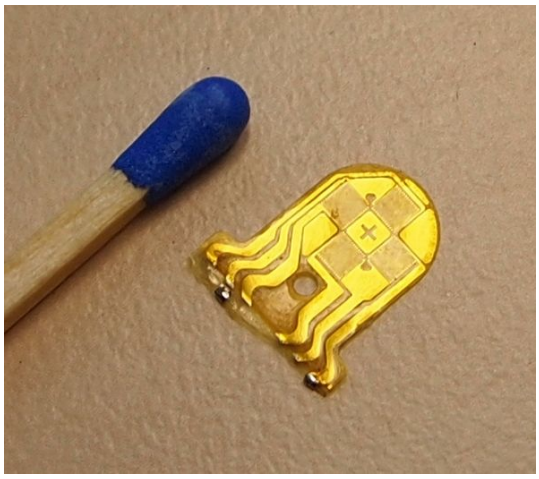

(b) Two axis strain gauge sensor element of the *TrackPoint* sensor.

Figure 4.20: Directional sensing, as for example using the two axis strain-gauge sensor found in *TrackPoint*, can further enrich the captured tactile data.

4.3.4 Future work

As an immediate next step, we plan to integrate the manufactured sensor fingertips into our Shadow Robot Hands [Figure 4.19]. However, we are continuing to test numerous sensor materials, in an endeavor to allow further miniaturization and possibly achieve even higher spatial resolutions.

As our resistive tactile sensor technology, used in the 3D-shaped sensor introduced in this section, can measure applied pressure in the normal direction only, adding additional sensors to also measure shear forces would significantly improve the sensor to have human-like sensor characteristic (see also Section 2.1 for further information about the human sense of touch and the related sensory organs). As our fingertip sensor design presented in this section only uses a fraction of the available space in the fingertip, numerous possibilities are available to add even a bulky strain-gauge based system into the available space. M3282 would be a possible 6D force-torque sensor candidate from SRI [SRI], developed especially towards robotic fingertips. Unfortunately it does not include the necessary signal conditioning electronics and the large sensor alone would take up all the available space inside the fingertip. A considerably less bulky option would be to use a dual-axis strain gauge foil directly, as found for example in *TrackPoint* input devices [Figure 4.20]. A preliminary experiment with a dummy solid fingertip instead of a (typical red) *TrackPoint* cap and custom electronics showed exceptional sensitivity and thus paves the way for this sensor technology to be included in future versions of fingertip sensors.

Another very interesting idea would be to equip robotic fingers with sensitive fingernails. With the addition of a multi-axis accelerometer to the fingernail, Sinapov *et al.* [SSSS11] showed promising surface classification capabilities by analyzing the frequency-domain signals. Another idea is to test the usability of surface microphones for this task.

Robotic grasping attention could also benefit from augmenting force/pressure sensors with pre-touch sensors, such as using the *seashell effect* [JS12]. This allows the technical system to sense the proximity of objects before actual contact is made, thus alerting the control system to proceed with higher concentration.

Finally, plans are in motion to integrate the developed fingertip sensor into hand prostheses, which holds the possibility of restoring patients' sense of touch in their fingertips. To convey the tactile data to the user, we are considering non-invasive information transmission using visual channels, such as a graphical tactile overlay map of fingertip taxels on see-through video goggles (such as Google's Glass [Goo]).

5 Conclusion

5.1 Concluding remarks

A sense of touch is more important than we typically give it credit for. The distributed nature of biological mechanoreceptors makes the sense of touch extremely robust and resistant to errors. Nevertheless, in these rare cases when haptic feedback is lost, the implications are significant. Not only is fine grasping and manipulation impossible due to unavailable feedback, even maintaining body posture, such as when simply standing up, is not possible if not actively controlled through another sensory channel.

Artificial sensory devices for sight and sound, the two other main sensory channels that humans possess, have been studied for decades. We can fall back on capable camera and microphone systems that exceed the capabilities of their human biological sensors in all major aspects, e.g., resolution, frequency spectrum, sensitivity and operating environment conditions. However, research on artificial tactile sensing has until now, unfortunately received only low to moderate interest, which easily explains why current robotic systems are still so clumsy when operating in non-deterministic environments.

Observing human haptics and extracting the salient information from the gathered data is not only a necessity if we are to try to understand the underlying cognitive processes, but should also give significant clues to designing future intelligent interactive systems. Such devices could one day take the burden of everyday tedious tasks away from us in a similar fashion to how industrial robots revolutionized manufacturing. The aim of the work in this thesis was to provide significant further steps along the path towards reaching this grand goal. In terms of the main goal of this thesis, namely to make haptics more observable, I argue that the high number of developed novel tactile sensors has clearly achieved this goal. These sensors make it possible to gather haptic interaction data from a wide spectrum of usage scenarios and provide new insights into haptics in numerous research fields such as robotics, rehabilitation, kinetics, psychology, ambient intelligence and human-machine interfaces.

The developed tactile sensors were presented in two parts, with Part A (Chapter 3) concentrating on sensor developments towards observing human tactile interactions and Part B (Chapter 4) discussing sensors for augmenting technical systems with the sense of touch. This division stems from the fact that many of the developed sensors were designed for an initial target application that fell into one of these two categories. The sensory device or the underlying sensor technology is in most cases not limited to these specific domains. Figure 5.1 provides a coarse estimate of the potential of the tactile sensor developments presented in this thesis to be used to observe haptics in humans or to augment technical systems with the sense of touch.

tacTiles, introduced in Section 3.1, were developed to capture human full-body interactions with large objects, such as sofas, mattresses, doormats, yoga mats, chairs, backpacks, walls or floors. However, by covering technical systems, such as industrial robot arms or mobile bots with tacTiles mats, a low spatial resolution artificial sense of touch can be realized on such systems. The performance of tacTiles might already suffice in many situ-

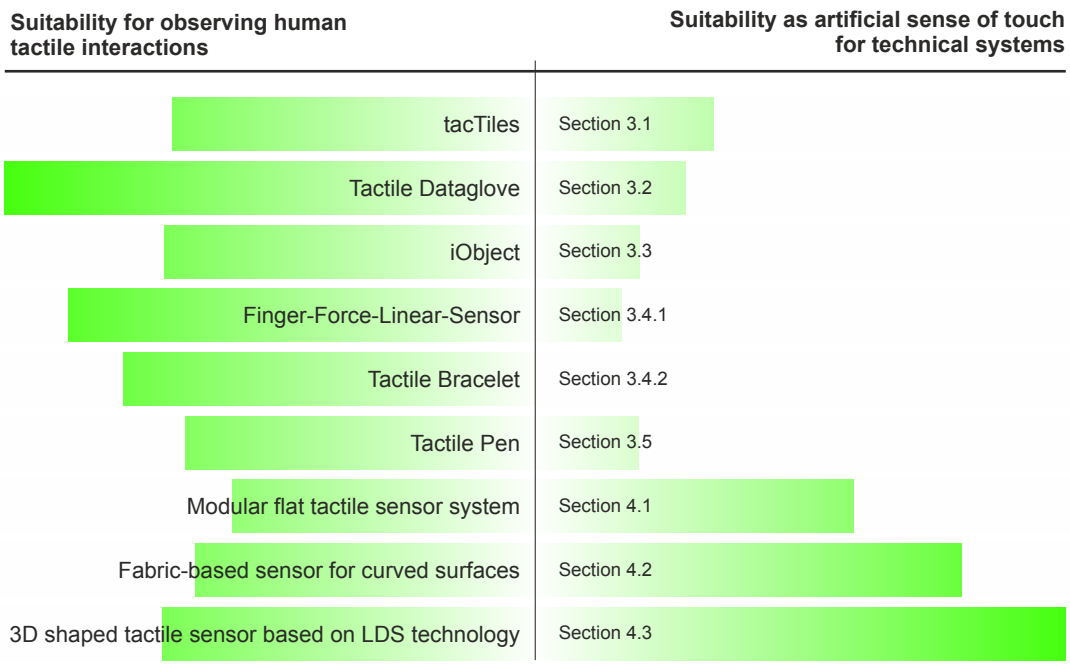

Figure 5.1: Chart estimating the suitability of the various developed tactile sensors in this thesis for the tasks of observing haptics in humans and augmenting technical systems with the sense of touch.

ations, e.g., for simple contact or collision detection with rough contact point localization. The requirement that tacTiles be very robust was proven to have been achieved during a 3 month hands-on experience exhibition called *Sonic Interaction Design* in Oslo's Technical Museum in Norway. Open to the general public, tacTiles in the form of a cover for an office chair, survived the sometimes rough handling it received from adults and children alike and continued operating without mechanical malfunction for the entire exhibition.

The *Tactile Dataglove* [Section 3.2], *iObject* [Section 3.3] and *Tactile Pen* [Section 3.5] were especially developed to observe human manual intelligence. Whereas, iObject allows motion sensing and a higher definition tactile signal to be captured than the tactile dataglove (220 taxels in the first iObject prototype versus 54 taxels in the glove), the wearable glove makes haptic interactions with arbitrary objects observable. The Tactile Pen was designed especially to measure the grip force during handwriting in order to better facilitate therapeutic treatment assessment. All three sensors possess great potential to help reveal some of the cognitive processes behind human manual interactions. Fitting the tactile dataglove over a suitable anthropomorphic robotic or prosthetic hand will enable such system to measure contact patterns in the fingers and in the palmar area of the hand. Grasp comparisons between humans and robots are future research directions made possible by these two devices.

The *modular flat tactile sensor system*, *fabric-based touch sensitive artificial skin* and *3D shaped tactile sensor* were developed to cover and to add touch sensing to the surfaces of technical systems. The rapid augmentation of systems with a sense of touch was the main goal of the modular flat tactile sensor system introduced in Section 4.1. Due to its modular construction, tactile sensitive surface areas in different shapes and sizes can be assembled using the 80×80mm modules in a very short time by simply interconnecting the modules to form a desired flat shape. A spatial resolution of only 5mm and a system

throughput of up to 500,000 taxels/second enable high fidelity tactile sensing for technical systems. On the other hand, when two or more modules are assembled on top of each other, instrumented graspable objects with touch sensitive outer surfaces can be created using this sensor technology, making human haptic interactions observable. The cover page of this thesis shows a haptic image of my hand on a 3×3 module unit. As many robots use curved surfaces, the usage of such rigid modules to cover their outer surface is however limited. The fabric-based tactile sensor, originally developed to form a tactile dataglove for human hands, can with minor modifications also function as an artificial skin for technical systems. Section 4.2 presented design ideas, currently in the prototype stage, to add a sense of touch to larger palmar areas of Shadow Robot hands. Although this sensor technology has not yet reached the high spatial resolutions of the modular flat tactile sensor system, it can conform to curved surfaces and thus is able to cover significantly greater surface shape variations of technical systems. The 3D shaped tactile sensor, presented in Section 4.3 is a ground-breaking novel tactile sensor development that can be produced in very high spatial resolutions and in almost arbitrary shapes. It is based on the 3D-shaped resistive tactile sensor electrodes that are produced using injection molding and Laser-Direct-Structuring (LDS). As a proof-of-concept, this thesis presented a sensor in the shape of a robotic fingertip with 12 taxels and embedded signal acquisition electronics. Not only can this be used to create almost arbitrary shaped tactile sensors, it allows for a very compact build by embedding the required data acquisition electronics directly on the back of the sensor surface. In my opinion, this 3D-sensor has a very high potential to change the tactile sensing capabilities of intelligent interactive systems in the near future. All three sensors discussed in this paragraph could also be used to build instrumented objects for observing human manual interactions. The 3D shaped tactile sensor technology allows the highest sensor fidelity and variations in object shape, and is therefore the candidate for constructing such objects.

The *Finger-Force-Linear-Sensor* and *tactile bracelet* are two novel sensors that were developed to allow more natural control of dexterous multi Degree-of-Freedom (DOF) hand prostheses. Instead of simply classifying postures as has been traditionally done, controlling the force of individual finger joints will, in our opinion, provide significant benefits especially when interacting with non-deformable objects. In order to develop and test the different mappings between generated single finger forces and muscle activations, a ground-truth measurement device that could capture the single finger forces, initially on able-bodied people was required. The Finger-Force-Linear-Sensor, introduced in Subsection 3.4.1, was developed for this purpose. Both, right and left hands, whether small or large in size, can be placed into the Finger-Force-Linear-Sensor to very accurately measure the forces generated by the fingers and the thumb. To intuitively gather the manual intentions of lower arm amputees a tactile bracelet, introduced in Subsection 3.4.2 was designed with the goal to provide a more robust means of control for multi-DOF hand prostheses. An experiment that used a flat tactile sensitive table to create a mapping between forces and muscle bulgings measured only in the ventral side of the arm showed very promising initial results. These findings suggest there is hope that tactile sensor technology can become a viable alternative to the current method of surface ElectroMyoGraphy (sEMG) in intention gathering tasks. The tactile bracelet, currently in development, will eventually cover the complete forearm circumference with high spatial resolution tactile sensitive surfaces. In a planned future experiment that will be done in cooperation with the Technical Orthopedic Department at Heidelberg University, the tactile bracelet will be exhaustively tested on a large number of lower arm amputees.

Already, the results of the first experiments conducted using the developed novel tactile sensors presented in this thesis show clearly that by observing humans with high-fidelity sensors as they perform manual interactions, we can enrich our understanding of human manual intelligence. Future technical systems will profit considerably from a sense of touch, regardless of whether they are interacting with the environment or humans. The high number of novel, practically usable, tactile sensors developed in this thesis is a significant step forward towards observable haptics.

5.2 Future outlook

Although some initial experiments using the numerous novel tactile sensor designs were presented in this thesis, there remain countless opportunities to devise clever new experiments involving the designed sensors. With the ultimate goal of understanding and later replicating human haptic cognitive processes in technical systems, many further experiments involving the sense of touch are necessary. Finding salient attributes in haptic data is a first step towards this high goal.

Due to time constraints, not all ideas and experiments were able to be executed in the timeframe of this PhD thesis. Devoting additional resources into further research and development would yield even better performing and optimized tactile sensors. The following paragraphs of this section present future plans for many projects, some with mature and thoroughly planned ideas just waiting to be executed in next available timeslot, and some still in their infancy requiring further work on specifications and details.

Tactile Dataglove. As an immediate next step, we want to integrate postural sensing into our wearable dataglove. The data acquisition electronics of a future prototype will receive an additional 9-DOF motion sensing device in the wrist unit, and the glove will become wireless by streaming live tactile data over radio waves for online capabilities or for an offline setup by recording the captured haptic interactions to an onboard memory card. In addition to planned tactile exploration experiments in our manual intelligence laboratory (MILAB), the wearable dataglove will be used by EU FP7 funded project *WEARHAP* (WEARable HAPtics) partners in future experiments, e.g., in the fields telerobotics, gaming and telehaptics.

iObject. An improved version of instrumented/intelligent Object, *iObjectPlus*, is currently under development. It will offer twice the spatial resolution of the original design and will be equipped with a higher bandwidth wireless communication. iObject plays a central role in a DFG-supported project called *Haptic Learning* which is a collaboration between our institute, led by Prof. Dr. Helge J. Ritter, the Department of Brain Robot Interface in Advanced Telecommunication Research Institute International (ATR) in Japan, led by Prof. Dr. Jun Morimoto, and the Computational Neurosciences Group in Göttingen University in Germany, led by Prof. Dr. Florentin Wörgötter. The goal of the project is to gain an insight into the brain processes during learning of haptic interactions. The participants have to learn a highly haptic driven task while manipulating iObject and while doing this functional-Magnetic-Resonance-Imaging (fMRI) is used to locate regions of activity in the brain. From the gathered data we wish to discover new insights in how haptic tasks are learned. Further experiments involving iObject are planned in our grasp lab, e.g., human/robot grasping task comparisons.

Augmenting our laboratory's robotic hands with the sense of touch. In an ongoing project in cooperation with the Shadow Robot Company, we will finish the fabric-based tactile artificial skin patches that are to be fitted onto the palm and proximal phalanges of the Shadow Robot hands in our laboratory. Additionally, the fingertip tactile sensors are soon going to be mounted onto the same robotic hands. Furthermore, initial ideas of adding directional force sensing, temperature sensing and embedding surface microphones into the fingertip sensors in order to have more robust slip detection have already been sketched. A prototype of an optical pre-touch sensor has been successfully developed that will further enrich the sensing capabilities, especially in solving grasping tasks.

Robust control of hand prostheses. Together with Dr. Claudio Castellini from the German Aerospace Center (DLR) and Mr. Merkur Alimusaj from the Technical Orthopedic Department at Heidelberg University, we will, after finishing the hardware of tactile bracelet, look into the mappings between single finger forces and haptic images of forearm using the Finger-Force-Linear-Sensor as a reference sensor. If these experiments prove fruitful, *tactile myography* can realistically be used to control future multi-DOF hand prostheses.

Various. In cooperation with the Ambient Intelligence group in our Institute, plans are afoot to create further large scale mats using the tacTiles technology in order to augment sofas and other pieces of furniture in our intelligent apartment.

Together with ergotherapist Gerhard Mahlich, we will continue our work on the tactile pen, to help adults and children alike with handwriting disorders.

Finally, the 3D shaped tactile sensor design is not limited to robotic fingertips. Its sturdy mechanical construction and relatively simple data acquisition electronics make this an obvious artificial sensor choice for a wide variety of future intelligent interactive systems.

6 Appendix

6.1 Tactile sensor performance measurement rig

In order to evaluate the performance of the tactile sensors introduced in this thesis, a measurement bench was developed that is capable of exerting forces from 0 to 80N [Figure 6.1a]. The reference force is measured by a calibrated ME-Messsysteme GmbH KD140-200 [ME-b] industrial strain gauge force sensor connected to a signal amplifier. The sensor has a great linear output with a relative error of only 0.02% and total accuracy of better than 0.1% over the measurement range. The strain gauge reference sensor is mounted on a vertical linear axis and its position is actuated by a stepper motor driven by the connected PC. The linear movement is transformed to a change in force via a coil-spring. Exchangeable probe tips made from different materials, and coming in different shapes and sizes can be mounted on the M5 threaded cap connected to the spring. The electrical axes drive unit, control software and measurement rig calibration, plus most of the measurement rig's mechanical construction was done by me.

A National Instruments PCIe-6259 data acquisition card is used to sample the reference sensor and the tactile sensor(s) being tested. The same card is also used to control the motion of the measurement bench axes and to provide an adjustable bias voltage, necessary for resistance measurements with a voltage divider circuitry.

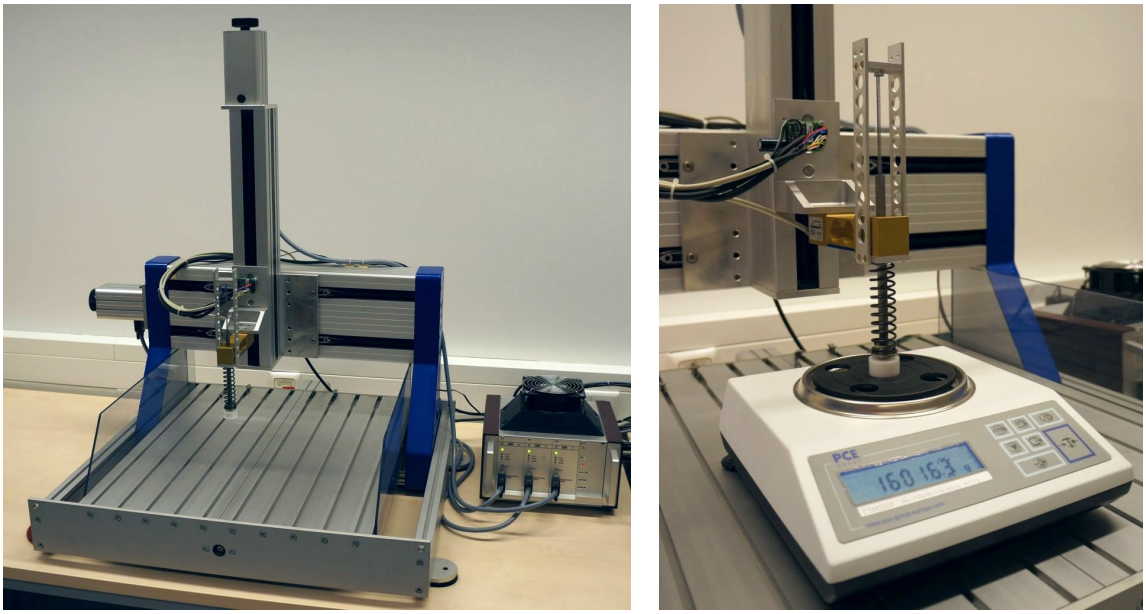

(a) Measurement rig. **(b)** Calibration process.

Figure 6.1: Custom built tactile sensor evaluation measurement rig with a calibrated industrial strain gauge reference sensor mounted on a numerically controlled linear axis. (b) depicts the calibration process using precision laboratory scale.

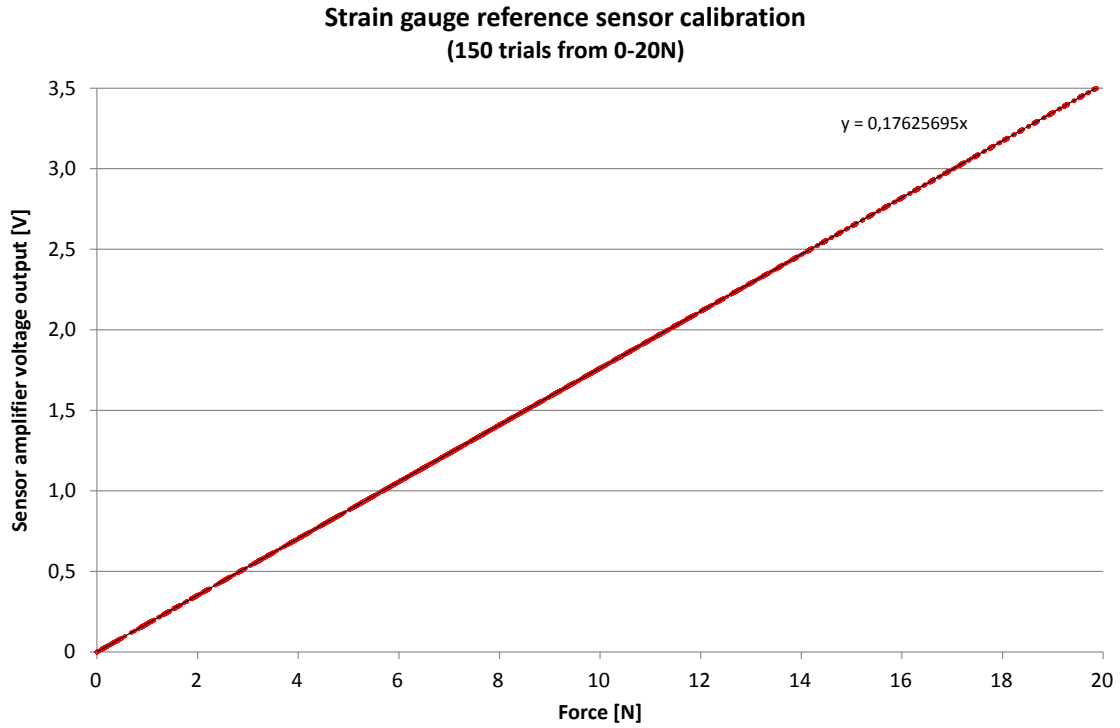

Figure 6.2: Strain gauge calibration result over 150 trials showing exceptional linearity and repeatability. The ground truth was taken from PCE-LSM2000 precision scale (assuming a gravitational field of $9.807 m/s^2$).

I developed a generic control software stack, allowing text-based scriptable control of axis and measurement triggering. Force application can be optionally controlled according to a reference sensor output and iterations can be programmed towards performing high-count automated measurement runs. The output of the measurements are saved in simple ASCII text files that are timestamped and in a delimited format so that they can be imported into arbitrary data analysis programs.

To calibrate and verify the operation of the measurement rig, I used LSM2000 laboratory scale from PCE [PCE] with a 2000g range and 0.1g accuracy [Figure 6.1b]. The integrated data communication port (RS-232C) of the LSM2000 scale allows scripted automated measurements to be made by the connected PC. Assuming a standard gravitational field (g) of $9.807 m/s^2$, we calculate the force, F, in Newtons by:

$$F = m * g \tag{6.1}$$

where the mass, m, is in kilograms.

Figure 6.2 displays the measurement results of the KD140 strain gauge sensor connected to PCIe-6259 analog input over 150 trials, while applying a ramp force from 0 to 20N using the vertical axis of the measurement rig setup. Over the course of a single ramp, the system made approximately 70 measurements, lasting 6 seconds each to stabilize the rig mechanics and scale reading, making a total experiment duration of ≈18 hours. The results verify the high linearity and exceptional repeatability of the sensor system and show the gain coefficient necessary for later tactile sensor measurements to convert the output voltage to force readings.

6.2 tacTiles electronic component list

C1-C16	100 nF
C17	10 μF / 16 V
C18	100 μF / 16 V
D1	1N4007
D2	blue LED 5mm
D3	red LED 5mm
IC1	L4940V5 low-drop positive voltage regulator, 5 V
IC2	PIC18F4580 8-bit microcontroller
IC3	MAX232A RS-232 line driver/receiver
IC4	4 MHz oscillator, 5 V
K1	5V relay, double pole double throw (DPDT)
R1	100 Ω, 1/4 W
R2	470 Ω, 1/4 W
R3	620 Ω, 1/4 W
R4	680 Ω, 1/4 W
R5-R7	2.7 KΩ, 1/4 W
R8-R17	10 KΩ, 1/4 W
R18	100 KΩ, 1/4 W
S1-S12	2-pin straight header, 2.54 mm grid
S13	5-pin angled header, 2.54 mm grid
S14	6-pin straight header, 2.54 mm grid
T1	BD238 PNP-transistor
T2	BC547 NPN-transistor
T3	BS170 N-channel field-effect-transistor (FET)
8x	Interlink Electronics FSR-406 force-sensitive-resistors (FSRs)
2x	reed switches, 100mA
1x	Free2move F2M01 Bluetooth module
1x	2-cell 1500mAh Lithium-Polymer Battery

6.3 iObject

6.3.1 iObject Main-Processing-Unit schematic

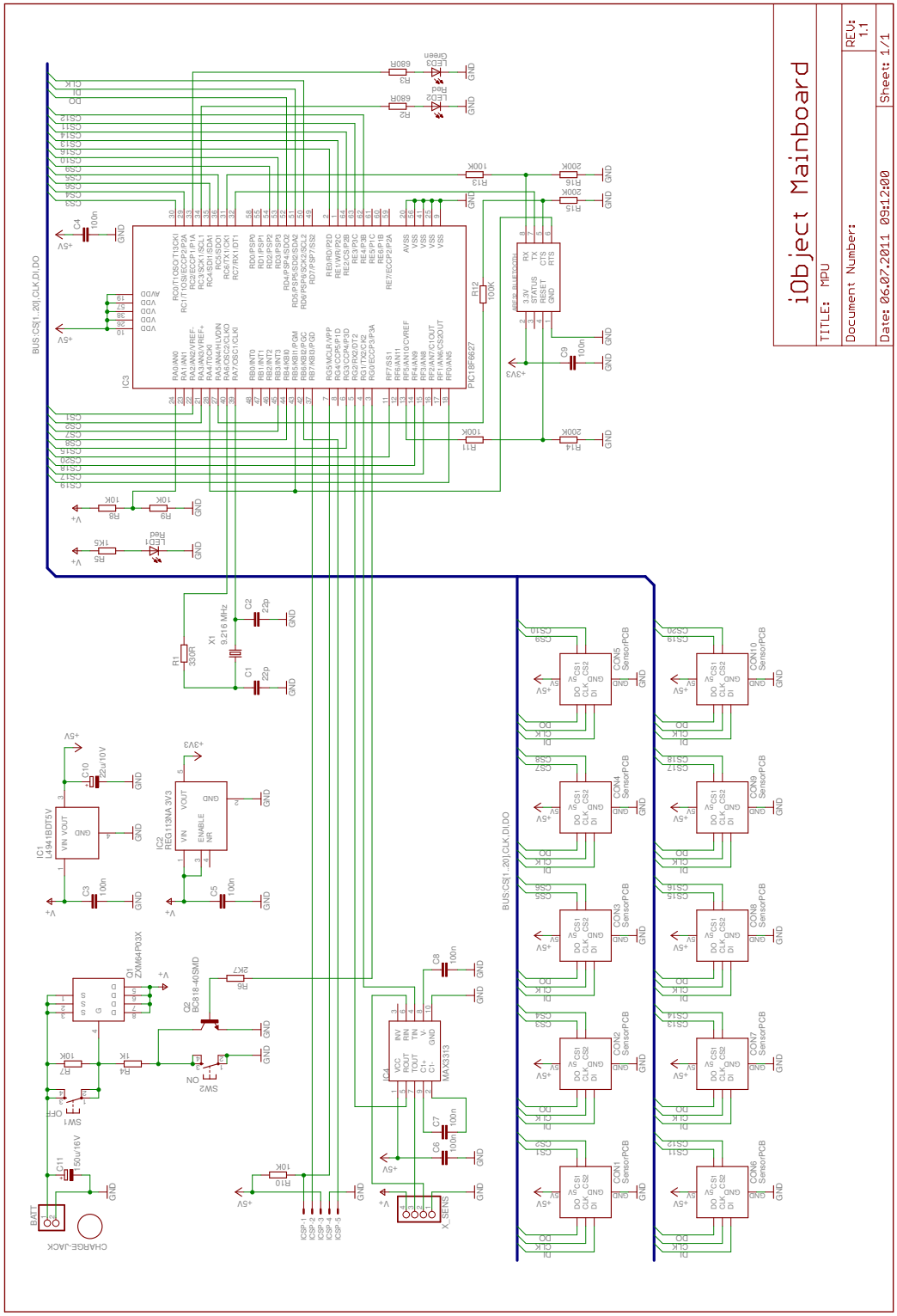

6.3.2 iObject MPU electronic components list

C1-C2	22 pF, 0603
C3-C9	100 nF, 0603
C10	22 μF / 10V, 3216-18
C11	150 μF / 16V, SMC-B
IC1	L4941BDT5V, DPAK
IC2	REG113NA-3V3, SOT23-5L
IC3	PIC18F6627, TQFP-64
IC4	MAX3313E, uMAX-10L
LED1-LED2	Red LED, 0805
LED3	Green LED, 0805
Q1	ZXM64P03X, MSOP-8
Q2	BC818-40SMD, SOT-23
R1	330 Ω, 0603
R2-R3	680 Ω, 0603
R4	1 KΩ, 0603
R5	1.5 KΩ, 0603
R6	2.7 KΩ, 0603
R7-R10	10 KΩ, 0603
R11-R13	100 KΩ, 0603
R14-R16	200 KΩ, 0603
SW1-SW2	SMD switch
X1	9.216 MHz X'tal

6.3.3 iObject sensorboard schematic

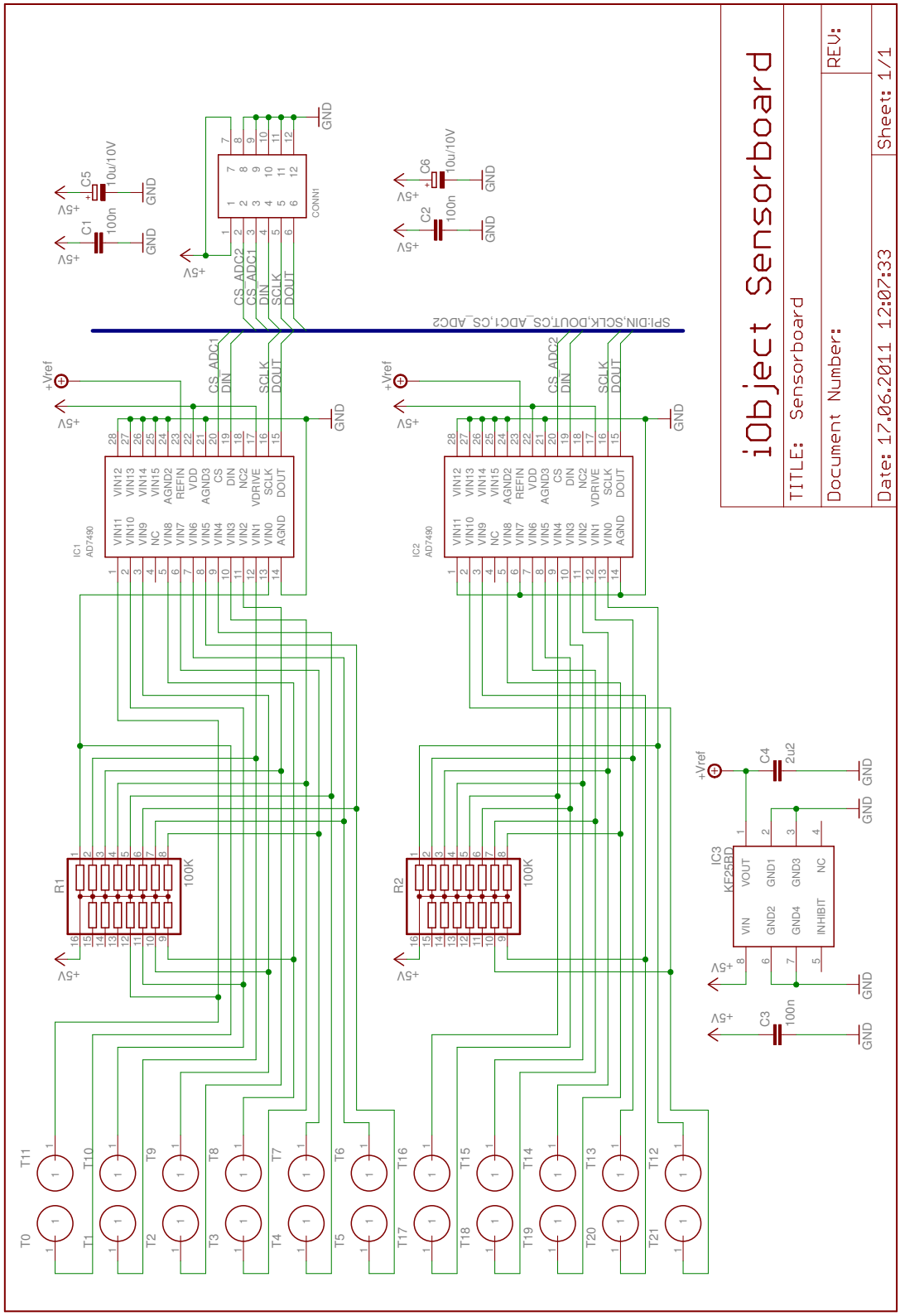

6.3.4 iObject sensorboard electronic components list

C1-C3	100 nF, 0805
C4	2.2 μF, 1206
C5-C6	10 μF / 10V, SMC-B
IC1-IC2	AD7490, TSSOP-28
IC3	KF25BD, SO-8
R1-R2	100 KΩ 15-resistor array, SO-16

6.3.5 Technical drawing of iObject's heavy loading mount

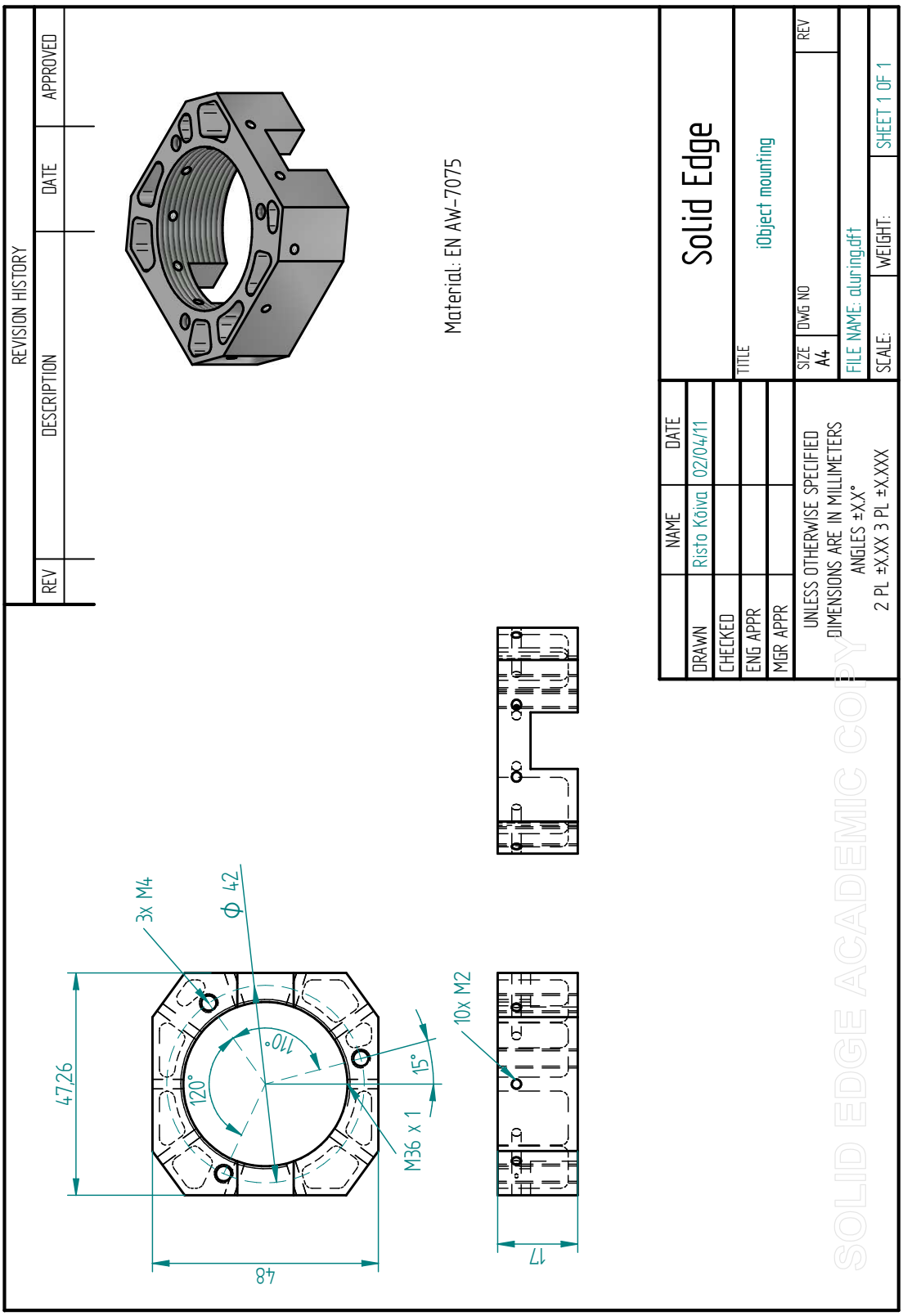

6.3.6 Technical drawing of iObject's magnetic mount

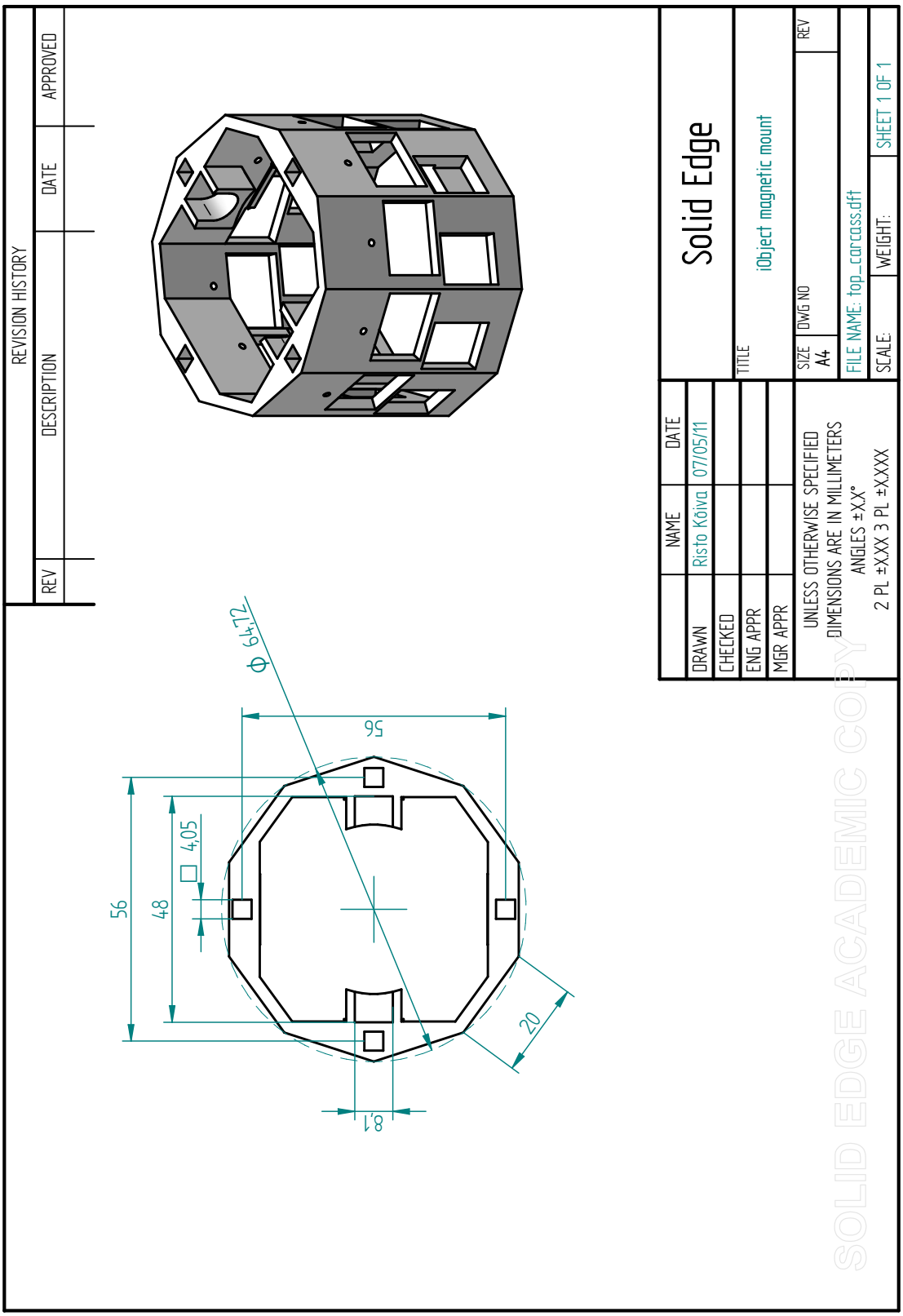

6.3.7 Xsens MTx motion tracking sensor internal

For motion tracking iObject uses the commercially available Xsens MTx sensor. This subsection describes the Xsens MTx internal states and low level communication protocol details that are relavant for iObject communication.

The Xsens MTx motion tracker module uses a proprietary communication protocol with two possible message formats: normal and extended message [Figure 6.3]. Normal message is used for sending a data payload of up to 254 bytes. The extended message is used for sending more data in a single packet with a maximum allowed limit of 2048 bytes.

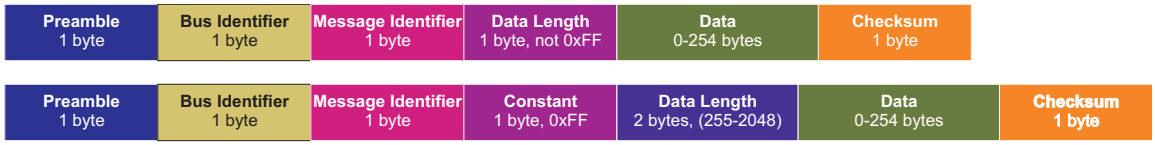

Figure 6.3: Normal and extended low-level protocol format used by Xsens MTx motion and orientation sensor.

Every Xsens communication protocol starts with a preamble, a constant byte *0xFA* is defined by manufacturer for this purpose. The next field in the communication protocol, the *Bus Identifier*, is evaluated only when using multiple Xsens sensor modules on a common bus. As the MTx motion tracker in iObject [Section 3.3] is used independently and not in a Xsens bus system with multiple sensors, values *0x01* (defining the first sensor on the bus) and *0xFF* (bus master) are both accepted by the Xsens MTx in the Bus Identifier (BID) field.

Below, an abbreviated list of possible Message Identifiers (MId), relevant for iObject usage, is presented (for a full list see the *MT Low Level Communication Protocol Documentation* available as part of the MT Software-Development-Kit (SDK) from Xsens [Xse]). In parentheses the message direction is indicated:

- *0x0C* - ReqConfiguration (to MTx)
- *0x0D* - Configuration (from MTx)
- *0x10* - GoToMeasurement (to MTx)
- *0x11* - GoToMeasurementAck (from MTx)
- *0x30* - GoToConfig (to MTx)
- *0x31* - GoToConfigAck (from MTx)
- *0x32* - MTData (from MTx)
- *0x34* - ReqData (to MTx)
- *0x3E* - WakeUp (from MTx)
- *0x3F* - WakeUpAck (to MTx)

A sharp reader will have already noticed that the acknowledge messages have always the MId incremented by one over the MId of the request, but not all messages are acknowledged

with a special acknowledge message (for example a *ReqData* message is acknowledged with a *MTData* message).

The checksum field is used for communication error detection and is calculated as a sum over all bytes excluding the preamble, but including the checksum field and should equate in case of error-free communication to a value whose least significant byte is *0x00*.

Xsens MTx internal states and wakeup procedure

Internally, the MTx motion and orientation sensor can be in 3 states: *WakeUp*, *Config* or *Measurement* [Figure 6.4].

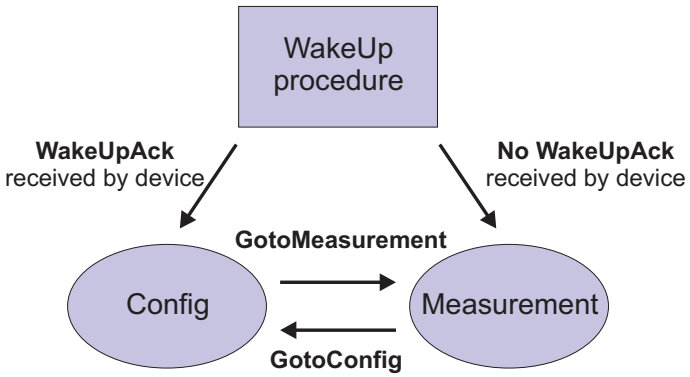

Figure 6.4: Internal Xsens MTx motion and orientation sensor states.

At power-up Xsens MTx sends a *WakeUp* message [Figure 6.5a]. If the message is acknowledged with *WakeUpAck* [Figure 6.5b] within 500ms, the Xsens MTx transfers into *Config* state, and otherwise it transfers into *Measurement* state.

(a) WakeUp packet.

(b) WakeUpAck packet.

Figure 6.5: Xsens MTx WakeUp and WakeUpAck packets.

At power-up Xsens MTx also sends, in addition to a *WakeUp* message one *Configuration* message with a 118 byte payload [Figure 6.6]. The payload includes information such as device ID, sampling period, output skip factor, synchronization settings, data and time formats and most importantly for further usage, the current output mode and settings. The output mode and settings define the coding used for the sensory data output packet - *MTData* packet, where for example orientation data can be output at different precisions (IEEE 754 standard float, 12.20 float or 16.32 high precision float) or in different formats (such as quaternions, Euler angles or 3×3 rotation matrix).

Figure 6.6: Xsens MTx configuration packet.

Xsens MTx request configuration packet

If the user wishes to validate the current configuration, and has missed the configuration packet sent automatically during the power-up, the information can be requested explicitly by issuing *RegConfig* packet [Figure 6.7].

Figure 6.7: Xsens MTx Request Configuration packet.

Xsens MTx data request packet

Depending on the configuration, the sensory data of Xsens MTx can be output periodically (automatically) or only when requested. If polling is configured (which is the case for iObject), *ReqData* packet needs to be sent each time data is to be output by Xsens MTx. Figure 6.8 displays the format of this packet.

Figure 6.8: Xsens MTx manual Request Data packet.

Xsens MTx sensor data packet

The *MTData* packet contains the output of the internal acceleration and magnetic sensor values. Depending on the configuration, raw, calibrated, or calculated values, such as quaternion orientation, can be output. Figure 6.9 displays two format examples of a *MTData* packet.

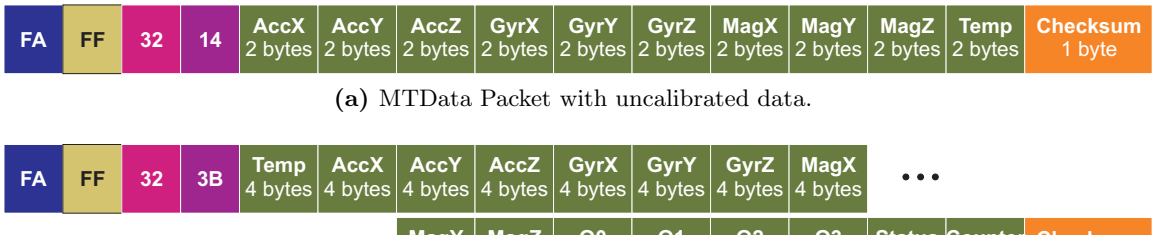

(a) MTData Packet with uncalibrated data.

(b) MTData Packet with calibrated data payload (orientation in quaternion mode).

Figure 6.9: Two possible examples of Xsens MTx MTData packets.

6.3.8 Low level communication of ARF32 Bluetooth module

An *Adeunis ARF32 Data* Bluetooth module is used in iObject to stream the captured tactile and motion data wirelessly to the host. Internally, the Adeunis ARF32 Bluetooth module uses a National Semiconductor LMX9830 Bluetooth Serial Port Module chip [LMX] and thus uses the communication protocol defined for LMX9830. A basic packet protocol scheme for LMX9830 can be seen in Figure 6.10.

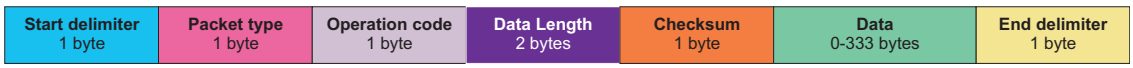

Figure 6.10: Adeunis ARF32 low-level protocol format.

LMX9830 uses *0x02* as the start delimiter and *0x03* as the end delimiter. There are 4 possibilities for Packet Types:

- *0x52* - Request
- *0x43* - Confirm (All correct requests are answered by LMX9830 by one confirm)
- *0x69* - Indication
- *0x72* - Response

The following *Operation codes* of LMX9830 are relevant for iObject operation (for a complete *Operation codes* list, see LMX9830 datasheet [LMX]):

- *0x0C* - SPP_INCOMING_LINK_ESTABLISHED
- *0x0E* - SPP_LINK_RELEASED
- *0x11* - SPP_TRANSPARENT_MODE
- *0x25* - LMX9830_READY

If the ARF32 module is powered up, it emits an indication packet with an operation code *0x25* (LMX9830_READY) and with a *Data length* of 5 bytes [Figure 6.11]. In the LMX9830_READY packet, the first byte of the payload gives the byte count of the following version number string. In the example below, the first byte in data part is *0x04*, meaning the next 4 bytes are for describing the version number. Decoding the version number from ASCII ($0x30 = 0$, $0x31 = 1$, $0x32 = 2$) results in a version number of 0212.

Figure 6.11: LMX9830_READY packet sent by the ARF32 Bluetooth module after applying power.

The checksum is calculated as a sum of the bytes starting from the packet type field to, and including, the data length field, modulo *0xFF*. For the LMX9830_READY packet [Figure 6.11] this calculates as $(0x69 + 0x25 + 0x05 + 0x00)$ & $0xFF = 0x93$.

Note that the actual data field in ARF32 is, contrary to what one might expect, not part of the checksum calculation, possibly to free the Bluetooth modules internal processor from overloading.

If an external communication partner connects over Bluetooth to ARF32/LMX9830, then the module will emit SPP_INCOMING_LINK_ESTABLISHED packet with the Bluetooth address of the remote device [Figure 6.12].

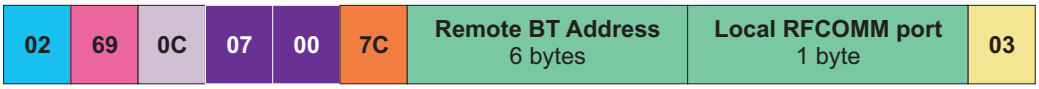

(a) Incoming link notification packet format.

(b) An example of incoming link notification packet when connected from Bluetooth host 01:23:45:67:89:AB. The local RFCOMM port chosen in iObject will always be *0x01*.

Figure 6.12: ARF32 Bluetooth module incoming link notification packet including an example.

After receiving the SPP_INCOMING_LINK_ESTABLISHED packet from the Bluetooth module, iObject internally enables the outgoing communication and starts querying the sensors and transmitting data over the connected Bluetooth link.

If the link is dropped due to a disconnect from the remote device or due to communication loss the ARF32/LMX9830 emits SPP_TRANSPARENT_MODE left and SPP_LINK_RELEASED packets [Figure 6.13].

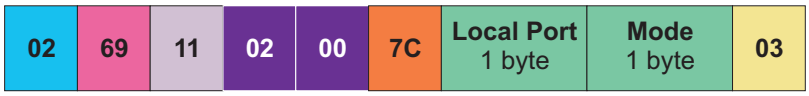

(a) SPP_TRANSPARENT_MODE packet. When leaving the transparent mode, the Mode field will be set to *0x00*.

(b) SPP_LINK_RELEASED paket.

Figure 6.13: Packets sent internally by ARF32 module after the Bluetooth link gets dropped.

Possible reasons for SPP_LINK_RELEASED can be:

- *0x00* - the local device has disconnected the Data-Link-Control (DLC)
- *0x01* - the remote device has disconnected the DLC
- *0x02* - Asynchronous-Connectionless-Link (ACL) link failure/ link supervision time-out
- *0x03* - Lower layer (e.g. Logical Link Control and Adaptation Protocol (L2CAP)) has disconnected the DLC

A normal triggered Bluetooth host disconnect would have a value of *0x01* in the protocol's *Reason* field.

6.3.9 iObjectPlus sensorboard schematic

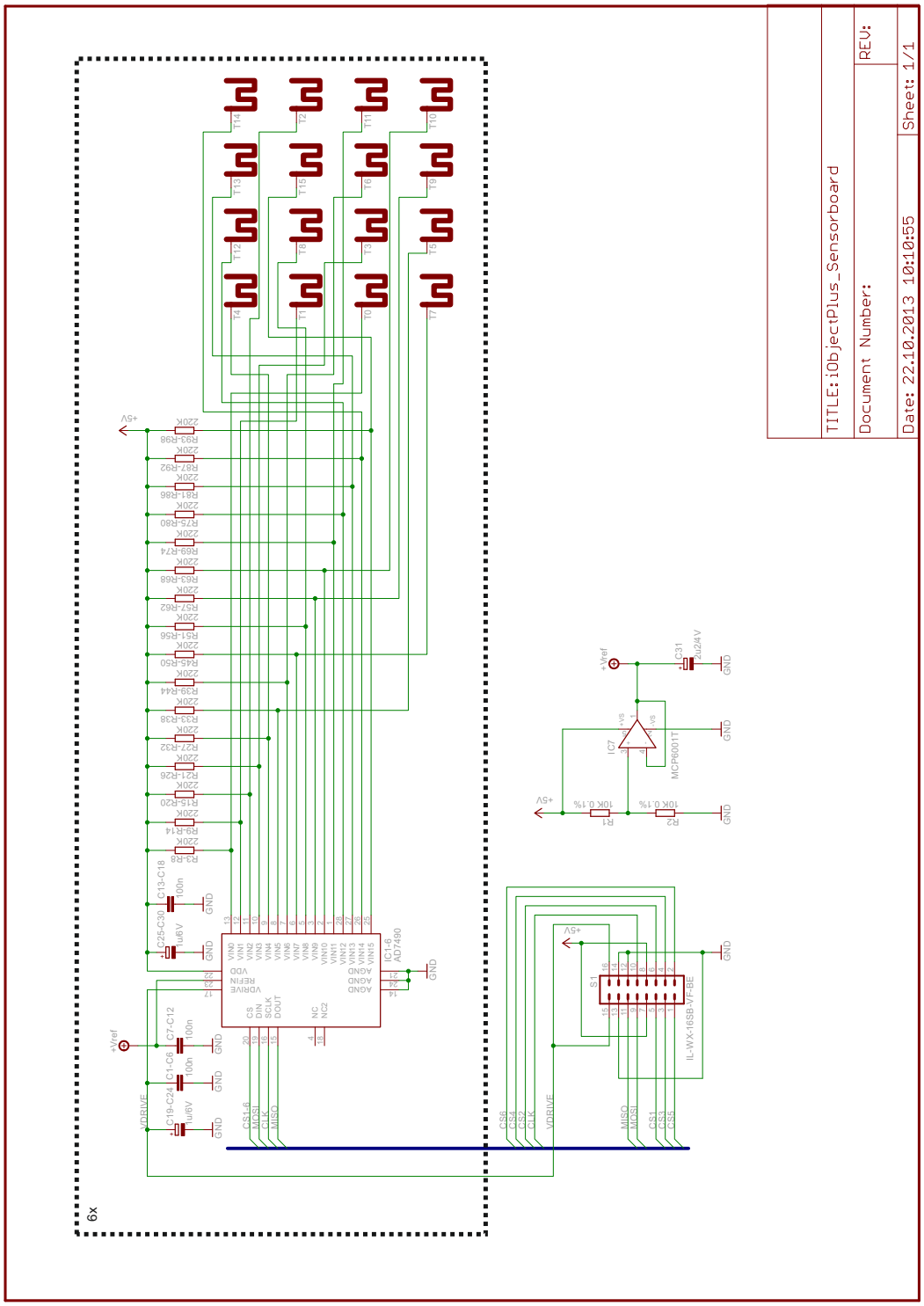

iObjectPlus sensorboard schematic with 4×24 taxels. Six 16-channel ADC's (AD7490) are used to capture the tactile data from 96 taxels. The taxel mapping shown is as on the physical device when looking at the electrode side.

6.3.10 iObjectPlus sensorboard electronic components list

C1-C18	100 nF, 0402
C19-C30	1μF / 6V, SMC-A
C31	2.2μF / 4V, 1206
IC1-IC6	AD7490, TSSOP-28
IC7	MCP6001T, SC70-5
R1-R2	10 KΩ 0.1%, 0402
R3-R98	220 KΩ, 0402
S1	JAE connector, IL-WX-16SB-VF-BE

6.4 Tactile Bracelet

6.4.1 Tactile Bracelet sensorboard schematic

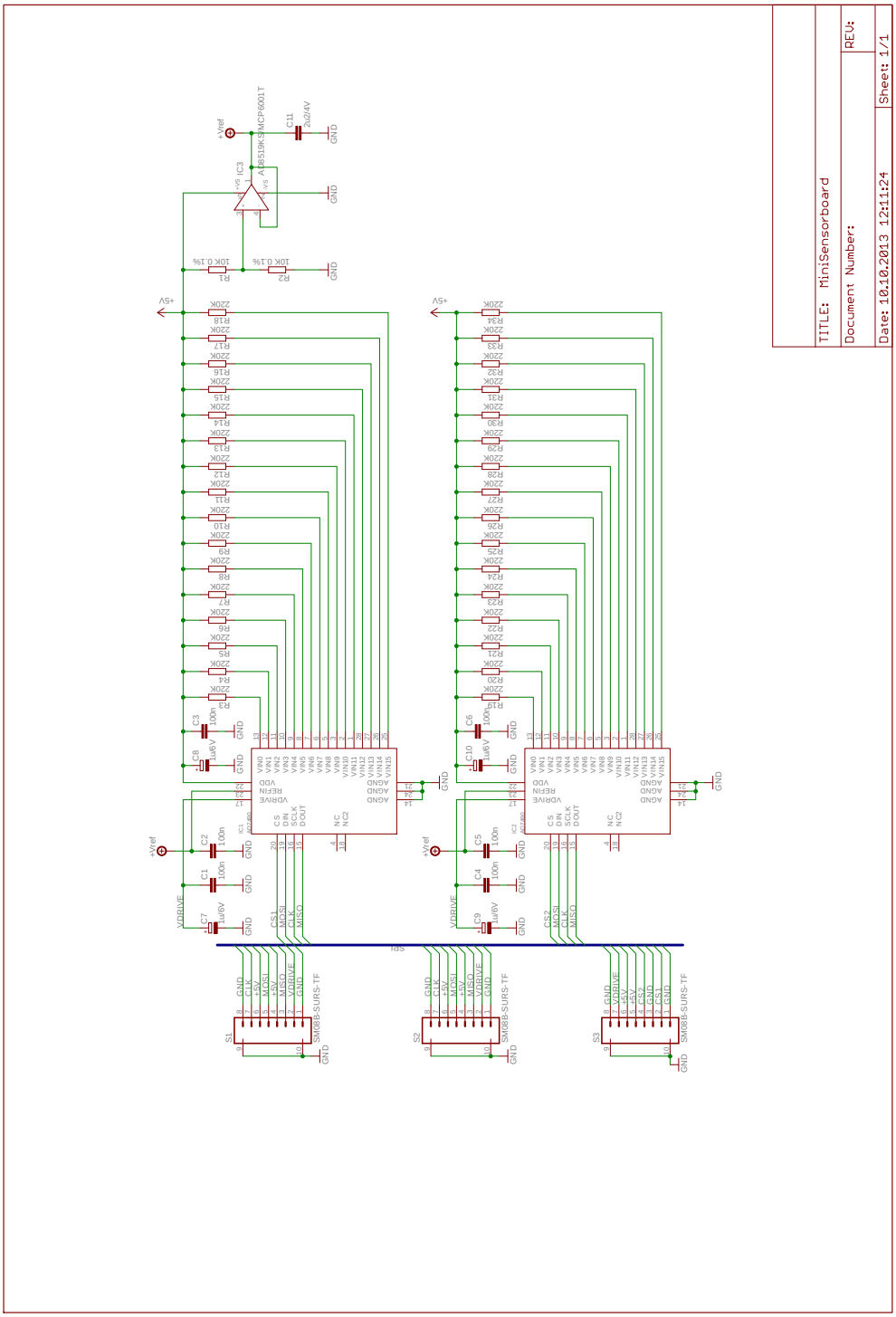

Tactile Bracelet sensorboard schematic implementing two 16-channel analog digital converters acting on the SPI-bus as slave devices.

6.4.2 Tactile Bracelet sensorboard electronic components list

C1-C6	100 nF, 0402
C7-C10	1 μF / 6V, SMC-A
C11	2.2 μF / 4V, 1206
IC1-IC2	AD7490, TSSOP-28
IC3	MCP6001T, SC70-5
R1-R2	10 KΩ 0.1%, 0402
R3-R34	220 KΩ, 0402
S1-S3	SM08B-SURS-TF (JST) connectors

6.4.3 Tactile Bracelet mainboard schematic

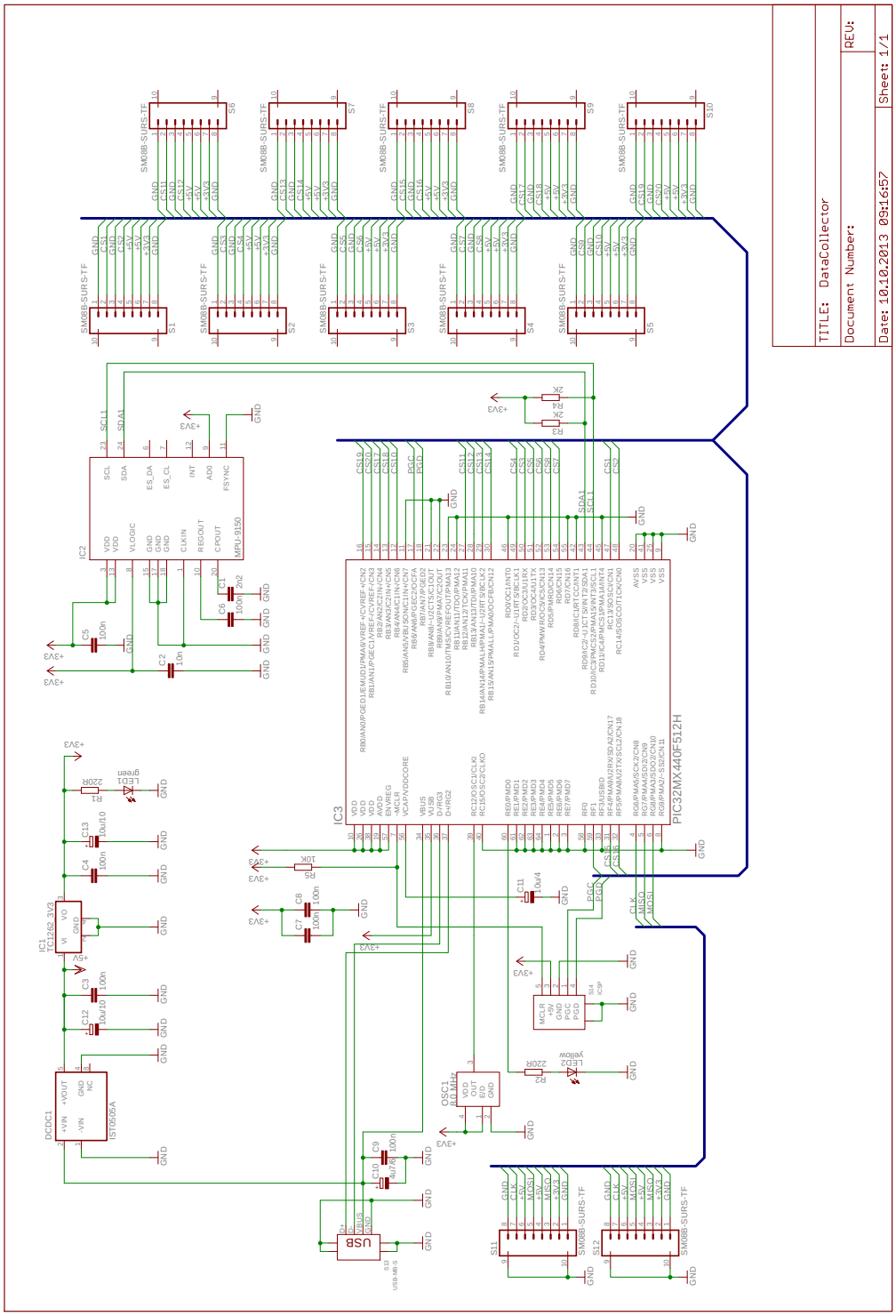

Tactile Bracelet mainboard schematic using a PIC32 microcontroller as the central data aggregator and an InvenSense MPU-9150 9-axis IMU-chip as a motion tracker. The gathered data can be relayed over a USB 2.0 bus to a data processing device (e.g., PC).

6.4.4 Tactile Bracelet mainboard electronic components list

C1	2.2 nF, 0603
C2	10 nF, 0603
C3-C9	100 nF, 0603
C10	4.7 μF / 6V, 7343
C11	10 μF / 4V, 1206
C12-C13	10 μF / 10V, 7343
DCDC1	IST0505A
IC1	TC1262-3V3, SOT-223
IC2	MPU-9150, QFN-24
IC3	PIC32MX440F512H, TQFP-64
LED1	LED green, 0603
LED2	LED yellow, 0603
OSC1	8.0 MHz (Aker S23305-8.000-X)
R1-R2	220 Ω, 0603
R3-R4	2 KΩ, 0603
R5	10 KΩ, 0402
S1-S12	SM08B-SURS-TF (JST) connectors
S13	Mini-USB (Molex 67503-1020) connector
S14	ICSP (Molex 53398-0571) 5-pin header

6.4.5 Tactile Bracelet connection diagram

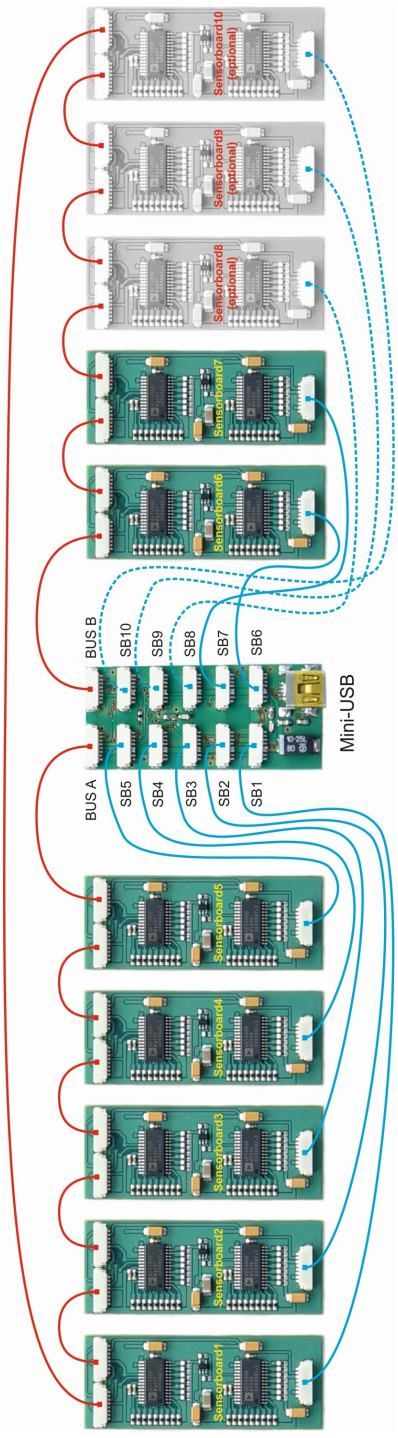

The Tactile Bracelet inter-board connection diagram. Red wires denote the SPI-Bus containing the clock (CLK), master in slave out (MISO), master out slave in (MOSI) signals; Blue wiring contains the chip select ($\overline{CS}$) signals for selecting the analog-digital converter to be active on the bus. Power (+3.3V DC and +5V DC) and reference (GND) are distributed over the red and blue wires.

6.5 Tactile fingertip sensor

6.5.1 Tactile fingertip sensor schematic

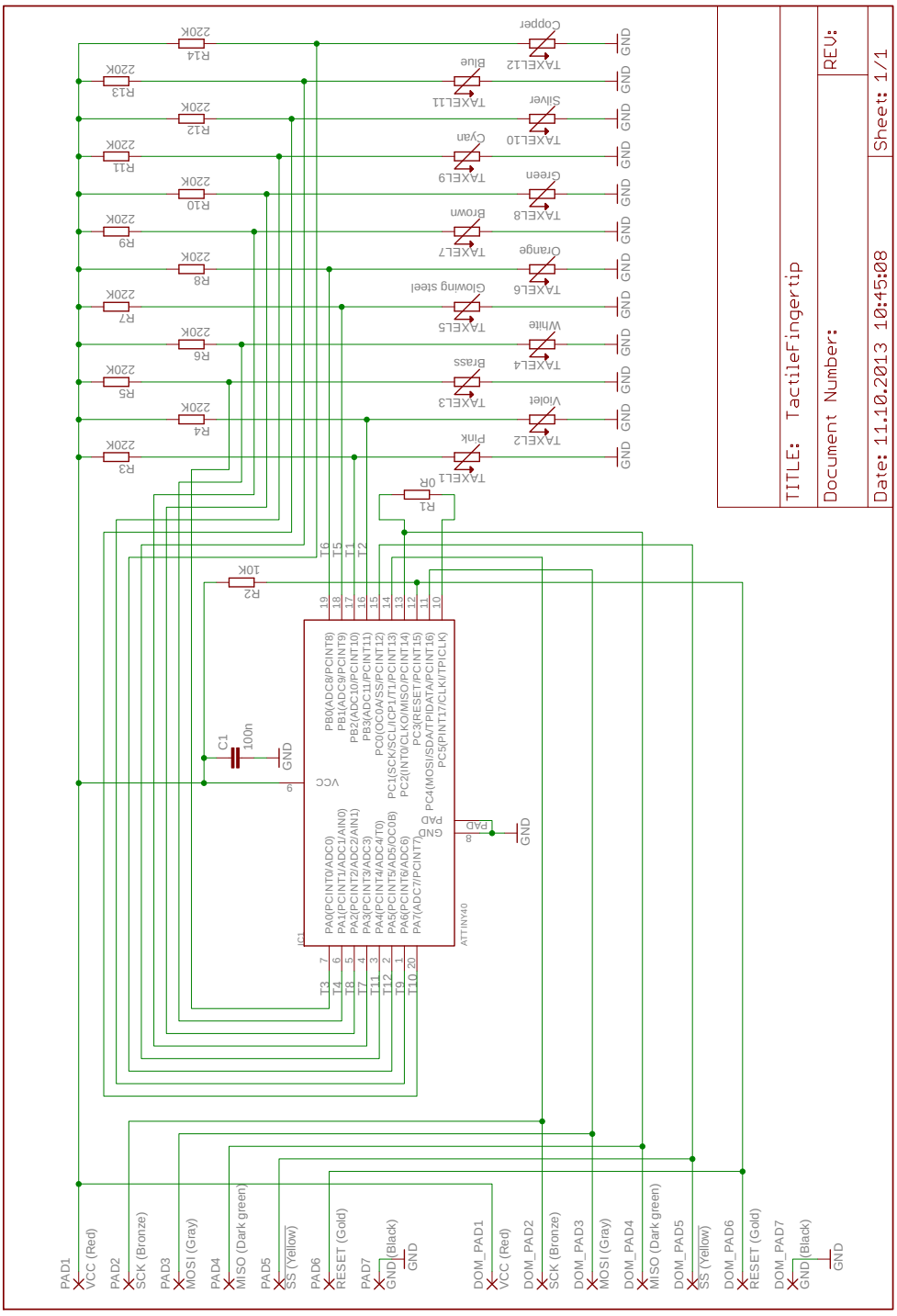

Tactile fingertip sensor schematic. The taxel color coding is according to mapping shown in Appendix 6.5.3.

6.5.2 Tactile fingertip electronic components list

C1	100n, 0603
IC1	ATTINY40, VQFN-20
R1	0 Ω, 1206
R2	10 KΩ, 0603
R3-R14	220 KΩ, 0603

6.5.3 Tactile fingertip sensor cell mapping

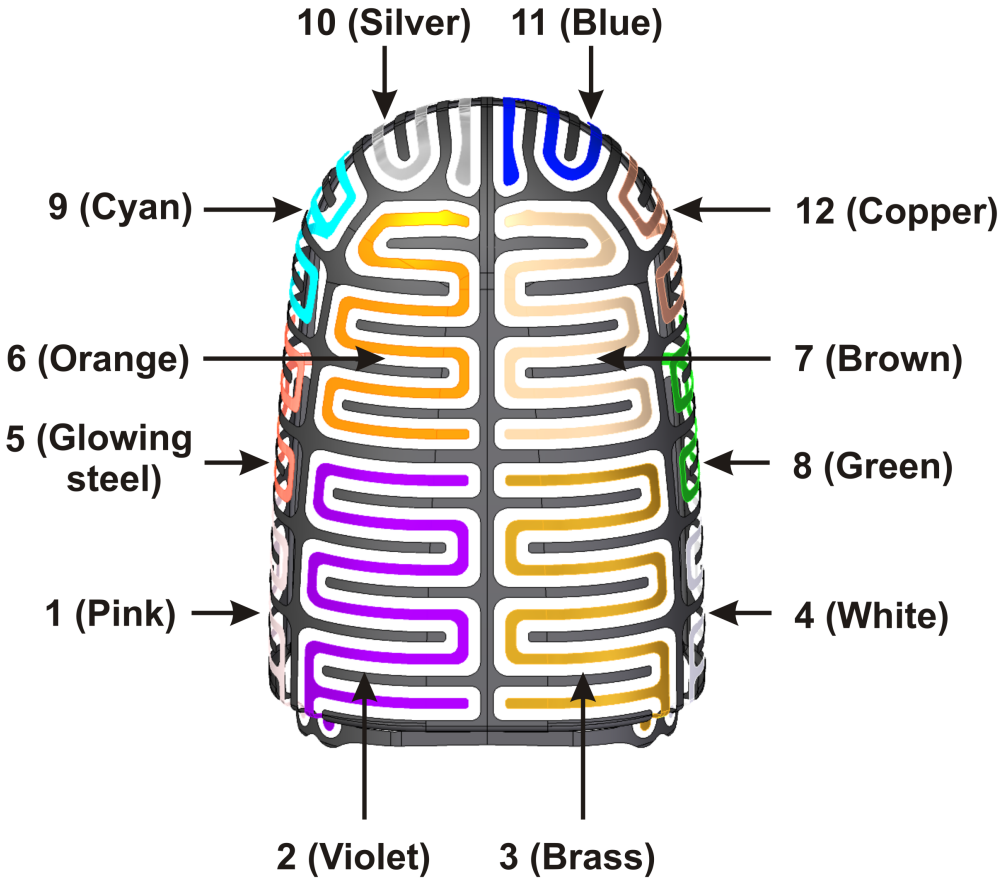

Color descriptions from Solid Edge CAD program.

Bibliography

[AGH10] Jan Anlauff, Tobias Großhauser, and Thomas Hermann. tacTiles: a low-cost modular tactile sensing system for floor interactions. In *Nordic Conference on Human-Computer Interaction: Extending Boundaries (NordiCHI)*, pages 591–594, Reykjavik, Iceland, 2010. ACM. URL: http://dx.doi.org/10.1145/1868914.1868981.

[AK10] Panagiotis K. Artemiadis and Kostas J. Kyriakopoulos. EMG-Based Control of a Robot Arm Using Low-Dimensional Embeddings. *IEEE Transactions on Robotics*, 26(2):393–398, 2010. URL: http://dx.doi.org/10.1109/TRO.2009.2039378.

[Alp] Alpha-Fit's Alphamat body pressure measurement system. http://www.alpha-fit.de/en/products/alphamat.html. Cited on Mar. 2013.

[ANK07] Hassan Alirezaei, Akihiko Nagakubo, and Yasuo Kuniyoshi. A highly stretchable tactile distribution sensor for smooth surfaced humanoids. In *IEEE-RAS International Conference on Humanoid Robots (Humanoids)*, Pittsburgh, Pennsylvania, USA, 2007. URL: http://dx.doi.org/10.1109/ICHR.2007.4813864.

[App] Apple Magic Mouse. http://www.apple.com/de/magicmouse/. Cited on Oct. 2013.

[ATC] Flock-of-Birds. Ascension Technology Corporation. http://www.ascension-tech.com/. Cited on Mar. 2013.

[Bü11] Gereon H. Büscher. Optimierung eines Datenhandschuhs, insbesondere Erweiterung um eine Taktilsensorik. Diploma thesis, Bielefeld University of Applied Sciences, Faculty of Mathematic and Technology, Bielefeld, Germany, Sept. 2011.

[Bec10] Travis W. Beck. *Application of Mechanomyography for Examining Muscle Function*. Transworld Research Network, 2010. URL: http://www.trnres.com/ebookcontents.php?id=82.

[BGLH01] J. Butterfass, M. Grebenstein, H. Liu, and G. Hirzinger. DLR-Hand II: next generation of a dextrous robot hand. In *IEEE International Conference on Robotics and Automation (ICRA)*, volume 1, pages 109–114, Seoul, Korea, 2001. URL: http://dx.doi.org/10.1109/ROBOT.2001.932538.

[BGV92] Bernhard E. Boser, Isabelle M. Guyon, and Vladimir N. Vapnik. A training algorithm for optimal margin classifiers. In *5th Annual Workshop on Computational Learning Theory (COLT)*, pages 144–152, Pittsburgh, Pennsylvania, USA, 1992. ACM. URL: http://doi.acm.org/10.1145/130385.130401.

[BJGVC88] S.J. Bolanowski Jr, G.A. Gescheider, R.T. Verrillo, and C.M. Checkosky. Four channels mediate the mechanical aspects of touch. *The Journal of the Acoustical society of America*, 84:1680–1694, 1988.

[BKS+] Gereon Büscher, Risto Kõiva, Carsten Schürmann, Robert Haschke, and Helge J. Ritter. Video: Tactile dataglove with fabric-based sensors. `http://www.youtube.com/watch?v=YFDfSIRei7c`. Cited on Mar. 2013.

[BKS+12] Gereon Büscher, Risto Kõiva, Carsten Schürmann, Robert Haschke, and Helge J. Ritter. Tactile dataglove with fabric-based sensors. In *IEEE-RAS International Conference on Humanoid Robots (Humanoids)*, Osaka, Japan, Nov. 2012.

[BKS+14] Gereon Büscher, Risto Kõiva, Carsten Schürmann, Robert Haschke, and Helge J. Ritter. Flexible and stretchable fabric-based tactile sensor. *Robotics and Autonomous Systems. Special Issue on Advances in Tactile Sensing and Touch-based Human-Robot Interaction*, Sept. 2014. URL: `http://dx.doi.org/10.1016/j.robot.2014.09.007`.

[Blua] Bluetooth SIG. Specification of the Bluetooth System 2.0+EDR. `http://www.bluetooth.com/`. Cited on Mar. 2013.

[Blub] Wikipedia, free encylopedia. User collected approximate wireless range of Bluetooth classes. `http://en.wikipedia.org/wiki/Bluetooth#Uses`. Cited on Mar. 2013.

[BMK+13] Gereon H. Büscher, Gerhard Mahlich, Risto Kõiva, Carsten Schürmann, Robert Haschke, and Helge J. Ritter. Schreibgeräthülle mit taktil-sensitivem schaft. Bielefeld, Germany, May 2013. Presented at the annual DVE Ergotherapy-Congress.

[Bot65] A. H. Bottomley. Myoelectric control of powered prostheses. *Journal of Bone & Joint Surgery*, B47:411–415, 1965.

[BvdS06] Sebastian Bitzer and Patrick van der Smagt. Learning EMG control of a robotic hand: towards active prostheses. In *IEEE International Conference on Robotics and Automation (ICRA)*, pages 2819–2823, Orlando, Florida, USA, 2006. URL: `http://dx.doi.org/10.1109/ROBOT.2006.1642128`.

[BVLZ06] Leonardo Bonanni, Cati Vaucelle, Jeff Lieberman, and Orit Zuckerman. TapTap: a haptic wearable for asynchronous distributed touch therapy. In *CHI'06 extended abstracts on Human factors in computing systems*, pages 580–585, Montréal, Québec, Canada, 2006. ACM. URL: `http://doi.acm.org/10.1145/1125451.1125573`.

[BXB+10] Ravi Balasubramanian, Ling Xu, Peter D. Brook, Joshua R. Smith, and Yoky Matsuoka. Human-Guided Grasp Measures Improve Grasp Robustness on Physical Robot. In *IEEE International Conference on Robotics and Automation (ICRA)*, pages 2294–2301, Anchorage, Alaska, USA, 2010. URL: `http://dx.doi.org/10.1109/ROBOT.2010.5509855`.

[CAC+11] Christian Cipriani, Christian Antfolk, Marco Controzzi, Göran Lundborg, Birgitta Rosén, Maria Chiara Carrozza, and Fredrik Sebelius. Online myoelectric control of a dexterous hand prosthesis by transradial amputees. *IEEE Transactions on Neural Systems and Rehabilitation Engineering*, 19(3):260–270, 2011. URL: `http://dx.doi.org/10.1109/TNSRE.2011.2108667`.

[CFC01] David J. Curcie, James A. Flint, and William Craelius. Biomimetic finger control by filtering of distributed forelimb pressures. *IEEE Transactions on Neural Systems and Rehabilitation Engineering*, 9(1):69–75, 2001. URL: `http://dx.doi.org/10.1109/7333.918278`.

[CFMdP03] Eris Chinellato, Robert B. Fisher, Antonio Morales, and Ángel P. del Pobil. Ranking planar grasp configurations for a three-finger hand. In *IEEE International Conference on Robotics and Automation (ICRA)*, volume 1, pages 1133–1138, Taipei, Taiwan, 2003. URL: `http://dx.doi.org/10.1109/ROBOT.2003.1241745`.

[CGDS09] Claudio Castellini, Emanuele Gruppioni, Angelo Davalli, and Giulio Sandini. Fine detection of grasp force and posture by amputees via surface electromyography. *Journal of Physiology-Paris*, 103(3-5):255–262, 2009. URL: `http://dx.doi.org/10.1016/j.jphysparis.2009.08.008`.

[CK12a] Claudio Castellini and Risto Kõiva. Intention gathering from muscle residual activity for the severely disabled. In *International Conference on Intelligent Robots and Systems (IROS). Workshop on Progress, Challenges and Future Perspectives in Navigation and Manipulation Assistance for Robotic Wheelchairs*, Vilamoura, Portugal, 2012.

[CK12b] Claudio Castellini and Risto Kõiva. Using surface electromyography to predict single finger forces. In *IEEE RAS EMBS International Conference on Biomedical Robotics and Biomechatronics (BioRob)*, pages 1266–1272, Rome, Italy, 2012. URL: `http://dx.doi.org/10.1109/BioRob.2012.6290294`.

[CK13] Claudio Castellini and Risto Kõiva. Using a high spatial resolution tactile sensor for intention detection. In *13th International Conference on Rehabilitation Robotics (ICORR)*, Seattle, Washington, USA, 2013.

[CMMS08] Giorgio Cannata, Marco Maggiali, Giorgio Metta, and Giulio Sandini. An embedded artificial skin for humanoid robots. In *International Conference on Multisensor Fusion and Integration for Intelligent Systems (MFI)*, Seoul, Korea, 2008. URL: `http://dx.doi.org/10.1109/MFI.2008.4648033`.

[Col95] Jonathan Cole. *Pride and a daily marathon*. Bradford Books, 1995.

[CSC04] Ed H. Chi, Jin Song, and Greg Corbin. "Killer App" of wearable computing: wireless force sensing body protectors for martial arts. In *ACM symposium on User Interface Software and Technology (UIST)*, pages 277–285, Santa Fe, New Mexico, USA, 2004. URL: `http://doi.acm.org/10.1145/1029632.1029680`.

[CST00] Nello Cristianini and John Shawe-Taylor. *An introduction to support Vector Machines: and other kernel-based learning methods*. Cambridge University Press, New York, NY, USA, 2000.

[CvdS09] Claudio Castellini and Patrick van der Smagt. Surface EMG in advanced hand prosthetics. *Biological Cybernetics*, 100(1):35–47, 2009. URL: `http://dx.doi.org/10.1007/s00422-008-0278-1`.

[Cyb] Cyber Glove Systems. `http://www.cyberglovesystems.com/`. Cited on Mar. 2013.

[DBS12] Jason M. DeFreitas, Travis W. Beck, and Matt S. Stock. Effects of strength training on mechanomyographic amplitude. *Physiological Measurement*, 33(8):1353, 2012. URL: `http://stacks.iop.org/0967-3334/33/i=8/a=1353`.

[De 97] Carlo J. De Luca. The use of surface electromyography in biomechanics. *Journal of Applied Biomechanics*, 13(2):135–163, 1997.

[dM78] Theodore du Moncel. *Le téléphone, le microphone et le phonographe.* Bibliothèque des merveilles, Hachette, Paris, 1878.

[DMVS10] Ravinder S. Dahiya, Giorgio Metta, Maurizio Valle, and Giulio Sandini. Tactile Sensing – From Humans to Humanoids. *IEEE Transactions on Robotics*, 26(1):1–20, Feb. 2010. URL: `http://dx.doi.org/10.1109/TRO.2009.2033627`.

[DSD08] Laura Dipietro, Angelo M. Sabatini, and Paolo Dario. A survey of glove-based systems and their applications. *IEEE Transactions on Systems, Man, and Cybernetics, Part C: Applications and Reviews*, 38(4):461–482, July 2008. URL: `http://dx.doi.org/10.1109/TSMCC.2008.923862`.

[DVDR+13] Marco Donati, Nicola Vitiello, Stefano Marco Maria De Rossi, Tommaso Lenzi, Simona Crea, Alessandro Persichetti, Francesco Giovacchini, Bram Koopman, Janez Podobnik, Marko Munih, and Maria Chiara Carrozza. A flexible sensor technology for the distributed measurement of interaction pressure. *Sensors*, 13(1):1021–1045, 2013. URL: `http://www.mdpi.com/1424-8220/13/1/1021`.

[DWA11] Hao Dang, Jonathan Weisz, and Peter K. Allen. Blind grasping: Stable robotic grasping using tactile feedback and hand kinematics. In *IEEE International Conference on Robotics and Automation (ICRA)*, Shanghai, China, 2011. URL: `http://dx.doi.org/10.1109/ICRA.2011.5979679`.

[ECL03] Jonathan Engel, Jack Chen, and Chang Liu. Development of a multi-modal, flexible tactile sensing skin using polymer micromachining. In *International Conference on Solid-State Sensors, Actuators and Microsystems (Transducers)*, volume 2, Bled, Slovenia, 2003. URL: `http://dx.doi.org/10.1109/SENSOR.2003.1216943`.

[Eeo] Eeonyx. Conductive & heat resistant fabrics, foams & textiles. `http://www.eeonyx.com/`. Cited on Mar. 2013.

[EFS11] Norbert Elkmann, Markus Fritzsche, and Erik Schulenburg. Tactile sensing for safe physical human-robot interaction. In *4th International Conference on Advances in Computer-Human Interactions (ACHI)*, pages 212–217, Gosier, France, 2011.

[FC92] Carlo Ferrari and John Canny. Planning optimal grasps. In *IEEE International Conference on Robotics and Automation (ICRA)*, volume 3, pages 2290–2295, Nice, France, May 1992. URL: http://dx.doi.org/10.1109/ROBOT.1992.219918.

[FDZ+05] Jodi Forlizzi, Carl DiSalvo, John Zimmerman, Bilge Mutlu, and Amy Hurst. The SenseChair: the lounge chair as an intelligent assistive device for elders. In *Conference on Designing for User eXperience (DUX)*, San Francisco, California, USA, 2005. AIGA: American Institute of Graphic Arts. URL: http://portal.acm.org/citation.cfm?id=1138235.1138272.

[FE09] Markus Fritzsche and Norbert Elkmann. An artificial skin for safe human-robot-interaction. In *International Conference on Humanoid Robots (Humanoids), Workshop on Tactile Sensing in Humanoids – Tactile Sensors and beyond*, pages 42–43, Paris, France, 2009.

[FOHK09] Yuki Fujimori, Yoshiyuki Ohmura, Tatsuya Harada, and Yasuo Kuniyoshi. Wearable motion capture suit with full-body tactile sensors. In *IEEE International Conference on Robotics and Automation (ICRA)*, pages 3186–3193, Kobe, Japan, May 2009. URL: http://dx.doi.org/10.1109/ROBOT.2009.5152758.

[Fra] Heinrich Hertz Institute Fraunhofer. Visible light communication. http://www.hhi.fraunhofer.de/fields-of-competence/photonic-networks-and-systems/research-topics/optical-indoor-networks/visible-light-communication.html Cited on Apr. 2013.

[Fre] Free2Move AB. http://www.free2move.se/. Cited on Mar. 2013.

[FSE12] Markus Fritzsche, José Saenz, and Norbert Elkmann. A tactile sensor for collision detection and human robot interaction on complexly-shaped industrial robots. In *IEEE/RSJ International Conference on Intelligent Robots and Systems (IROS), Workshop on Advances in tactile sensing and touch-based human-robot interaction*, Vilamoura, Portugal, Oct. 2012.

[GAC+] Arjan Gijsberts, Manfredo Atzori, Claudio Castellini, Henning Müller, and Barbara Caputo. Measuring movement classification performance with the movement error rate. *IEEE Transactions on Neural Systems and Rehabilitation Engineering*. In Review.

[GBH+11] Ulf Großekathöfer, Alexandra Barchunova, Robert Haschke, Thomas Hermann, Mathias Franzius, and Helge J. Ritter. Learning of object manipulation operations from continuous multimodal input. In *IEEE-RAS International Conference on Humanoid Robots (Humanoids)*, pages 507–512, Bled, Slovenia, 2011. URL: http://dx.doi.org/10.1109/Humanoids.2011.6100880.

[GDFY03] Francine Gemperle, Carl DiSalvo, Jodi Forlizzi, and Willy Yonkers. The Hug: a new form for communication. In *Conference on Designing for user experiences (DUX)*, pages 1–4, San Francisco, California, USA, 2003. ACM. URL: http://doi.acm.org/10.1145/997078.997103.

[GGW09] Dirk Göger, Nicolas Gorges, and Heinz Wörn. Tactile sensing for an anthropomorphic robotic hand: Hardware and signal processing. In *IEEE International Conference on Robotics and Automation (ICRA 2009)*, pages 895–901, Kobe, Japan, May 2009. URL: `http://dx.doi.org/10.1109/ROBOT.2009.5152650`.

[GK90] S.C. Gandevia and S.L. Kilbreath. Accuracy of weight estimation for weights lifted by proximal and distal muscles of the human upper limb. *The Journal of Physiology*, 423(1):299–310, 1990. URL: `http://jp.physoc.org/content/423/1/299.abstract`.

[Goo] Google Glass. `http://google.com/glass/`. Cited on Sept. 2013.

[GV79] G.A. Gescheider and R.T. Verrillo. Vibrotactile frequency characteristics as determined by adaptation and masking procedures. *Sensory functions of the skin of humans*, pages 183–205, 1979.

[Hal11] John E. Hall. *Textbook of Medical Physiology*. Saunders, 12th edition, Apr. 2011.

[HHR06] Thomas Hermann, Oliver Höner, and Helge Ritter. AcouMotion – An Interactive Sonification System for Acoustic Motion Control. In Sylvie Gibet, Nicolas Courty, and Jean-François Kamp, editors, *Gesture in Human-Computer Interaction and Simulation*, volume 3881 of *Lecture Notes in Computer Science*, pages 312–323. Springer Berlin / Heidelberg, 2006. URL: `http://dx.doi.org/10.1007/11678816_35`.

[HK08] Thomas Hermann and Risto Kõiva. tacTiles for Ambient Intelligence and Interactive Sonification. In Antti Pirhonen and Stephen A. Brewster, editors, *3rd International Workshop on Haptic and Audio Interaction Design (HAID)*, volume LNCS 5720 of *Lecture Notes in Computer Science*, pages 91–101, Jyväskylä, Finland, Sep. 2008. Springer.

[HK11] Thomas Hermann and Risto Kõiva. *SonicChair, Sonic Interaction Design - Exhibition Catalogue*. BEK: Bergen Center for Electronic Arts, 2011.

[HMS07] Ekbert Hering, Rolf Martin, and Martin Stroher. *Physik für Ingenieure*, volume 10. Springer Verlag, 2007.

[Hona] Honigmann Industrielle Elektronik GmbH. Datasheet, RFS-150 XY, Radial force sensor with 2 axis. `http://www.honigmann.com/bilder/download/TDE_RFS150XY_05.pdf`. Cited on Sept. 2013.

[Honb] Honigmann Industrielle Elektronik GmbH. Datasheet, TENSIOTRON TS 503 Strain Gauge Measuring Amplifier. `http://www.honigmann.com/bilder/download/TDE_TS503_9-03.pdf`. Cited on Sept. 2013.

[IEE08] IEEE Standard for Floating-Point Arithmetic. *IEEE Std 754-2008*, pages 1–70, Aug. 2008. URL: `http://dx.doi.org/10.1109/IEEESTD.2008.4610935`.

[IHN+96] Masayuki Inaba, Yukiko Hoshino, Kenichiro Nagasaka, Tatsuo Ninomiya, Satoshi Kagami, and Hirochika Inoue. A full-body tactile sensor suit using

electrically conductive fabric and strings. In *IEEE/RSJ International Conference on Intelligent Robots and Systems (IROS)*, volume 2, pages 450–457, Osaka, Japan, 1996. URL: http://dx.doi.org/10.1109/IROS.1996.570816.

[Int] Interlink Electronics Inc. http://www.interlinkelectronics.com/. Cited on Mar. 2013.

[Inv] InvenSense MPU-9250 nine axis MEMS MotionTracking device. http://www.invensense.com/mems/gyro/mpu9250.html. Cited on Oct. 2014.

[JF09] Roland S. Johansson and J. Randall Flanagan. Coding and use of tactile signals from the fingertips in object manipulation tasks. *Nature reviews. Neuroscience*, 10:345–359, May 2009. URL: http://ukpmc.ac.uk/abstract/MED/19352402.

[JP81] Kenneth O. Johnson and John R. Phillips. Tactile spatial resolution. I. Two-point discrimination, gap detection, grating resolution, and letter recognition. *Journal of Neurophysiology*, 46(6):1177–1192, 1981.

[JRW91] Todd R. Jensen, Robert G. Radwin, and John G. Webster. A conductive polymer sensor for measuring external finger forces. *Journal of Biomechanics*, 24(9):851–858, 1991. URL: http://dx.doi.org/10.1016/0021-9290(91)90310-J.

[JS12] Liang-Ting Jiang and Joshua R. Smith. Seashell effect pretouch sensing for robotic grasping. In *IEEE International Conference on Robotics and Automation (ICRA)*, pages 2851–2858, St. Paul, Minnesota, USA, 2012. URL: http://dx.doi.org/10.1109/ICRA.2012.6224985.

[JV79] Roland S. Johansson and Åke B. Vallbo. Tactile sensibility in the human hand: relative and absolute densities of four types of mechanoreceptive units in glabrous skin. *The Journal of physiology*, (1979):283–300, 1979. URL: http://jp.physoc.org/content/286/1/283.short.

[JW87] Roland S. Johansson and Göran Westling. Signals in tactile afferents from the fingers eliciting adaptive motor responses during precision grip. *Experimental Brain Research*, 66:141–154, 1987. 10.1007/BF00236210. URL: http://dx.doi.org/10.1007/BF00236210.

[Kat] Hirokazu Kato. Artoolkit homepage. http://www.hitl.washington.edu/artoolkit/. Cited on Mar. 2013.

[KHC12] Risto Kõiva, Barbara Hilsenbeck, and Claudio Castellini. FFLS: An accurate linear device for measuring synergistic finger contractions. In *International Conference of the IEEE Engineering in Medicine & Biology Society (EMBC)*, pages 531–534, San Diego, California, USA, 2012. URL: http://dx.doi.org/10.1109/EMBC.2012.6345985.

[KHC13] Risto Kõiva, Barbara Hilsenbeck, and Claudio Castellini. Evaluating subsampling strategies for semg-based prediction of voluntary muscle contractions. In *13th International Conference on Rehabilitation Robotics (ICORR)*, Seattle, Washington, USA, 2013.

[KHR11] Risto Kõiva, Robert Haschke, and Helge J. Ritter. Development of an intelligent object for grasp and manipulation research. In *15th International Conference on Advanced Robotics (ICAR)*, pages 204–210, Tallinn, Estonia, June 2011. URL: http://dx.doi.org/10.1109/ICAR.2011.6088549.

[Kin] Microsoft Kinect. http://www.xbox.com/kinect/. Cited on Mar. 2013.

[KKYS10] G. S Kim, H. M Kim, J.W. Yoon, and H.S. Shin. Development of cylindrical type finger-force measuring system for measuring grasping finger-force of human. In *IEEE International Conference on Robotics and Biomimetics (ROBIO)*, pages 1734–1739, Tianjin, China, 2010. URL: http://dx.doi.org/10.1109/ROBIO.2010.5723593.

[KLK+09] Kunnyun Kim, Kang Ryeol Lee, Won Hyo Kim, Kwang-Bum Park, Tae-Hyung Kim, Jin-Sang Kim, and James Jungho Pak. Polymer-based flexible tactile sensor up to 32×32 arrays integrated with interconnection terminals. *Sensors and Actuators*, 156(2):284–291, 2009. URL: http://dx.doi.org/10.1016/j.sna.2009.08.015.

[KMSW11] Rebecca K. Kramer, Carmel Majidi, Ranjana Sahai, and Robert J. Wood. Soft curvature sensors for joint angle proprioception. In *IEEE/RSJ International Conference on Intelligent Robots and Systems (IROS)*, pages 1919–1926, San Francisco, California, USA, 2011. URL: http://dx.doi.org/10.1109/IROS.2011.6094701.

[Kon] Konami Digital Entertainment, Inc. DanceDanceRevolution. http://www.konami.com/ddr/. Cited on Mar. 2013.

[Kra94] Gregory Kramer. *Auditory display: Sonification, audification, and auditory interfaces*. Addison-Wesley, 1994.

[Kra02] Jan Krause. Bau eines haptischen Interfaces zur Echtzeitkontrolle von Sonifikationsmodellen, Aug. 2002.

[KS12] Risto Kõiva and Carsten Schürmann. Sensors for capturing tactile interaction patterns. In *International Conference on Human-Robot Interaction (HRI). Workshop on Advances in tactile sensing and touch based human-robot interaction*, Boston, Massachusetts, USA, Mar. 2012.

[KSJ10] Eric R. Kandel, James H. Schwartz, and Thomas M. Jessell. *Principles of Neural Science*. Mcgraw-Hill Professional, 4 edition, July 2010.

[KUMO04] Masahiro Kondo, Jun Ueda, Yoshio Matsumoto, and Tsukasa Ogasawara. Perception of human manipulation based on contact state transition. In *IEEE/RSJ International Conference on Intelligent Robots and Systems (IROS)*, volume 1, pages 100–105, Sendai, Japan, Sept. 2004. URL: http://dx.doi.org/10.1109/IROS.2004.1389336.

[KUO08] Masahiro Kondo, Jun Ueda, and Tsukasa Ogasawara. Recognition of in-hand manipulation using contact state transition for multifingered robot hand control. *Robotics and Autonomous Systems*, 56(1):66–81, 2008. URL: http://dx.doi.org/10.1016/j.robot.2007.09.018.

[KWM+09] Dieter F. Kutz, Alexander Wölfel, Tobias Meindl, Dagmar Timmann, and Florian P. Kolb. Spatio-temporal human grip force analysis via sensor arrays. *Sensors*, 9(8):6330–6345, 2009. URL: http://dx.doi.org/10.3390/s90806330.

[KWW03] Oliver Kerpa, Karsten Weiss, and Heinz Wörn. Development of a flexible tactile sensor system for a humanoid robot. In *IEEE/RSJ International Conference on Intelligent Robots and Systems (IROS)*, Las Vegas, Nevada, USA, 2003. URL: http://dx.doi.org/10.1109/IROS.2003.1250596.

[KZS+13] Risto Kõiva, Matthias Zenker, Carsten Schürmann, Robert Haschke, and Helge J. Ritter. A highly sensitive 3D-shaped tactile sensor. In *IEEE/ASME International Conference on Advanced Intelligent Mechatronics (AIM)*, pages 1084–1089, Wollongong, Australia, July 2013. URL: http://dx.doi.org/10.1109/AIM.2013.6584238.

[Lea] Leap Motion. http://www.leapmotion.com/. Cited on Mar. 2013.

[LGLM11] M. Leon, J.M. Gutierrez, L. Leija, and R. Munoz. EMG pattern recognition using Support Vector Machines classifier for myoelectric control purposes. In *Pan American Health Care Exchanges (PAHCE)*, pages 175–178, Rio de Janeiro, Brazil, 2011. URL: http://dx.doi.org/10.1109/PAHCE.2011.5871873.

[LHSS06] Paul Lukowicz, Friedrich Hanser, Christoph Szubski, and Wolfgang Schobersberger. Detecting and interpreting muscle activity with wearable force sensors. In Kenneth P. Fishkin, Bernt Schiele, Paddy Nixon, and Aaron Quigley, editors, *Pervasive Computing*, volume 3968 of *Lecture Notes in Computer Science*, pages 101–116. Springer Berlin Heidelberg, 2006. URL: http://dx.doi.org/10.1007/11748625_7.

[LKL66] L. F. Lucaccini, P. K. Kaiser, and J. Lyman. The French electric hand: Some observations and conclusions. *Bulletin of Prosthetics Research*, 10(6):31–51, 1966.

[LKLP04] Mark Lowe, Alison King, Elizabeth Lovett, and Thomas Papakostas. Flexible tactile sensor technology: bringing haptics to life. *Sensor Review*, 24(1), 2004.

[LMX] National Semiconductor Corporation. LMX9830 Bluetooth Serial Port Module. http://www.national.com/ds/LM/LMX9830.pdf. Cited on Mar. 2013.

[LP93] Susan J. Lederman and Dianne T. Pawluk. *Lessons From the Study of Biological Touch for Robotic Tactile Sensing*, chapter 8, pages 151–192. 1993. URL: http://dx.doi.org/10.1142/9789814355964_0008.

[LPK12] LPKF Laser & Electronics AG. 3-Dimensional Circuitry, Laser Direct Structuring Technology (LPKF-LDS™) for moulded interconnect devices. http://www.lpkf.com/_mediafiles/1797-lpkf-lds-process.pdf, 2012. Cited on Sept. 2013.

[LUK] LUKOtronic Motion Capturing. http://www.lukotronic.com/. Cited on Mar. 2013.

[LVX] LVX System homepage. http://www.lvx-system.com/. Cited on Apr. 2013.

[MA99] Andrew T. Miller and Peter K. Allen. Examples of 3D grasp quality computations. In *IEEE International Conference on Robotics and Automation (ICRA)*, volume 2, pages 1240–1246, Detroit, Michigan, USA, May 1999. URL: http://dx.doi.org/10.1109/ROBOT.1999.772531.

[MA01] Stephen A. Mascaro and Harry H. Asada. Photoplethysmograph fingernail sensors for measuring finger forces without haptic obstruction. *IEEE Transactions on Robotics and Automation*, 17(5):698–708, 2001. URL: http://dx.doi.org/10.1109/70.964669.

[MAB+10a] Roberto Merletti, Matteo Aventaggiato, Alberto Botter, Ales Holobar, Hamid Marateb, and Taian M.M. Vieira. Advances in Surface EMG: Recent Progress in Clinical Research Applications. *Critical Reviews in Biomedical Engineering*, 38(4):347–379, 2010.

[MAB+10b] Roberto Merletti, Matteo Aventaggiato, Alberto Botter, Ales Holobar, Hamid Marateb, and Taian M.M. Vieira. Advances in Surface EMG: Recent Progress in Detection and Processing Techniques. *Critical Reviews in Biomedical Engineering*, 38(4):305–345, 2010.

[Mat] Mattel Inc. http://www.mattel.com/. Cited on Mar. 2013.

[MC11] Philipp Mittendorfer and Gordon Cheng. Humanoid multimodal tactile-sensing modules. *IEEE Transactions on Robotics*, 27(3):401–410, 2011. URL: http://dx.doi.org/10.1109/TRO.2011.2106330.

[MDE+10] Jonathan Maycock, Daniel Dornbusch, Christof Elbrechter, Robert Haschke, Thomas Schack, and Helge J. Ritter. Approaching manual intelligence. *KI - Künstliche Intelligenz*, 24:287–294, 2010.

[ME-a] ME-Meßsysteme GmbH. Datasheet, Force Sensor GSV1L. http://www.me-systeme.de/de/datasheets/gsv1l-gsv1m.pdf.

[ME-b] ME-Meßsysteme GmbH. Datasheet, Force Sensor KD140. http://www.me-systeme.de/de/datasheets/kd140.pdf. Cited on Sept. 2013.

[ME-c] ME-Meßsysteme GmbH. Datasheet, Force Sensor KD60. http://www.me-systeme.de/en/datasheets/kd60.pdf. Cited on Sept. 2013.

[MEH+11] Jonathan Maycock, Kai Essig, Robert Haschke, Thomas Schack, and Helge J. Ritter. Towards an understanding of grasping using a multi-sensing approach. In *IEEE International Conference on Robotics and Automation (ICRA), Workshop on Autonomous Grasping*, Shanghai, China, 2011.

[Mic] Microchip Technology Inc. MPLAB X Integrated Development Environment (IDE). http://www.microchip.com/pagehandler/en-us/family/mplabx/. Cited on Nov. 2013.

[MMH+09] Kazuya Matsuo, Kouji Murakami, Tsutomu Hasegawa, Kenji Tahara, and Ryo Kurazume. Segmentation method of human manipulation task based on measurement of force imposed by a human hand on a grasped object. In *IEEE/RSJ International Conference on Intelligent Robots and Systems (IROS)*, Oct. 2009.

[MN08] Frederic H. Martini and Judi L. Nath. *Fundamentals of Anatomy & Physiology*. Benjamin Cummings, 8 edition, Apr. 2008.

[Mov] NeuroScript LLC. MovAlyzerR software to automatically analyze and quantify human movement. `http://www.neuroscript.net/`. Cited on Nov. 2013.

[MVG+05] Florian 'Floyd' Mueller, Frank Vetere, Martin R. Gibbs, Jesper Kjeldskov, Sonja Pedell, and Steve Howard. Hug over a distance. In *CHI '05 Extended Abstracts on Human Factors in Computing Systems*, pages 1673–1676, Portland, Oregon, USA, 2005. ACM. URL: `http://doi.acm.org/10.1145/1056808.1056994`.

[Nap56] John R. Napier. The prehensile movements of the human hand. *Journal of bone and Joint surgery*, 38(4):902–913, 1956.

[Nd04] Yvonne Nolan and Annraoi dePaor. The mechanomyogram as a channel of communication and control for the disabled. In *IEEE International Conference of the Engineering in Medicine and Biology Society (EMBS)*, volume 2, pages 4928–4931, San Francisco, California, USA, 2004. URL: `http://dx.doi.org/10.1109/IEMBS.2004.1404362`.

[Nex] Nexonar - next generation sonar technology. `http://www.nexonar.com/`. Cited on Mar. 2013.

[NHJ+11] Johnny L.G. Nielsen, Steffen Holmgaard, Ning Jiang, Kevin B. Englehart, Dario Farina, and Phil A. Parker. Simultaneous and proportional force estimation for multifunction myoelectric prostheses using mirrored bilateral training. *IEEE Transactions on Biomedical Engineering*, 58(3):681–688, 2011. URL: `http://dx.doi.org/10.1109/TBME.2010.2068298`.

[Nin] Nintendo Wii Fit. `http://www.wiifit.com/`. Cited on Mar. 2013.

[NKK+06] Hiroyuki Nakamoto, Futoshi Kobayashi, Fumio Kojima, Nobuaki Imamura, and Hidenori Shirasawa. Universal robot hand equipped with tactile and joint torque sensors (development and experiments on stiffness control and object recognition). In *The 10th World Multi-conference on Systemics, Cybernetics and Informatics (WMSCI 2006)*, volume 2, pages 347–352, Orlando, Florida, USA, July 2006.

[NME13] Abdeldjallil Naceri, Alessandro Moscatelli, and Marc O. Ernst. Modulation of digit normal forces and locations during unconstrained grasping. In *IEEE International Conference on Robotics and Automation (ICRA). Workshop on Hand synergies - how to tame the complexity of grasping*, pages 56–61, Karlsruhe, Germany, May 2013.

[noD] noDNA shop for makers. `http://nodna.de/`. Cited on Mar. 2013.

[OBMC09] Calogero M. Oddo, Lucia Beccai, Giovanni G. Muscolo, and Maria Chiara Carrozza. A biomimetic MEMS-based tactile sensor array with fingerprints integrated in a robotic fingertip for artificial roughness encoding. In *IEEE International Conference on Robotics and Biomimetics (ROBIO 2009)*, pages 894–900, Guilin, Guangxi, China, Dec. 2009. URL: `http://dx.doi.org/10.1109/ROBIO.2009.5420491`.

[OKN06] Yoshiyuki Ohmura, Yasuo Kuniyoshi, and Akihiko Nagakubo. Conformable and scalable tactile sensor skin for curved surfaces. In *IEEE International Conference on Robotics and Automation (ICRA)*, Orlando, Florida, USA, 2006. URL: http://dx.doi.org/10.1109/ROBOT.2006.1641896.

[Ori05] Claudio Orizio. *Surface Mechanomyogram*, pages 305–322. John Wiley & Sons, Inc., 2005. URL: http://dx.doi.org/10.1002/0471678384.ch11.

[OTK+09] Masahiro Ohka, Jumpei Takata, Hiroaki Kobayashi, Hirofumi Suzuki, Nobuyuki Morisawa, and Hanafiah Bin Yussof. Object exploration and manipulation using a robotic finger equipped with an optical three-axis tactile sensor. *Robotica*, 27:763–770, Sept. 2009. URL: http://journals.cambridge.org/article_S0263574708005213.

[Ott] Ottobock Michelangelo hand prosthesis. http://www.living-with-michelangelo.com/ Cited on Sept. 2013.

[Oxf09] *The Oxford English Dictionary*. Oxford University Press, Oct. 2009. URL: http://oxforddictionaries.com/.

[Pat] Pattex. Henkel AG & Co. KGaA. http://www.pattex.de/ Cited on Mar. 2013.

[PBW+11] Bart Peerdeman, Daphne Boere, Heidi Witteveen, Rianne Huis in 't Veld, Hermie Hermens, Stefano Stramigioli, Hans Rietman, Peter Veltink, and Sarthak Misra. Myoelectric forearm prostheses: State of the art from a user-centered perspective. *Journal of rehabilitation research and development*, 48(6):719–738, 2011.

[PCE] PCE Instruments. http://www.pce-instruments.com/. Cited on Sept. 2013.

[Per] The Peregrine. http://theperegrine.com/. Cited on Mar. 2013.

[PHA] Phantom 6-DOF haptic device. http://geomagic.com/en/products/phantom-premium-6dof/overview/. Cited on Oct. 2013.

[PHG09] Ryan M. Peters, Erik Hackeman, and Daniel Goldreich. Diminutive digits discern delicate details: Fingertip size and the sex difference in tactile spatial acuity. *The Journal of Neuroscience*, 29(50):15756–15761, 2009. URL: http://dx.doi.org/10.1523/JNEUROSCI.3684-09.2009.

[PLK+12] Changhyun Pang, Gil-Yong Lee, Tae-il Kim, Sang Moon Kim, Hong Nam Kim, Sung-Hoon Ahn, and Kahp-Yang Suh. A flexible and highly sensitive strain-gauge sensor using reversible interlocking of nanofibres. *Nature Materials*, 11:795–801, 2012. URL: http://dx.doi.org/10.1038/nmat3380.

[PRAS+07] O. Portillo-Rodriguez, C.A. Avizzano, E. Sotgiu, S. Pabon, A. Frisoli, J. Ortiz, and M. Bergamasco. A wireless bluetooth dataglove based on a novel goniometric sensors. In *16th IEEE International Symposium on Robot and Human interactive Communication (RO-MAN)*, pages 1185–1190, Jeju, Korea, Aug. 2007. URL: http://dx.doi.org/10.1109/ROMAN.2007.4415259.

[Pri] PrimeSense. http://www.primesense.com/. Cited on Mar. 2013.

[PSS+97] Jean Ponce, Steve Sullivan, Attawith Sudsang, Jean-Daniel Boissonnat, and Jean-Pierre Merlet. On Computing Four-Finger Equilibrium and Force-Closure Grasps of Polyhedral Objects. *The International Journal of Robotics Research*, 1997.

[PW] Hannah Perner-Wilson. Plusea. `http://www.plusea.at/`. Cited on Mar. 2013.

[RDLT06] Gabriel Robles-De-La-Torre. The importance of the sense of touch in virtual and real environments. *IEEE Multimedia*, 13(3):24–30, July-Sept. 2006. URL: `http://dx.doi.org/10.1109/MMUL.2006.69`.

[RHN+11] Joseph M. Romano, Kaijen Hsiao, Günter Niemeyer, Sachin Chitta, and Katherine J. Kuchenbecker. Human-inspired robotic grasp control with tactile sensing. *IEEE Transactions on Robotics*, 27(6):1067–1079, 2011. URL: `http://dx.doi.org/10.1109/TRO.2011.2162271`.

[RHS07] Helge J. Ritter, Robert Haschke, and Jochen J. Steil. A dual interaction perspective for robot cognition: Grasping as a "Rosetta Stone". In Barbara Hammer and Pascal Hitzler, editors, *Perspectives of Neural-Symbolic Integration*, volume 77 of *Studies in Computational Intelligence*, pages 159–178. Springer Berlin / Heidelberg, 2007.

[RKC12] Maximo A. Roa, Risto Kõiva, and Claudio Castellini. Experimental evaluation of human grasps using a sensorized object. In *4th IEEE RAS EMBS International Conference on Biomedical Robotics and Biomechatronics (BioRob)*, pages 1662–1668, Rome, Italy, June 2012. URL: `http://dx.doi.org/10.1109/BioRob.2012.6290670`.

[RLFP04] Bruce Richardson, Krispin Leydon, Mikael Fernstrom, and Joseph A. Paradiso. Z-tiles: building blocks for modular, pressure-sensing floorspaces. In *Extended Abstracts on Human Factors in Computing Systems (CHI)*, pages 1529–1532, Vienna, Austria, 2004. ACM. URL: `http://dx.doi.org/10.1145/985921.986107`.

[RRL12] Sridhar Rajagopal, Richard D. Roberts, and Sang-Kyu Lim. IEEE 802.15.7 visible light communication: modulation schemes and dimming support. *IEEE Communications Magazine*, 50(3):72–82, 2012. URL: `http://dx.doi.org/10.1109/MCOM.2012.6163585`.

[RSL] RSLSteeper BeBionic3 hand prosthesis. `http://bebionic.com/` Cited on Sept. 2013.

[RvHC96] David A. Rosenbaum, Caroline M. van Heugten, and Graham E. Caldwell. From cognition to biomechanics and back: The end-state comfort effect and the middle-is-faster effect. *Acta Psychologica*, 94(1):59–85, 1996. URL: `http://dx.doi.org/10.1016/0001-6918(95)00062-3`.

[SBQK05] Prashant Srinivasan, David Birchfield, Gang Qian, and Assegid Kidanè. Design of a pressure sensitive floor for multimodal sensing. In *International Conference on Information Visualisation (IV)*, pages 41–46, London, United Kingdom, July 2005. URL: `http://dx.doi.org/10.1109/IV.2005.40`.

[Sch99] Stefan Schaal. Is imitation learning the route to humanoid robots? *Trends in Cognitive Sciences*, 3(6):233–242, 1999. URL: `http://dx.doi.org/10.1016/S1364-6613(99)01327-3`.

[Sch08] Carsten Schürmann. Entwicklung eines modularen und intelligenten Taktilsensorsystems mit Standard Imaging Interface zur Hochgeschwindigkeitsbildübermittlung. Diploma thesis, Bielefeld University, Faculty of Technology, Bielefeld, Germany, 2008.

[SEHR10] Jan Steffen, Christof Elbrechter, Robert Haschke, and Helge J. Ritter. Bio-inspired motion strategies for a bimanual manipulation task. In *IEEE-RAS International Conference on Humanoid Robots (Humanoids)*, pages 625–630, Nashville, Tennessee, USA, Dec. 2010. URL: `http://dx.doi.org/10.1109/ICHR.2010.5686830`.

[Sha] Shadow Robot Company. Shadow Robot Hand. `http://www.shadowrobot.com/` Cited on Sept. 2013.

[Shi96] Karun B. Shimoga. Robot Grasp Synthesis Algorithms: A Survey. *The International Journal of Robotics Research*, 15(3):230–266, 1996.

[SKHR11] Carsten Schürmann, Risto Kõiva, Robert Haschke, and Helge J. Ritter. A modular high-speed tactile sensor for human manipulation research. In *IEEE World Haptics Conference (WHC)*, pages 339–344, Istanbul, Turkey, 2011. URL: `http://dx.doi.org/10.1109/WHC.2011.5945509`.

[SKHR12] Carsten Schürmann, Risto Kõiva, Robert Haschke, and Helge J. Ritter. Analysis of human grasping under task anticipation using a multi sensory tactile book. In *IEEE-RAS International Conference on Humanoid Robots (Humanoids)*, pages 773–778, Osaka, Japan, Nov. 2012. URL: `http://dx.doi.org/10.1109/HUMANOIDS.2012.6651607`.

[SLPD09] Julien Scheibert, S. Leurent, Alexis Prevost, and Georges Debrégeas. The role of fingerprints in the coding of tactile information probed with a biomimetic sensor. *Science*, 323(5920):1503–1506, 2009. URL: `http://dx.doi.org/10.1126/science.1166467`.

[Sma] Alpha-Fit's Smart Sock – tactile sensitive sock. `http://www.alpha-fit.de/en/products/smartsock.html`. Cited on Mar. 2013.

[SMM+11] Alexander Schmitz, Perla Maiolino, Marco Maggiali, Lorenzo Natale, Giorgio Cannata, and Giorgio Metta. Methods and technologies for the implementation of large-scale robot tactile sensors. *IEEE Transactions on Robotics*, 27(3):389–400, 2011. URL: `http://dx.doi.org/10.1109/TRO.2011.2132930`.

[SMR11] Jan Steffen, Jonathan Maycock, and Helge J. Ritter. Robust dataglove mapping for recording human hand postures. In *4th International Conference on Intelligent Robotics and Applications (ICIRA)*, Aachen, Germany, 2011.

[SNI+04] Makoto Shimojo, Akio Namiki, Masatoshi Ishikawa, Ryota Makino, and Kunihiko Mabuchi. A tactile sensor sheet using pressure conductive rubber with

electrical-wires stitched method. *IEEE Sensors Journal*, 4(5), 2004. URL: http://dx.doi.org/10.1109/JSEN.2004.833152.

[Sof] SoftKinetic. http://www.softkinetic.com/. Cited on Mar. 2013.

[SOK+11] Takashi Sagisaka, Yoshiyuki Ohmura, Yasuo Kuniyoshi, Akihiko Nagakubo, and Kazuyuki Ozaki. High-density conformable tactile sensing glove. In *IEEE-RAS International Conference on Humanoid Robots (Humanoids)*, pages 537–542, 2011. URL: http://dx.doi.org/10.1109/Humanoids.2011.6100898.

[Spe] Spectra Symbol. http://www.spectrasymbol.com/. Cited on Mar. 2013.

[SPH12] Munehiko Sato, Ivan Poupyrev, and Chris Harrison. Touché: enhancing touch interaction on humans, screens, liquids, and everyday objects. In *SIGCHI Conference on Human Factors in Computing Systems (CHI)*, pages 483–492, Austin, Texas, USA, 2012. ACM. URL: http://doi.acm.org/10.1145/2207676.2207743.

[SPR+12] Hooman Aghaebrahimi Samani, Rahul Parsani, Lenis Tejada Rodriguez, Elham Saadatian, Kumudu Harshadeva Dissanayake, and Adrian David Cheok. Kissenger: design of a kiss transmission device. In *Designing Interactive Systems Conference (DIS)*, pages 48–57, Newcastle Upon Tyne, United Kingdom, 2012. ACM. URL: http://doi.acm.org/10.1145/2317956.2317965.

[SPW] Mika Satomi and Hannah Perner-Wilson. KOBAKANT DIY Wearable Technology database. http://www.kobakant.at/. Cited on Mar. 2013.

[SRI] SRI Sensor. 6-axis Force/Torque sensor. http://srisensor.com/pdf/2013SRIProductCatalogV1.3English.pdf. Cited on Sept. 2013.

[SRL05] Fredrik C.P. Sebelius, Birgitta N. Rosén, and Göran N. Lundborg. Refined myoelectric control in below-elbow amputees using artificial neural networks and a data glove. *The Journal of Hand Surgery*, 30(4):780–789, 2005. URL: http://dx.doi.org/10.1016/j.jhsa.2005.01.002.

[SSPR10] Matthias Schöpfer, Carsten Schürmann, Michael Pardowitz, and Helge J. Ritter. Using a piezo-resistive tactile sensor for detection of incipient slippage. In *International Symposium on Robotics (ISR)*, Munich, Germany, 2010.

[SSS+96] Sigeru Sato, Makoto Shimojo, Yoshikazu Seki, Akihiko Takahashi, and Shunji Shimizu. Measuring system for grasping. In *5th IEEE International Workshop on Robot and Human Communication (RO-MAN)*, pages 292–297, Tsukuba, Japan, Nov. 1996. URL: http://dx.doi.org/10.1109/ROMAN.1996.568852.

[SSS+09] Matthias Schöpfer, Carsten Schürmann, Florian P. Schmidt, Michael Pardowitz, and Helge J. Ritter. Handling of deformable material using tactile sensors in a bi-manual scenario. In *International Conference on Humanoid Robots (Humanoids), Workshop on Tactile Sensing in Humanoids – Tactile Sensors and beyond*, pages 61–63, Paris, France, 2009.

[SSSS11] Jivko Sinapov, Vladimir Sukhoy, Ritika Sahai, and Alexander Stoytchev. Vibrotactile recognition and categorization of surfaces by a humanoid robot.

IEEE Transactions on Robotics, 27(3):488–497, 2011. URL: http://dx.doi.org/10.1109/TRO.2011.2127130.

[Ste10] Jan Steffen. *Structured Manifolds for Motion Production and Segmentation – A Structured Kernel Regression Approach.* PhD Thesis, Bielefeld University, Faculty of Technology, Neuroinformatics Group, Bielefeld, Germany, Jan. 2010.

[Str] Stratasys Ltd. FDM Technology. http://www.stratasys.com/3d-printers/technology/fdm-technology. Cited on Nov. 2013.

[Str12] Michael Strohmayr. *Artificial Skin in Robotics: a comprehensive interface for system-environment interaction.* PhD thesis, Karlsruher Institut für Technologie (KIT), Karlsruhe, Germany, 2012.

[Syn] SynTouch BioTac robotic fingertip tactile sensor. http://www.syntouchllc.com/Products/BioTac/. Cited on Nov. 2013.

[SZ96] K. Sathian and A. Zangaladze. Tactile spatial acuity at the human fingertip and lip: bilateral symmetry and interdigit variability. *Neurology*, 46(5):1464–1466, 1996. URL: http://www.ncbi.nlm.nih.gov/pubmed/8628503.

[TDSM68] William H. Talbot, Kornhuber Hans H. Darian-Smith, Ian and, and Vernon B. Mountcastle. The sense of flutter-vibration: comparison of the human capacity with response patterns of mechanoreceptive afferents from the monkey hand. *Journal of Neurophysiology*, 31:301–334, Mar. 1968. URL: http://ukpmc.ac.uk/abstract/MED/4972033.

[Teka] Tekscan Inc. Body Pressure Measurement System. http://www.tekscan.com/body-pressure-measurement/. Cited on Mar. 2013.

[Tekb] Tekscan Inc. Tactile grip force and pressure measurement. http://www.tekscan.com/grip-pressure-measurement/. Cited on Mar. 2013.

[TFR13] Lukas Twardon, Andrea Finke, and Helge J. Ritter. Exploiting eye-hand coordination: a novel approach to remote manipulation. In *IEEE/RSJ International Conference on Intelligent Robots and Systems (IROS)*, Tokyo, Japan, 2013.

[TM81] Julia M. Thornbury and Charlotte M. Mistretta. Tactile sensitivity as a function of age. *Journal of Gerontology*, 36(1):34–39, 1981. URL: http://www.ncbi.nlm.nih.gov/pubmed/7451834.

[TMD+05] François Tremblay, Annie-Claude Mireault, Liam Dessureault, Hélène Manning, and Heidi Sveistrup. Postural stabilization from fingertip contact. *Experimental Brain Research*, 164:155–164, 2005. URL: http://dx.doi.org/10.1007/s00221-005-2238-5.

[TOO+11] Nobuhiro Takahashi, Ryuta Okazaki, Hiroyuki Okabe, Hiromi Yoshikawa, Kanako Aou, Shumpei Yamakawa, Maki Yokoyama, and Hiroyuki Kajimoto. Sense-roid: Emotional haptic communication with yourself. In *Virtual Reality International Conference (VRIC)*, Laval, France, Apr. 2011.

[TRF+09] Francesco V.G. Tenore, Ander Ramos, Amir Fahmy, Soumyadipta Acharya, Ralph Etienne-Cummings, and Nitish V. Thakor. Decoding of individuated finger movements using surface electromyography. *IEEE Transactions on Biomedical Engineering*, 56(5):1427–1434, 2009. URL: `http://dx.doi.org/10.1109/TBME.2008.2005485`.

[TSP01] Hong Z. Tan, Lynne A. Slivovsky, and Alex Pentland. A sensing chair using pressure distribution sensors. *IEEE/ASME Transactions on Mechatronics*, 6(3):261 –268, Sep. 2001. URL: `http://dx.doi.org/10.1109/3516.951364`.

[VCvdS11] Jörn Vogel, Claudio Castellini, and Patrick van der Smagt. EMG-based teleoperation and manipulation with the DLR LWR-III. In *IEEE/RSJ International Conference on Intelligent Robots and Systems (IROS)*, pages 672–678, San Francisco, California, USA, 2011. URL: `http://dx.doi.org/10.1109/IROS.2011.6094739`.

[VHK+00] Robert W. Van Boven, R. H. Hamilton, T. Kauffman, J. P. Keenan, and A. Pascual-Leone. Tactile spatial resolution in blind braille readers. 55(10):1597, 2000. URL: `http://www.ncbi.nlm.nih.gov/pubmed/11094135`.

[Vic] Vicon Motion Systems. `http://www.vicon.com/`. Cited on Mar. 2013.

[Vir] Virtual Realities, Ltd. `http://www.vrealities.com/`. Cited on Mar. 2013.

[VIR+09] Nicolas Villar, Shahram Izadi, Dan Rosenfeld, Hrvoje Benko, John Helmes, Jonathan Westhues, Steve Hodges, Eyal Ofek, Alex Butler, Xiang Cao, and Billy Chen. Mouse 2.0: multi-touch meets the mouse. In *ACM Symposium on User Interface Software and Technology (UIST)*, pages 33–42, Victoria, BC, Canada, 2009. ACM. URL: `http://doi.acm.org/10.1145/1622176.1622184`.

[VJ84] Åke B. Vallbo and Roland S. Johansson. Properties of cutaneous mechanoreceptors in the human hand related to touch sensation. *Human Neurobiology*, 3:3–14, 1984. URL: `http://ci.nii.ac.jp/naid/10012460874/en/`.

[WB11] Raphael Wimmer and Patrick Baudisch. Modular and deformable touch-sensitive surfaces based on time domain reflectometry. In *24th annual ACM symposium on User interface software and technology (UIST)*, pages 517–526, Santa Barbara, California, USA, 2011. ACM. URL: `http://doi.acm.org/10.1145/2047196.2047264`.

[WEA] WEARHAP (WEARable HAPtics). EU funded project no. 601165. `http://www.wearhap.eu/`. Cited on Nov. 2013.

[Wei] Weiss Robotics GmbH & Co.KG. `http://www.weiss-robotics.de/`. Cited on Mar. 2013.

[Wei68] Sidney Weinstein. Intensive and extensive aspects of tactile sensitivity as a function of body part, sex and laterality. In *The First Int'l symp. on the Skin Senses*, 1968.

[WHB07] Zheng Wang, Jens Hoelldampf, and Martin Buss. Design and performance of a haptic data acquisition glove. In *Proceedings of the 10th Annual International Workshop on Presence (PRESENCE)*, pages 349–357, Barcelona, Spain, 2007.

[WJ84] Göran Westling and Roland S. Johansson. Factors influencing the force control during precision grip. *Experimental Brain Research*, 53, 1984.

[WJ87] Göran Westling and Roland S. Johansson. Responses in glabrous skin mechanoreceptors during precision grip in humans. *Experimental Brain Research*, 66:128–140, 1987. URL: `http://dx.doi.org/10.1007/BF00236209`.

[WKC08] Michael Wininger, N Kim, and William Craelius. Pressure signature of forearm as predictor of grip force. *Journal of Rehabilitation Research and Development*, 45(6):883–892, 2008.

[WL11] Nicholas Wettels and Gerald E. Loeb. Haptic feature extraction from a biomimetic tactile sensor: Force, contact location and curvature. In *IEEE International Conference on Robotics and Biomimetics (ROBIO 2011)*, pages 2471–2478, Phuket, Thailand, 2011. URL: `http://dx.doi.org/10.1109/ROBIO.2011.6181676`.

[WNMS12] S. Wattanasarn, K. Noda, K. Matsumoto, and I. Shimoyama. 3D flexible tactile sensor using electromagnetic induction coils. In *IEEE 25th International Conference on Micro Electro Mechanical Systems (MEMS 2012)*, pages 488–491, Paris, France, 2012. URL: `http://dx.doi.org/10.1109/MEMSYS.2012.6170230`.

[WW04] Karsten Weiss and Heinz Wörn. Tactile sensor system for an anthropomorphic robotic hand. In *IEEE International Conference on Manipulation and Grasping (IMG 2004)*, volume 7, Genova, Italy, July 2004.

[WW05] Karsten Weiß and Heinz Wörn. The working principle of resistive tactile sensor cells. In *IEEE International Conference on Mechatronics and Automation (ICMA)*, volume 1, pages 471–476, Niagara Falls, Ontario, Canada, July 2005. URL: `http://dx.doi.org/10.1109/ICMA.2005.1626593`.

[Xse] Xsens 3D Motion Tracking. `http://www.xsens.com/`. Cited on Mar. 2013.

[YBL+12] Ming Ying, Andrew P. Bonifas, Nanshu Lu, Yewang Su, Rui Li, Huanyu Cheng, Abid Ameen, Yonggang Huang, and John A. Rogers. Silicon nanomembranes for fingertip electronics. *Nanotechnology*, 23(34):344004, 2012. URL: `http://stacks.iop.org/0957-4484/23/i=34/a=344004`.

[YC12] Don Yungher and William Craelius. Improving fine motor function after brain injury using gesture recognition biofeedback. *Disability and Rehabilitation: Assistive Technology*, 7(6):464–468, 2012.

[YKA09] Zhao Feng Yang, Dinesh Kant Kumar, and Sridhar Poosapadi Arjunan. Mechanomyogram for identifying muscle activity and fatigue. In *IEEE International Conference of the Engineering in Medicine and Biology Society (EMBC)*, pages 408–411, Minneapolis, Minnesota, USA, 2009. URL: `http://dx.doi.org/10.1109/IEMBS.2009.5333666`.

[YWB+11] Don A. Yungher, Michael T. Wininger, J.B. Barr, William Craelius, and A. Joseph Threlkeld. Surface muscle pressure as a measure of active and passive behavior of muscles during gait. *Medical Engineering & Physics*, 33(4):464–471, 2011. URL: `http://dx.doi.org/10.1016/j.medengphy.2010.11.012`.

[ZMCD02] Massimiliano Zecca, Silvestro Micera, Maria Chiara Carrozza, and Paolo Dario. Control of multifunctional prosthetic hands by processing the electromyographic signal. *Critical Reviews in Biomedical Engineering*, 30(4-6):459–485, 2002.

Index